

THE FILTRATION PROPERTIES OF A DIMORPHIC YEAST

Submitted by: Tony McCarthy BSc.

For the qualification of PhD

At Dublin City University,

School of Biotechnology

Under the Supervision of

Dr. Greg Foley and Dr. Padraig Walsh

April 2001

I hereby certify that this material, which I now submit for assessment on the programme of study leading to the award of PhD (Biotechnology) is entirely my own work and has not been taken from the work of others save and to the extent that such work has been cited and acknowledged within the text of my work.

Signed: Zeng Mc Carthy
candidate

ID No.: 94971218

Date: 17 April 2001

Published papers related to the work in this thesis:

McCarthy A. A., O'Shea D.G., Murray N.T., Walsh P.K. and G. Foley (1998).
The effect of cell morphology on the filtration characteristics of the dimorphic yeast Kluyveromyces marxianus var. marxianus NRRYLy2415.

Biotechnol. Prog. 14(2) 279-285

McCarthy A. A., Conroy H., Walsh P.K. and G. Foley (1998).

The effect of pressure on the specific resistance of yeast filter cakes during dead-end filtration in the range 30-500kPa.

Biotech. Tech., 12, 909-912

McCarthy A. A., Gilboy P., Walsh P.K. and G. Foley (1999).

Characterisation of cake compressibility in dead-end microfiltration of microbial suspensions.

Chem. Eng. Commun., 173, 79-90.

*'I have no love of knowledge just a fear of
stupidity'*

FOR THOSE WHO WENT HOME EARLY

*The world went on in mizzly motion
But those who drank the dizzy potion
Soon forgot the busy commotion
And slipped away, from the hectic fray*

WINTERS RAIN

*Viscously flowing down the window pane
Like a tear held heavy in sorrow
Blinded by the invisible
The genius of simplicity is complete
And there is beauty in the irreversible*

TABLE OF CONTENTS

Abstract:	ix
Acknowledgements:.....	xii
Nomenclature:.....	xiv
List of Figures:....	xix
List of Tables	xxiii

CHAPTER 1: Overview of Membrane Filtration Processes

1.1 Introduction	1
1.2 Classification of membrane filtration techniques	1
1.3 Filtration techniques	3
1.3.1 Modes of operation	3
1.3.2 Modules and system configurations	5
1.4 Membranes.	6
1.5 Applications of microfiltration	7
1.6 Conclusions	8

CHAPTER 2: Dead-End and Crossflow Filtration of Microbial Suspensions

2.1 Introduction	9
2.1.1 Fundamental concepts in filtration	9
2.1.2 Factors that influence filtrate flux in filtration.....	11
2.2 Dead-end filtration of micro-organisms	14
2.2.1 Flow through packed beds and filter cakes.....	14
2.2.1.1 Influence of particle morphology and packing arrangement on voidage.....	16
2.2.1.2 Particle size and size distribution effects.....	20
2.2.1.3 Factors affecting Kozeny's constant.....	21
2.2.2 Membrane effects	22
2.2.2.1 Membrane fouling by macrosolutes	22
2.2.3 Particle surface properties and solution properties effects	25

2.2.4	Filter cake compressibility	25
2.2.4.1	Factors affecting compressibility and mechanisms of compressibility	26
2.2.4.2	Filter-cake compression theory	28
2.3	Crossflow microfiltration.....	29
2.3.1	Flux behaviour in crossflow microfiltration	30
2.3.2	Cake formation in crossflow microfiltration	32
2.3.3	Fouling in crossflow filtration	34
2.3.4	Influence of process variables.....	36
2.3.4.1	Temperature of feed solution.....	36
2.3.4.2	Transmembrane pressure drop.....	37
2.3.4.3	Crossflow velocity	37
2.3.5	The critical flux concept	39
2.3.6	Feed suspension characteristics	40
2.3.6.1	Particle concentration	40
2.3.6.2	Particle morphology.....	41
2.3.7	Specific resistance in crossflow filtration.....	42
2.3.8	Theoretical studies in crossflow filtration	43
2.3.8.1	Convective models.....	43
2.3.8.2	Shear-induced diffusion.....	44
2.3.8.3	Force balance models.....	45
2.3.8.4	Empirical models	45
2.4	Conclusions	45

CHAPTER 3: Materials and Experimental Methods

3.1	Organism.....	47
3.2	Autoclaving procedure.....	47
3.3	Media preparation.....	47
3.3.1	YEPD medium.....	47
3.3.2	YEPD medium (solid)	48
3.3.3	YEPL medium	48
3.3.4	Glycerol medium	48
3.3.5	Whey-based medium	48

3.4	Culturing on solid medium	48
3.5	Shake flask cultures	49
3.6	2L “Life Sciences” fermenter	49
3.6.1	Fermenter configuration	49
3.6.2	Fermenter set-up: batch mode.....	50
3.6.3	Fermenter set-up: continuous mode.....	51
3.6.4	Fermenter operation.....	52
3.7	Cultivation conditions required to produce different morphological forms of <i>K. Marxianus</i>	52
3.7.1	Cultivation conditions for yeast-like cells	52
3.7.2	Cultivation conditions for cultures containing a mixture of yeast-like cells and filaments	52
3.7.3	Cultivation conditions for cultures containing a mixture of filaments and mycelia	53
3.8	Wet weight cell concentration	53
3.9	Cell density determination.....	54
3.10	Centrifugation pellet voidage.....	55
3.11	Centrifugation studies.....	55
3.11.1	Centrifugation speed	55
3.11.2	Determination of unstressed pellet voidage-‘Water Drop Test’	56
3.12	Dead-end filtration.....	57
3.12.1	Sample preparation	57
3.12.2	Filtration set-up.....	58
3.12.3	Determination of membrane resistance	58
3.12.4	Determination of the mean specific resistance	59
3.12.5	Reversibility studies.....	60
3.13	Image analysis.....	60
3.14	Crossflow filtration.....	64
3.14.1	Culturing conditions and suspension preparation for crossflow filtration	64
3.14.1.1	Growth media used for cell suspensions filtered by crossflow filtration suspensions	64
3.14.1.2	Cultivation conditions.....	65
3.14.1.3	Suspension preparation for crossflow filtration experiments.	65

3.14.2	Crossflow filtration module	66
3.14.3	Crossflow filtration setup.....	67
3.14.5	Water source for crossflow filtration experiments	68
3.14.6	Determination of R_m	69
3.14.7	Membrane cleaning.....	70
3.14.8	Preparation of module for crossflow filtration	70
3.14.9	Crossflow filtration operation.....	70
3.14.10	Switching feed to saline and crossflow filter cake recovery	71
3.14.11	Determination of recovered crossflow filter cake mass.....	72
3.14.12	Determination of filter cake mass as a function of filtration time	73

CHAPTER 4: Dead-End Filtration Behaviour of *K. Marxianus*

4.1	Introduction	75
4.2	Morphological characteristics of <i>K. marxianus</i> broths.....	76
4.3	Effect of mean cell morphology on dead-end filtration characteristics.....	79
4.3.1	Effect of pressure on specific resistance.....	79
4.3.2	Effect of cell morphology on unstressed cake resistance	82
4.4	The effect of L_{dm} on centrifugation pellet voidage	83
4.4.1	The effect of centrifugation speed on pellet voidage.....	85
4.4.2	Time dependent decompression of centrifugation pellets	86
4.4.3	Determination of unstressed centrifugation pellet voidage	88
4.4.2	The relationship between unstressed pellet voidage and L_{dm}	90
4.5	Calculation of the Kozeny constant	92
4.6	Effect of mean morphology on filter cake compressibility	95
4.7	Conclusions	101

CHAPTER 5: Compressibility of Filter Cakes

5.1	Introduction	102
5.2	Characterisation of cake compressibility.....	103
5.3	Conclusions	108

CHAPTER 6: Modelling Filter Cake Compressibility

6.1 Introduction 110
6.2 Model development 111
6.3 Solution method 113
6.4 Model predictions of relationship between α_{av} and ΔP 114
6.5 An alternative approach to the linearity between α_{av} and ΔP 120
6.6 The affect of null stress voidage on filter cake compression 122
6.7 Model predictions for the voidage gradient in filter cakes and calculation
of the average cake voidage 124
6.8 Implications of applying the Kozeny-Carman equation directly to
filtration data 127
6.9 Conclusions 130

CHAPTER 7: Crossflow Filtration Characteristics of *K. marxianus*

7.1 Introduction 132
7.2 General observations in crossflow microfiltration..... 135
7.3 Flux patterns in crossflow microfiltration 136
7.4 Spent medium and fresh media studies..... 143
7.5 Washed suspensions 148
7.5.1 Cake formation and flux behaviour of washed cell suspensions 149
7.5.2 Reversibility of fouling and cake recovery 159
7.5.3 Cake formation and morphology effects 161
7.5.4 Evolution of specific resistance in crossflow microfiltration 168
7.5.5 Crossflow velocity 178
7.6 Unwashed suspensions 181
7.7 Conclusions 189

CHAPTER 8: Summary and Future Work

8.1 Summary 191
8.2 Recommendations for future work 194

Appendix A: Cake formation in crossflow filtration: equations..... 196
References: 199

THE FILTRATION PROPERTIES OF A DIMORPHIC YEAST

ABSTRACT

A dimorphic yeast *Kluyveromyces marxianus* var. *marxianus* NRRLy2415 which exhibits a wide range of mean morphological forms was used as a model organism to investigate the role of cell morphology on the dead-end and crossflow filtration behaviour. Varying the culturing conditions produced cell suspensions of different mean morphology. Batch fermentations were used to produce yeast-like morphologies and continuous cultures produced cells more mycelial in nature. Semi-automated image analysis was used to measure the mean specific surface area, S_v , and the mean ratio of cell length to equivalent cylindrical diameter, L_{dm} . The parameter L_{dm} was used to describe the mean cell morphology, whereby increasing values of L_{dm} indicate that the mean cell morphology is more mycelial in nature.

It was shown that a linear relationship was found to exist between the mean specific resistance, α_{av} , and applied pressure, ΔP , over the entire range of pressures employed and for all morphologies of *K. marxianus* filtered. The linear relationship, i.e. $\alpha_{av} = \alpha_o(1 + k_c \Delta P)$ allowed the null stress resistance, α_o , to be determined, thus uncoupling cake packing and compressibility effects. The voidage of cell pellets formed in a bench-top centrifuge was measured for a range of cell suspensions of different mean morphologies, and in all cases, the pellet voidage decreased linearly with centrifugation speed. This decrease became more pronounced as L_{dm} increased. The extrapolated null stress pellet porosity, ϵ_o , was correlated with L_{dm} by the expression $\epsilon_o = 1 - 1/(1.24 + 0.062L_{dm})$. The ratio $\alpha_o \rho_c / S_v^2$ decreased with increasing L_{dm} , a finding that was qualitatively consistent with the pellet voidage data and the Kozeny-Carman equation. Considerably better agreement with the experimental data was obtained when the Kozeny constant, k_o , was treated as a variable and related to L_{dm} by the equation $k_o = 10.1 + 0.34L_{dm}$.

It was shown that as L_{dm} increases that filter cake compressibility defined as k_c increases. The reversibility of filter cake compression was determined by measuring the specific resistance of a pre-formed filter cake, exposing the cake to a higher pressure and then re-determining α_{av} at the lower pressure. It was found that the compression of filter cakes of *K. marxianus* and bakers yeast was predominantly reversible, whereas with filter cakes of calcium carbonate, compression was completely irreversible. A model was presented to qualitatively describe filter cake compression. The model was found to predict a near linear relationship between α_{av} and ΔP , as was found to occur with *K. marxianus* and other yeast suspensions. It was also shown that the Tiller relationship relating α_{av} and ΔP could be reduced to a linear expression if the index of compressibility, $n1$, is equal to 2. Furthermore it was shown theoretically that the coefficient of compressibility increases with null stress porosity, thus partially explaining the increase in k_c with L_{dm} .

Crossflow filtration studies were conducted with a tubular carboxepharse membrane. In crossflow filtration experiments, cake formation, fouling and evolution of mean specific resistance of suspensions of *K. marxianus* was studied. Suspensions washed in saline and unwashed suspensions of *K. marxianus* grown in different media and of various mean morphologies, were used to analyse cake formation and fouling. It was shown that fouling is significant during crossflow filtration whilst it is negligible during dead-end filtration. Varying the cell morphology influenced the filtration behaviour more than using different growth media for both washed and unwashed cell suspensions.

Spent media separated from the cells by dead-end filtration was used to study the effect of media components on fouling. The filtration flux of spent medium was found to be independent of the growth conditions and only slightly influenced by the culturing media. For unwashed suspensions there appeared to be considerable rejection of macrosolutes during crossflow filtration that resulted in fluxes an order of magnitude lower than for washed suspensions. By switching the feed to saline solution during the pseudo steady state period it was shown that the cell cake remains largely intact and thus is not significantly influenced by shear.

A novel technique to determine cake mass during crossflow filtration was developed. The cake mass was determined by conducting dry weight analysis on samples withdrawn from the feed reservoir during filtration and subsequently doing a mass balance on the system. For the washed cell suspensions, it was shown that with increasing L_{dm} , the mass of cake formed decreased from approximately 6g to 2g. Furthermore preferential deposition of small cells does not appear to occur with washed yeast-like suspensions as indicated by the cake formation rate and image analysis data. However, preferential deposition of smaller cells was found to occur with unwashed yeast suspensions and possibly occurred with both washed and unwashed mycelial suspensions. Recovery of filter cakes comprised of yeast cells was significantly higher than with mycelial filter cakes, indicating possible differences in cake structure and cell membrane interactions.

The specific resistance of washed cell suspensions increases throughout filtration and is higher than observed during dead-end filtration even if membrane fouling is considered. This indicated a degree of cake fouling by fines occurring during crossflow filtration. Also the specific resistances of the recovered crossflow filter cakes, measured by dead-end filtration, were significantly greater than those for the feed suspensions. The apparent specific resistances of mycelial filter cakes were greater than those determined for yeast morphologies. This is in contrast to dead-end filtration where the specific resistance was less for mycelial suspensions than for yeast suspensions.

The effect of varying the crossflow velocity with washed yeast-like suspensions was studied. It was shown that the cake mass decreased and filtrate flux increased with increasing crossflow velocity. Furthermore it was shown the specific resistance decreases with crossflow velocity. It was shown that this was probably attributable to the pressure drop across the filter cake decreasing due to decreasing cake mass, and hence less cake compression. There was also evidence of fouling decreasing with increasing crossflow velocity.

ACKNOWLEDGEMENTS

Thanks to Greg Foley, who through faith, guidance and superior knowledge of the intricacies of the English language helped mould experimental findings into this thesis. Greg you played the role of Devil's advocate amicably. Thanks to Pdraig for being there.

Much thanks to Donal O'Shea, my fellow internee during those badger infested days and nights of the Hampstead. Without your guidance in fundamental lab techniques, I would still be filtering contaminated cultures. Those coffee breaks were often a fruitful forum for discussing biochemical engineering and more often than not lead, to exhausted intellects seeking solace in a pint or dozen of bad Guinness or cheap promotion beer.

Thanks also to the girls, Una Cusack, Miriam O'Shea and Audrey McNulty who were amicable drinking partners and annoying lab adversaries (the latter two), and who all brought vastly different characters into our little microcosm. Thanks to those who came afterwards Sara and Therese who if nothing else, helped me realise it was time to leave.

Many thanks to my fourth years throughout the years (mine and those I temporarily adopted). Ye always brought a bit of more character and humour to the lab. Basically the rest of us were sick of the sight of each other. Special thanks to Niamh T. Murray, Pat Gilboy and Zita Woods who did some outstanding work and contributed in a very real way to the findings in this thesis.

Special thanks to John Quinn a fellow house-mate and drinking partner from undergraduate days. Your unique view point of everything taught me a lot, especially about human nature, may it take you far.

Thanks to all the other post-grads throughout all those years who are/were friends/drinking buddies or perplexed acquaintances of mine. Special thanks to the women, for being women.

Thanks to my family for their encouragement and support and providing a safe haven from the boredom of DCU.

Thanks to all at DPS who helped show me that the 'Real World' is just as bitchy and personality driven as that little island, the DCU Biology department. I can't believe as I write this I have been working for a year *and a half* + a bit more.

This thesis is dedicated to the memory of my father, whose strength of character I model my own on and to David Gantley a great friend.

NOMENCLATURE

Symbol	Meaning	Units
A	Active filtration area	m^2
a	Constant in power law expression for dead-end filtration, equation 2.9	-
A_p	Projected cell area	m^2
b	Compressibility factor	Pa^{-1}
c	Wet weight cell concentration	kg/m^3
c_{app}	Apparent cell concentration	kg/m^3
c_{dex1}	Concentration of stock dextran solution	kg/m^3
c_{dex2}	Concentration of dextran after centrifugation	kg/m^3
c_{dw}	Dry weight cell concentration	kg/m^3
c_o	Cell concentration, equations 7.3-7.7	kg/m^3
c_s	Concentration of saline	kg/m^3
c_t	Cell concentration at time, t	kg/m^3
c_l	Cell concentration, equations 7.4-7.7	kg/m^3
d	Particle diameter	m
D_i	Equivalent cylindrical diameter of i^{th} cell in image analysis sample	m
D_rW	Wet weight to dry weight ratio	-
I	Mass of interstitial water in centrifugation pellet	kg

Symbol	Meaning	Units
J	Filtrate flux	$\text{m}^3/\text{m}^2/\text{s}$ (m/s)
J_0	Initial flux	m/s
$J_{2\text{hrs}}$	Filtrate flux after two hours crossflow microfiltration	m/s
K_1	Cross sectional factor, equation 2.7	-
K_{f1}	Fouling coefficient in crossflow filtration	m^{-4}
K_{f2}	Fouling coefficient in crossflow filtration	m^{-4}
k_c	Coefficient of compressibility	Pa^{-1}
k_0	Kozeny's constant	-
k'	Kozeny's constant, equation 6.16	-
k''	Kozeny's constant, equation 6.13	-
L	Cell length	m
L_b	Depth of bed or filter cake	m
L_{dm}	Mean aspect ratio	-
L_E	Average length of the streamlines in packed bed	m
L_i	Length of i^{th} cell in image analysis sample	m
M	Mass of deposited cake per unit membrane area	kg/m^2
M_d	Mass of dry matter in crossflow microfiltration samples	kg
M_t	Cake mass, equation 7.3 and 7.5	kg
M_1	Cake mass at the end of the initial batch crossflow filtration period, equation 7.5	kg
m	Power law constant equation 2.16	-

Symbol	Meaning	Units
N	Number of cells in image analysis sample	-
n	Index of compressibility, equation 2.9	-
n_1	Index of compressibility equation 2.12, 6.2	-
P_{feed}	Feed suspension pressure in crossflow filtration	Pa
P_{fil}	Filtrate pressure in crossflow filtration	Pa
P_L	Local hydraulic pressure	Pa
P_1	Pressure at membrane cake interface	Pa
P_m	Pellet mass	kg
P_{ret}	Retentate pressure in crossflow filtration	Pa
P_s	Local compressive pressure	Pa
P_x	Scaling factor in equations 2.11, 2.12 and 6.2	Pa
R_c	Cake resistance	m^{-1}
R_{irev}	Irreversible fouling resistance	m^{-1}
R_m	Membrane resistance	m^{-1}
R_{mo}	Initial clean membrane resistance	m^{-1}
R_{rev}	Reversible fouling resistance	m^{-1}
R_T	Total resistance	m^{-1}
S	Slope of plots of R_T versus V_f	m^{-4}
S_v	Mean specific particle surface area	m^{-1}
S_i	Surface area of i^{th} cell in sample	m^2
T	Tortuosity	-
t	Filtration time	s

Symbol	Meaning	Units
u	Crossflow velocity	m/s
u_0	Superficial velocity through packed bed	m/s
$V_{2\text{hrs}}$	Filtrate volume after 2 hours of crossflow filtration	m^3
V_{dex}	Volume of dextran added to centrifugation tube	m^3
V_f	Filtrate volume	m^3
V_i	Volume of i^{th} cell in sample	m^3
V_s	Volume of suspension filtered	m^3
V_{si}	Volume of sample taken for crossflow microfiltration cake mass determination	m^3
V_t	Volume of centrifuge tube	m^3
V_1	Filtrate volume collected in batch mode, equation 7.6 and equation 7.7	m^3
W	Cell width	m
w_1	Weight of full centrifuge tube	kg
w_2	Weight of cells in centrifuge tube	kg
w_m	Mass fraction of interstitial water in centrifugation pellets	-
z	Position within filter-cake	m
ΔP	Applied pressure	Pa
ΔP_c	Pressure drop across filter cake	Pa
ΔP_{tm}	Trans-membrane pressure drop	Pa
ΔP_{tmc}	Critical trans-membrane pressure drop	Pa
α	Local specific cake resistance	m/kg
α_{app}	Apparent specific cake resistance crossflow microfiltration	m/kg

Symbol	Meaning	Units
α_{av}	Mean specific resistance measured in dead-end filtration	m/kg
α_{avc}	Mean specific resistance of recovered crossflow filter cake measured in dead-end filtration	m/kg
α_0	Unstressed specific cake resistance	m/kg
$\alpha_{0/eq6.3}$	α_0 as predicted by equation 6.3	m/kg
$\alpha_{0/model}$	α_0 as predicted by model	m/kg
α_{true}	True specific cake resistance in crossflow microfiltration	m/kg
β	Index of compressibility, equation 2.11	-
ϵ	Voidage, local voidage	-
ϵ_{av}	Average voidage	-
ϵ_{avl}	Average voidage predicted by Kozeny-Carman equation	-
ϵ_l	Voidage at membrane-cake interface	-
ϵ_0	Unstressed cake voidage	-
μ	Viscosity of filtrate	Pa s
ρ_c	Cell density	kg/m ³
ρ_p	Particle density	kg/m ³
ρ_w	Density of water	kg/m ³
τ_w	Shear stress	Pa

LIST OF FIGURES

- Figure 1.1** Schematic of dead-end and crossflow filtration
- Figure 1.2** Modes of operation in crossflow filtration
- Figure 2.1** Schematic of cake formation in filtration
- Figure 2.2** Typical flux decline in filtration
- Figure 2.3** Schematic diagram of filter cake
- Figure 3.1** Fermenter configuration for chemostat operation
- Figure 3.2** Dead-end filtration set-up
- Figure 3.3** Morphological classes of *K. marxianus*
- Figure 3.4** Schematic of crossflow filtration set-up
- Figure 4.1** Examples of three broths of *K. marxianus* and the corresponding L_{dm} value
- Figure 4.2** Relation between S_v and L_{dm} for all broths filtered
- Figure 4.3** $\text{Log}(\alpha_{av})$ versus $\text{Log}(\Delta P)$ for three different morphologies
- Figure 4.4** α_{av} versus ΔP plotted on a linear scale
- Figure 4.5** $\alpha_o \rho_c / S_v^2$ versus L_{dm} for all broths filtered
- Figure 4.6** Voidage of cell pellets formed at 3500 rpm as a function of L_{dm}
- Figure 4.7** Variation in pellet voidage with centrifugation speed
- Figure 4.8** The effect of time delay in decanting the supernatant on pellet voidage
- Figure 4.9** Water drop test results
- Figure 4.10** Relationship between unstressed voidage, ϵ_o , and L_{dm}
- Figure 4.11** $\alpha_o \rho_c / S_v^2$ versus L_{dm} for all broths filtered
- Figure 4.12** Relationship between the Kozeny constant and L_{dm}
- Figure 4.13** Compressibility coefficient, k_c , versus L_{dm}
- Figure 4.14** Example of 'hinge compression' of a mycelial cell

- Figure 4.15** Example of deformation at a branch point of a branched mycelium
- Figure 5.1** Specific cake resistance *versus* applied pressure for yeast like and mycelial broths of *K. marxianus*
- Figure 5.2** Specific cake resistance *versus* applied pressure for unwashed resuspended yeast and washed resuspended yeast
- Figure 5.3** Specific cake resistance *versus* applied pressure for cultured bakers yeast
- Figure 5.4** Specific resistance *versus* applied pressure for calcium carbonate
- Figure 5.5** α_0/S_v^2 *versus* L_{dm} for all yeast suspensions
- Figure 5.6** k_c *versus* L_{dm} for all yeast suspensions
- Figure 6.1** Relationship between α_{av} and ΔP , Verhoff and Furnaic model, constant k_0
- Figure 6.2** Relationship between α_{av} and ΔP , Verhoff and Furnaic model, variable k_0 .
- Figure 6.3** Relationship between α_{av} and ΔP , Zydney and Colton model, constant k_0 .
- Figure 6.4** Relationship between α_{av} and ΔP , Zydney and Colton model, variable k_0 .
- Figure 6.5** Relationship between α_{av} and ΔP , Verhoff and Furnaic model, k_0 varies according to equation 6.9.
- Figure 6.6** Relationship between α_{av} and ΔP , Zydney and Colton model, k_0 varies according to equation 6.9.
- Figure 6.7** Plots of ϵ_0 *versus* k_c/b
- Figure 6.8** Relationship between ϵ_{av} and ΔP
- Figure 6.9** Relationship between ϵ and fractional position from cake membrane interface
- Figure 6.10** The effect of using the Kozeny-Carman equation to predict ϵ_{av1}
- Figure 6.11** k'/k_0 *versus* ΔP for various values of b

- Figure 7.1** Filtration flux as a function of filtration time for a predominantly yeast-like morphology of *K. marxianus* grown in whey medium
- Figure 7.2** Filtration behaviour of *K. marxianus* grown in YEP_NL medium
- Figure 7.3** Dead-end filtration behaviour of *K. marxianus* grown in various media
- Figure 7.4** Total resistance as a function of filtrate volume for *K. marxianus* grown in YEP_NL medium
- Figure 7.5** Filtration behaviour of spent and original media
- Figure 7.6** Comparison between dead-end filtration and crossflow filtration of fresh YEP_NL medium
- Figure 7.7** Filtrate flux and cake formation for a washed suspension of *K. marxianus*
- Figure 7.8** Cake formation during cross flow filtration of washed suspensions of *K. marxianus*
- Figure 7.9** The effect of switching the feed suspension from cell suspensions to saline for YEP_NL medium
- Figure 7.10** YEP_NL medium 500 rpm batch culture
- Figure 7.11** Effect of cell morphology on filtration behaviour of *K. marxianus*
- Figure 7.12** The effect of growth medium on the filtration flux of washed cell suspensions
- Figure 7.13** Cake mass as function of filtrate volume
- Figure 7.14** Relationship between filtrate flux and S_v
- Figure 7.15** Evolution of the apparent specific resistance in crossflow microfiltration and comparison with dead-end filtration resistances
- Figure 7.16** R_T as a function of filtrate volume
- Figure 7.17** The specific resistance as a function of filtrate volume for batch (800 rpm) suspensions

- Figure 7.18** The specific resistance as a function of filtration time for 500 rpm batch cultures
- Figure 7.19** Apparent specific resistance as a function of filtration time for mycelial suspensions
- Figure 7.20** The effect of crossflow velocity on the pseudo steady state cake mass and filtration flux
- Figure 7.21** The effect of crossflow velocity on the *true* specific resistance determined after two hours of filtration
- Figure 7.22** Effect of morphology on the filtration flux for unwashed suspensions
- Figure 7.23** Effect of media on filtration flux of unwashed suspensions
- Figure 7.24** Specific resistance measured during dead-end filtration *versus* applied pressure for YEP_{NL} media in 800 rpm batch culture.
- Figure 7.25** Saline filtration for unwashed suspensions grown in YEP_{NL} medium

LIST OF TABLES

Table 3.1	YEPD medium formulation
Table 3.2	Life Sciences fermenter configuration
Table 3.3	Calculation of surface area and volume for cells of different morphology
Table 3.4	Description of crossflow filtration set-up
Table 3.5	Fouling behaviour of water from different sources
Table 3.6	Saline filtration and crossflow filtration filter cake recovery
Table 4.1	Distribution of cell morphologies by percentage volume
Table 6.1	Model predictions for various null stress voidages and values of b
Table 6.2	The effect of applied pressure on average cake voidage for highly compressible filter cakes
Table 7.1	Two hour fluxes and fouling behaviour for spent and fresh media
Table 7.2	Two hour fluxes, fouling behaviour and cake recovery for washed cell suspensions
Table 7.3	Image analysis data for washed cell suspensions and recovered crossflow filter cakes
Table 7.4	Fouling coefficient for the 800 rpm batch cultures
Table 7.5	Effect of crossflow velocity on filtration flux and resistances for washed suspensions
Table 7.6	Two hour fluxes and fouling behaviour for unwashed suspensions
Table 7.7	Cake masses after 2 hours for unwashed cell suspensions
Table 7.8	Morphology data for feed suspensions and recovered cakes for unwashed cell suspensions

CHAPTER 1

OVERVIEW OF MEMBRANE FILTRATION PROCESSES

1.1 Introduction

Filtration is an important separation technique and is often used in downstream processing of chemicals and biochemicals. There is a broad range of filtration techniques, such as depth filtration, dead-end and crossflow filtration. The filtration technique utilised will depend on the application. Filtration can be used for a variety of applications such as removing particulates from gases, purifying water supplies, removing contaminants from waste streams, clarification of product, product concentration and/or product washing.

This thesis will focus on the membrane-based filtration techniques of dead-end and crossflow microfiltration of suspensions of microorganisms. In this chapter, a brief outline of the principles of operation and applications of dead-end and crossflow filtration is given. An in-depth review of dead-end and crossflow microfiltration experimental work and theory is given in Chapter 2.

1.2 Classification of membrane filtration techniques

Membrane separations are primarily based on particle size and are achieved using a porous material commonly referred to as a membrane or filter. In theory, all components in a suspension that are smaller than the pore size of the membrane will pass through the membrane and particles larger than the pores will be retained on the upstream side of the membrane. The filtration techniques are classified by the direction of the flow of the feed suspension that is being processed. The dead-end filtration technique involves the suspension flowing perpendicular to the membrane surface as shown in Figure 1.1 (A). In crossflow filtration, the feed suspension flows tangential to the membrane surface as shown in Figure 1.1 (B).

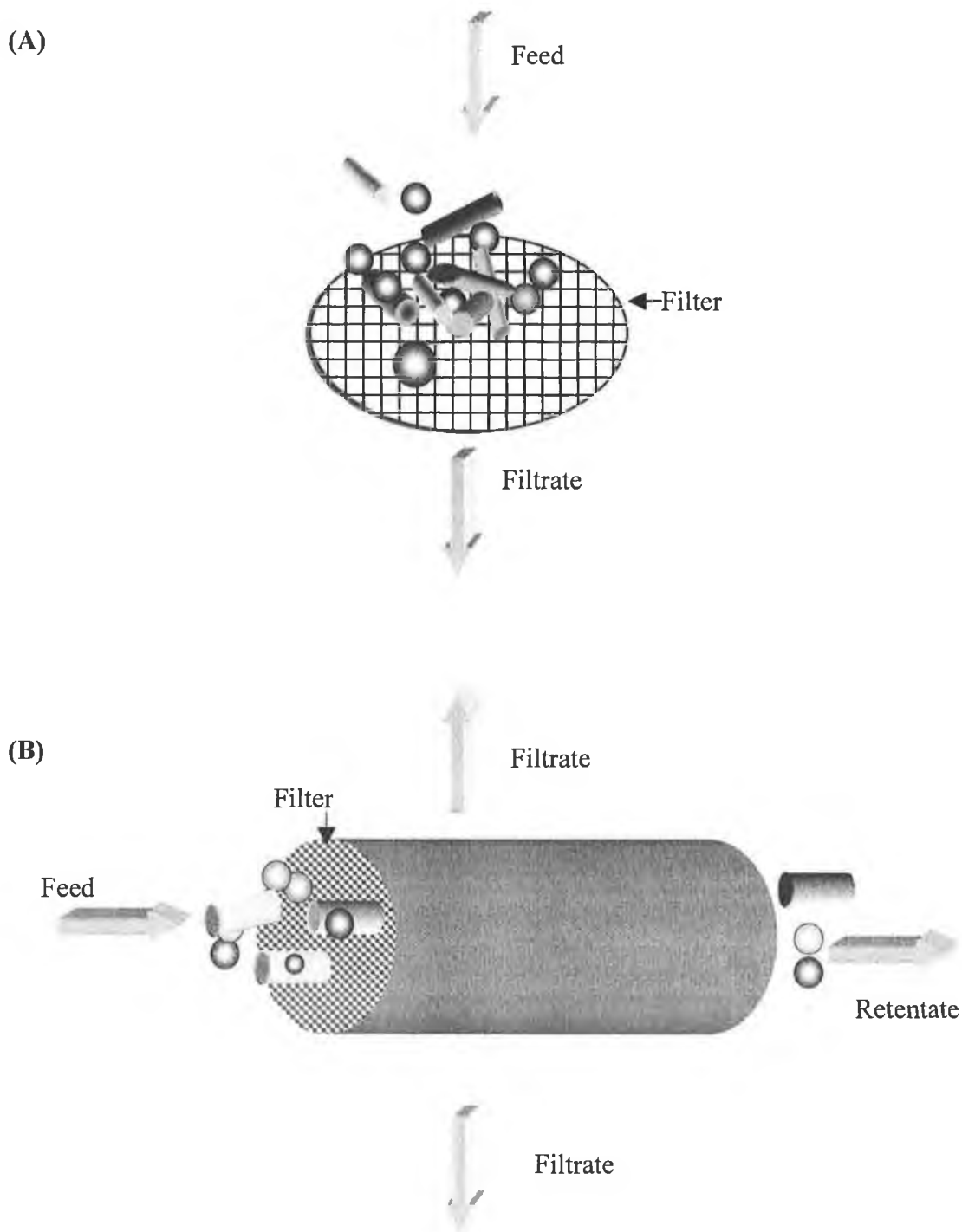


Figure 1.1 Schematic of (A) dead-end and (B) crossflow filtration.

Membrane filtration techniques can be further classified according to the size of separation. Reverse osmosis membranes are impermeable to solutes of molecular dimensions. A typical application of this technique is the desalination of water. Ultrafiltration (UF) membranes are impermeable to macromolecules such as

proteins, polypeptides and polysaccharides. This type of membrane is used in product recovery where the product is a macrosolute such as a protein or polysaccharide. Alternatively it can be used in media clarification. Microfiltration membranes are impermeable to particulate matter of approximately a tenth of a micron or greater. These are used for filtration of microbial broths or suspensions of inorganic aggregates.

1.3 Filtration techniques

Filtration involves the separation of particles from a gas or liquid suspension. The mode of operation chosen is based on the nature of the feed solution. Dead-end filtration systems are usually of a simpler configuration than crossflow filtration and generally require less capital outlay and have smaller maintenance requirements. It is the preferred method when the particle load in the feed suspension is low, e.g. purification of gases or clarification of fermentation media. Crossflow filtration operation is preferred when dead-end filtration performance is poor, due to the high resistance to filtrate flow by rejected material.

1.3.1 Modes of operation

Dead-end filtration is primarily configured in a one step arrangement, the purpose being to separate particles from a feed suspension. The feed suspension is separated into two distinct phases: (i) particle free filtrate and (ii) the rejected particles, known as the filter cake. After the particles have been removed from the suspension, the particle cake can be washed with water or buffer. The particle cake can also be dried by hot air or it can be subjected to a further pressure to remove interstitial liquid, a technique referred to as *expression*.

Crossflow filtration can be operated in batch or continuous modes (Figure 1.2, A & B). Biological applications are typically conducted in batch mode for cell harvesting, macrosolute recovery or cell concentration prior to cell disruption. This can be followed by a diafiltration (washing) step (Figure 1.2 C).

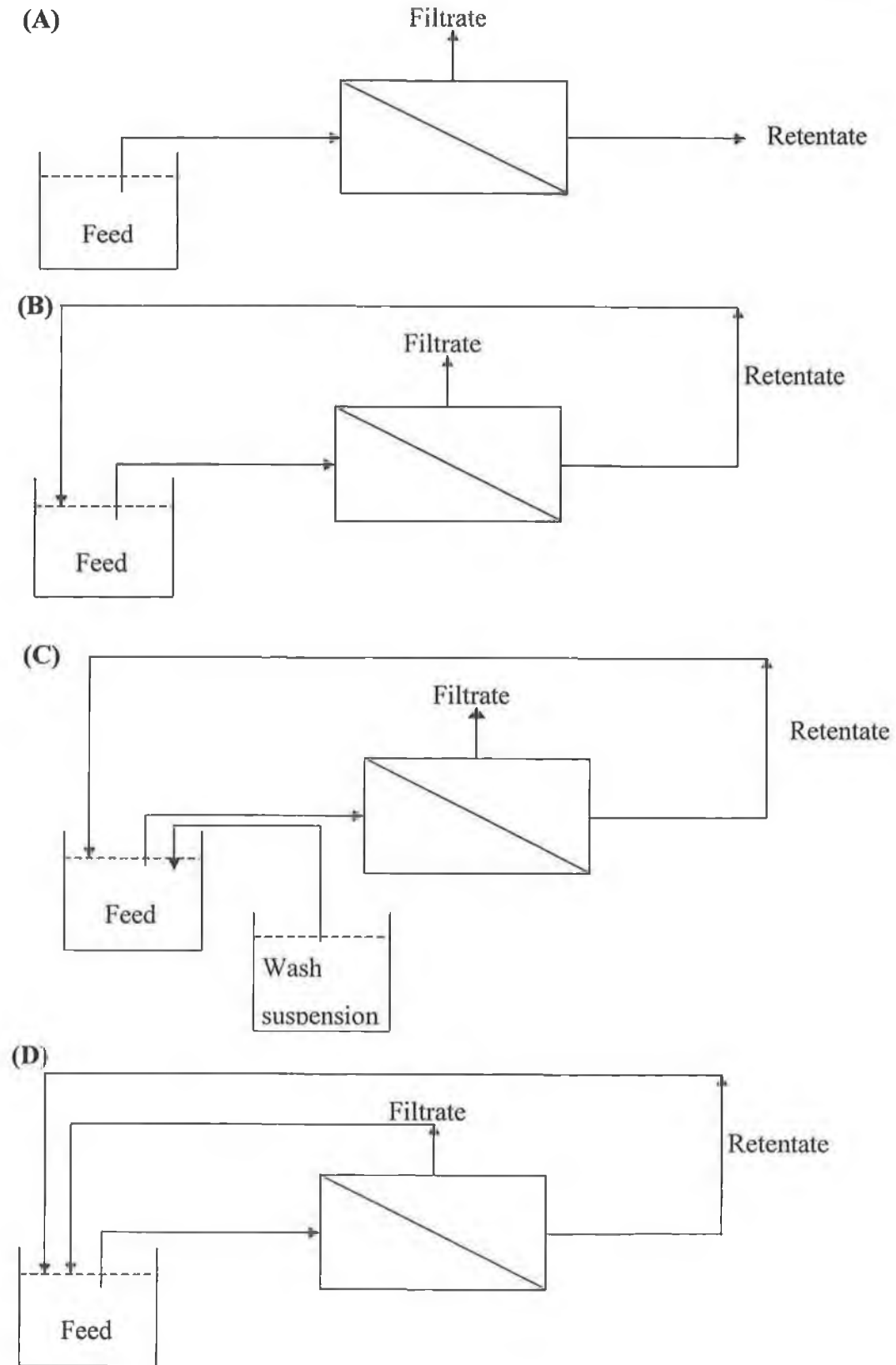


Figure 1.2 Modes of operation in crossflow filtration, (A) continuous, (B) batch, (C) diafiltration and (D) total recycle mode.

This is used to remove impurities from cell suspensions or to maximise product recovery when the product is in the filtrate. Experimental studies are normally conducted in total recycle mode (Figure 1.2 D). This approximates continuous mode if the reservoir volume is sufficiently large. This allows the feed concentration to remain relatively constant and simplifies interpretation of experimental data, compared with batch filtration where the particle concentration in the system increases with time.

1.3.2 Modules and system configurations

Membranes are available in a variety of housings or modules. The most common dead-end filtration module is the plate and frame filter. This consists of layers of filters, which are separated by plates and frames to maximise the filtration area in as small a volume as possible. Rotary drum vacuum filters and stirred cell filters are similar to dead-end filters except the mass of deposited particles can be controlled by a blade (rotary vacuum filter) or stirrer (stirred cell). In laboratory research, dead-end filtration experiments are normally carried out in a filter holder, which consists of a filter supported by a porous plate.

In crossflow filtration, a variety of module configurations can be used which are dependent on the membrane geometry, the most common geometries being stacked-sheet, hollow fibre and tubular. Hollow fibre and tubular modules have a shell and tube configuration. However, hollow fibre modules usually consist of a greater number of tubes with a smaller diameter than the tubes used in tubular modules. Stacked-sheet modules are available in flat-sheet or spirally-wound configurations. Fluid flow in stacked-sheet and hollow fibre modules is generally laminar, which is important when filtering shear-sensitive cells. With tubular modules, the flow is usually turbulent which can result in improved filtrate performance.

More complex configurations are used to improve filtration performance. Inserts such as baffles can be placed in the filtration modules to generate turbulence. Membranes may be pleated or curved (e.g., Moulin *et al.*, 1996). The direction of tangential flow can be reversed periodically (e.g., Howell *et al.*, 1993) or the direction of filtrate flow can be reversed (e.g., Tanaka *et al.*, 1995).

1.4 Membranes

Membranes are classified according to their pore size and membrane structure. Microfiltration membranes generally have a pore size range in the range of 0.1-1.0 μm . The structure of the membrane varies depending on the material of which it is made and the method of production. The most common membrane materials are (i) polymer based such as cellulose, polysulphone, polycarbonate, polyvinylidene fluoride (PVDF) and (ii) ceramic membranes such as alumina or zirconia.

Membranes can be symmetric or asymmetric. An asymmetric membrane consists of a thick porous layer that is covered with a thin layer of low porosity. Microfiltration membranes are generally symmetric in nature (Bowen, 1993), whereas UF membranes are asymmetric.

The membrane type can have a considerable impact on filtration performance because the membrane plays a crucial role in determining the rejection of particles from the feed, particularly at the start of filtration operations. However, the deposited cake layer often dominates filtration behaviour and the membrane type may be of little significance. For example, it has been shown using PVDF membranes in crossflow microfiltration of baker's yeast that the decrease in filtration performance throughout the filtration run was solely due to cake formation (Tanaka *et al.*, 1993).

1.5 Applications of microfiltration

There are many applications of microfiltration and it is normally used when other separation techniques such as centrifugation or sedimentation are unfeasible. This can occur when the particles to be separated are small in size or the density difference between particle and fluid phases are small. In some applications, sterile separation is imperative and this can be achieved with most microfiltration configurations.

The feed can be organic or inorganic in nature. A large variety of biological suspensions can be processed using microfiltration. Predominantly, it is suspensions of microorganisms that are filtered. The product can be the microorganisms themselves, as in cell harvesting of yeast (Bell and Davies, 1987), bacteria (Mourot *et al.*, 1989) and mycelial suspensions (Sims and Cheryan, 1986). The product may also be extracellular such as enzymes (Kroner *et al.*, 1984), polysaccharides (Gehlert *et al.*, 1998) and beer (Le, 1987). The product may also be intracellular, which requires cell disruption prior to the removal of cell debris. Another application is the removal of heavy metals by bioaccumulation using yeast cells entrapped in a crossflow microfiltration system (Brady *et al.*, 1994). A further application is the treatment of wastewater (e.g., Le and Biligheimer, 1985).

Microfiltration is also used in animal cell culture separations. However, appropriate modules, which generate low shear, must be used to avoid loss in viability of these shear sensitive cells (Maiorella *et al.*, 1991). Microfiltration is also used in the field of plasmapheresis where red blood cells are removed from blood to produce plasma (Zydney, 1985).

Membrane fermenters are growing in popularity. These predominantly consist of fermenters attached to external crossflow microfiltration modules (e.g., Li *et al.*, 1996). The fermentation broth is pumped through the microfiltration module and the retentate is returned to the fermenter. Fresh medium is added as filtrate is removed from the system. This configuration allows simultaneous product formation and recovery. It also has many benefits over conventional batch fermentation. These include higher biomass yields and the removal of growth and

product formation inhibitors (Li *et al.*, 1996). It also is possible to have the membrane within the fermenter itself. Examples of the use of membrane fermenters include the processing of methanogenic waste by anaerobic fermentation (Elmaleh and Abdelmoumni, 1997) and the extraction of lactic acid across a hollow fibre membrane (Tong *et al.*, 1998).

1.6 Conclusions

Dead-end and crossflow microfiltration are under researched techniques in the processing of microbial suspensions. In particular, dead-end microfiltration of microbial suspensions has received little attention, in spite of wide scale use in industry. As a consequence, a detailed understanding of this technique is not yet available. The newer unit operation of crossflow microfiltration has been the focus of much research in the last two decades. However there is a considerable amount of research to be carried out before a comprehensive understanding of the factors that influence microfiltration performance is achieved.

This thesis is concerned with the fundamental mechanisms governing filtration performance in the microfiltration of microbial suspensions. In particular the role of cell morphology on microfiltration behaviour will be studied. In Chapter 2, recent research into dead-end and crossflow microfiltration will be reviewed.

CHAPTER 2

DEAD-END AND CROSSFLOW MICROFILTRATION OF MICROBIAL SUSPENSIONS

2.1 Introduction

Microfiltration is a widely used separation process that has many different configurations and applications. There has been a considerable amount of research into many different areas of microfiltration. Consequently, it can be considered to be quite a mature technology. Despite this, there are areas in this field which are either relatively new developments and hence require further research, or have received scant attention in the literature. The latter can be considered to be true for dead-end microfiltration of suspensions of microorganisms, while the former can be considered true for crossflow microfiltration of suspensions of microorganisms.

The objective of this chapter is to critically review current opinion in microfiltration. The fundamental principles of dead-end and crossflow filtration will be outlined. Primary focus will be placed on microfiltration of microorganisms. Particular emphasis will be placed on filter cake properties and the role of particle morphology in microfiltration behaviour.

2.1.1 Fundamental concepts in filtration

Filtration involves the separation of particles from a particle/fluid mixture and the separation is primarily achieved due to differences in particle size. During filtration, particles that are larger than the pore size of the membrane deposit to form a filter cake on the upstream side of the membrane. However, interaction between macromolecules or fines with the deposited filter cake or membrane can result in particles smaller than the membrane pores being rejected.

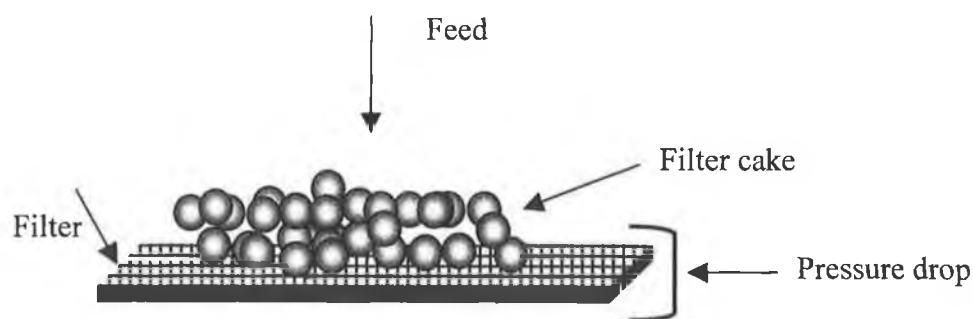


Figure 2.1 Schematic of cake formation in filtration.

The driving force for filtration is a pressure difference across the filter and its associated filter cake which forces fluid through the filter cake and filter, as shown in Figure 2.1. The pressure gradient can be achieved either by applying a pressure in a sealed environment by a compressed gas, piston or pump, or it can be achieved by applying a vacuum to the filtrate side of the membrane.

During filtration, suspended particles in the suspension are rejected at the membrane to form a filter cake. In dead-end filtration, the mass of the filter cake grows until all the cells or particles are deposited or until the capacity of the filter has been reached, in which case further filtration is not possible. However, during crossflow filtration, particles stop depositing due to tangential forces generated by the crossflow. The filtration rate decreases with filtration time, as shown in Figure 2.2. This is due to the formation of the filter cake or fouling of the cake layer and membrane by macromolecules in the suspension. Filtration performance is usually expressed in terms of the filtrate flux, J . The filtrate flux is defined as the volume of filtrate that passes through a unit area of the membrane in a unit time. In crossflow filtration, the filtrate flux can, in theory, attain a constant value when cake formation ceases. However, in practice, this is rarely obtained.

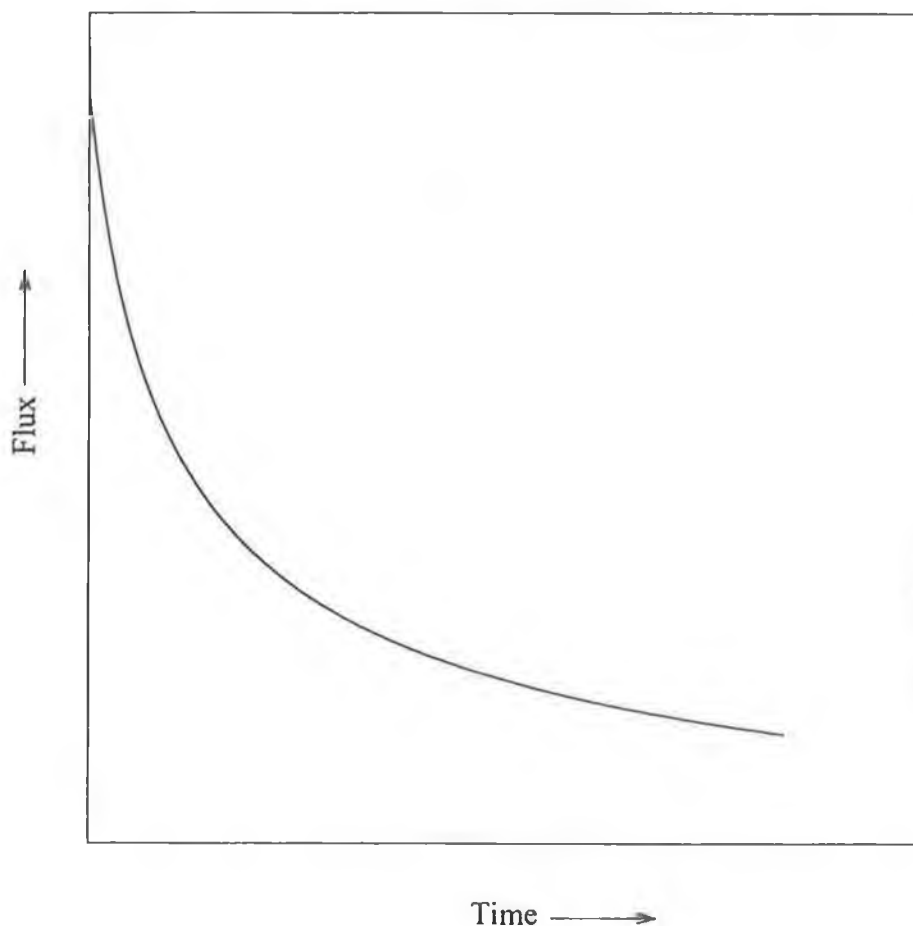


Figure 2.2 Typical flux decline in filtration.

2.1.2 Factors that influence filtrate flux in filtration

This section outlines the factors that cause the filtrate flux to decline and thus ultimately affect the filtration performance. As filtration progresses, the filtrate flowrate declines and this is attributable to the build up of the cake layer on the membrane surface or fouling of the membrane or cake layer. It is the properties of the cake layer and the nature of the fluid, membrane and particle interactions that ultimately determine the rate of fluid flow through the cake layer and membrane.

Usually it is the formation of the cake layer that is the dominant cause of the steep decline in the filtrate flux. Other phenomena, such as membrane fouling by macrosolutes, pore plugging by particles and filter cake clogging by macrosolutes or fines, can also contribute to the flux decline. These phenomena are collectively described by the generic term, fouling. In the literature any drop in filtration performance, is often described as 'fouling'. Here the term shall be restricted to any decrease in filtration performance other than that attributable to cake formation.

As described previously, the filtrate flux declines throughout filtration. In filtration theory, the filtrate flux, J , is expressed by the Darcy equation, equation 2.1, which describes fluid flow through a packed bed,

$$J = \frac{\Delta P}{\mu R_T} \quad [2.1]$$

where ΔP is the applied pressure, μ is the viscosity of the filtrate and R_T is the total resistance to fluid flow.

Filtration relationships based on the Darcy equation are used to describe filtration behaviour (Hermia, 1982). These relationships are as follows: (i) the complete blocking model which assumes each particle that deposits on the membrane will seal a membrane pore, (ii) the intermediate blocking filtration model which assumes only a portion of the deposited particles seal a pore, (iii) the standard blocking model, which assumes the pore volume will decrease proportionally to filtrate volume by deposition of solids on the pore walls and (iv) the cake filtration model which assumes the cake resistance is proportional to the filtrate volume.

When the formation of a particle cake is the sole reason for flux decline, the filtrate flux is a function of the mass of deposited solids and the properties of the filter cake. Filtration can then be described by the two resistances model,

$$J = \frac{dV_f}{A dt} = \frac{\Delta P}{\mu [R_m + R_c]} \quad [2.2]$$

where V_f is the filtrate volume, t is the filtration time, A is the active filtration area, R_m is the membrane resistance and R_c is the cake resistance.

The cake resistance R_c is expressed by,

$$R_c = \alpha_{av} M \quad [2.3]$$

where α_{av} is the mean specific resistance and M is the mass of filter cake deposited per unit membrane area. The principal difference between dead-end and crossflow filtration is that the thickness of the filter cake can be limited in crossflow filtration. Therefore, in theory, filtration performance should be superior to that in dead-end filtration. However, the properties of the cake layer can be substantially different in crossflow filtration. In particular, α_{av} can be greater than in dead-end filtration (Foley, 1994).

In dead-end filtration, the filter cake mass will increase throughout microfiltration and is proportional to the filtrate volume when particle settling is negligible. Equation 2.2 can be integrated with respect to time to give,

$$\frac{t}{V_f} = \left[\frac{c\mu\alpha_{av}}{2A^2 \Delta P} \right] V_f + \frac{\mu R_m}{A \Delta P} \quad [2.4]$$

where c is the particle concentration in the feed suspension. The cell concentration is usually expressed as the cell mass per unit suspension volume and hence equation 2.4 neglects moisture retained in the filter cake. If the cell concentration is sufficiently large or the retained moisture content is large, the deposited cake mass, cV_f and hence the specific cake resistance, can be in error.

For constant pressure filtration, equation 2.4 predicts that plots of t/V_f versus V_f are linear when both α_{av} and R_m are constant. This is generally referred to as parabolic filtration behaviour. However, non-parabolic filtration behaviour is also possible, such as when membrane fouling by macrosolutes occurs or when cake clogging occurs due to fines in the suspension (Tiller *et al.*, 1981; Willis *et al.*, 1983). Also, filtration behaviour is non-parabolic when sedimentation is significant such that the mass of deposited cake is not proportional to the volume of filtrate (Takai *et al.*, 1987). Alternatively, non-parabolic behaviour can be caused by changes in the pressure drop across the cake during the initial stages of filtration (Willis *et al.*, 1983).

2.2 Dead-end filtration of microorganisms

When filtering microorganisms, the cake resistance is usually much larger than the membrane resistance such that the filter cake dominates the filtration performance. Therefore the properties of the cake layer, expressed as the mean specific resistance is of most interest. However, Sorensen *et al.* (1996), suggest that for highly compressible material where the filtrate flux becomes independent of pressure at low to moderate pressures, the specific filtrate flowrate (maximum attainable flux value) may be of more practical use.

The mean specific resistance of a filter cake is dependent on many factors such as particle shape and size, particle surface properties, fluid properties, membrane properties and filter cake compressibility. Filter cake compressibility is the phenomenon where the mean specific resistance increases with increasing applied pressure. These factors are discussed in detail in the following sections.

2.2.1 Flow through packed beds and filter cakes

A filter cake can be viewed as a packed bed and hence microfiltration is equivalent to flow through packed beds when membrane effects can be neglected. The packing arrangement of particles in a filter cake has a large influence on the mean specific resistance of the filter cake. The filter cake voidage, ϵ , is the volume

fraction of the filter cake which is available to fluid flow and therefore higher filter cake voidage should give higher filtrate flowrates. Other factors such as filter cake tortuosity and specific surface area of the particles also influence filtrate flowrates.

The specific resistance is often estimated from an empirical expression such as the Kozeny-Carman equation. The Kozeny-Carman equation describes the fluid flow through a packed bed (Carman, 1937), and can be written,

$$u_0 = \frac{\varepsilon^3}{k_0 S_v^2 (1-\varepsilon)^2} \frac{\Delta P}{\mu L_b} \quad [2.5]$$

where u_0 is the superficial velocity through the packed bed, k_0 is the Kozeny constant, ε is the void fraction of the packed bed, S_v is the specific particle surface area and L_b is the bed depth.

The Kozeny-Carman equation, which was developed for packed beds, is often applied to microfiltration studies (e.g., Nakanishi *et al.*, 1987). To relate the mean specific resistance with the filter cake properties, equation 2.5 can be arranged using equation 2.1 and equation 2.3 to give,

$$\alpha_{av} = \frac{k_0 [1-\varepsilon] S_v^2}{\varepsilon^3 \rho_p} \quad [2.6]$$

where ρ_p is the particle density.

The Kozeny constant is taken to be equal to 5 ± 0.5 , for a wide range of particle shapes (Grace, 1953) and this value is commonly used in the literature. However, as shall be discussed later, k_0 is dependant on other parameters and can vary outside this range. It can be seen from equation 2.6 that the specific resistance is extremely dependent on the filter cake voidage. A small reduction in the filter cake voidage brings about a large change in the specific resistance. The parameters on

the right hand side of the Kozeny-Carman equation, k_0 , ϵ and S_v are, to varying degrees, influenced by the morphology of the particles in the filter cake.

The applicability of the Kozeny-Carman equation to the microfiltration of microorganisms is the subject of some debate. Nakanishi *et al.* (1987), using a Kozeny constant of 5.0 and the theoretical dense-packed voidage for spheres (0.4), found that the Kozeny-Carman equation underestimated the specific resistance by as much as one to three orders of magnitude, depending on the microorganism filtered. This could be partly attributed to the voidage value used. Ogden and Davis (1990) found that for baker's yeast, using a theoretical voidage of 0.4, the Kozeny-Carman equation underestimated the specific resistance by a factor of five. However, using a voidage value of 0.27 obtained from work done elsewhere (Ofsthun, 1989), the predicted resistance was within a few percent of the measured resistance. Other researchers have used experimentally determined voidages and applied them to the Kozeny-Carman equation to determine Kozeny's constant (Oolman and Liu, 1991).

2.2.1.1 Influence of particle morphology and packing arrangement on voidage

The packing arrangements of cells in microbial filter cakes have rarely been investigated. However, there has been considerable research into the packing arrangements of fibres and hard spheres in packed beds formed under gravity. In those studies it has been shown that the shape of the particles and the packing arrangement of particles can substantially affect the bed voidage. Therefore the packing arrangement of particles or cells in a filter cake can be expected to have a large impact on the filter cake voidage and on α_{av} .

The voidage of a packed bed depends on both the packing arrangement and morphology of the particles that comprise the bed. There are two main packing arrangement groups for particles that form a packed bed: (i) ordered packing and (ii) random packing. Within both groups, different packing arrangements are possible even for monodisperse particles. Therefore, in theory it is possible that a

particle population can be arranged in many different ways to give packed beds of a wide range of voidages.

With ordered packing, the structure and local voidage of the bed is homogenous and the particles in the bed form lattice-like structures. The voidage of the bed will depend on the packing arrangement in the bed. For monodisperse rods, there are two packing arrangements, cubic and orthorhombic. The voidage attained in each arrangement is 0.215 and 0.093 respectively (Nakanishi *et al.*, 1987). For spheres the packing voidage can vary between 0.259 for pyramidal packing and 0.476 for cubic packing, with other packing arrangements giving voidages between these two limits.

With randomly packed beds, the structure of the bed is heterogeneous. The voidage can vary substantially within the bed and the local voidage is dependant on the local packing arrangement. Randomly packed beds can exist between two limiting states, random loose packed and random dense packing. Loose packed beds are formed when the particles are carefully poured into a container. Dense packed beds are formed when the loose packed beds are tapped until there is no further reduction in the bed height and hence voidage. When the voidage of a randomly packed bed is at a minimum, the packing is referred to as random dense packing. Loose random packing gives the maximum voidage for a system and is limited by gravitational stability. Intermediate states can also exist between these limits.

Beds of randomly packed spheres have voidages between 0.364 for dense random packing and 0.445 for loose random packing (Nolan and Kavanagh, 1992). For random packing of cylindrical particles, the voidage of the packed bed increases with increasing particle length to diameter ratio, for both loose and dense packing (Milewski, 1978; Zou and Yu, 1996a, 1996b). This is in contrast to ordered packing of cylindrical particles, where the bed voidage is only dependent on the packing arrangement and is independent of the length to diameter ratio. Furthermore, randomly packed beds of cylindrical particles can have voidages greater than beds of randomly packed spheres. This is also in contrast to ordered packing where the cylinders will always give lower voidages than spheres.

For random packed beds of non-spherical particles, it is generally accepted that the bed voidage increases as the sphericity of the particles that form the bed decreases (Zou and Yu, 1996a). (Sphericity is a measure of how spherical a particle is, where a sphericity of unity corresponds to spherical particles and decreasing sphericity reflects the particles being either more irregular or elongated in nature). Thus the particle morphology can have a substantial effect on packed bed voidage and subsequently can be expected to have a similar effect on microfiltration.

There have been some theoretical studies into simulating the packing structures of particles in constant pressure microfiltration (Hwang *et al.*, 1996; Lu and Hwang, 1993). Computer simulations by Hwang *et al.* (1996), showed that when the particle shape deviates from spherical, the cake voidage will increase, i.e. similar to increasing voidage with increasing length to width ratio in random packed beds of cylinders. The voidage values obtained in these simulations were in good agreement with voidage values in packed bed studies, when the particles are near spherical. However, there was less agreement with packed bed studies as the particle sphericity decreased. The simulated voidages were less than the voidages determined in packed bed studies. This was due to most of the particles in the simulated filter cake having the major axis aligned with the direction of fluid flow. Consequently, when particle alignment occurs, the voidage will decrease as the structure will tend to a more ordered packing arrangement. Elsewhere, theoretical studies by Kawakatsu *et al.* (1995) on the packing of spheres within filter cakes, found the predicted voidage of 0.37 to be in agreement with packed bed studies.

There is some evidence of ordered packing occurring in microfiltration. For example Zydney *et al.* (1989) showed blood cells packing in a hexagonal arrangement. Nakanishi *et al.* (1987) found, when filtering microorganisms of different morphologies, spherical morphologies gave lower specific cake resistances at all pressures than rod-shaped particles, a finding which could not be explained by particle size alone. The authors suggested that if the cells being filtered pack in an ordered state, spherical particles should form filter cakes of higher voidage than rod shaped particles, thus explaining the lower resistances of

cell suspensions of ellipsoidal cells. There is also some indirect evidence that this may occur. Fowler and Robertson (1991), showed, using scanning electron microscopy, that *Escherichia coli* cells predominantly orientated in the direction of fluid flow, when medium was passed through an immobilised cell aggregate.

However, there is also evidence of random packing in dead-end filter cakes of microorganisms. Cross-sectional images of filter cakes produced by scanning electron microscopy, show random packing of ellipsoidal *Corynebacterium glutamicum* and rod shaped *Bacillus subtilis* (Tanaka *et al.*, 1994a) and *E. coli* (Tanaka *et al.*, 1994b). Ju and Ho (1988) measured the voidage of cell pellets formed by centrifugation of cells with different shapes, namely elliptical *Saccharomyces cerevisiae*, rod-shaped *E. coli* and mycelial *Penicillium chrysogenum*. It was found that as the sphericity of the cells decrease, the voidage of the pellets formed increased, in agreement with random packing behaviour. However, the measured voidages were less than theoretically predicted voidages for random dense packing. This was attributed to compression of the cell pellets due to centrifugal forces. Another possible reason is that microbial suspensions usually have a distribution in cell size and it can be expected that they will pack more tightly than monodisperse suspensions.

Factors other than the packing arrangement may also affect microfiltration performance. It has been shown when filtering a well-mixed suspension of baker's yeast, that cakes formed under pressure give higher fluxes at the same applied pressure than cakes formed by gravity settling (Arora and Davis, 1994). This was attributed to microchannelling within the filter cakes.

2.2.1.2 Particle size and size distribution effects

Particle size strongly affects microfiltration resistances. According to the Kozeny-Carman equation, the specific resistance is proportional to the square of the specific surface area, S_v . For a spherical particle, S_v is equal to $6/d$ and for a cylindrical particle is equal to $4/d$, where d is the particle diameter. Therefore increasing particle size will cause a reduction in the resistance to filtrate flow. This can clearly be seen with work done with spherical latex particles (Nakanishi *et al.*, 1989; Ogden and Davis, 1990) and glass and silica particles (Chellam and Wiesner, 1998). Particle size can also affect packing arrangement with other inorganic suspensions. Tiller *et al.* (1987) have shown that the filter cake voidage decreases with increasing particle size. This was attributed to increased repulsion between particles due to increasing charge concentration with decreasing particle size. Shimizu *et al.* (1994) showed with baker's yeast, that the specific resistance increased when the particle size was reduced by cell breakage. It can be seen in the work with microbial suspensions of Nakanishi *et al.* (1987) that increasing S_v is accompanied by an increase in α_{av} for elliptical and rod-shaped cells.

Another important factor affecting packing voidages is the size distribution of particles in the packed bed. Broadening of the size distribution of particles in a packed bed causes a reduction in packed bed voidages (Nolan and Kavanagh, 1993; Sohn and Moreland, 1968; Wakeman, 1975). This can be attributed to smaller particles filling the voids between larger particles. The effect of particle size and size distribution on packing voidage has been comprehensively studied for powders. Decreasing size can result in increasing voidage due to the formation of agglomerates or aggregates (Tiller *et al.*, 1987). However, the formation of aggregates of unicellular microorganisms does not occur in most cases. The effect of particle size, size distribution and particle shape has been accounted for in packed bed studies using empirically relationships (Yu *et al.*, 1997; Zou and Yu, 1996b).

2.2.1.3 Factors affecting Kozeny's constant.

Kozeny's constant is normally reported in the literature as having a value of 5 ± 0.5 (Grace, 1953). However, it is known that it can vary outside this range for microbial suspensions (Oolman and Liu, 1991). The value of Kozeny's constant is dependant on the tortuosity of the filter cake. The relationship between tortuosity and Kozeny's constant (k_o) is given by (Mota *et al.*, 1998)

$$k_o = K_1 T^2 \quad [2.7]$$

The cross-sectional factor, K_1 , is dependent on the shape of the capillary cross section. It is equal to 2 for a circular capillary (Dolejs and Mikulasek, 1997). The tortuosity of the filter-bed, T , is defined as

$$T = \frac{L_E}{L_b} \quad [2.8]$$

where L_E is the average length of the streamlines and L_b is the thickness of the packed bed.

For a packed bed of spherical particles with the capillaries deviating at an average of 45° from the net direction of fluid flow, the value for T is $\sqrt{2}$ (Carman, 1937). The tortuosity of the packed bed decreases with increasing bed voidage and approaches unity as the voidage of the bed approaches unity (Mauret and Renaud, 1997; Puncochar and Drahos, 1993). Therefore, k_o would be expected to decrease with increasing voidage. However, k_o is known to increase with increasing voidage (e.g. Mauret and Renaud, 1997). The authors in that case attributed this to the flow in the bed being non-capillary like. It can be seen in the microfiltration data of Oolman and Liu (1991) and Liu and Yu (1993) that increasing filter cake voidage coincides with an increase in the calculated Kozeny constant.

Recent theoretical and experimental study has shown that broadening the size distribution of the particles in the feed suspension can cause the mean specific

resistance to increase (Free *et al.*, 1998). The measured voidage and mean particle size remained constant for each feed suspension tested. It was shown theoretically that the increase in the specific resistance could be attributed to the pore size distribution in the filter cake increasing. The Kozeny constant was found to increase with increases in the pore size distribution, as all the other parameters in the Kozeny-Carman equation were constant for each suspension filtered.

2.2.2 Membrane effects

Membrane fouling is a generic term used to describe any phenomenon that causes the membrane resistance to increase during microfiltration. It is usually caused by macromolecules which are absorbed or are deposited within the membrane pores or on the membrane surface. It can also be due to particles in the feed suspension sealing the pores. The latter phenomenon is usually referred to as pore plugging (Kawakatsu *et al.*, 1995). Fouling will cause a decrease in filtration efficiency and it can be especially significant when the product is a macromolecule, resulting in product losses. The percentage of product that is recovered in the filtrate is defined as the percentage transmission. Transmission of macromolecules and fouling properties depends on membrane properties such as inherent charge and composition as much as on pore size (Bowen and Cao, 1998). Suspension properties such as the pH, ionic strength and charge properties also influence fouling.

2.2.2.1 Membrane fouling by macromolecules

When filtering biological suspensions, proteins are normally the main membrane foulant, however, other macromolecules such as polysaccharides, lipids and antifoams can contribute significantly. Fouling can be affected by many factors such as pH, ionic strength, protein structure, degree of hydration of the protein, membrane surface chemistry, magnitude and polarity of the protein and membrane surface charge and applied pressure (Bowen, 1993).

Internal pore fouling is more important with microfiltration membranes than ultrafiltration membranes where protein molecules are normally retained at the membrane surface (Bowen, 1993). Tracey and Davis (1994) demonstrated using bovine serum albumin (BSA) suspensions, that the reduction in flux when using small pore size membranes ($0.05\mu\text{m}$) is caused by the build-up of a cake layer of aggregates, while with the larger pore size membranes ($0.2\mu\text{m}$), fouling is caused by the constant reduction in the pore radius. Scanning electron microscopy showed that fouling of polycarbonate membranes with BSA is not evenly distributed throughout the pore, but is instead concentrated near the pore entrances (Tracey and Davis, 1994). Membrane properties such as the degree of hydrophilicity affect fouling behaviour. It has been shown that the more hydrophilic the membrane the better the antifouling properties of the membrane (Capannelli *et al.*, 1990). Modifying the surface properties of polyacrylonitrile membranes with charged groups has been shown to improve the retention of dextran and *E. coli* cells (Kobayashi *et al.*, 1998).

Fouling is caused in part by absorption of molecules onto the membrane. However, shear forces are believed to play an important role in altering protein conformation resulting in greater fouling than can be explained by absorption alone. Bowen and Gan (1991) found during microfiltration of BSA solutions, that fouling is much greater than can be explained by the adsorption of protein or concentration polarisation. This is believed to be due to shear forces generated by the fluid flow. Increasing applied pressure increases shear forces that result in protein denaturation. Kelly *et al.* (1993) observed that fouling increases with increases in the number of denatured protein monomers in solution. Higher applied pressures and hence higher shear forces have been found to result in greater fouling with beer (Blanpain *et al.*, 1993), with BSA (Bowen and Gan, 1991) and with colloids (Visvanathan and Ben Aim, 1989).

Since the pore size of microfiltration membranes is typically much larger than the macromolecules being filtered, fouling is believed to be influenced by aggregates. The fouling can be due to protein depositing on the membrane surface or within the membrane pores. For example, Maa and Hsu (1996) showed that membrane

fouling increased with increasing size and number of aggregates of human growth hormone. Prolonged pumping can produce protein aggregates (Chandavarkar and Cooney, 1990).

Altering the pH of suspension will alter the net charge of the protein, change the degree of hydration and alter its conformational state, and alter the net charge of the membrane (Bowen and Gan, 1991). Consequently, the relationship between pH and protein adsorption can be complex (Bowen and Gan, 1991). In that study it was shown with BSA suspensions, that as the pH was reduced from pH 7.0 to the isoelectric point of the protein, pH 4.5, protein adsorption increased. This was due to the degree of hydration of the protein decreasing to a minimum. Below pH 4.5, the adsorption of protein decreased due the degree of hydration increasing. However, at lower pH values it increased again to a maximum because the protein and membrane have opposite charges. Elsewhere with non-ionic membranes it has been shown that maximum adsorption occurs at the isoelectric point of the protein (Fane *et al.*, 1983). It has also been shown that increasing the pH can result in less fouling due to less aggregation caused by increased repulsion between macromolecules (Maa and Hsu, 1996). Therefore the role of pH in the fouling of membranes and product recovery will vary depending on the nature of the feed suspension and membrane.

Increasing the ionic strength has been shown to increase fouling due to aggregation of macromolecules (Blanpain *et al.*, 1993), suggesting that electrostatic repulsion plays an important role in fouling. However, it has be shown that increasing the ionic strength had no impact on the fouling characteristics of BSA, except at the isoelectric point where protein adsorption decreased when the electrolyte was NaCl (Bowen and Gan, 1991). The nature of the electrolyte is also important as certain ions may bind more readily with proteins than others. It was shown when using CaCl₂, protein binding with BSA suspensions was enhanced and increased with electrolyte concentration to a greater extent than with sodium based salts (Bowen and Gan, 1991).

2.2.3 Particle surface properties and solution properties effects

Experimental studies by Hodgson *et al.* (1993) focused on the role of the extracellular matrix. It was shown when the extracellular matrix of the gram-negative marine bacteria SW8 was modified by using Ethylene Diamine Tetraacetic Acid (EDTA) or proanase, that the specific resistance decreased. The size of the SW8 cells was found to be unaffected by the modification. It was concluded in that study that the extracellular matrix had a significant role in affecting microfiltration behaviour probably due to 'enmeshment' of the extracellular matrix. The nature of the enmeshment was assumed to be a function of pressure, ionic strength and surface treatment. The latter was demonstrated in that study.

Repulsive forces, due to the charge on the surface of the particles, will tend to increase voidage. This is commonly referred to as the *double layer* theory (Defrise and Gekas, 1988; Fane *et al.*, 1991). The effect of the repulsive force will increase as the net charge on the particle surface increases (Defrise and Gekas, 1988). As particle size decreases the voidage will increase due to a greater charge density (Tiller *et al.*, 1987; Wakeman *et al.*, 1991a).

The ionic strength and pH of the solutions filtered will also affect the double layer. High ionic strength solutions used when filtering *E. coli*, have been found to result in higher specific resistances than low ionic strength solutions (Fane *et al.*, 1989). This was attributed to high ionic strength solutions suppressing double layer repulsive forces.

2.2.4 Filter cake compressibility

Filter cake compressibility is the phenomenon whereby the resistance of the filter cake increases with increasing applied pressure. Filter cake compression causes a reduction in cake voidage and can also be associated with increases in the specific surface area of the particles (Chase and Willis, 1992). The pressure dependence of the specific resistance is described by the empirical expression (Leu, 1986)

$$\alpha_{av} = a\Delta P^n \quad [2.9]$$

where a is a constant and n is the index of compressibility. A value of zero for n represents an incompressible filter cake and increasing values of n represents increasing filter cake compressibility. In the filtration studies of non-microbial suspensions, equation 2.9 has generally been found to accurately represent the pressure dependence of the specific resistance at high pressures, (Tiller *et al.*, 1987). However, the value of n is pressure dependant, whereby it decreases at high pressures (Tiller and Kwon, 1998), therefore equation 2.9 applies over a limited range of pressures. Equation 2.9 has been found to be less accurate for microbial suspensions which are generally filtered at low to moderate pressures (<200kPa). For example, Nakanishi *et al.* (1987) observed non-linearity in log-log plots of α_{av} versus ΔP and estimated the compressibility factor, n , by arbitrarily fitting equation 2.9 to a linear portion of the plot, at the higher end of the pressure range employed. Other workers have employed a similar approach (Tanaka *et al.*, 1994a).

More recently it has been shown that a linear relationship exists between α_{av} and ΔP for a number of different yeast suspensions (Tanaka *et al.*, 1997). This is consistent with the findings of Riesmeier *et al.* (1987), where a linear dependence between α_{av} and ΔP was found to exist for *E. coli* suspensions. Similar results have been found by Cleveland *et al.* (1996) where it was shown that when filtering highly compactable biosolids, the average specific resistance is proportional to the pressure drop across the filter cake, ΔP_c , i.e. a linear relationship exists between α_{av} and ΔP_c .

2.2.4.1 Factors affecting compressibility and mechanisms of compressibility

All available literature for microorganisms show that microbial suspensions exhibit some degree of compressibility. Microbial suspensions can be classified as between moderately and extremely compressible. There is evidence that filter cake compressibility is morphology dependent, for example, the compressibility index of filter cakes produced from elliptical cells has been found to be lower than those of cakes formed by rod-shaped cells (Nakanishi *et al.*, 1987; Tanaka *et al.*, 1994a). Similarly, Oolman and Liu (1991) and Liu and Yu (1993) have showed that the

compressibility index increased when the cell morphology changed from predominantly filaments to predominantly pellets.

Many factors contribute to the degree of compressibility. These include particle size, particle shape, surface charge of particles, solution conductivity, degree of particle aggregation and rigidity of particle. Inorganic particles greater than 20-50 μm in size form tightly-packed incompressible filter cakes (Tiller *et al.*, 1987). Suspensions of aggregated particles will form more porous filter cakes than if the particles are freely dispersed in suspension. However, filter cakes formed by aggregated particles will be more sensitive to pressure and consequently will be more compressible. The degree of filter cake compressibility is also believed to be dependant on the null stress voidage, ϵ_0 , of the cake, whereby n increases with ϵ_0 (Tiller and Kwon, 1998). However, the reason for this dependence is unknown.

When filtering inorganic suspensions, cake compression is caused by the partial collapse of the filter cake structure. The compressive pressure on the filter cake forces particles into existing voids, thereby reducing the voidage of the filter cake. This is almost completely an irreversible process, i.e. the voidage of the filter cake will not increase to the null state voidage after the pressure exerted on the filter cake has been removed, (Tiller, 1953; Tiller *et al.*, 1987). Alternatively, the reduction in the filter cake voidage can be the result of particle deformation, whereby the particles deform due to compressive forces. For inorganic suspensions this is believed to occur at very high pressures (Tiller *et al.*, 1987). Another possible mechanism of compression involves the applied pressure overcoming repulsive forces from equally charged particles, resulting in a tightening of the cake structure (McDonagh *et al.*, 1984). This has been predicted to occur in theoretical simulations (Hwang *et al.*, 1998).

The mechanism of compression of filter cakes of microorganisms has received scant attention. One possible mechanism involves particle rearrangement within the filter cake, which was shown to occur with fluid flow through aggregates of *E. coli* (Fowler and Robertson, 1991). This process also showed degrees of reversibility, whereby the hydraulic resistance of the aggregates decreased when

the applied pressure was decreased. Another possible mechanism involves the deformation of cells under compressive forces (Kawakatsu *et al.*, 1993). Microbial cells are known to be deformable at high pressures (Smith *et al.*, 1998). Therefore cell deformation may play a role in compression. However, it is not known whether cells will deform under the pressures normally employed during microfiltration.

2.2.4.2 Filter cake compression theory

Filter cake compression results in voidage and local resistance gradients throughout the filter cake. The voidage is at a minimum and the local resistance at a maximum at the membrane, as shown in Figure 2.3. At the cake-slurry interface, the voidage is equal to the voidage of an unstressed cake, ϵ_0 . The voidage of the cake decreases throughout the cake where it is at a minimum at the membrane, ϵ_1 . Increasing the applied pressure causes a reduction of the voidage, ϵ_1 , and voidage throughout the filter cake, but the voidage at the cake-slurry interface is independent of the applied pressure. The mean specific resistance of a compressible filter cake is the integrated resistance throughout the entire depth of the filter cake.

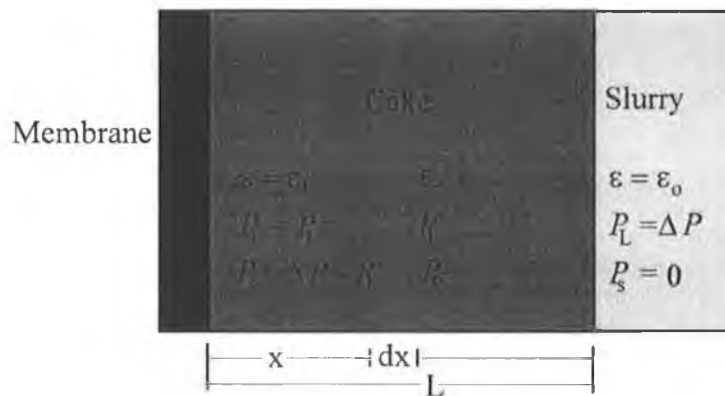


Figure 2.3 Schematic diagram of filter cake.

In Figure 2.3, P_L is the hydraulic pressure, P_s is the solid compressive pressure and the subscripts 1 and 0 denote the membrane/cake and cake/slurry interface respectively. The compressive pressure is also known as the effective pressure. It is a measure of the frictional drag on particles due to fluid flow. At any point in the

filter cake it is equal to the difference between the applied and hydraulic pressure, i.e.,

$$P_s = \Delta P - P_L \quad [2.10]$$

It can be seen that the liquid pressure, P_L , is equal to the applied pressure, ΔP , at the cake slurry interface and decreases to the pressure drop across the membrane, P_1 , at the membrane. Similarly the solid compressive pressure is at a minimum at the cake-slurry interface and increases to a maximum at the membrane. Empirical relationships are used to describe the relationship between the solid compressive pressure, P_s , and the local filter cake voidage, ϵ , and local specific resistance, α (e.g., Tiller and Leu, 1980). These can be written as

$$(1 - \epsilon) = (1 - \epsilon_o) \left[1 + \frac{P_s}{P_x} \right]^\beta \quad [2.11]$$

$$\alpha = \alpha_o \left(1 + \frac{P_s}{P_x} \right)^{n1} \quad [2.12]$$

where P_x is a scaling factor and ϵ_o and α_o are the unstressed cake voidage and unstressed specific cake resistance respectively. The parameters β and $n1$ are material characteristics which specify the degree of compressibility. These values are partly correlated such that a high value of β indicates a high value of $n1$. Integrating equations 2.11 and 2.12 allows the mean specific resistance, α_{av} and average voidage ϵ_{av} to be determined.

2.3 Crossflow microfiltration

Crossflow microfiltration is a relatively new technology that has been the focus of a significant amount of research over the last two decades. In particular, a considerable portion of this research has been applied to understanding the

microfiltration behaviour of biological suspensions. This research has focussed on the effect of process variables, cake formation, cake properties, fouling, flux enhancement and modelling crossflow microfiltration behaviour. However, there is a considerable amount of research to be done to elucidate the factors that comprehensively determine microfiltration performance.

The popularity of crossflow microfiltration research compared with dead-end microfiltration of microorganisms is probably due to its perceived advantage over dead-end microfiltration, insofar as the particle layer that forms on the membrane surface is limited by the tangential flow of the feed solution. Therefore, in theory, high steady state fluxes are possible. However, in practice, fluxes are often low and elimination of fouling and cake formation is, in most instances, not possible.

Many factors affect filtration performance in crossflow microfiltration. These include operating conditions such as transmembrane pressure drop and crossflow velocity. Filtration performance is also affected by feed suspension properties including particle properties and the amount and nature of the macromolecules in the medium. The above factors will be dealt with in more depth in the following sections.

2.3.1 Flux behaviour in crossflow microfiltration

In crossflow microfiltration, the flux declines rapidly as a cake layer of rejected particles deposit on the membrane surface. Then the cake layer reaches a limiting thickness due to the tangential forces, caused by the fluid flow, acting on the particles and cake. In theory, when cake formation ceases, the filtrate flux will reach a constant value, i.e. steady state flux. In practice, however, the flux may continue to decline at a slower rate due to fouling (e.g., Schluep and Widmer, 1996), i.e. pseudo steady state. Therefore, the decline in flux during crossflow microfiltration can normally be attributed to cake layer formation or fouling of the membrane or cake layer by macrosolutes.

In crossflow microfiltration, the Darcy equation is often rewritten as:

$$J = \frac{\Delta P_{tm}}{\mu R_T} \quad [2.13]$$

where ΔP_{tm} is the transmembrane pressure drop and is determined from the following expression,

$$\Delta P_{tm} = \frac{P_{feed} + P_{ret}}{2} - P_{fil} \quad [2.14]$$

where P_{feed} is the pressure of the feed suspension entering the microfiltration module, P_{ret} is the pressure of the retentate exiting the microfiltration module and P_{fil} is the filtrate pressure, which in most applications, will be equal to zero. The total resistance to flow, R_T , can be expressed as (Boyaval *et al.*, 1996)

$$R_T = R_m + R_{rev} + R_{irrev} \quad [2.15]$$

where R_{rev} is the reversible component of fouling, i.e. the fouling layer that is removed by rinsing with water at the end of microfiltration. It is normally assumed that reversible fouling is attributable to the deposited cake layer or concentration polarisation of macrosolutes. In equation 2.15, R_{irrev} is the irreversible component of fouling, i.e. fouling that cannot be removed by rinsing with water. This is normally assumed to be attributable to membrane fouling, i.e. the adsorption and entrapment of fermentation broth components, such as proteins, mineral salts, polysaccharides and cell debris (Nagata *et al.*, 1989).

Even though optimising process variables can considerably improve microfiltration performance, the filtrate flux is often too low to make it commercially attractive. Therefore, there has been a growing field of research into improving filtrate flux. Many of the techniques employed focus on reducing the cake layer thickness. The main techniques used to improve filtrate flux include backflushing (Redkar *et al.*, 1996; Tanaka *et al.*, 1995) and introducing air slugs into the feed stream (Li *et al.*, 1996; Tanaka *et al.*, 1995). Other techniques employed include using modules which generate very high shear (Belfort, 1998; Moulin *et al.*, 1996; Winzeler and Belfort, 1993) and pulsatile flow systems, where the feed pressure varies cyclically

(Hadzismajlovic and Bertram, 1998) or flow direction reverses (Howell *et al.*, 1993).

2.3.2 Cake formation in crossflow microfiltration

There is strong evidence of cake formation occurring in crossflow microfiltration, (e.g. Riesmeier *et al.*, 1987, 1989; Tanaka *et al.*, 1993). A number of different techniques have been employed to study cake formation in crossflow formation. These include direct methods such as flow visualisation (Davis and Birdsell, 1987), fibre optic sensors (Flemming *et al.*, 1997), a laser distance sensor (Schluep and Widmer, 1996), electron microscopy (Gatenholm *et al.*, 1988; Tanaka *et al.*, 1994b), a cell lysis technique (Riesmeier *et al.*, 1987), manually weighing the cake at the end of microfiltration (Tanaka *et al.*, 1993) or measuring the cake thickness (Fordham and Ladva, 1989) after microfiltration has been interrupted. Also, indirect methods based on monitoring the particle concentration in the feed reservoir have been utilised (Flynn *et al.*, 1990).

Two types of filter cake can form during microfiltration. The first is a stagnant cake which has been observed with flow visualisation techniques (Davis and Birdsell, 1987) or can be inferred to occur when a cake can be observed at the end of microfiltration (Tanaka, 1993). The second is a flowing cake which is believed to form over the stagnant layer (Davis and Birdsell, 1987). However, the contribution of a flowing cake to the total resistance is believed to be small (Romero and Davis, 1991).

Initially cake formation is believed to occur in a similar manner to dead-end microfiltration (Fordham and Ladva, 1989; Tanaka *et al.*, 1993). Cake growth ceases when the tangential forces on the particles exceed the forces due to the filtrate flow or when the rate of particle removal from the filter cake equals the rate of particle deposition. Modelling cake formation has attracted considerable research and a brief overview of these models is given in section 2.3.8.

Cake mass has been observed to increase with transmembrane pressure (Flynn *et al.*, 1990), feed particle concentration and membrane pore size (Flynn *et al.*, 1990; Gatenholm *et al.*, 1988; Riesmeier *et al.*, 1989) and decrease with crossflow velocity (Flynn *et al.*, 1990; Tanaka *et al.*, 1998). The topology of the membrane usually defined as the membrane rugosity (degree of roughness), is also believed to influence cake formation. Increasing membrane rugosity aids cake formation as it will protect deposited particles from the influences of fluid flow (Flynn *et al.*, 1990; Gatenholm *et al.*, 1988).

The cake layer thickness can increase over the length of filtration channel as predicted by the shear induced diffusion model (e.g., Bashir and Reuss, 1992). However, the cake layer thickness has been shown to decrease over the length of the filtration channel (Riesmeier *et al.*, 1987). This is attributed to a reduction in the transmembrane pressure drop over the length of microfiltration channel. Alternatively, there is evidence that cake formation occurs evenly over the entire filter length (Fordham and Ladva, 1989).

There is evidence that cake formation is largely irreversible, whereby particles forming the cake layer are difficult to remove (Fordham and Ladva, 1989). Increasing crossflow velocity during the pseudo steady state period of microfiltration, does not increase flux (Redkar and Davis, 1993). However, back washing is effective for flux recovery (Redkar and Davis, 1995). In the latter case, it was postulated that decompression of the cake or shock waves (caused during backwashing) are required for effective removal of cake. Alternatively it has been shown during microfiltration of *Lactobacillus helveticus*, that when the transmembrane pressure was reduced during microfiltration, the total resistance was not reduced (Boyaval *et al.*, 1996). It was suggested that the filter cake was in a consolidated state that could not be removed by erosion or shear induced diffusion. This would suggest that the back transport of particles from the cake during microfiltration is minimal. However, particles have been shown to be removed from the filter cake due to shear forces (e.g. Aubert *et al.*, 1993).

Many authors use wall shear stress as the fundamental parameter for controlling re-entrainment of particles. Aubert *et al.* (1993) suggest that there is a minimum shear stress required for cake erosion to occur. Furthermore these researchers found that the shear stress required for cake erosion increases with membrane pore size and ΔP_{tm} .

2.3.3 Fouling in crossflow microfiltration

Fouling studies conducted in dead-end microfiltration (as described in Section 2.2.3), are normally conducted with macrosolute suspensions, i.e. in the absence of cells. When filtering microbial suspensions in dead-end microfiltration, membrane effects and membrane fouling are often ignored. This can be justified when the cake layer contributes the bulk of the hydraulic resistance. However, in crossflow microfiltration the cake layer thickness is controlled by the tangential flow. Hence the membrane may contribute significantly to the overall microfiltration performance. It can be difficult to separate the effects of cake formation and membrane fouling. The possible impact of membrane fouling is often ignored in ascertaining reasons for flux decline and especially in modelling microfiltration behaviour.

When filtering fermentation broths, components in the broth such as proteins, lipids, polysaccharides, antifoams and other components can cause membrane fouling and subsequently cause low flux values. Many of the factors that influence fouling in dead-end microfiltration (as described in Section 2.2.3.1) can be considered to be applicable in crossflow microfiltration. However, fouling behaviour may be influenced by the presence of cells or tangential forces.

The negative impact of media components on filtrate flux has been clearly shown by comparing the microfiltration fluxes of cell suspensions in original fermentation media with those of cells resuspended in either water or buffer (Kroner *et al.*, 1984). Fouling effects have been elucidated by comparing cells suspended in water and simulated media (e.g. Patel *et al.*, 1987). It has been shown that membrane fouling can be the dominant effect in causing an increase in microfiltration

resistance (Foley *et al.*, 1995b) with resuspended baker's yeast. This was achieved by comparing filtration fluxes of washed and unwashed suspensions of resuspended active dry yeast and supernatant generated from centrifugation of unwashed suspensions. Furthermore it was shown that the combined resistances of the washed cell suspension and supernatant was greater than that of the unwashed suspension. Consequently, it was suggested that the cake layer could protect the membrane from fouling by leaked cell material. Similarly, varying the mixture of different solutes it is possible to determine the combined effect of particles and macrosolutes on filtration performance. This can be achieved by filtering particle suspensions and macromolecule suspensions separately and when mixed. It has been demonstrated that mixing of the solutions leads to lower transmission of the macrosolutes and lower fluxes (Kawakatsu *et al.*, 1993; Jiraratananon *et al.*, 1998).

However, there is also evidence that the media components have no effect on microfiltration performance as was found by Tanaka *et al.* (1993) using baker's yeast grown on Yeast Extract Peptone Dextrose (YEPD) media. Elsewhere, Riesemeir *et al.* (1987) showed that no significant difference existed in the filtrate fluxes between minimal and complex media. This may in part be due to the media compositions. Junker *et al.* (1994) showed that when filtering different types of cell-free media, the filtrate flux decreased by 60% when the total solid content was above 90g/L. Furthermore those authors showed that the harvest cell concentration does not significantly impact on flux when the medium has a high total solid content.

Fouling will be influenced by the nature of the macrosolutes in the feed suspension. Antifoams have been shown to have a significant influence on microfiltration behaviour (Cabral *et al.*, 1985; Kroner *et al.* 1984). Tanaka *et al.* (1993) found when cell suspensions grown in molasses medium were filtered, that the fluxes were an order of magnitude lower than when cell suspensions grown in YEPD media were filtered. The lower fluxes were attributed to fine particles in the molasses suspensions fouling the cake layer. In addition, magnesium ammonium phosphate precipitate, formed during sterilisation, was found to be the medium component which caused the greatest degree of fouling during the crossflow

microfiltration of a bacterial suspension (Nagata *et al.*, 1989). In addition, it has been shown that medium components play a relatively greater role in the fouling phenomenon at low cell concentrations (Patel *et al.*, 1987).

However, it should be noted that rejection of macrosolutes and fouling by macrosolutes can occur in the cake layer. This has been demonstrated by Jiraratananon *et al.* (1998) with dextran and polyethylene glycol (PEG) molecules mixed with bentonite. Gesan *et al.* (1995) suggested that the build up of a reversible layer of calcium phosphate aggregates on the membrane could entrap proteins when filtering whey suspensions. Proteins and polysaccharides in the spent medium of *Corynebacterium glutamicum* broth were found to form a gel layer on the filter cake after the cells stopped depositing (Tanaka *et al.*, 1998). Similarly, fines in spent molasses medium were believed to foul the deposited cell cake rather than the membrane (Tanaka *et al.*, 1994c). There is some evidence that the rejection of enzymes or other macrosolutes is dependant on the molecular weight of the enzyme (Quirk and Woodrow, 1984). Therefore it may be expected that properties of the cake layer such as voidage and pore size may determine if the macrosolutes are entrapped in the cake itself.

2.3.4 Influence of process variables

Process variables such as transmembrane pressure drop, crossflow velocity and membrane properties can impact upon cake formation and fouling in crossflow microfiltration. Consequently, crossflow filtration performance is dependent on many more factors than is the case in dead-end microfiltration. The influence of process variables on crossflow microfiltration performance is outlined below.

2.3.4.1 Temperature of the feed solution

Temperature affects microfiltration performance through variation in the viscosity of the filtrate. Kroner *et al.* (1984) noted when filtering *E. coli* suspensions, that the filtrate flux was greater at 20°C than at 5°C. When filtering biological suspensions, large increases in temperature could result in reduction of cell viability or denaturation of proteins and enzymes. It should be noted that temperature will have

a similar impact on filtrate viscosity in dead-end microfiltration. In crossflow microfiltration, temperature will also affect the retentate viscosity which will affect shear forces and consequently can affect cake formation.

2.3.4.2 Transmembrane pressure drop

The transmembrane pressure drop, ΔP_{tm} , is the driving force for microfiltration. Increasing ΔP_{tm} results in a greater driving force for microfiltration, thus increasing filtrate fluxes. However, this is counterbalanced by increasing cake layer thickness (Riesmeier *et al.*, 1987; Tanaka *et al.*, 1993), causing an increase in cake resistance. Also, increasing pressure can increase the specific cake resistance due to filter cake compressibility, as in dead-end microfiltration.

Higher transmembrane pressures result in higher initial fluxes. However, the filtrate flux declines much more rapidly than at lower pressures (e.g. Field *et al.*, 1995; Riesmeier *et al.*, 1987). Consequently, the filtrate flux at steady state does not increase linearly with pressure for all pressures.

It has been found when increasing ΔP_{tm} at low pressures that the flux increases linearly until a critical pressure, ΔP_{tmc} , is obtained. The value of ΔP_{tmc} will depend on the module used and nature of the feed suspension and other process parameters. For example, it has been shown that ΔP_{tmc} increases with increasing crossflow velocity (Liberge *et al.*, 1994) and at higher cell concentrations the flux is independent of pressure at lower pressures (Patel *et al.*, 1987).

Above ΔP_{tmc} , increases in ΔP_{tm} can result in the flux decreasing (Li *et al.*, 1996; Liberge *et al.*, 1994; Sakai *et al.*, 1989) or the filtrate flux may become independent of ΔP_{tm} (Taddei *et al.*, 1990).

2.3.4.3 Crossflow velocity

Increasing the crossflow velocity results in an increase in wall shear stress, τ_w . If the shear stress is sufficient, then particles will no longer be deposited to form a

filter cake or alternatively particle removal from the cake will increase. It is this phenomenon, which results in the cake thickness reaching a limiting value. At the beginning of microfiltration the flux is similar for all crossflow velocities and it has been concluded that cake formation is similar to dead-end microfiltration (Nakao *et al.*, 1990).

Increase in crossflow velocity result in thinner cakes being formed (Fordham and Ladva, 1989; Riesmeier *et al.*, 1987; Riesmeier *et al.*, 1989; Tanaka *et al.*, 1993) and the filtrate flux normally increases (e.g. Sakai *et al.*, 1989; Li *et al.*, 1996) due to a reduction in the cake resistance. It has been shown that high crossflow velocities can result in the elimination of fouling with methanogenic waste (Elmaleh and Abdelmoumni, 1997). At high crossflow velocities, the high tangential forces generated can cause a reduction in cell viability (Chan *et al.*, 1991). However, low crossflow velocities can result in part of the channel of the crossflow microfiltration module becoming plugged (Tanaka *et al.*, 1993), thus reducing the area of the membrane available for microfiltration and hence lowering filtrate fluxes.

Most researchers have found a power law relationship between filtrate flux and crossflow velocity, i.e.,

$$J \propto u^m \quad [2.16]$$

The value for m can vary depending on the suspension type, module used or operating conditions. It is generally found to be between 0.4 - 1.2. For example, Le *et al.* (1984b) found that when filtering *S. cerevisiae* suspensions the value of m was 1.1. Sims and Cheryan (1986) found that the value of m was 1.1 in turbulent flow. Le *et al.*, (1984a) showed that when filtering *Pseudomonas fluorescens* lysate, m was 0.5. The value of m is dependent on the flow conditions and module used.

Although the filtrate flux normally increases with crossflow velocity it has also been shown to decrease or become independent (Liberge *et al.*, 1994; Wakeman

and Tarleton, 1991b) of crossflow velocity. This is probably due to increases in specific resistance as will be discussed in Section 2.3.7.

2.3.5 The critical flux concept

Recent research has focused on the effect of the flux to shear stress ratio on microfiltration behaviour. It has been shown that the flux to shear stress ratio is critical in determining microfiltration performance, and a low J/τ_w ratio improves the microfiltration flux in the long term (Gesán *et al.*, 1995). Boyaval *et al.* (1996) demonstrated that an increase in R_T was faster and more severe when the value of J/τ_w was greater than $1.1 \text{ L}^{-1} \text{ h}^{-1} \text{ m}^{-2} \text{ Pa}^{-1}$. Below this value, R_T was low and increased only slightly with J/τ_w . Above this value, fouling was severe and increased dramatically with J/τ_w . Alternatively, Schluep and Widmer (1996) used the relation between $\Delta P_{tm}/\tau_w$ to relate cake formation to process parameters. The authors showed that increasing $\Delta P_{tm}/\tau_w$ results in increasing cake height and also greater cake resistance.

If the filtrate flux is sufficiently low, then increases in R_T do not occur (Field *et al.*, 1995). This is due to the tangential forces acting on the particles being sufficiently strong to prevent cake layer formation. Microfiltration performance can be improved if the initial flux is kept low so as to avoid fouling early in the microfiltration run. It is well noted that at low pressure, the reduction in filtrate flux is not as drastic as at high transmembrane pressure (Howell *et al.*, 1993; Riesmeier *et al.*, 1987). Protocols have been developed where microfiltration is carried out at constant flux (below the critical flux) where the overall microfiltration performance is much better than traditional constant pressure crossflow microfiltration (Field *et al.*, 1995).

For constant flux filtration, it has been demonstrated that a slow transient regime (whereby the flux is increased slowly to its set value) gives considerably lower fouling than a fast transient regime (Boyaval *et al.*, 1996). This was attributed to a more ordered packing of the cake in the slow transient regime which results in less fouling by medium components. While a high initial flux can result in considerable

cake formation, this can be offset by the cake that is formed being loosely packed (Boyaval *et al.*, 1996). Rushton *et al.* (1980) reported that the voidage of filter cakes of calcium salts and magnesium carbonates depends on the order of deposition of the particles, which is ruled by the rate of arrival of the particles. It has been shown that a high initial flux results in better protein transmission but paradoxically this is offset by poorer microfiltration performance later (Gesau *et al.*, 1995). More porous filter cakes can be capable of capturing small sized species such as aggregates and result in low fluxes later in the microfiltration run (Wakeman and Tarleton, 1991b).

2.3.6 Feed suspension characteristics

2.3.6.1 Particle concentration

Increasing particle concentration usually results in a reduction in filtrate flux. However, the results differ somewhat when comparing batch and continuous crossflow microfiltration. With batch crossflow microfiltration, plots of flux *versus* particle concentration can be sigmoidal (Kroner *et al.*, 1984; Pritchard and Howell, 1990). During batch crossflow microfiltration, the filtrate flux drops significantly initially. The filtrate flux then reaches a pseudo steady state where it becomes independent of particle concentration. At higher particle concentrations the flux can either increase (Pritchard and Howell, 1990) or decrease (Kroner *et al.*, 1984). Both these changes have been attributed to increases in the feed suspension viscosity at high particle concentrations (Pritchard and Howell, 1990). Furthermore it was shown theoretically that the observed flux behaviour in batch crossflow microfiltration can be attributed to increases in the feed suspension viscosity (McCarthy *et al.*, 1996).

In continuous microfiltration the steady state cake mass has been shown to increase with increasing particle concentration, c , (Riesmeier *et al.*, 1987; Tanaka *et al.*, 1993) and the filtrate flux has been shown to decrease (e.g. Liberge *et al.*, 1994; Riesmeier *et al.*, 1987). Some data indicate that the flux is proportional to c^{-m} where $m \approx 0.4$ (Riesmeier *et al.*, 1987, Warren *et al.*, 1991). Other data suggest that the flux decreases linearly with $\ln(c)$ in a similar manner to that found in

ultrafiltration of macromolecules (Kavanagh and Brown, 1987; Le and Billigheimer, 1985; Nagata *et al.*, 1989)

2.3.6.2 Particle morphology

Particle morphology can have a large impact on microfiltration behaviour, as is the case in dead-end microfiltration. Particle size, shape and size distribution can all impact on the properties of the filter cake as in dead-end microfiltration. Further phenomena are observed in crossflow microfiltration such as preferential deposition of smaller cells (Foley, 1993) and shear-induced arrangement of cells (Tanaka *et al.*, 1994b).

Preferential deposition occurs due to particle polydispersity in the feed solution. Larger particles experience more tangential drag than smaller particles. Consequently, when the tangential drag is sufficient, smaller particles will deposit while larger particles will not. This will result in the filter cake having a smaller mean particle size than the feed suspension. This phenomena was extensively modelled by Foley *et al.* (1995a), where it was shown that the mean specific resistance increased with increasing R_m and crossflow velocity but decreases with ΔP_{tm} (increases in the mean specific resistance reflect a greater degree of preferential deposition).

With rod shaped cells such as *B. subtilis* and *E. coli*, it has been shown that particle packing in the filter cake is influenced by shear (Tanaka *et al.*, 1994b; Tanaka *et al.*, 1996). At low crossflow velocities and during the initial stages of cake formation at higher crossflow velocities, particles pack in a random manner similar to that observed in dead-end microfiltration. However, when the crossflow velocity to flux ratio is high, particles depositing on the cake become aligned with the membrane and subsequently pack tighter (ordered packing), hence increasing the mean specific resistance. If backwashing is utilised during microfiltration, then the cake will form in a random manner between backwash intervals. This can result in considerably improvement in microfiltration performance (Tanaka *et al.*, 1996).

Yamasaki *et al.* (1993a, 1993b) studied the effect of cell morphology on the microfiltration performance during crossflow microfiltration of suspensions of the dimorphic organism *Aureobasidium pullans*. It was found that the yeast-like morphology gave better microfiltration fluxes and pullulan transmission than the more mycelial morphology. The reason for this was not elucidated.

Hooper *et al.* (1998) demonstrated that higher fluxes are obtained when *Streptomyces rimosus* suspensions were pre-treated by acidification, which results in cell aggregates disassociating. Acidification also resulted in lower feed suspension viscosity and subsequently lower transmembrane pressures and lower pumping costs.

2.3.7 Specific resistance in crossflow microfiltration

During the initial stages of microfiltration, there is evidence that the specific resistance in crossflow microfiltration is similar to that found in dead-end microfiltration (Taddei *et al.*, 1990; Tanaka *et al.*, 1993; Tanaka *et al.*, 1996) and is not affected by the shear rate (Fordham and Ladva, 1989). However, when the filtrate flux reaches a pseudo steady state the specific resistance may be similar to dead-end microfiltration (Tanaka *et al.*, 1993), lower than in dead-end microfiltration (Xu-Jiang *et al.*, 1995) or greater than in dead-end microfiltration (Baker *et al.*, 1985; Matsumoto and Totsuka, 1992; Riesmeier *et al.*, 1989; Tanaka *et al.*, 1996). However, it should be noted that the work of Xu-Jiang *et al.* (1995) was conducted using a talc powder suspension. Furthermore, lower specific resistance of filter-cakes formed by crossflow microfiltration as opposed to dead-end microfiltration has not been shown to occur with microbial suspensions. Higher specific resistance than dead-end microfiltration is the most common finding in crossflow microfiltration studies.

The specific resistance in crossflow microfiltration has been shown to increase with filtration time (Riesmeier *et al.*, 1987). This has been attributed to time dependent compaction of the cake layer, although no evidence was provided to support this assertion. Furthermore the specific resistance has been shown to

exhibit a minimum with respect to transmembrane pressure (Baker *et al.*, 1985; Riesmeier *et al.*, 1989; Schluep and Widmer, 1996) and to be independent of crossflow velocity (Baker *et al.*, 1985; Riesmeier *et al.*, 1989) or to increase with crossflow velocity (Baker *et al.*, 1985; Riesmeier *et al.*, 1987, 1989). However, in the above research it is assumed that the membrane resistance is constant throughout microfiltration. It has been demonstrated qualitatively, that many of the above phenomena can occur as a result of membrane fouling (Foley, 1994).

Higher specific resistances measured in crossflow microfiltration compared to dead-end microfiltration have been shown to be caused by the filter cake being clogged by fines (Tanaka *et al.*, 1993), fouling of the cake layer (Tanaka *et al.*, 1998) and preferential deposition of smaller particles (Baker *et al.*, 1985). It can also be attributed to shear induced arrangement of particles resulting in reduced cake voidage (Tanaka *et al.*, 1994b, 1996). It has been noted with synthetic spherical particles that the mean specific resistance can increase as a result of increased cake compactness (Mackley and Sherman, 1992). Similar results were shown with glass/silica particles (Chellam and Wiesner, 1998) where the mean specific resistance was greater in crossflow microfiltration than in dead-end microfiltration. In the latter study, this could only be partially explained by the increase in fines in the crossflow cakes suggesting the cakes were more compact.

2.3.8 Theoretical studies in crossflow microfiltration

There has been considerable research into theoretically analysing crossflow microfiltration. The models are nearly exclusively centred on describing cake formation and in most cases ignore fouling affects. Most fouling models are based on the blocking models of Hermia (1982) or modified forms of the same (e.g. Foley *et al.*, 1995b). Cake formation models are briefly described in the following sections.

2.3.8.1 Convective models

With convective models or flowing cake models the deposition of particles on the membrane is balanced by the flow of particles tangential to the membrane (Davis

and Birdsell, 1987; Vassilieff, 1992). The concentration of particles in the flowing layer is considerably higher than in the bulk suspension. However, the existence of a stagnant layer can only be accommodated by assuming non-Newtonian flow in the cake layer, e.g. Bingham plastic behaviour.

2.3.8.2 Shear-Induced Diffusion

With shear-induced diffusion models, the deposition of particles is balanced by diffusion of particles away from the cake. Using Brownian diffusion coefficients results in the under-prediction of flux by one to two orders of magnitude (Davis and Leighton, 1987). The higher than expected fluxes were attributed to shear forces caused by the tangential flow, enhancing the back diffusion of particles into the retentate stream. Consequently, shear induced models were developed, using experimentally determined shear-induced diffusion coefficients to predict cake formation and flux behaviour. The shear-induced diffusion coefficients are a function of the shear rate, particle concentration and particle size (Leighton and Acrivos, 1987).

2.3.8.3 Force balance models

These models analyse the forces exerted on an isolated particle depositing on the filter cake. Particles will stop depositing on the cake layer when the tangential forces are sufficient to overcome the normal drag forces caused by the permeate flow. Therefore, larger particles are more likely to escape in the retentate due to their larger tangential forces. Models of this kind can be used to describe preferential particle deposition (Blake *et al.*, 1992; Foley *et al.*, 1995a).

2.3.8.4 Empirical models

These models are normally based on the Darcy equation whereby the cake resistance is related to process parameters by empirical correlation (Riesmeier *et al.*, 1989; Warren *et al.*, 1991). However, the predictive capabilities of these models is limited to the suspensions studied. Furthermore these models are unable to elucidate the fundamental mechanisms of crossflow microfiltration.

2.4 Conclusions

Many potential parameters that may influence filtration behaviour during dead-end microfiltration, have received scant attention. In particular particle morphology, packing arrangements and filter cake compressibility may have considerable impact on microfiltration performance as outlined in Section 2.2. However, there has been limited research conducted into filter cake properties, particularly when microbial suspensions are being filtered.

In Chapter 4 the dead-end microfiltration properties of a dimorphic yeast, *Kluyveromyces marxianus*, will be presented and analysed. The specific strain of this organism used in this study was selected because it can exhibit a wide variety of morphological forms. Potential mechanisms for filter cake compression will be analysed in Chapter 5. In Chapter 6, the modelling of filter cake compression will be addressed.

Crossflow microfiltration has attracted considerable research as outlined in Section 2.3. However, only a fraction of this research has been devoted to elucidating cake formation combined with membrane fouling. Furthermore little work has been done into the role of cell morphology on microfiltration performance. These factors will be addressed in Chapter 7.

CHAPTER 3

MATERIALS AND EXPERIMENTAL METHODS

3.1 Organism

The organism used for all studies was *Kluyveromyces marxianus* var. *marxianus* (formerly *fragilis*) NRRLy2415 (Northern Regional Research Laboratories, Peoria, IL). This organism is also recognised as NCYC1425 (National Collection of Yeast Cultures, England). It is a polymorphic strain of *K. marxianus*, which can exhibit a wide range of morphological forms. It was because *K. marxianus* can be grown to give suspensions with a wide range of mean morphology, that it was used in this thesis to study the affect of cell morphology on filtration behaviour.

3.2 Autoclaving procedure

All media, both solid and liquid, were sterilised by autoclaving at 121°C (15 psig) for 15 minutes in a Tomy SS-325 autoclave (Tomy Seiko Co., Ltd., Japan).

3.3 Media preparation

3.3.1 Yeast extract peptone dextrose (YEPD) medium

The YEPD medium contained the components listed in Table 3.1, resuspended in deionised water.

Table 3.1 YEPD medium formulation.

Constituent	Manufacturer	Concentration (g/L)
Yeast extract	Oxoid	10
Bacteriological peptone	Oxoid	20
Glucose monohydrate	BDH	20

3.3.2 YEPD medium (solid)

This medium was as listed in Table 3.1, along with the addition of 30g/L Oxoid Technical Agar No. 3 (Basingstoke, England).

3.3.3 Yeast extract peptone lactose (YEPL) medium

This medium was as listed in Table 3.1 but with 20g/L lactose monohydrate (BDH, Poole, England) instead of glucose monohydrate.

3.3.4 Glycerol medium

This medium was as listed in Table 3.1 but with the replacement of glucose monohydrate by 20g/L of glycerol (BDH, Poole, England).

3.3.5 Whey-based medium

Whey-based medium was prepared by resuspending 57.14 g/L commercial whey powder (Avonmore plc, Kilkenny, Ireland) in deionised water and removing excess protein in a Romicon PM40 hollow fibre ultrafiltration unit, (Romicon Inc. Woburn, MA). The resulting permeate contained a lactose concentration of 40 g/L as determined by DNS assay (O'Shea, 1998). Fermentation medium was produced by diluting the resulting whey permeate to 5, 10, 15 or 20 g/L lactose with deionised water and supplementing with yeast extract (0.5g/g of lactose), ammonium sulphate (Riedel de Haen) (0.25g/g of lactose) and the pH was adjusted to 4.5 using concentrated HCl (BDH).

3.4 Culturing on solid medium

The organism was maintained on solid YEPD agar plates. Subculturing was done on a monthly basis to ensure viable cultures. A loopful of cells from a single colony was taken from a stock plate and streaked on to a fresh YEPD agar plate. Plates were incubated at 30°C for 24 hours and thereafter stored at 4°C.

3.5 Shake flask cultures

All starter cultures for both batch (in 2L bioreactor) and continuous fermentations were grown in 1L Erlenmeyer flasks containing 400mL YEPL medium. A loopful of cells from a single colony was transferred to the flask and the flask was incubated at 30°C on an orbital shaker (133 rpm) for 24 hours. Batch cultures (shake flask cultures) grown specifically for filtration studies were inoculated in a similar manner.

3.6 2L “Life Sciences” fermenter

Batch and chemostat fermentations were conducted in a 2 L (working volume 1-1.5L) bioreactor (Life Sciences, Luton, England). Fermentations were based on the work of O’Shea (1998).

3.6.1 Fermenter configuration

The bioreactor (Life Sciences Laboratories, Luton, U.K.) was fabricated in borosilicate glass mounted in a stainless steel collar supported on a three membered frame and base ring. The vessel had a hemispherical base and was surrounded by an external jacket to allow for heat transfer. The vessel had eleven ports on the head plate. During batch culturing, ports were used for the following: feed addition, culture removal, air addition, off gas outlet with condenser, antifoam addition and inoculum addition. During continuous culturing, ports were used for the following: feed addition, effluent removal, air addition, off gas outlet with condenser, antifoam addition and inoculum addition. The vessel was agitated using a top-driven stainless steel shaft mounted with two Rushton turbine impellers. The fermenter was aerated by open pipe aeration. For a schematic of the fermenter see Figure 3.1. For measured parameters see Table 3.2.

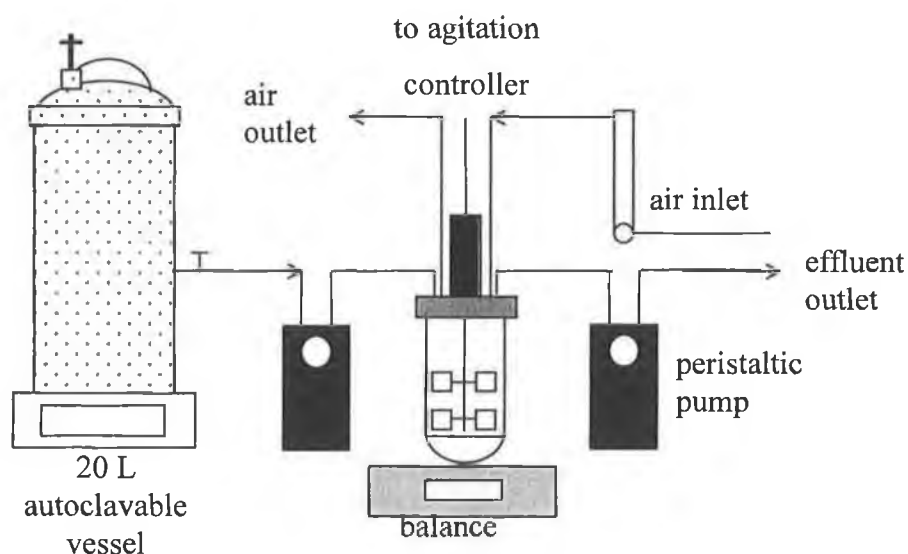


Figure 3.1 Fermenter configuration for chemostat operation.

Table 3.2 Life Sciences fermenter configuration.

Measurement	Quantity
Tank diameter	110 mm
Tank depth	230 mm
Impeller diameter	55mm
Number of impellers	2
Blades per impeller	6
Dimensions of blade	10mm x 10mm
Inter-impeller distance	70 mm
Sparger to 1 st impeller	20 mm

3.6.2 Fermenter set-up: batch mode

The fermenter was autoclaved containing 600 mL of YEPL medium. The fermenter was then inoculated with 400 mL of a 24 hour shake flask culture. The culture was then allowed to grow for 24 hours, after which the culture was removed using a Watson Marlow peristaltic pump (Cornwall, England) connected to a sterile line which ran to within 2 cm of the bottom of the fermenter. After the culture was removed, approximately 40 mL of culture remained at the bottom of the fermenter.

This was used as the starter culture for subsequent fermentations. Fresh sterile medium was pumped from a feed reservoir (20L) until the desired volume (determined by mass balance) in the fermenter was obtained (1.0-1.5L). The container used as the feed reservoir was a modified autoclave (Dixons Surgical Instruments Ltd, Sheffield, England) which had a maximum autoclavable volume of approximately 20L. A feed line ran from a port in the side of the autoclave to the fermenter, which was closed during autoclaving. A sterile air filter (Millipore Millex 0.22 μ m) was placed on a port on top of the autoclave to allow the vessel compensate for the loss of medium volume during feeding. The volume in the fermenter was monitored by a balance placed underneath the bioreactor. In this way the fermenter could be run in batch mode and kept contamination free, typically for a period of 2-4 weeks.

3.6.3 Fermenter set-up: continuous mode

When the fermenter was operated in chemostat mode it was set-up and inoculated as described above for batch mode. The fermentation was allowed to proceed in batch mode for a 24 hour period after inoculation and was then switched to chemostat mode.

The effluent was removed using a weir system, set at a height that allowed the working volume of the bioreactor to remain at 1L. Again the volume in the fermenter was monitored by a balance placed underneath the bioreactor. Pumping of both feed medium (from 20L reservoir) and effluent was achieved using Watson Marlow peristaltic pumps equipped with silicone tubing. The inlet pump was calibrated prior to use, using similar grade silicone tubing (5mm internal diameter). A pump setting was chosen, the pump primed and the output volume was collected for a fixed time interval. Thus pump setting was related to feed rate. The outlet pump setting was set to ensure the required steady state volume in the bioreactor. The fermenter typically reached steady state (biomass and morphology) after a throughput of 3-4 L of medium (O'Shea, 1998).

3.6.4 Fermenter operation

Agitation in the fermenter was set using a potentiometer on the front of the fermenter controller. Temperature was regulated at 30°C, by circulating water through the jacket from a heating-cooling water bath (B. Braun, Buckinghamshire, U.K.). Aeration was supplied from a fish pump regulated by a rotameter (Platon) (2 L/min maximum air throughput). Air sterilisation was achieved using in line autoclavable Millipore Millex (Molsheim, France) 0.22µm air filters. Organic antifoam (Sigma, St. Louis, Missouri) was added manually through a septum port on top of the vessel using a sterile syringe and needle.

3.7 Cultivation conditions required to produce different morphological forms of *K. marxianus*

The fermentation conditions used to give different morphological forms of *Kluyveromyces marxianus* were based on the experimental work of O'Shea (1998). A brief outline of fermentation conditions used to produce different morphological forms is given here.

3.7.1 Cultivation conditions for yeast-like cells

1000-mL Erlenmeyer flasks (either baffled or unbaffled) containing 300 or 400 mL of glycerol medium (glycerol, 20 or 40 g/L) were prepared and autoclaved. The flasks were then aseptically inoculated with a loop of *K. marxianus* and placed on an orbital shaker (133 rpm). Samples were withdrawn at time periods of 48 to 72 hours.

3.7.2 Cultivation conditions for cultures containing a mixture of yeast-like cells and filaments

Batch fermentations were carried out in 1000-mL Erlenmeyer flasks (either baffled or unbaffled) containing 300 or 400 mL of whey medium (20g/L lactose). In addition batch fermentations using whey medium (20 g/L lactose) were conducted for a period of 24 hours in the Life Sciences bioreactor (working volume 1000 to 1500mL). The range of agitation speeds varied between 50 and 800 rpm and the aeration rate was either 500 or 1000 mL/min.

3.7.3 Cultivation conditions for cultures containing a mixture of filaments and mycelia

Continuous culture fermentations were conducted in the Life Sciences fermenter using a working volume of 1000 mL, agitated at 800 rpm and aerated at a rate of 1000 mL/min. The fermentation medium used was a whey permeate medium containing 5, 10, 15 or 20 g/L lactose. The dilution rate was varied between 0.1 and 0.42 h⁻¹.

3.8 Wet weight cell concentration

In filtration studies, cell concentrations of microbial suspensions are usually expressed as a mass of wet pellet per unit volume of suspension (c_{app}) or as a dry weight concentration. A more accurate measurement is the mass of *wet cells* per unit volume of suspension (c). This concentration was determined using a modified form of the methods used by Ju and Ho (1988).

Well mixed cell suspensions were poured into pre-weighed centrifuge tubes. The weight of suspension added to the tubes was determined by weighing the tube after the addition of suspension. Cell suspensions were centrifuged at 3500 rpm for 15 minutes in a Labofuge 400 centrifuge (Hereaus, Germany). The supernatant was decanted. The pellet was washed twice with deionised water. After the second wash the supernatant was decanted. The interior of the centrifuge tube was carefully wiped with absorbent tissue so as to remove any water droplets that cling to the side of the centrifuge tube. The centrifuge tube was then weighed to determine the mass of the pellet. A dextran solution of known concentration (8-10% by weight) was added to the centrifuge tube (the volume of dextran solution added to the centrifuge tube was typically twice the pellet mass). The pellet and the dextran solution were thoroughly mixed and centrifuged again. The mass of interstitial water in the pellet, I , can be determined from the following expression

$$I = \rho_w V_{dex} \left[\frac{c_{dex1}}{c_{dex2}} - 1 \right] \quad [3.1]$$

where V_{dex} is the volume of dextran stock added to the centrifuge tube, ρ_w is the density of water, c_{dex1} is the concentration of the stock dextran and c_{dex2} is the concentration of dextran in the supernatant after the pellet and dextran solution mixture have been centrifuged.

The dextran concentrations were determined gravimetrically. Known volumes of dextran solutions were added to glass sample bottles of known weight (pre-dried in a 140 °C oven overnight). The sample bottles containing the dextran solutions were then placed in a 140 °C oven overnight. The sample bottles containing the dried dextran were reweighed allowing the mass of dry dextran to be determined and hence the dextran concentration in the samples was calculated.

The mass fraction of interstitial water in the pellet, w_m , is

$$w_m = \frac{I}{P_m} \quad [3.2]$$

where P_m is the pellet mass determined after the wash stage. Subsequently the true wet cell concentration, c , can be determined as follows,

$$c = c_{app} [1 - w_m] \quad [3.3]$$

3.9 Cell density determination

The cell density, ρ_c , was determined by the method of Ju and Ho (1988). The volume of a centrifuge tube was determined by filling the tube with de-ionised water. A cover glass was placed upon the tube mouth while air bubbles were carefully excluded and the full tube was then weighed. The volume of the tube, V_t , was determined as the weight of water in the tube divided by the density of pure water (1000 kg/m³).

The tube was then dried and tared. A known volume of cell suspension was added to the tube and it was then centrifuged at 3500rpm. The resulting cell pellet was

washed with de-ionised water and re-centrifuged at 3500rpm. De-ionised water was slowly added to the tube. A cover glass was placed upon the tube mouth while air bubbles were excluded and the tube contents were then weighed, w_1 . The mass of cells in the pellet, w_2 , was determined as the product of the volume of suspension centrifuged and cell concentration determined separately, as outlined in Section 3.8. The cell density was determined from the following equation,

$$\rho_c = \frac{w_2}{V_t - (w_1 - w_2) / \rho_w} \quad [3.4]$$

The cell density, ρ_c , within experimental error was found to equal 1080 kg/m^3 for all mean morphological forms.

3.10 Centrifuged pellet voidage

The average voidage of centrifuged pellets, ϵ_{av} , expressed as the volume fraction of the pellet unoccupied by cells was determined by the following expression,

$$\epsilon_{av} = \frac{w_m}{\left[(1 - w_m) \frac{\rho_w}{\rho_c} + w_m \right]} \quad [3.5]$$

where ρ_w is the density of water taken to be equal to 1000 kg/m^3 .

3.11 Centrifugation studies

3.11.1 Effect of centrifugation speed

The wet weight concentration was determined at 3500 rpm as described in Section 3.8. Also the wet cell concentration was determined at a centrifugation speed of 1500 rpm for a number of suspensions spanning the entire range of morphologies filtered. Since the wet cell concentrations for the two centrifugation speeds were found to be in excellent agreement with each other, it was assumed that the wet cell weight was independent of centrifugation speed.

Centrifugation studies were performed to elucidate if the centrifugation speed effects the measured pellet voidage. This would be expected as varying the centrifugation speed changes the centrifugal forces exerted on the cell pellets. Centrifugation was carried out for 10 minutes for all samples examined, at a range of speeds between 1500 rpm and 3500 rpm. The supernatant was poured off and the interior of the tube was wiped with absorbent tissue. The weight of pellet formed was then determined at each centrifugation speed, P_m (without washing stages). The weight of cells in the centrifugation pellets, w_2 , was determined as the product of the wet cell concentration (determined as described in Section 3.8) and volume of sample centrifuged. Subsequently the mass fraction of water in centrifuged pellets could be determined using the following expression,

$$w_m = \frac{P_m - w_2}{P_m} \quad [3.6]$$

Hence cell voidage could be determined using equation 3.5. Therefore by applying this method the voidage of the pellet could be determined without using washing stages.

3.11.2 Determination of unstressed pellet voidage - 'Water Drop Test'

To verify that the pellets undergo decompression after removal of the centrifugal forces, the following procedure was used. Pellets were formed by centrifugation at 3500 rpm for 10 minutes. When the centrifuge speed returned to zero, a timer was activated. The centrifuge tubes were removed after different periods of time and the supernatant decanted. The time at which the supernatant was decanted was noted. The pellet weight was then determined as usual. The weight of cells in the centrifugation pellet, w_2 , was determined as the product of the wet cell concentration (determined as described in Section 3.8) and volume of sample centrifuged. The pellet voidage at each time point was determined by again using equation 3.5 and equation 3.6.

A test was designed to determine the voidage of unstressed pellets, i.e. corresponding to a centrifugation speed of zero. It was noticed when determining

the pellet wet weight concentration, that the supernatant remaining in the centrifuge tube (after taking a sample to determine the dextran concentration) appeared to be absorbed by the pellet, when the pellet was formed from mycelial suspensions. Therefore, it was assumed that the pellet slowly decompresses after removal from the centrifuge and subsequently can absorb liquid as the voidage of the pellet increases. Furthermore it was assumed that the pellet weight, determined when the pellet ceases to absorb moisture, is equivalent to an unstressed pellet weight. Based on this phenomenon a procedure for determining the unstressed pellet voidage was designed and is referred to here as the 'Water Drop Test'.

Pellets were formed by centrifugation at 3500 rpm with mycelial suspensions. After centrifugation, the supernatant was discarded. The walls of the centrifuge tube were wiped and the pellet weight was determined. Water was carefully added to the centrifuge tube until a thin layer covered the surface of the pellet (typically 0.2 or 0.3 mL). The pellet was reweighed so as to determine the amount of water added. When all the water was absorbed by the pellet, fresh water was added and the pellet was reweighed again. This process was repeated until the pellet stopped absorbing water. The pellet weight measured immediately before the pellet stopped absorbing water was taken as the weight of an unstressed pellet and the voidage was determined by using equation 3.5 and equation 3.6 and the wet weight concentration determined separately as outlined in Section 3.8.

3.12 Dead-end filtration

3.12.1 Sample preparation

As the pH was not controlled during the fermentation, the pH of the cell broths collected varied between pH 3 and pH 7. All samples were adjusted to pH 5 using either H₂SO₄ or NaOH solution. A pH of 5 was chosen as the pH of most broths had a pH close to this value. The temperature of the cell suspension was equilibrated to 20 °C prior to filtration.

3.12.2 Filtration set-up

The dead-end filtration set-up is shown in Figure 3.2. Filtration was performed in a 200 mL stainless steel dead-end filtration module using 47 mm diameter Supor 0.45 μm nominal pore diameter polysulfone membranes. The module consists of a stainless steel base containing a stainless steel mesh 26 mm in diameter, through which filtrate leaves the module. A new membrane was used for each run. The pressure was applied from a nitrogen cylinder (250 bar) and reduced to operating conditions by an attached gas regulating valve. The applied pressure was set (between 20-180kPa) by adjusting a valve on the gas regulator.

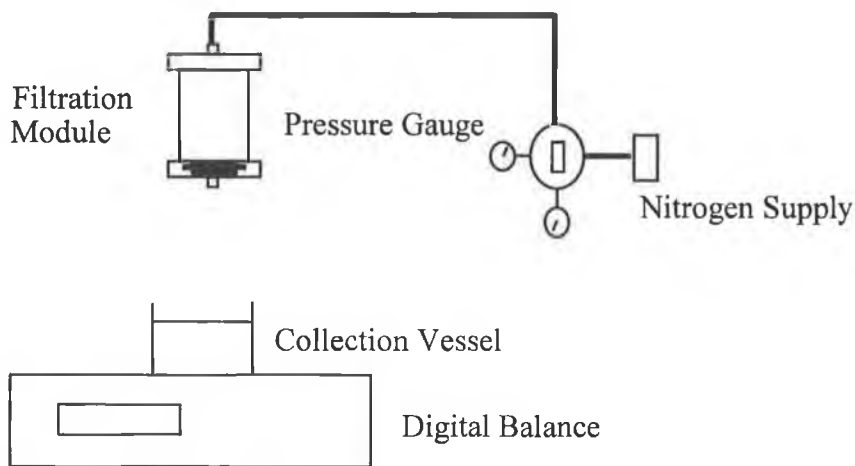


Figure 3.2 Dead-end filtration set-up.

3.12.3 Determination of membrane resistance

The membrane resistance, R_m , was measured by passing 150 mL of deionised water through the filter at 20 kPa pressure. R_m was calculated from the following expression

$$R_m = \Delta P / J\mu \quad [3.7]$$

where J is the filtrate flux and μ is the filtrate viscosity. The filtrate volume was determined at various times using a Mettler electronic balance and the flux determined as $\Delta V / [A\Delta t]$ where ΔV is the change in filtrate volume during a time period Δt .

The filtrate viscosities were determined at 20 °C using a Brookfield V1 (Harlow, England) cone and plate viscometer.

The value of R_m was typically between $1.4 \times 10^{10} \text{ m}^{-1}$ and $1.9 \times 10^{10} \text{ m}^{-1}$. After filtration of the cell suspension was complete, the cake was removed and the filter was washed in de-ionised water. The membrane resistance was determined again using de-ionised water. The membrane resistance usually increased by 20-50% during filtration. On occasion, the resistance increased by between 100 to 150 %.

3.12.4 Determination of the mean specific resistance

The mean specific resistance, α_{av} of the filter-cake was determined using the steady state method of Nakanishi *et al.* (1987). A known volume of suspension (typically 150 mL) was filtered at a pressure of 20 or 30 kPa. Once the initial filtration was complete, the pressure was released. The temperature of the filtrate was measured and adjusted to 20 °C if necessary. The filtrate was then carefully returned to the filtration module. The pressure was set at 20 or 30 kPa (the pressure employed was the same as that used to form the filter cake) and filtration recommenced. Accuracy in the estimation of α_{av} was ensured by monitoring the flux over a period of time until a steady-state filtrate flux was achieved. Steady state flux was achieved almost instantly when the filter cake was exposed to a change in pressure. The specific resistance could then be calculated from the Darcy equation (ref. Section 2.1.2) rearranged as follows,

$$\alpha_{av} = \frac{A(\Delta P - J\mu R_m)}{J\mu c V_s} \quad [3.8]$$

where c is the concentration of cells in the suspension, V_s is the volume of filtered suspension and R_m is the fouled membrane resistance as determined above. The specific resistance was measured at between four and seven further pressures up to 180 kPa by incrementing the pressure. In this manner, specific resistance measurements over the desired range of pressures could be achieved in a single pass through the module.

3.12.5 Reversibility studies

For two *K. marxianus* suspensions of different morphologies, suspensions of resuspended and cultured baker's yeast and calcium carbonate, the reversibility of filter cake compression was studied. The resuspended baker's yeast suspensions were produced by adding a defined weight of cell pellets to a defined volume of de-ionised water and mixing the suspensions at 30°C for 30 minutes. In all cases, the filter cake was formed at 30 kPa applied pressure. After the specific resistance was measured at the five pressures between 30 and 180 kPa as outlined above (Run 1), the pressure was released. The filtrate was returned to the module and the pressure was again set at 30 kPa. The specific resistance was determined at the same five pressures in the same manner as used previously (Run 2).

3.13 Image analysis

Image analysis of cells was carried out using a Leica Q500MC image processing and analysis system as described by O'Shea and Walsh (1996) and O'Shea (1998). A semi-automatic image analysis program was developed for the purpose of (i) morphologically classifying the population into one of six different classes and (ii) evaluating morphological parameters such as cell length, width and projected area. To determine these parameters accurately, cells with different shape (Figure 3.3) needed to be treated with different image processing regimes. For single cells, the length, width, projected area and perimeter were measured directly from their images. For double cells, the length, width and projected area of each sub-unit (mother/daughter cell) were measured. This was achieved by separating each double cell into its two sub-units using a process known as segmentation (O'Shea and Walsh, 1996). For mycelia, the overall length, perimeter and projected area were measured. This was achieved with the aid of an image analysis process known as skeletonization (O'Shea and Walsh, 1996). In the following, the term cell is understood to mean a single object in a binary image (prior to segmentation), whether it be a single cell, a double cell or a mycelium.

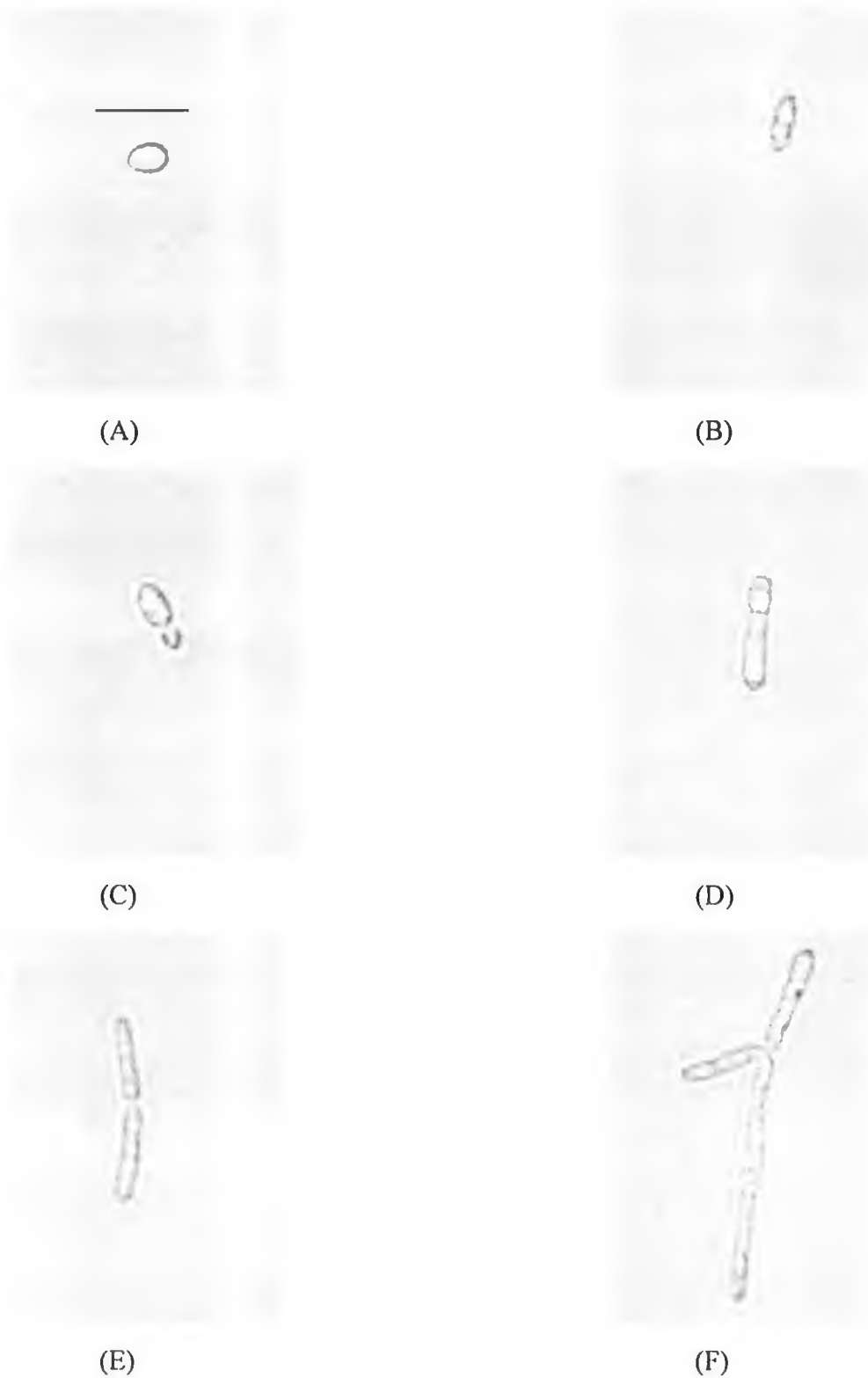


Figure 3.3 Morphological classes of *K. marxianus*. (A) yeast (B) elongated yeast, (C) double yeast, (D) filament, (E) double filament and (F) mycelium. Bar indicates 10 μm .

Two distinct geometries of cells and sub-units of cells were defined. Cells or sub-units were considered to be prolate ellipsoidal if their ratio of length to width was computed to be less than or equal to 4:1. Cells or sub-units with a length to width ratio greater than 4:1 were deemed to be cylindrical. It should be noted that the selection of the 4:1 ratio is entirely arbitrary. However, the conclusions reached in this thesis were unaffected by selecting alternative ratios in the range 3:1 to 5:1. Once a cell or sub-unit could be classified as ellipsoidal or cylindrical, its surface area and volume was calculated as described in Table 3.3. It should be noted that elongated yeast are defined as ellipsoidal cells with a length to width ratio between 2.5:1 and 4:1. This class is retained purely to remain consistent with previous work (O'Shea and Walsh, 1996).

Having computed the necessary characteristics of individual cells, the mean morphology could then be computed. The specific cell surface area was approximated using the expression

$$S_v = \frac{\sum_{i=1}^N S_i}{\sum_{i=1}^N V_i} \quad [3.9]$$

where N is the total number of cells in each image analysis sample and S_i and V_i are the surface area and volume of individual cells respectively. At least 200 cells were analysed in all cases.

The mean aspect ratio, L_{dm} , is used throughout this thesis as a simple measure of mean cell shape and is defined by the expression

$$L_{dm} = \frac{\sum_{i=1}^N L_i}{\sum_{i=1}^N D_i} \quad [3.10]$$

Table 3.3 Calculation of surface area and volume for cells of different morphology

Class	Surface area of cell/ subunit	Volume of cell/subunit
Y, EY, DY ^a	$\frac{WL\pi}{2} \left\{ \frac{\arcsin[1 - (W^2 / L^2)]^{1/2}}{[1 - (W^2 / L^2)]^{1/2}} + \frac{W}{L} \right\}$	$\frac{\pi LW^2}{6}$
F, DF ^b	$\pi W^2 + \pi W(L - W)$	$\frac{\pi W^3}{6} + \frac{\pi(L - W)W^2}{4}$
M ^c	πLW	$\frac{\pi LW^2}{4}$

^aYeast(Y), elongated yeast (EY) and each subunit of a double yeast (DY) were treated as being ellipsoidal. The cell width, *W*, and cell length, *L*, were measured directly from the images. For double yeast cells the total surface area and total volume are the sums of the surface areas and volumes of the two subunits respectively.

^b Filaments (F) and each subunit of a double filament (DF) were treated as being cylindrical with hemispherical ends. Because of cell curvature (i.e, in the same sense as a banana is curved), the true cell width, *W*, could not be measured directly. Therefore it was estimated using the expression (where *A_p* is the projected area of the cells).

$$W = \left\{ -L + \left[L^2 + 4\left(\frac{\pi}{4} - 1\right)A_p \right]^{1/2} \right\} / \left[2\left(\frac{\pi}{4} - 1\right) \right]$$

^c The mycelium (M) image was eroded to a single pixel line. The overall length was determined by dividing the measured perimeter by 2. The width was estimated by dividing the projected area by the length. End effects were neglected.

where L_i and D_i are the length and equivalent cylindrical diameter of the i^{th} cell in the sample. The equivalent cylindrical diameter (i.e. the diameter of a cylinder with the same volume and length as the cell) of a cell can be calculated from the volume using the following expression,

$$D_i = \sqrt{\frac{4V_i}{\pi L_i}} \quad [3.11]$$

The equivalent cylindrical diameter was chosen as the most appropriate universal measure of width for the range of morphological classes displayed by the culture. It obviates the need for weighting the width contribution, from the two sub-units of double cells.

3.14 Crossflow filtration

3.14.1 Culturing conditions and suspension preparation for crossflow filtration

K. marxianus was cultured in four different media. For each medium used fermentation conditions were varied to produce either 2 or 3 distinct morphologies. Three crossflow filtration runs were carried out for each distinct fermentation suspension. These were as follows: (i) cell-free spent medium, produced by collecting filtrate from dead-end filtration of *K. marxianus* suspensions, (ii) *K. marxianus* in fermentation broth, referred to as unwashed suspensions, diluted to 17.5 g/L with cell free spent medium and (iii) washed *K. marxianus* suspensions, 17.5 g/L, resuspended in 1% saline. Also non-fermented autoclaved medium was filtered for each different medium used.

3.14.1.1 Growth media used for cell suspensions filtered by crossflow filtration

K. marxianus was cultured in four different media. These were: (i) Whey based medium (20g/L lactose) as used for the dead-end filtration studies, (ii) YEPL medium (20g/L lactose) as outlined in Section 3.3.3, (iii) YEP_NL medium, identical

to the YEPL medium except with neutralised bacteriological peptone (20 g/L) (Oxoid, Basingstoke, England) instead of bacteriological peptone and (iv) Whey2, identical to (i) except with the addition of yeast extract (0.5 g/g of lactose) and ammonium sulphate (0.25 g/g of lactose) to the whey permeate, pH adjusted to pH 4.5, and boiled at 100°C for 10 minutes. The medium was again ultrafiltered and the permeate used as the medium.

3.14.1.2 Cultivation conditions

Cell suspensions were produced using three different culturing conditions: (i) batch fermentation, agitated at 800 rpm with a suspension volume of 1.1L and aerated at 1.1L/min, (yeast-like morphology), (ii) batch fermentation, agitated at 500 rpm with a suspension volume of 1.4L and aerated at 1.1L/min, (yeast-like morphology but mean cell morphology more elongated than (i)) and (iii) continuous culture agitated at 800 rpm with a reactor volume of 1L, aerated at 1L/min and a dilution rate in the range of 0.17 to 0.19 h⁻¹ (mycelial morphology).

3.14.1.3 Suspension preparation for crossflow filtration experiments

All crossflow filtration experiments were conducted with fresh *K. marxianus* cultures. Wet weight cell concentrations varied with fermentation conditions and the medium used. Prior to fermenting cell suspensions for filtration studies, trial fermentations were performed. The wet weight cell concentration of the trial fermentation was then determined as described in Section 3.8. Cell suspensions grown for filtration studies, were diluted to approximately 17.5 g/L by assuming that the wet weight cell concentration was the same as that determined for the trial fermentation. The *true* cell concentration of the cell suspensions used for crossflow filtration experiments was determined by doing wet weight analysis on the diluted suspensions. Consequently, the cell suspensions could be filtered fresh while also ensuring that the cell concentration was constant, i.e., approximately 17.5 g/L. Furthermore, the *true* cell concentration, was used in subsequent calculations for cake masses.

Cell-free spent media: Cell suspensions of *K. marxianus* were filtered using 47mm diameter, 0.45 mm Supor membranes, by dead-end filtration using vacuum. The filtrate was collected and stored at 4°C until filtered.

Unwashed suspensions of K. marxianus: Suspensions of *K. marxianus* were diluted to 17.5 g/L using cell free spent media collected from dead-end filtration of the same suspension. This was achieved by assuming the concentration of the cell suspension was the same as the trial fermentation.

Washed suspensions of K. marxianus: Again assuming the cell concentration was the same as the trial fermentation, a volume of cell suspension was vacuum filtered so as to produce a washed suspension of 1.5 L volume and a cell concentration of 17.5 g/L. After the initial filtration was complete, the filter cakes produced were washed with 1% NaCl solution. The volume of washing solution used was approximately 40-50% the original volume of suspension filtered. After the washing of the filter cakes was complete the filter cakes were then re-suspended in 1% saline. When re-suspending the filter-cakes in saline and transferring the resultant suspension to another vessel for mixing, some cell suspension is invariably lost. To account for this the cell concentration was made up to an estimated 18g/L. The actual cell concentration was determined using the wet weight technique outlined in Section 3.8.

In all cases, the pH of the suspension was adjusted to pH 7 prior to filtration.

3.14.2 Crossflow filtration module

The crossflow filtration (CFF) module consists of a stainless steel outer shell. The module holds a tubular Carbosepharose membrane (Techsep, France). The membrane was 0.40 m in length and had an inner diameter of 6 mm and an outer diameter of 9 mm. The nominal pore size of the membrane used in all experiments was 0.45 μm .

3.14.3 Crossflow filtration set-up

In Figure 3.4, a schematic flow-sheet for the crossflow filtration module is shown. Fluid is pumped through the system by a variable speed Millipore 'Easyload' peristaltic pump (Millipore, Bedford, MA). Volumetric feed flow rate through the module is controlled by adjusting the speed setting on the pump and adjusting the flow through the bypass line. The feed flow rate is monitored by a rotameter on the feed line. By controlling the flowrate of the feed flowing through the bypass line, oscillations produced in the fluid flow by the pump could be dampened, and for the filtration run an essentially steady flow could be achieved. Feed pressure, retentate pressure and filtrate pressure were monitored by bourbon pressure gauges (0 – 400 kPa). Mean transmembrane pressure drop, ΔP_{tm} , is defined as follows

$$\Delta P_{tm} = (P_{feed} + P_{ret})/2 - P_{fil} \quad [3.12]$$

where P_{feed} is the feed pressure, P_{ret} is the retentate pressure and P_{fil} is the filtrate pressure. The feed and retentate pressures and hence mean transmembrane pressure drop was controlled by adjusting valve V3, Figure 3.4. During the filtration run the temperature of the feed solution was kept at 20 ± 0.5 °C. Constant temperature was ensured by passing water, from a cooler, at 17.5 °C through a jacket in reservoir A, Figure 3.4. All suspensions in Reservoir A were mixed at 220-240 rpm throughout the filtration experiments.

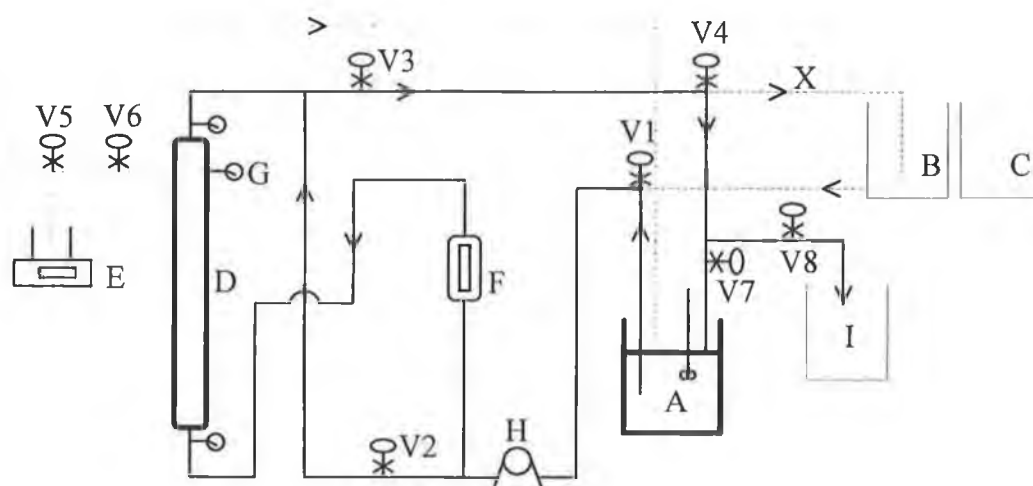


Figure 3.4 Schematic of crossflow filtration set-up. For description of parts see Table 3.4.

Table 3.4 Description of crossflow filtration set-up.

Symbol	Description
A	Jacketed vessel (Reservoir A) for cell suspensions
B	Saline reservoir (Reservoir B)
C	Reservoir C
D	Filtration module, housing tubular membrane
E	Mass balance
F	Volumetric flowmeter
G	Pressure gauges
H	Peristaltic pump
I	Waste Collection Vessel
X	Tubing
V1	3 way valve; to change feed from reservoir A to reservoir B
V2	Needle valve on bypass line; controls flowrate to filtration module
V3	Needle valve; controls transmembrane pressure
V4	3 way valve; to change retentate to reservoir B from reservoir A
V5	3 way valve; to collect filtrate samples to determine fluxes
V6	On/Off valve; for opening/closing filtrate line
V7	On/Off valve; used in combination with V8
V8	On/Off valve; used in combination with V7, Allows system to drain of fluid

3.14.5 Water source for crossflow filtration experiments

Initial, trial crossflow filtration experiments showed, that with some cell suspensions, the membrane resistance could be a large portion of the total resistance even after several hours of filtration and hence membrane fouling was an important factor. Therefore trials were conducted to compare the degree of fouling using water from different sources. Water from five sources were compared.

These were: (i) deionised (DI) water, (ii) DI water filtered through a 0.8 μ m Supor membrane, (iii) DI water filtered through a 0.45 μ m Supor membrane (iv) distilled water and (v) ultrafiltered (UF) water filtered with the Romicon ultrafilter (as described in Section 3.3.5). To determine the degree of fouling with water from different sources, batch crossflow filtration experiments were conducted. These were conducted at a crossflow velocity of 0.47 m/s and ΔP_{tm} of 100 kPa. The water was filtered in batch mode until at least 1L of filtrate was collected. The degree of fouling was determined as the percentage (%) increase in R_m after 1L of filtrate was collected. The degree of fouling by water from different sources is shown in Table 3.5. It can be seen that using UF water or distilled water results in the lowest degree of fouling. Subsequently UF water was used as the water source at all stages, e.g. media preparation, suspension washing, membrane washing, flushing, etc. Since the UF module was also used in the preparation of whey based media, it had to be thoroughly cleaned with 1% NaOH and 1% HCl before it was used to filter water.

Table 3.5 Fouling behaviour of water from different sources.

Water Source	Percentage increase in R_m after 1L water filtered
DI water	112
DI prefiltered-0.8 μ m	54
DI prefiltered-0.45 μ m	19
Ultrafiltered water	9
Distilled water	11

3.14.6 Determination of R_m

Prior to the filtration of cell suspensions, the resistance of the clean membrane was measured using 1% saline or UF water. This was done at a transmembrane pressure drop of 100 kPa and the volumetric flow rate through the module was 0.8 L/min (an inlet crossflow velocity of 0.47m/s). The clean membrane resistance was estimated to be $5.1 \times 10^{11} \text{ m}^{-1}$ and filtration experiments were conducted when the measured value was within 10% of this value.

3.14.7 Membrane cleaning

Prior to conducting crossflow filtration experiments the membrane was cleaned to ensure that the membrane resistance was within 10% of the clean membrane resistance. The membrane was cleaned with 1% NaOH followed by 2% Sodium hypochlorite, followed by 2% Nitric acid and finally 1% NaOH. Approximately 2L of washing suspension at 70-80 °C was used in each case. With each washing solution, approximately 0.5L of the cleaning agent was allowed to pass through the membrane at ΔP_{tm} of 100 kPa. Then the filtrate line was closed and the cleaning solution was allowed to circulate through the module for 15-20 minutes at $\Delta P_{tm} = 0.0$ kPa. After each cleaning agent, the membrane was thoroughly flushed with UF water. The membrane resistance was checked at the end of the cleaning process and the protocol repeated if the membrane resistance was not within the desired limits.

3.14.8 Preparation of module for crossflow filtration

When filtering suspensions of *K. marxianus*, the filtrate line and the line connecting reservoir B to valve V1 was primed with 1% saline, (Figure 3.4), and the entire system was then flushed with 1% saline. When filtering washed suspensions, the saline used was from the same batch that was used to wash and resuspend the cells. At the end of the flushing period the saline was drained from reservoir A and from the feed and retentate lines.

3.14.9 Crossflow filtration operation

A known volume of suspension, typically $1L \pm .02L$, was placed in reservoir A and mixed at a rate of 200 rpm. The filtrate valve V6 was closed and the pressure control valve V3 was fully opened ($\Delta P_{tm} \approx 0.0$ Bar). The suspension was allowed to circulate in the system for approximately 2 minutes (to allow mixing of suspension with saline trapped in the system, bends etc).

The filtration experiments were carried out at 20 °C for 2 hours in total recycle mode. However, the first 80 mL of filtrate was collected in batch mode, with filtrate readings taken every 10 to 20 mL. This ensured more datapoints could be

recorded at the start of filtration, during the period of rapid flux decline, than if total recycle mode was used. The volume collected during the initial batch period was kept sufficiently small so as not to impact filtration performance significantly. After the initial sample was collected it was returned to reservoir A and valve V5 was switched to direct the filtrate back into to reservoir A. Valve V5 was used to collect filtrate samples throughout the filtration period. After each sample was collected it was returned to reservoir A. Flux values were determined by recording the length of time taken to collect a known volume of filtrate (typically sample sizes of 10-20 mL). The transmembrane pressure was controlled using valve V3 and the flowrate of suspension through the module was controlled by adjusting valve V2.

3.14.10 Switching feed to saline and crossflow filter cake recovery

After 2 hours of filtration of washed and unwashed suspensions of *K. marxianus*, the feed was switched to saline from reservoir B, as described in Table 3.6 (steps 1 to 3). This was done to ascertain the effect that changing the feed suspension had on the filtration flux. The method described in Table 3.6 allows the feed suspension to be changed without stopping filtration. Filtration of the saline solution was carried out for a further 30 minutes.

After filtration of the saline solution was complete, the crossflow filter cake was recovered as outlined in Table 3.6 (step 5 to 16). The cake is recovered into reservoir C using saline to flush the system. Cake recovery is aided by reducing the transmembrane pressure to zero and introducing air-slugs into the system. The cake recovery process was deemed to be complete when no cells were apparent in reservoir B after step 14 and after no further improvement in the membrane resistance was observed. Note, most of the cake appeared to be recovered after two flushing stages (i.e., steps 7 to 15 done twice). Further flushing stages were required to ensure the membrane resistance had reached a constant value.

Table 3.6 Saline filtration and crossflow filtration filter cake recovery

Step	Description
1.	After 2 hours filtration, open valve V8 and close V7 allowing retentate to go to waste collection
2.	Switch feed from reservoir A to reservoir B using valve V1
3.	When the retentate is clear (approximately 1 minute), switch flow from waste collection to reservoir B using valve V4
4.	Record flux readings for further 30 minutes
5.	Stop pump
6.	Close filtrate valve V6 and reduce pressure by adjusting valve V3
7.	Place line X into reservoir C to recover cells. Pump suspension into reservoir C
8.	Stop pump
9.	Add fresh saline, approximately 200 to 300 mLs into reservoir B
10.	Flush system into reservoir C
11.	Stop pump
12.	Add fresh saline into reservoir B
13.	Place line X into reservoir B
14.	Pump suspension through system for 15 minutes approximately. occasionally letting air slugs enter the system
15.	Determine membrane resistance, by assuming the membrane resistance, R_m , is equal to the total resistance, R_T
16.	Repeat steps 7-15 until reservoir B is clear of cells after step 14 and membrane resistance is constant.

3.14.11 Determination of recovered crossflow filter cake mass

The recovered filter cake suspension (reservoir C) had a volume of approximately 1.5-3.0L. This suspension was too dilute to accurately determine the cell concentration using the method described in Section 3.8. To overcome this, a known volume of the recovered cake suspension, (200-400 mL for washed suspensions, approximately 70-100% of the suspension volume of unwashed suspensions), was concentrated using dead-end filtration, in the dead-end filtration

apparatus described in Section 3.12.2. After filtration was complete, the filter cake and membrane was carefully removed and placed in a universal. DI water was then added to the universal. The contents of the universal were then well mixed. The membrane was then removed using a forceps. The wet weight of cells in the universal was determined using the wet weight technique, described in Section 3.8. Hence the total mass of recovered filter cake can be subsequently determined.

3.14.12 Determination of filter cake mass as a function of filtration time

Prior to filtration, a known volume of a cell suspension, V_s , which has a known cell concentration, is placed in reservoir A. As described previously, the suspension is allowed to circulate in the system for approximately 2 minutes to mix saline trapped within the system with the suspension. This causes a dilution of the suspension, typically in the region of 5%. Two samples were taken from reservoir A to determine the initial cell concentration, c_i .

In total recycle filtration mode, the concentration of cell suspension in the reservoir will drop as a filter cake forms on the membrane. Therefore if the concentration of the cells in the reservoir can be determined during the filtration run it should be possible to determine the mass of cells on the membrane.

Wet weight analysis is normally used to determine cell concentration. However the volume of the sample required, 30 mL, was prohibitive. Another method for determining cell concentration was then developed. It is based on a dry to wet weight ratio for the cell suspension. For each washed suspension, the dry weight concentration was determined as outlined by O'Shea (1998) and wet weight analysis was carried out on a sample of the *K. marxianus* suspension. Therefore a wet to dry cell ratio, D_rW , could be defined as follows.

$$D_rW = \frac{c}{c_{dw}} \quad [3.13]$$

Samples of 10 mL were withdrawn from the reservoir at different intervals throughout the filtration run. The samples were placed in clean pre-dried glass bottles of known mass. The bottles were then placed in an oven at 140 °C, overnight. The amount of dry matter, M_d , in the sample is then determined gravimetrically. This dry matter also contains dry NaCl from the saline and this is accounted for when calculating c_{dw} .

$$c_{dw} = \frac{M_d}{V_{s1}} - c_s \quad [3.14]$$

In equation 3.14, V_{s1} is the volume of the sample taken for analysis and c_s is the concentration of the saline suspension used and was determined gravimetrically. By dividing the concentration of dry cell matter in the sample by the dry to wet cell ratio, the wet weight concentration can be determined using equation 3.13. The cake mass at any time can be determined by doing a mass balance for the entire system. Subsequently the difference in concentration between the sample and the initial sample (taken after circulation of suspension through the system for 2 minutes), allows the determination of the mass of cells on the membrane at the time the sample was obtained, i.e.,

$$M = V_i c_i - V_s c - \left[\sum_{N2=0}^{N2=N1-1} V_{s1}(N2) c(N2) \right] \quad [3.15]$$

In equation 3.15, V_i is the initial suspension volume. The summation term in equation 3.15 takes into account cells removed by previous samples; i.e. $N1$ is the sample number (3 or greater), $V_{s1}(N2)$ is the volume of sample $N2$, $c(N2)$ is the cell concentration of sample $N2$ where c is the cell concentration determined from equations 3.13 and 3.14. The suspension volume, V_s , at the time of taking the sample is determined from the following expression,

$$V_s = V_i - \sum_{N2=0}^{N2=N1-1} V_{s1}(N2) \quad [3.16]$$

CHAPTER 4

DEAD-END FILTRATION BEHAVIOUR OF *K. marxianus*

4.1 Introduction

While there have been many studies devoted to filtration of microorganisms in recent years, most of them have focused on the newer technique of crossflow filtration, as already outlined in Chapter 2. However, there are many factors that affect dead-end filtration behaviour including particle shape, particle size, surface properties, solute properties and membrane properties. Consequently, there remains a general lack of information on the dead-end filtration behaviour of microbial broths. In particular, the effect of cell morphology on dead-end filtration characteristics of fermentation broths has not been the subject of systematic study. However, as outlined in Chapter 2, cell morphology could potentially have an important role in filtration behaviour. Cell morphology can be expected to affect filter cake packing (Lu and Hwang, 1993; Hwang *et al.*, 1996) and consequently, filter cake voidage and specific resistance (Nakanishi *et al.*, 1987). Furthermore there is considerable evidence that filter cake compressibility is morphology dependent (Liu and Yu, 1993; Nakanishi *et al.*, 1987; Oolman and Liu, 1991). However, the reason for this is not known.

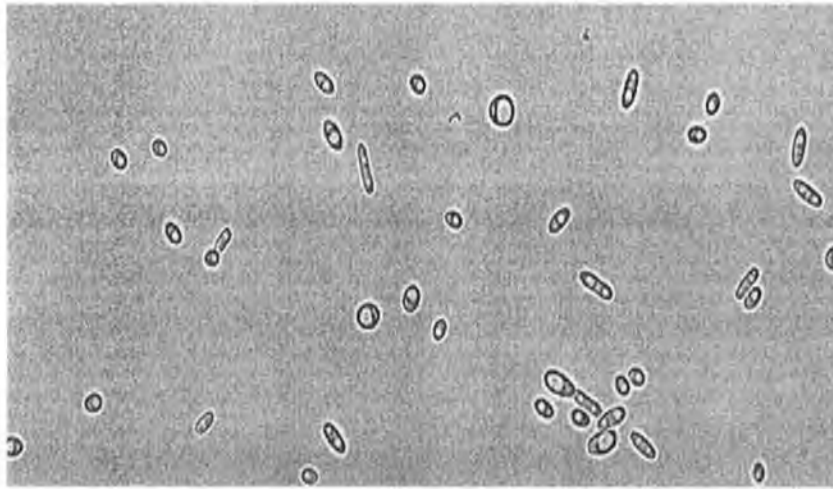
The objective of this chapter is to ascertain the contribution of cell morphology to the filtration characteristics of the dimorphic yeast *Kluyveromyces marxianus* var. *marxianus* NRRLy2415. This work describes a systematic investigation of the effect of cell morphology on the filtration behaviour using *K. marxianus* as a model microorganism. By using a single microorganism which can exhibit a variety of morphological forms, the precise effects of cell size and shape on filtration behaviour were elucidated more clearly than if a number of different microorganisms had been used.

4.2 Morphological characteristics of *K. marxianus* broths

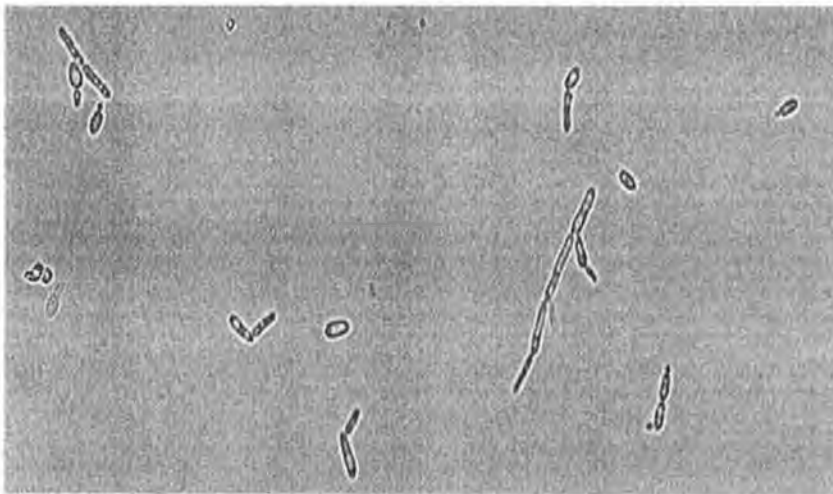
Batch cell cultures grown in Erlenmeyer flasks (1000-mL, baffled or unbaffled) employing glycerol medium were predominantly yeast-like in nature and gave mean aspect ratios, L_{dm} , ranging from 1.72 to 2.33. Higher values of L_{dm} were obtained (2.89-7.41) when the cells were grown on whey medium in batch mode in Erlenmeyer flasks (1000-mL, baffled or unbaffled) or in the 2000-mL bioreactor. When using the 2000-mL bioreactor, decreasing the agitation or aeration usually increases the L_{dm} of the fermentation broths. Continuous culture on whey medium produced L_{dm} values from 8.03 upwards. L_{dm} increases with dilution rate up to dilution rates of approximately 0.3 h^{-1} , (above this dilution rate, L_{dm} decreases) and also increases with increasing lactose concentration in the feed. A more complete analysis of the effect of growth conditions on culture morphology of *K. marxianus* is given in a related thesis (O'Shea, 1998).

Figure 4.1 shows examples of fermentation cultures with different mean cell morphology. It can be seen from Figure 4.1 that as the L_{dm} of the cell population increases the cells become more mycelial in nature. Furthermore, selected data are presented in Table 4.1 to illustrate how L_{dm} relates to the distribution of cell classes in a given broth. It is clear that low values of L_{dm} can be associated with yeast-like morphologies, while high values of L_{dm} reflect a more filamentous morphology. At intermediate values of L_{dm} , it can be seen that there is a broad distribution of cell classes within the broth. However, as will be seen in subsequent sections, a reasonably good understanding of the filtration behaviour of broadly distributed broths is possible even if one correlates data solely in terms of mean morphology parameters.

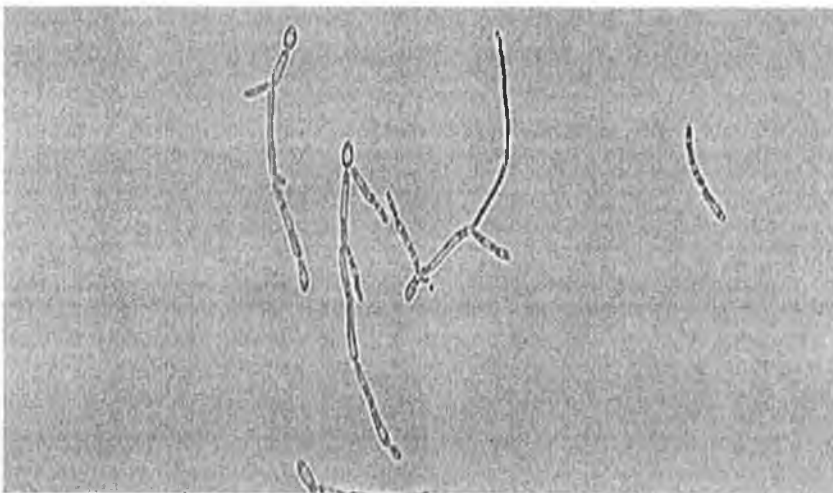
Figure 4.2 is a plot of S_v versus L_{dm} for all broths filtered. It can be seen that the broths used in this study cover a wide range of mean cell size and shape. There is a general tendency for S_v to increase with L_{dm} at low to intermediate values of L_{dm} . This is due to a decrease in cell width as the cells become more elongated. At higher values of L_{dm} (continuous cell cultures), S_v is independent of L_{dm} .



(A) $L_{dm} = 2.5$



(B) $L_{dm} = 7.5$



(C) $L_{dm} = 40.0$

Figure 4.1 Examples of three broths of *K. marxianus* and the corresponding L_{dm} value (200 X magnification).

TABLE 4.1 Distribution of cell morphologies by percentage (%) volume.

L_{dm}	Y (%)	EY (%)	DY (%)	F (%)	DF (%)	M (%)
1.94	89	5	4	0	2	0
3.63	30	9	53	5	1	2
5.39	11	12	39	3	28	7
7.41	9	7	38	4	15	27
10.0	4	10	20	6	24	36
20.1	1	2	6	11	9	71
48.4	0	0	1	1	6	92

Yeast (Y), elongated yeast (EY), double yeast (DY), filament (F), double filament (DF), mycelium (M).

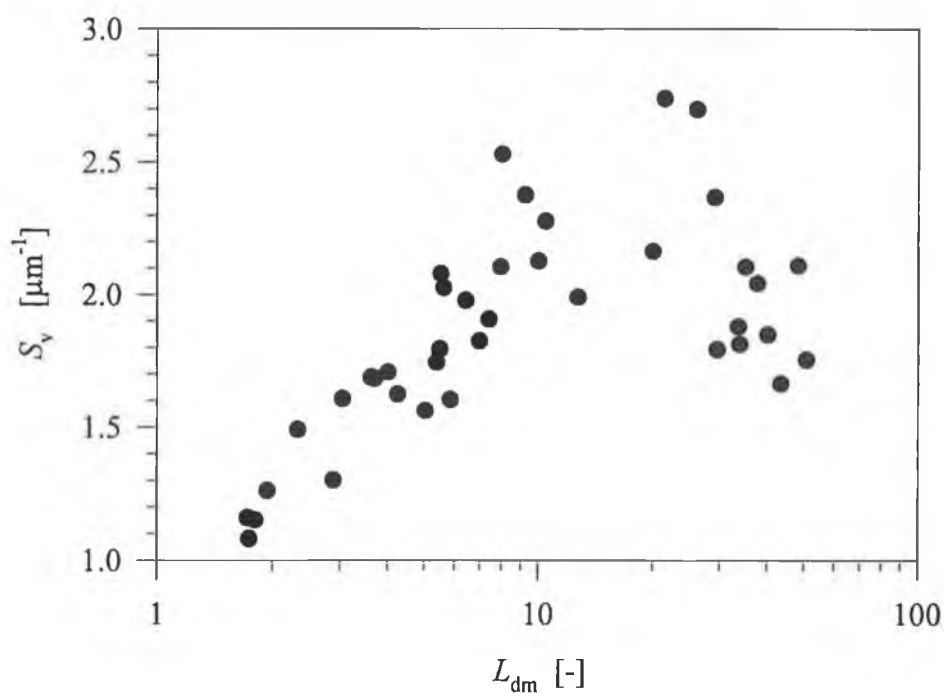


Figure 4.2 Relation between S_v and L_{dm} for all broths filtered.

For continuous cultures, cell width and hence L_{dm} is dependent on both the substrate feed concentration and dilution rate, (O'Shea *et al.*, 1998). Furthermore, when L_{dm} is in the range of 3 to 6, no anomalies are apparent in the S_v values. Therefore it appears that using two basic cell geometries of ellipsoids and cylinders with hemispherical caps is adequate in describing the geometry of the cells and sub-units.

4.3 Effect of mean cell morphology on the dead-end filtration characteristics

In this section the effect of mean cell morphology, described by L_{dm} and S_v on the filtration behaviour of *K. marxianus* will be analysed.

4.3.1 Effect of Pressure on Specific Resistance

Traditionally, the specific resistance has been correlated with pressure using a power law relationship of the form,

$$\alpha_{av} = a\Delta P^n \quad [4.1]$$

where a is a constant and n is the index of compressibility. For non microbial suspensions, which are typically filtered at higher pressures than microbial suspensions, this equation give a good description of the dependence of the specific cake resistance on pressure (Tiller *et al.*, 1987; Wakeman *et al.*, 1991a). For microbial suspensions, typically filtered at lower pressures (<200 kPa), plots of $\log(\alpha_{av})$ versus $\log(\Delta P)$ are generally non-linear. Nevertheless, attempts have been made to fit equation 4.1 to the data at the higher end of the pressure range (e.g. Nakanishi *et al.*, 1987; Tanaka *et al.*, 1994a).

Typical log-log plots of α_{av} versus ΔP , for three suspensions of *K marxianus* of different morphology, are shown in Figure 4.3. In Figure 4.3, it can be seen that these plots are non-linear and thus a power-law relationship is inadequate at describing the relationship between α_{av} and ΔP over the entire range of pressure used in this study. Furthermore, it was found to be difficult to fit equation 4.1 to a

linear portion of the curve in a consistent manner. Figure 4.4 shows the data shown in Figure 4.3 re-plotted on a linear scale. There is clearly a linear relationship between α_{av} and ΔP . For all mean morphologies examined the linear relationship was found to exist. The linear relationship can be applied to the entire range of pressures used in this study (i.e. 20-200 kPa).

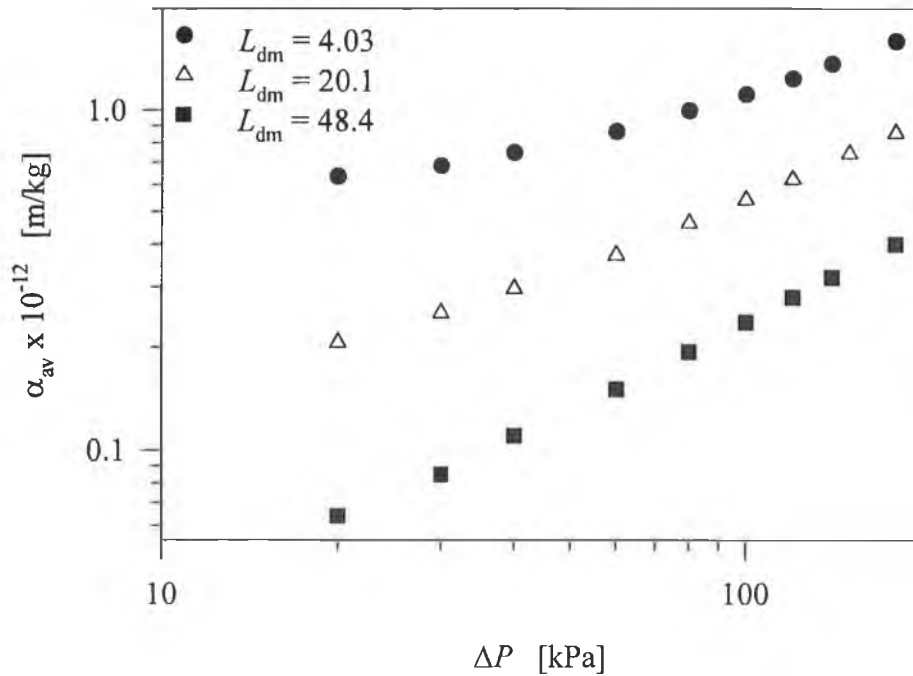


Figure 4.3 $\text{Log}(\alpha_{av})$ versus $\text{Log}(\Delta P)$ for three different cell morphologies.

A linear relationship between α_{av} and ΔP has been shown to occur when filtering *E. coli* suspensions for pressures up to 100 kPa (Riesemeir *et al.*, 1989). More recently a linear relationship was found to exist between α_{av} and ΔP for a number of yeast suspensions, (Tanaka *et al.*, 1997). In this study the relation between α_{av} and ΔP is written as follows;

$$\alpha_{av} = \alpha_o (1 + k_c \Delta P) \quad [4.2]$$

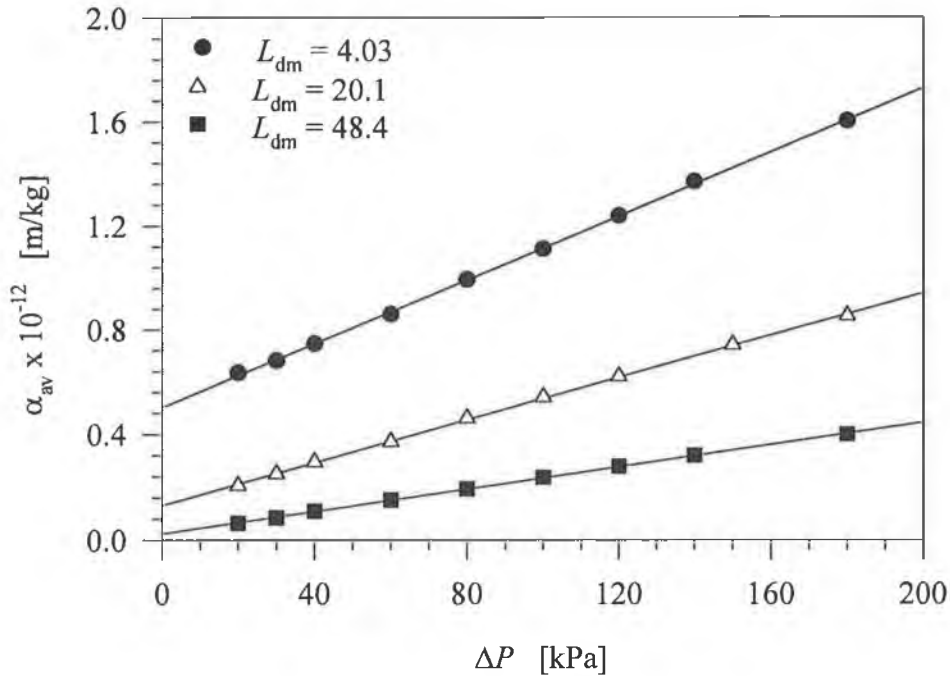


Figure 4.4 α_{av} versus ΔP plotted on a linear scale. Lines: linear regression through data.

Assuming the linearity holds as ΔP approaches zero, the constant α_0 represents the specific resistance of the unstressed cake. The coefficient, k_c , is a measure of cake compressibility, i.e. when k_c is zero the filter cake is incompressible and increasing values of k_c represents increasing filter cake compressibility. For all broths, the specific resistance of an unstressed cake, α_0 , is determined from the intercept of linear plots of α_{av} versus ΔP and the coefficient of compressibility, k_c , is determined from the slope divided by the intercept, α_0 .

For each fermentation broth filtered, equation 4.2 successfully describes the specific resistance and applied pressure relationship. Therefore it should be possible to simplify the analysis of the filtration data by correlating the cell morphology with the unstressed resistance and compressibility separately. This approach is taken in the following sections.

4.3.2 Effect of cell morphology on unstressed cake resistance

Correlation of filtration data with cell morphology requires consideration of both cell size and cell shape. At zero pressure, it is reasonable to correlate specific resistance data using the Kozeny-Carman equation (Grace *et al.*, 1953). Since S_v is not constant and independent of L_{dm} , as seen in Figure 4.2, equation 2.6 can be rearranged to give

$$\frac{\alpha_o \rho_c}{S_v^2} = \frac{k_o [1 - \epsilon_o]}{\epsilon_o^3} \quad [4.3]$$

Figure 4.5 shows a plot $\alpha_o \rho_c / S_v^2$ versus L_{dm} . By plotting the unstressed specific resistance in this way it is possible to account for variation in S_v with L_{dm} . The pressure that the filter cake is formed at does not appear to significantly affect the unstressed specific resistance and L_{dm} relationship. It can be seen that as L_{dm} increases, $\alpha_o \rho_c / S_v^2$ decreases. Equation 4.3 suggests that the unstressed filter cake voidage increases with increasing L_{dm} . Therefore it appears that when filtering *K. marxianus*, yeast like morphologies form tightly packed cakes, whereas more mycelial-like morphologies form more porous filter cakes. This is in agreement with the packed bed studies of Zou and Yu (1996a), who showed that the voidage of a packed bed of cylindrical particles increases as the aspect ratio of the particles in the bed increases. It is also in agreement with theoretical simulations of Hwang *et al.* (1996), where it was shown that the voidage of the filter cakes comprised of ellipsoidal particles increases as the aspect ratio of the particles increases.

It was not feasible to determine the voidage of the filter cakes produced in this study. Therefore, in order to validate the hypothesis that increasing L_{dm} results in increasing filter cake voidage, the voidage of centrifugation pellets was studied.

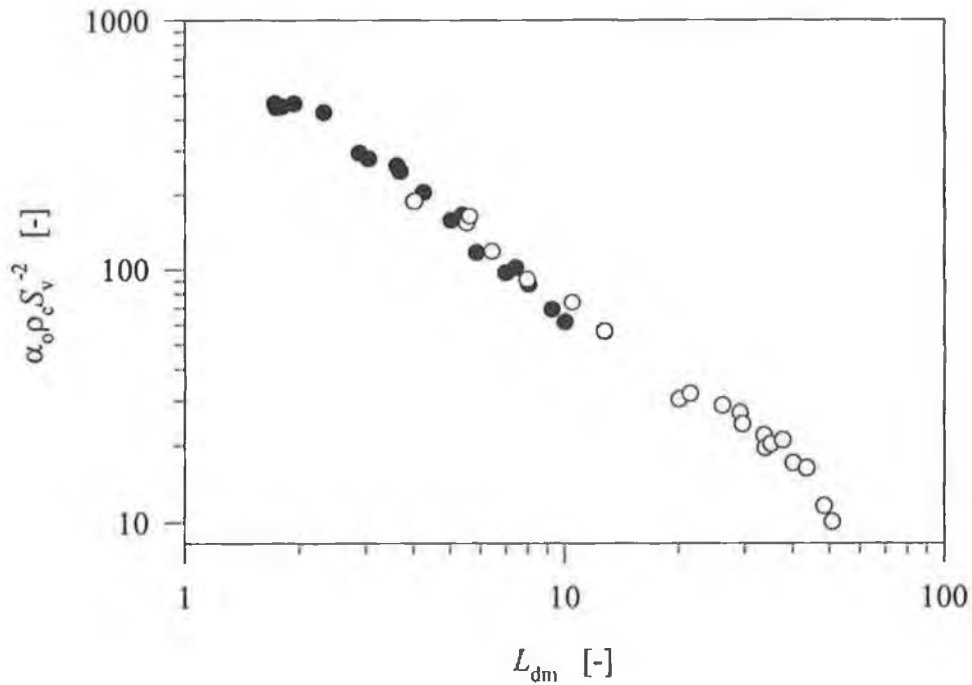


Figure 4.5 $\alpha_0 \rho_c / S_v^2$ versus L_{dm} for all broths filtered. Symbols: ● Filter cakes formed at 30 kPa and ○ Filter-cakes formed at 20 kPa.

4.4 The effect of L_{dm} on centrifugation pellet voidage

Figure 4.6 shows the variation in voidage of centrifugation pellets, formed at 3500 rpm, with L_{dm} . It can be seen that as L_{dm} of the fermentation broths increases the voidage of the centrifugation pellets increases. This trend is in qualitative agreement with the observed decrease in $\alpha_0 \rho_c / S_v^2$ with L_{dm} . Furthermore it is in qualitative agreement with the computer simulations of Nolan and Kavanagh (1993) and packed bed data of Zou and Yu (1996a). Therefore it would appear the cells in the centrifugation pellet pack in a random manner.

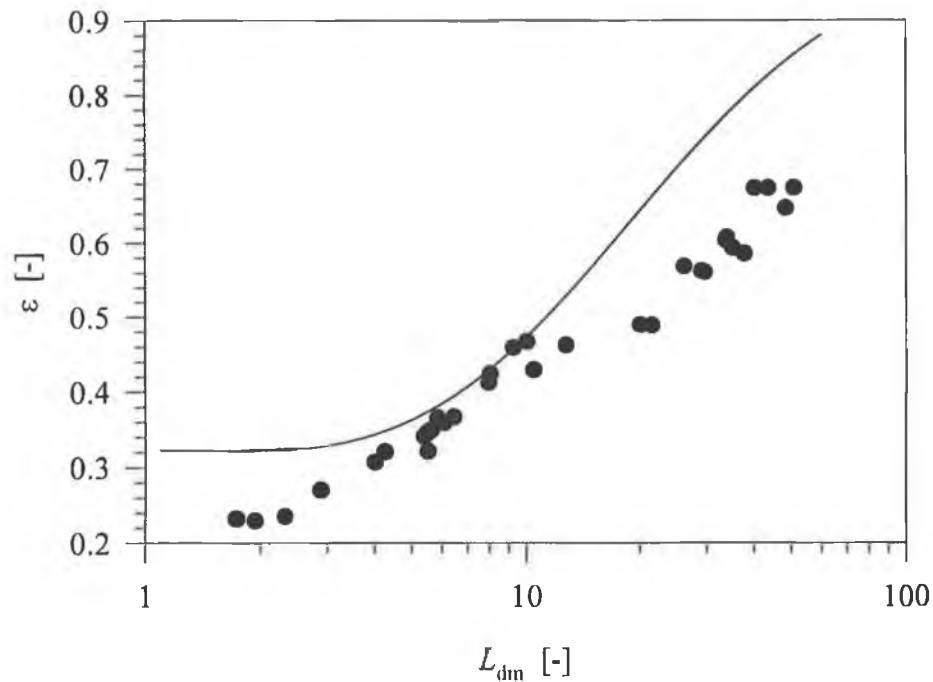


Figure 4.6 Voidage of cell pellets formed at 3500 rpm as a function of L_{dm} . The solid line represents Zou and Yu's (1996a) correlation for random close packing of cylinders.

The solid line in Figure 4.6 represents Zou and Yu's (1996a) correlation for random close packing of cylinders. It can be seen that the predicted voidages are lower than those predicted by packing theory. This is in agreement with the experimental results of Ju and Ho (1988) who determined voidages of centrifugation pellets formed from microorganisms of different morphology. The authors in that study attributed the lower than predicted voidages to compression of the centrifugation pellets. It should be noted that during centrifugation, the pellet is subjected to substantial compressive pressure, (Zydney and Colton, 1989), hence the lower pellet voidages. Therefore the effect of centrifugation speed on pellet voidage was studied for a wide range of morphologies.

4.4.1 The effect of centrifugation speed on pellet voidage

The compressive pressure exerted on the centrifugation pellet will increase with centrifugal force. Hence the compressive pressure exerted on the pellet will increase with centrifugation speed. Figure 4.7 shows the effect of centrifugation speed on pellet voidage for selected morphologies. It can be seen from Figure 4.7, that in all cases, increasing centrifugation speed causes a reduction in pellet voidage. The change in pellet voidage with centrifugation speed becomes more pronounced as the L_{dm} value of the cell population increases. The solid lines in Figure 4.7 are linear regression lines through the data. It can be seen that the decrease in pellet voidage with centrifugation speed is approximately linear.

There are a number of points worth noting. Firstly it should be noted that the compressive pressures exerted on the pellets at any speed will vary depending on the size of the pellet formed, i.e. the cell morphology and biomass of the broth. Larger pellets of the same suspension (obtained by centrifuging more biomass) are subjected to greater compressive forces than smaller pellets and thus will have a smaller average voidage (Zydney and Colton, 1989). It should be noted that for each morphology shown on Figure 4.7, the amount of cell suspension centrifuged at each speed varied by no more than 5%, therefore the decrease in voidage can be attributed solely to increased compressive pressure brought about by increased speed.

Pellets formed with suspensions of high L_{dm} were invariably larger than those with low L_{dm} despite similar biomass concentrations. In most cases, this was due to higher pellet voidage. Consequently, pellets formed from mycelia suspensions experienced higher compressive pressures than yeast like suspensions. This may explain why at high L_{dm} the measured voidages at 3500 rpm are much lower than those predicted by theory, as seen in Figure 4.6.

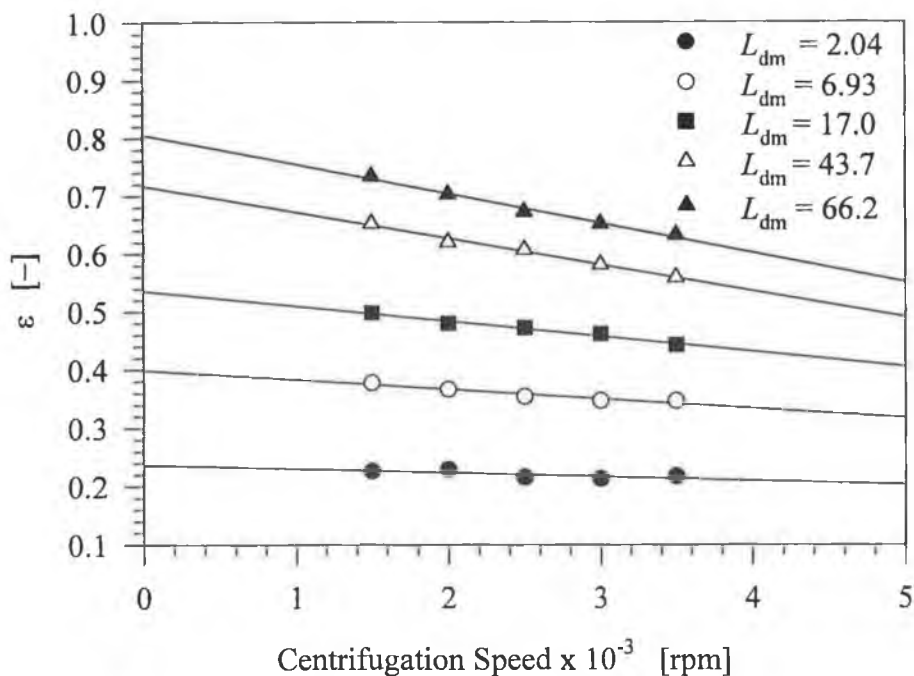


Figure 4.7 Variation in pellet voidage with centrifugation speed. Lines represent linear regression through the data.

Finally it should be noted that when the cell biomass was determined at 1500 rpm and 3500 rpm, the predicted cell concentrations were in excellent agreement with each other for all morphologies. This suggests that the decrease in cell voidage with centrifugation speed is not due to a reduction in cell volume.

4.4.2 Time dependent decompression of centrifugation pellets

In Figure 4.8, the effect of the time delay in decanting the supernatant for a mycelial suspension, (time defined as the time after the centrifuge has slowed down to zero), on the pellet voidage is shown. It can be seen that the apparent pellet voidage increases the longer the supernatant is allowed in contact with the pellet after centrifugation. It should be noted that for yeast like suspensions it was not possible to show a similar effect. This can be attributed to the fact that yeast pellets are only slightly compressible, as seen in Figure 4.7.

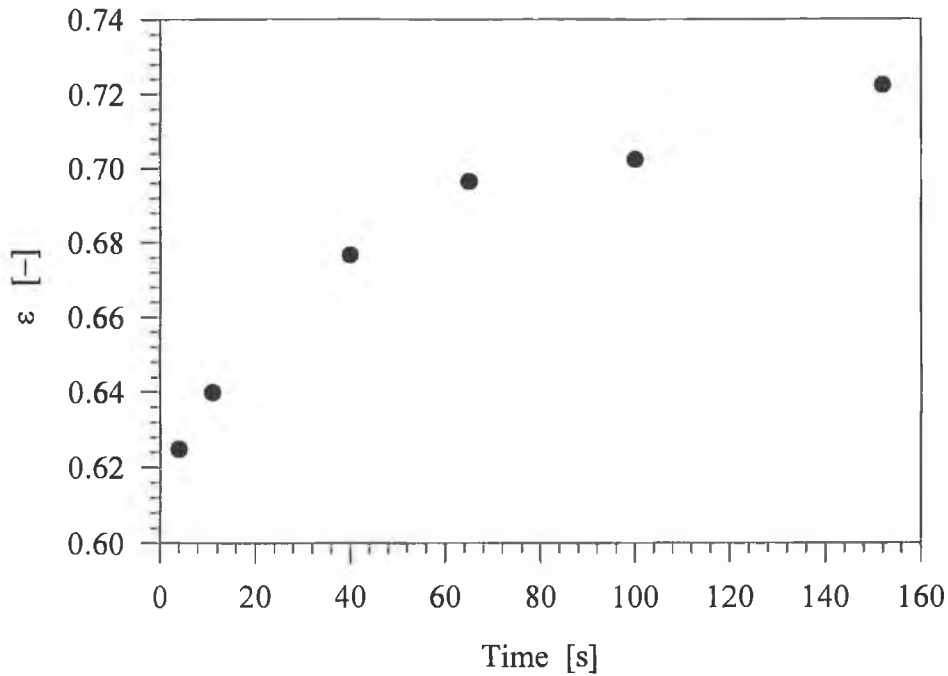


Figure 4.8 The effect of time delay in decanting the supernatant on pellet voidage. $L_{dm} = 66.2$, pellet formed at 3500 rpm.

The pellets appear to decompress if allowed to contact with the supernatant (They may continue to decompress after removal of supernatant and the voids may become filled with air rather than fluid. In this instance, no increase in pellet weight, hence voidage would be detected). If the pellet was left in contact with the supernatant long enough it may fully decompress. However, it should be noted that if left together for a long period of time, cells will tend to lift off when the supernatant is poured off. Due to this, a small fraction of the cells were lost for the last two samples in Figure 4.8. Therefore, it is not possible to continue to do this analysis indefinitely. Also it should be noted that it takes approximately 35 seconds for the centrifuge to slow down from 3500 rpm to zero, therefore decompression of the pellet may already have taken place before the centrifuge stops.

Thus it may not be accurate to relate the measured voidage to the compressive pressure at a particular speed. It should be noted the voidage data presented in Figure 4.6 and Figure 4.7 was taken as the average from two centrifuge tubes, where the supernatant was poured off, after less than 8 (approximately) seconds in contact with the pellet, after the centrifuge had stopped.

4.4.3 Determination of the voidage of an unstressed centrifugation pellet

If a relationship can be established between unstressed pellet voidage and L_{dm} , then it should be possible to determine the Kozeny constant from the filtration data and equation 4.3. In Figure 4.7, it can be seen that the dependence of pellet voidage on centrifugation speed is approximately linear. Extrapolation of the relationship to zero compressive pressure, i.e., zero speed, should give the value for the unstressed pellet voidage. However, there is potentially scope for large errors, in particular with cell suspensions of high L_{dm} as these suspensions display the greatest change in voidage with change in centrifugation speed.

The 'water drop test' was developed to determine the unstressed pellet voidage formed from cultures of high L_{dm} . The precise experimental procedure has been outlined in Chapter 3. The test is based on the pellets decompressing when the centrifugation is complete as discussed in the previous section. It was discovered that after the supernatant was removed and the interior of the tube wiped, the pellet readily absorbed water added to the tube. It is assumed that when the pellet stops absorbing water, the pellets are completely decompressed and all the voids are filled with water. The test was only used with morphologies with high L_{dm} because for more yeast-like suspensions the pellets undergo only slight compression and, as a result, water absorption was not found to occur. However, it may be possible to apply this method to yeast-like morphologies if much larger centrifugation pellets are obtained.

Results of the water drop test are shown in Figure 4.9. In Figure 4.9, it can be seen that the extrapolated unstressed pellet voidage is in excellent agreement with the unstressed pellet voidage determined by the 'water drop test'. For cell populations of low L_{dm} , extrapolation of the relationship to zero speed is unlikely to cause significant error because the pellet voidage is only slightly reduced by increasing the centrifugation speed. Therefore it is assumed that the unstressed pellet voidage can be determined for all morphologies by extrapolating the voidage data obtained from 1500 to 3500 rpm.

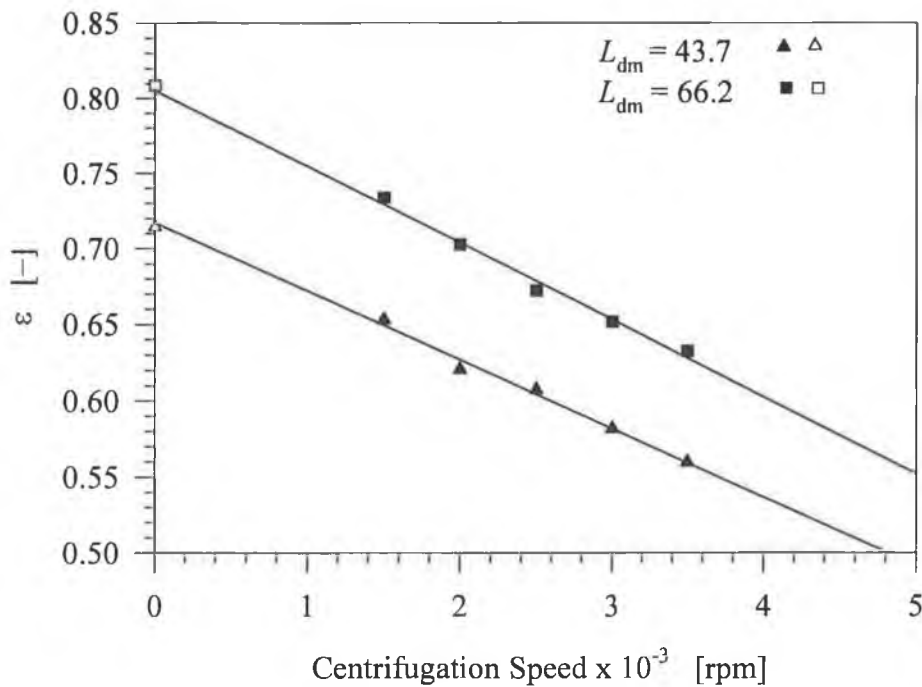


Figure 4.9 Water drop test results. Lines represent linear regression of data between 1500-3500 rpm. Open symbols represent voidages determined by water drop test. Closed symbols represent voidages determined by the standard method as described in section 3.11.1

4.4.2 The relationship between unstressed pellet voidage and L_{dm}

The unstressed pellet voidage was determined for a number of suspensions covering a large range of mean cell morphology. The results are shown in Figure 4.10. Also shown on Figure 4.10 are the pellet voidages determined at 3500 rpm. It can be seen that, at low L_{dm} , the unstressed pellet voidage is similar to that of pellets formed at 3500rpm. As L_{dm} increases the difference between the null stress voidage and that of pellets formed at 3500rpm increases. Furthermore the null stress voidage is in excellent agreement with the correlation of Zou and Yu (1996a) for random packing of monodisperse cylinders at intermediate values of L_{dm} . At high values of L_{dm} the extrapolated null stress voidage is slightly lower than that predicted by the correlation of Zou and Yu (1996a). This may be due to the high degree of branching of these cultures or due to the broad distribution of mycelia that are in these suspensions.

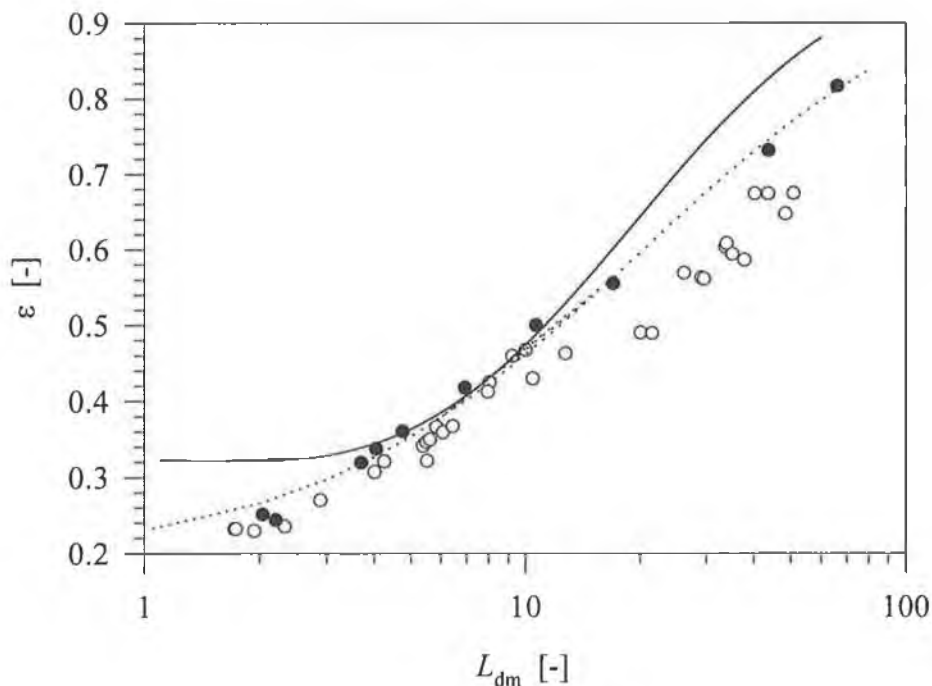


Figure 4.10 Relationship between voidage and L_{dm} . Closed symbols: unstressed voidage; open symbols: voidage at 3500 rpm; Solid line: correlation of Zou and Yu (1996a); dashed line: equation 4.4.

At low values of L_{dm} , there is considerable discrepancy between Zou and Yu's (1996a) correlation and the experimental data here. Furthermore, it should be noted that cell suspensions at low L_{dm} are predominantly yeast-like and therefore tending to be near spherical in geometry. The voidage of close randomly packed beds of spheres is approximately 0.38 (Nolan and Kavanagh, 1993), which is considerably larger than the voidage of cylinders with low L_{dm} ($L_{dm} \approx 0.3$). Therefore the discrepancy between theoretical and experimental voidage is even greater than shown in Figure 4.10.

However, similarly low pellet voidages have been measured by Ju and Ho, (1988) for suspensions of *Saccharomyces cerevisiae*. Furthermore recent work by Tanaka *et al.* (1997) estimated the null stress voidages of filter cakes using the Kozeny-Carmen equation, for a number of different yeasts, and predicted voidages between 0.2-0.4. In the former case, it was suggested that the lower than expected voidages was due to compression, however, compression is accounted for in Figure 4.10.

One possible explanation for the lower than expected voidage is presence of carbon dioxide bubbles on the surface of the cells that would reduce the pore liquid volume (Ofthsun, 1989). It is probable however, that the washing stages during the biomass determination will have significantly reduced the presence of such bubbles. However, a thorough analysis of this problem is a suitable subject for further study.

Another possible reason for the reduced voidage may be that the suspensions are polydisperse. It has been demonstrated experimentally (Wakeman, 1975) and by computer simulation (Nolan and Kavanagh, 1993), that polydispersity leads to reduced voidage in packed beds. All the broths used in this study exhibit a degree of polydispersity. However, the problem of polydispersity in this instance is rather complex, as cell populations have distributions of both cell size and cell shape. Therefore it is difficult to ascertain how exactly polydispersity may impact on the filtration data here.

For convenience and for calculations in the next section the following best-fit curve was obtained to relate unstressed pellet voidage to L_{dm} :

$$\varepsilon_o = 1 - \frac{1}{1.24 + .062L_{dm}} \quad [4.4]$$

A correlation coefficient, R^2 , of 0.995 was obtained.

4.5 Calculation of the Kozeny constant

Figure 4.11 shows the unstressed cake resistance data already shown in Figure 4.5. The dashed line on Figure 4.11, is the prediction of the Kozeny-Carman equation, equation 4.3, a Kozeny constant of 5.0 and the voidage data predicted by equation 4.4. It can be seen that the model prediction is in good qualitative agreement with the observed experimental behaviour. The solid curve in Figure 4.11 represents a fit of the Kozeny equation with k_o allowed to vary according to the equation,

$$k_o = 10.1 + 0.34L_{dm} \quad [4.5]$$

This expression was obtained by computing the Kozeny constant based on a voidage predicted by equation 4.4 and the measured value of $\alpha_o\rho/S_v^2$ for each individual filtration experiment and obtaining the best-fit line as indicated in Figure 4.12. It can be seen from Figure 4.12 that Kozeny constants of 10 to 30 are predicted. These values are significantly higher than the often reported value of 5 ± 0.5 (Grace, 1953). However, there is evidence of k_o varying outside the narrow range of 5 ± 0.5 for fungal suspensions (Oolman and Liu, 1991; Liu and Yu, 1993). The tendency for k_o to increase as the filter cakes become more porous (i.e. L_{dm} increasing), is also consistent with these authors findings.

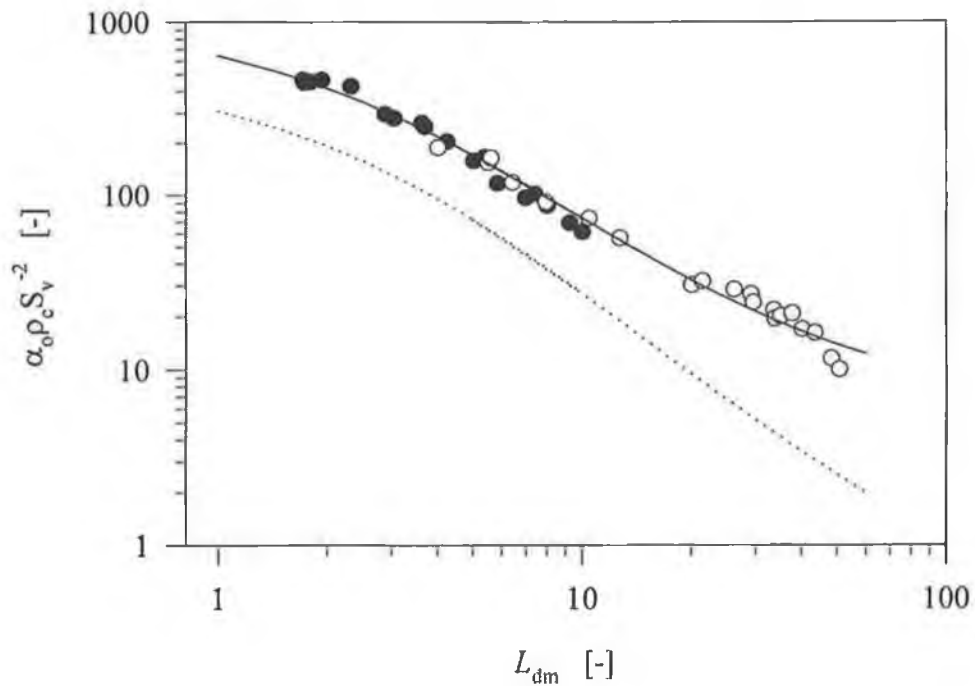


Figure 4.11 $\alpha_0 \rho_c / S_v^2$ versus L_{dm} for all broths filtered. Lines: — Kozeny-Carman equation, with k_0 varying according to equation 4.5 and Kozeny-Carman equation with $k_0 = 5.0$.

Furthermore it is commonly accepted that k_0 is dependent on voidage. One such relationship that relates k_0 with voidage can be expressed as (Happel and Brenner, 1965)

$$k_0 = \frac{2\varepsilon^3}{(1-\varepsilon) \left[\ln \left\{ \frac{1}{1-\varepsilon} \right\} - \frac{(1-[1-\varepsilon]^2)}{(1+[1-\varepsilon]^2)} \right]} \quad [4.6]$$

Also shown in Figure 4.12 is a plot of k_0 versus L_{dm} based on equation 4.6. It can be seen that the results presented here are in good qualitative agreement with those predicted by equation 4.6. However, the magnitude of k_0 determined experimentally is significantly larger than predicted.

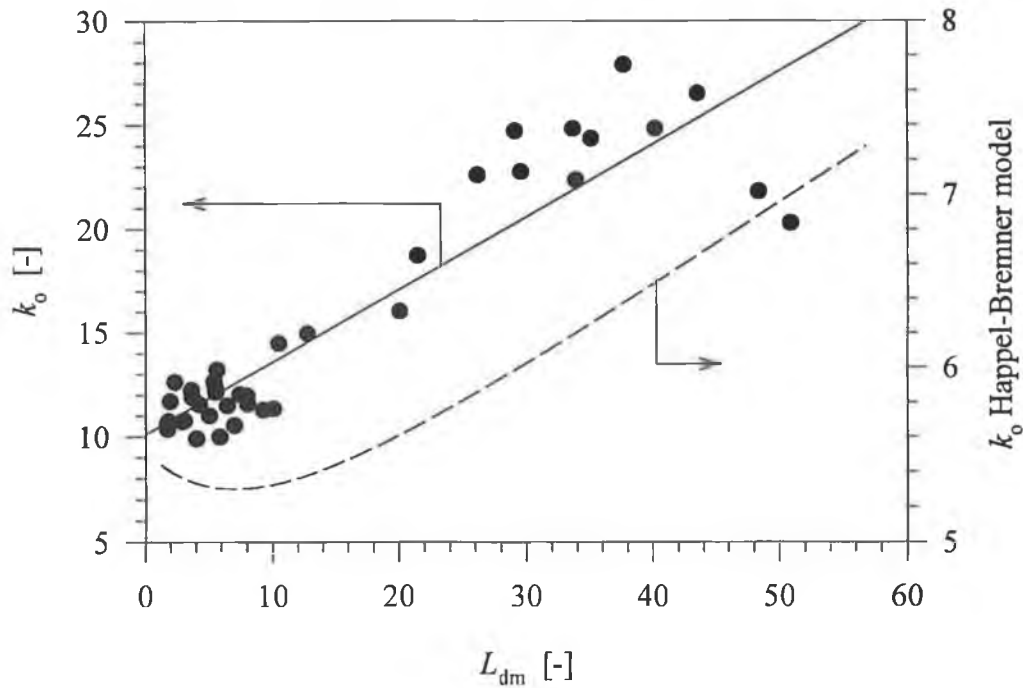


Figure 4.12 Relationship between the Kozeny constant and L_{dm} . Lines: — linear regression through data and ---- Happel-Brenner model.

One reason for this may be due to the distribution of morphology of the samples filtered. The Kozeny-Carman equation is based on the Poiseuille equation using an average pore size (Free *et al.*, 1998). However, when the particles have a size distribution, the pore sizes can vary substantially. Recent work by Free *et al.*, (1998) showed that Kozeny's constant increases with particle size distribution. Therefore the higher than expected values for k_0 may be due to the fact that all suspensions of *K. marxianus* filtered had a significant size distribution.

Obviously any difference between the predicted null stress voidage and the true null stress voidage could impact greatly on the calculation of k_0 . For instance, if ϵ_0 was slightly overestimated, then the subsequent values of k_0 would be significantly over-predicted. Alternatively the voidage of the filter cakes produced may be slightly different to pellets formed by centrifugation. This could occur if cells become aligned in the direction of fluid flow during filtration as was shown to occur with *E. coli* cells immobilised on a membrane (Fowler and Robertson, 1991). Therefore the results produced here should be considered more for the qualitative behaviour than quantitative.

4.6 Effect of mean morphology on filter cake compressibility

Figure 4.13 illustrates the relationship between the coefficient of compressibility, k_c and L_{dm} . It can be seen that as the mean cell morphology becomes more elongated, the coefficient of compressibility, k_c , increases. The tendency for cake compressibility to increase as the cells become more elongated has been observed previously for yeast and bacterial suspensions (Nakanishi *et al.*, 1987; Tanaka *et al.*, 1994). In addition, the increase of cake compressibility with cake voidage has been observed for fungal suspensions (Liu and Yu, 1993; Oolman and Lu, 1991). Furthermore it has been shown that the index of compressibility, n (equation 4.1), increases with ϵ_o (Tiller and Kwon, 1998).

The dependence of compression on morphology can also be seen in Figure 4.7. There it can be clearly seen that the decrease in voidage with centrifugation speed becomes greater as L_{dm} increases, i.e. greater compression. Therefore the centrifugation studies appear to 'mirror' the filtration studies.

Although the relationship between cell morphology and compressibility is well defined in this case, the reason for this is not known. This is fundamentally due to the lack of research into the mechanism of microbial filter cake compression. With inorganic suspensions compression is usually due to the breakdown of aggregates (Tiller *et al.*, 1987). Aggregated particles form more porous cakes that are more susceptible to compression than cakes formed by freely dispersed suspensions. However, in the study here, the cells were freely dispersed. Furthermore the centrifugation studies suggest that the pellets pack in a dense random manner. Therefore if filter cakes pack in a similar manner to the centrifugation pellets, the voidage can only be reduced by (1) rearrangement of the cells in the filter cake to form a more densely packed structure, or (2) deformation of the cells into the voids in the cake, thus reducing cake voidage. The latter could be accompanied by increases in S_v if the cell volume or shape changes significantly. In the case of the former, it is difficult to envisage the particles having sufficient space to move to reduce the voidage significantly, as the filter cake is assumed to be densely packed.

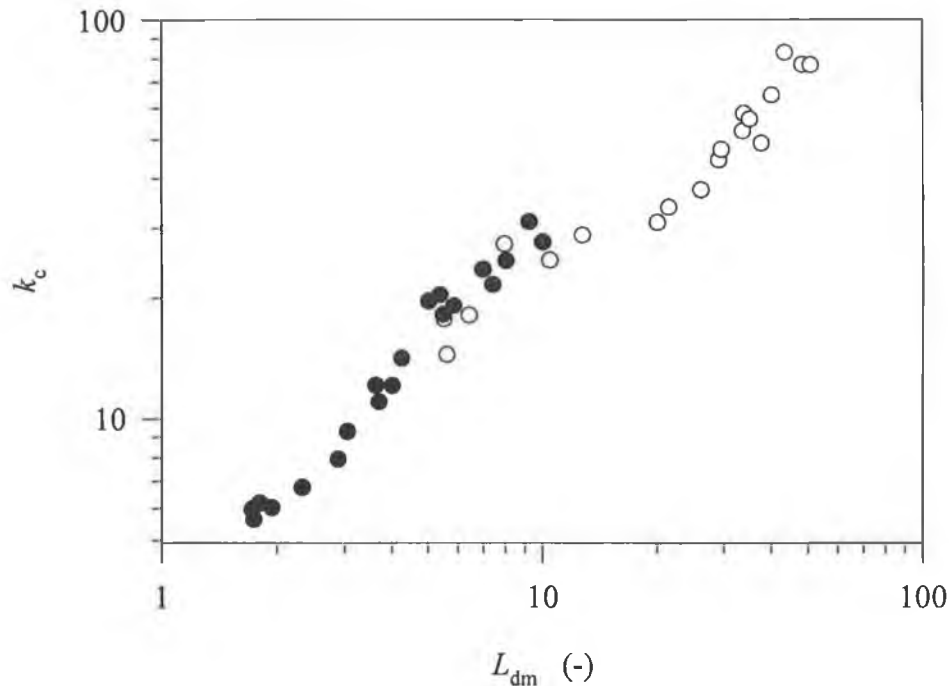


Figure 4.13 Compressibility coefficient, k_c , versus L_{dm} . Symbols: ● filter cakes formed at 30 kPa and ○ filter cakes formed at 20 kPa.

In particular the centrifugation studies suggest dense random packing is occurring as shown in Figure 4.6 and Figure 4.10, as the measured voidages are less than those predicted for dense random packing by Zu and Yu's (1996a) correlation for packed beds of cylindrical particles. It is possible that some bridging structures within the filter cake will collapse as the pressure is increased. This mechanism would most likely be irreversible. Compression reversibility will be dealt with in more detail in Chapter 5.

In the case of the cell deformation causing cake compression, there are conflicting reports about the deformability of microbial cells. Hodgson *et al.*, (1993) suggests that the cell wall will not deform under filtration pressures as yeast and bacteria cells are able to maintain osmotic pressure across the wall of the cells an order of magnitude greater than filtration pressure. However, the authors in that case suggest that deformation of the extracellular matrix of bacterial cells may be possible. Since *K. marxianus* does not have an extracellular matrix this can be

ruled out as a cause for compression. Alternatively scanning electron micrographs by Kawakatsu *et al.* (1993) suggest deformation of yeast under filtration pressure. However, the evidence presented in that case did not show conclusively that deformation was occurring.

An alternative mechanism of compression may occur here. It may be that deformation may be principally restricted to the region of cell wall connecting the mother and daughter cells, i.e. regions of budding or hyphal extension. Shown in Figure 4.14 are images of a mycelial cell undergoing deformation. The samples were viewed under a microscope and the images were captured using the image analysis system. The cells studied were situated near an air bubble. The sequence in which the images were taken was A-B-C-D-E-F. The deformation is caused by constriction of the aqueous phase over time, due to evaporation. When the liquid/air interface comes into contact with the cell, a force due to the water surface tension is exerted on the cell. It was not possible to determine the magnitude of this force. It can be clearly seen that the sub-unit, which first comes into contact with the liquid/air interface, is pulled back so as to straighten out the whole cell. Essentially it appears that the cell wall at the mother/daughter joint behaves like a hinge.

A further example of this is shown with a more elongated mycelium, in Figure 4.15. The sequence in which the images were taken was A-B-C-D. Here it can be clearly seen the 'hinge like' compression occurs at a branching point. In fact there appears to be greater compression at the branch point than at the join of the two sub-units in a chain. The sub-unit joins can be seen on the left of the images. Therefore the cell wall deformation is possibly greater at branch points than at contact points when the sub-units are in a chain. It should be noted that branching only becomes significant once L_{dm} reaches approximately 20.0.

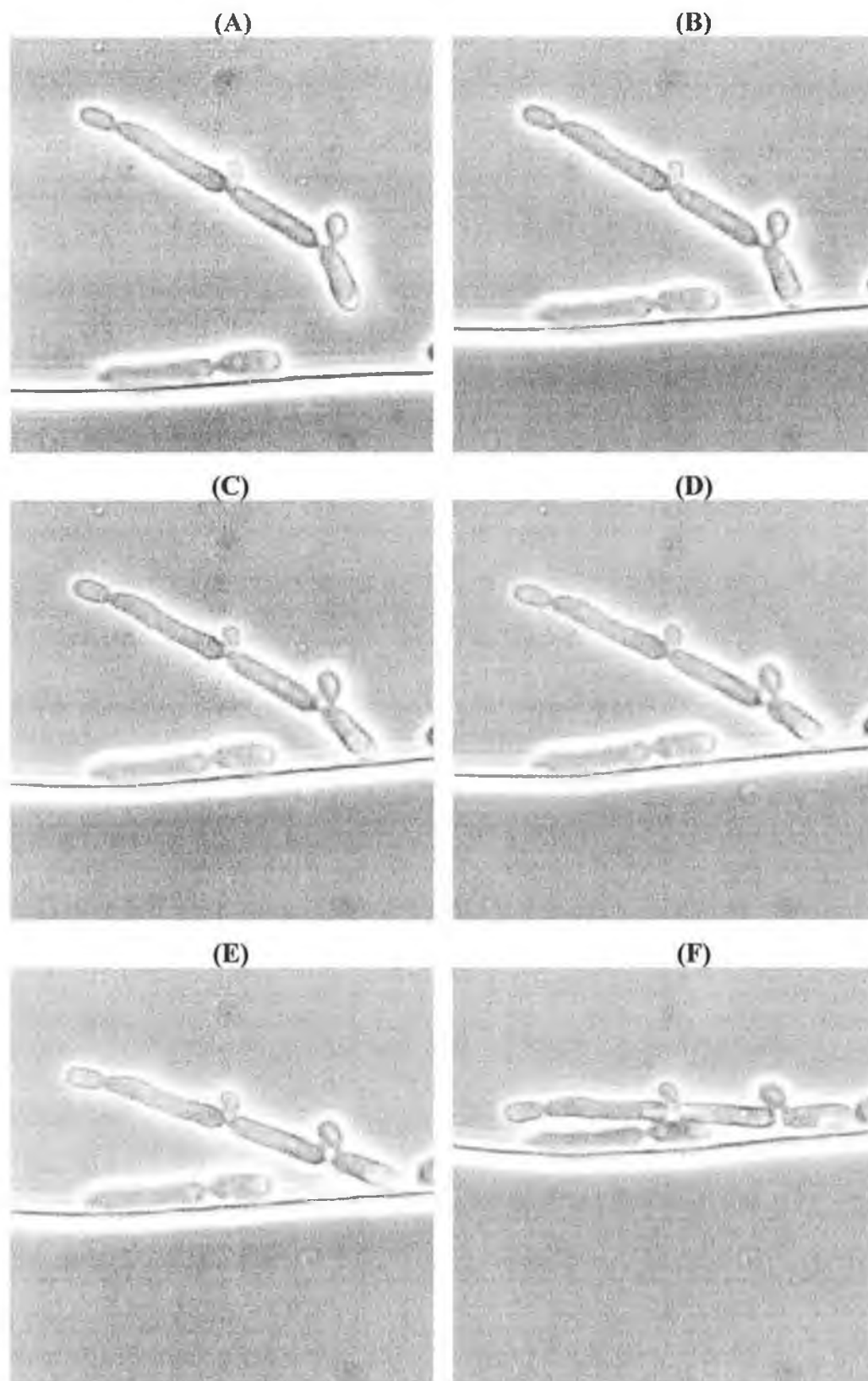


Figure 4.14 Example of 'Hinge compression' of a mycelium cell. (Magnification factor of 400 X)

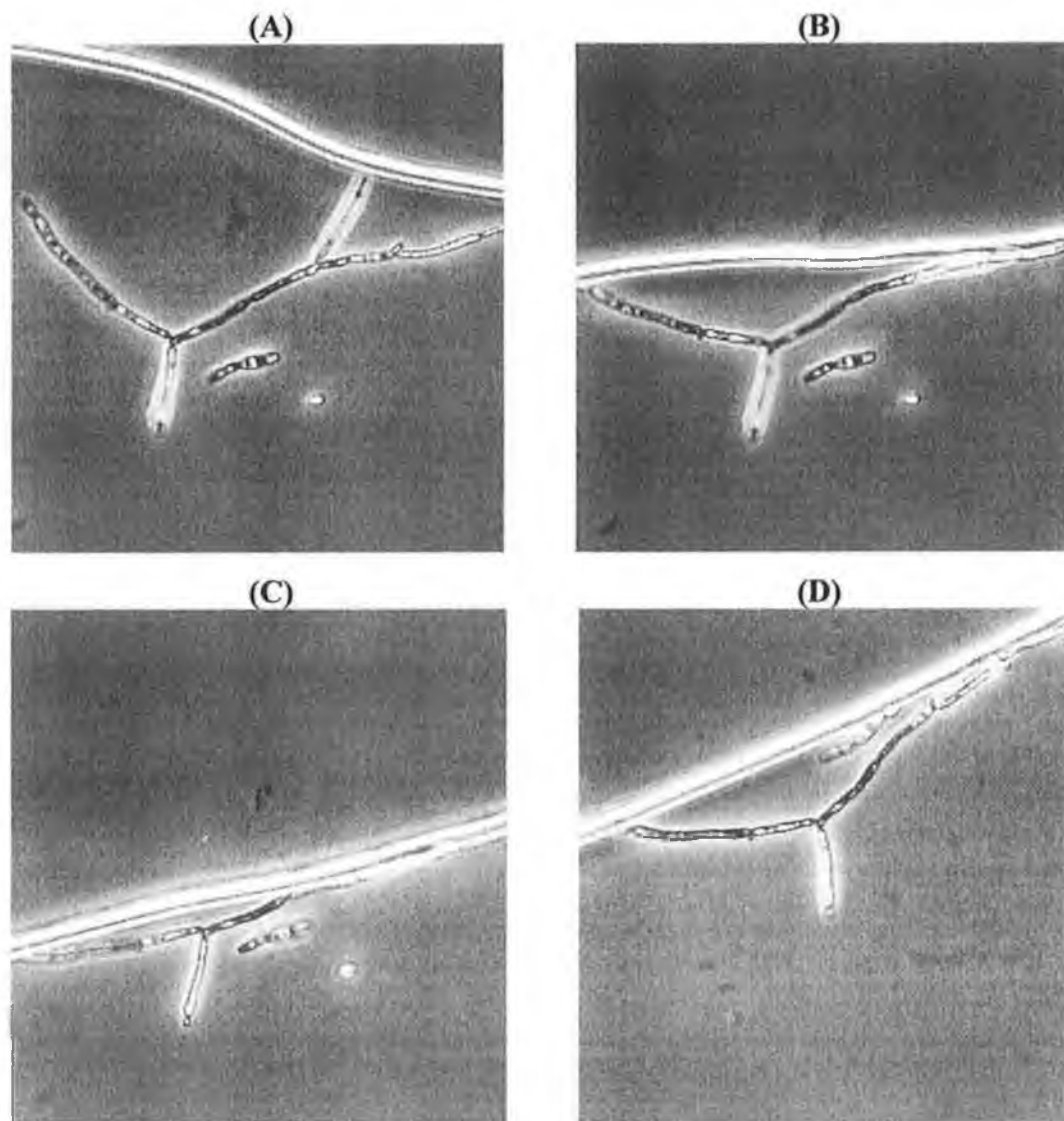


Figure 4.15 Example of deformation at a branch point of a branched mycelium. (Magnification factor 200 X)

Therefore, it could be hypothesised that as L_{dm} increases that compressibility increases due to greater numbers of double cells and mycelia in the suspensions, i.e. more branch points and join points. These cells could lead to increased compression, as they would deform more than unicellular populations. However, this hypothesis doesn't explain compression of unicellular organisms. In particular cell suspensions of *K. marxianus* grown in glycerol consists nearly entirely of single cells, as shown in Table 4.1, yet the filter cakes produced were still compressible. Therefore, it may be that the cell wall may deform in all regions of

the cell. However, wall deformation may be greatest at sub-unit joins and branch points. It should be noted that filter cakes produced with suspensions of low L_{dm} have the lowest voidage and compressibility, therefore the compressibility can be accounted for by only a slight change in voidage. Consequently, only slight deformation is required to account for the filter cake compression.

Another noteworthy feature in Figure 4.15 is that deformation appears to be reversible to a certain degree. It can be seen in Figure 4.15(D) that the cell appears to spring partially away from the air/liquid barrier and regain some of its original shape.

4.7 Conclusions

The use of a dimorphic microorganism and computer-aided image analysis has proved to be a powerful tool combination in elucidating the fundamental relationships between mean cell morphology and filtration behaviour. Also, centrifugation studies proved valuable in elucidating the filtration behaviour.

A linear relationship was found to exist between α_{av} and ΔP for all morphologies and pressures. As well as adequately describing the dependence of α_{av} on ΔP , it proved useful in determining the null stress resistance, thus uncoupling cake packing and compressibility effects. The null stress resistance was found to decrease as the mean morphology became more mycelial in nature, suggesting random packing of cells in the filter cake. The Kozeny-Carman equation coupled with a relationship for ϵ_0 and L_{dm} gives a reasonably good description of the relation between morphology and cake voidage at zero compressive pressure. Furthermore centrifugation studies supported the observed dependence of α_0 on morphology.

The tentative conclusion of other workers that the less spherical the cells in a broth, the greater the compressibility, has been demonstrated to be true for *K. marxianus*. Furthermore a possible mechanism for compression was described which could account for the dependence of compression on cell morphology. The mechanism is based on cells being most deformable at sub-unit joins and branch points.

CHAPTER 5

COMPRESSIBILITY OF FILTER CAKES

5.1 Introduction

Filter cake compressibility appears to be a universal problem when filtering microbial suspensions. While there has been a considerable amount of research into the compressibility of inorganic filter cakes (Tiller *et al.*, 1981, 1987), cake compressibility of microbial filter cakes has received scant attention. In particular the mechanism of compressibility is poorly understood. When filtering inorganic suspensions such as powders, compressibility is predominantly caused by the breakdown of aggregates. Therefore, the degree of compressibility is influenced by the factors that affect particle aggregation such as pH, surface charge and particle size (Tiller *et al.*, 1987).

Traditionally the specific resistance has been related to pressure by a power law expression. However, it was shown that a linear relationship exists between α_{av} and ΔP over the entire range of morphologies and pressures used in Chapter 4. Furthermore it was shown that compressibility was morphology dependent, which is in agreement with other observations in the literature (Liu and Yu, 1993; Nakanishi *et al.*, 1987; Oolman and Liu, 1991; Tanaka *et al.*, 1994)

In this chapter, the linearity of the relationship between α_{av} and ΔP is investigated for a range of yeast suspensions. In addition, the mechanism of cake compressibility was investigated by studying the reversibility of cake compression. The filtration data obtained for the yeast suspensions is compared with data for suspensions of calcium carbonate.

5.2 Characterisation of cake compressibility

Plots of α_{av} versus ΔP for two cell suspensions of *K. marxianus*, resuspended baker's yeast and cultured baker's yeast are shown in Figure 5.1 to Figure 5.3. It can be seen that the baker's yeast suspensions show a linear relationship between α_{av} and ΔP , which is in agreement with the results obtained with *K. marxianus* in Chapter 4. Furthermore it is in agreement with the results of Riesmeier *et al.*, (1989) who found a linear relationship between α_{av} and ΔP for *E. coli* suspensions and with results obtained for a wide range of cultured yeast suspensions (Tanaka *et al.*, 1997). The linearity is also consistent with the upward curvature seen in log-log plots of α_{av} versus ΔP for a number of microbial suspensions (Nakanishi *et al.*, 1987).

Also shown in Figure 5.1 to Figure 5.3 are plots of α_{av} versus ΔP for Run 2, where the filter cake has previously been exposed to a higher pressure (refer to section 3.12.5, Chapter 3). It can be seen that the results are similar to Run 1 results. This indicates that during Run 2, the filter cakes are not affected by having been exposed to a higher pressure, i.e. compressibility is nearly entirely reversible for all yeast suspensions. This is in agreement with the findings of Fowler and Robertson (1991) where it was shown the hydraulic resistance of an immobilised aggregate of *E. coli* decreases, after the pressure the aggregate is subjected to is reduced. However, for the resuspended active dry yeast (ADY) there is noticeable irreversibility particularly with the unwashed suspension.

By comparison, filtration data for Run 1 and Run 2 for a calcium carbonate suspension is shown in Figure 5.4. It can be seen that, for Run 1, there is curvature in the linear plot of α_{av} versus ΔP . Furthermore it can be seen that filter cake compressibility is nearly entirely irreversible, i.e. the mean specific resistance for Run 2 is the same as that measured at the highest pressure the filter cake was exposed to in Run 1. This finding is consistent with compressibility behaviour of powders, (Tiller *et al.*, 1987). Thus it appears that there are fundamental differences in the mechanism of compressibility for powder suspensions and microbial suspensions.

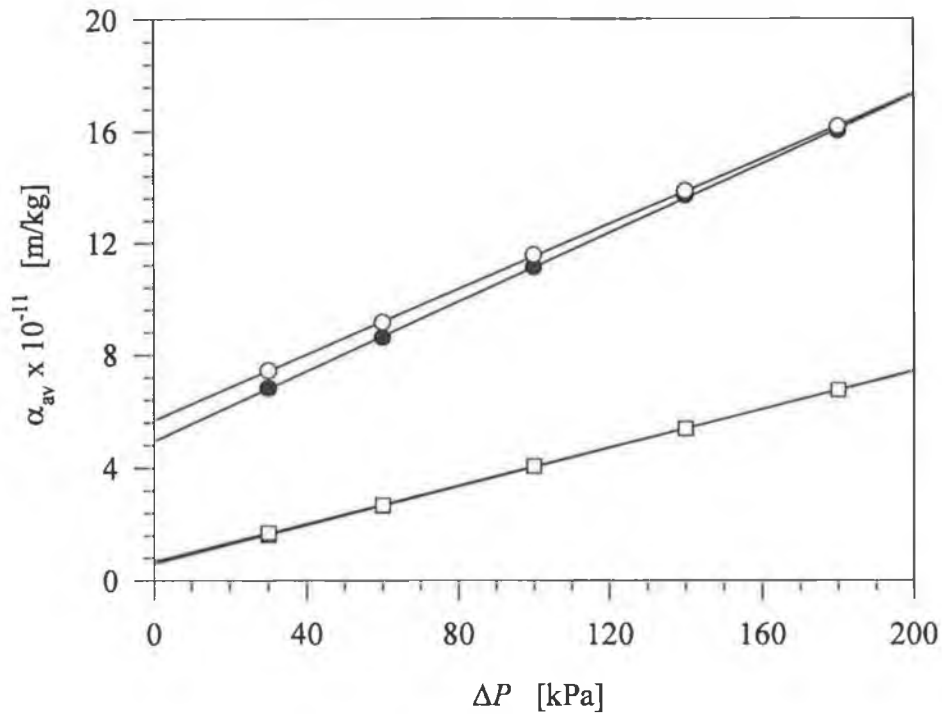


Figure 5.1 Specific cake resistance *versus* applied pressure, for yeast-like, (KM1: Run 1, \bullet and Run 2, \circ) and mycelial, (KM2: Run 1, \blacksquare and Run 2, \square (Note Run 1 and Run 2 results overlap)) broths of *K. marxianus*.

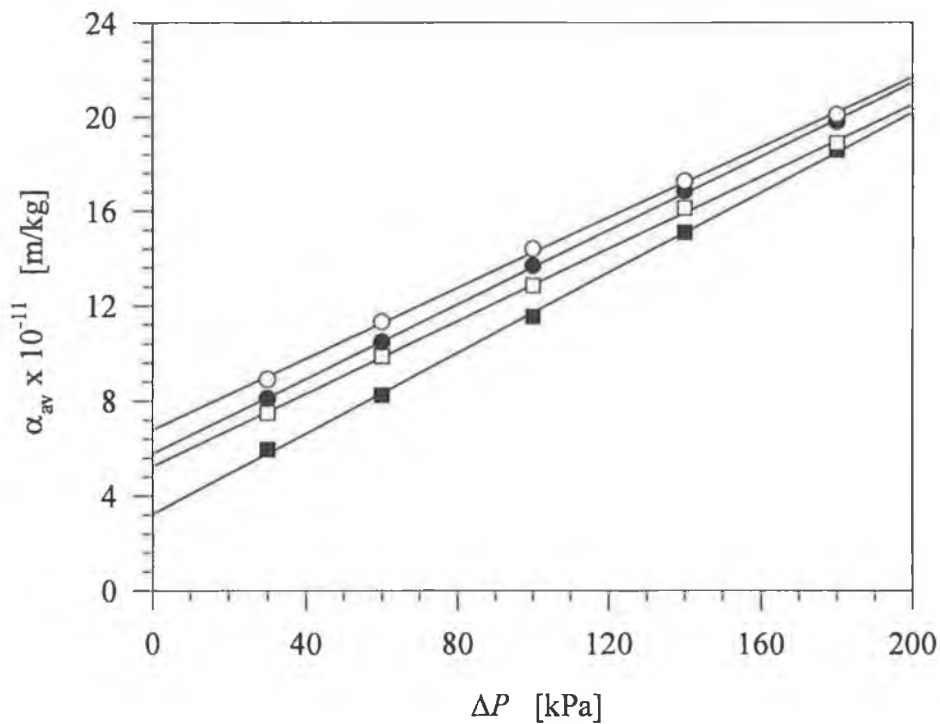


Figure 5.2 Specific cake resistance *versus* applied pressure, for unwashed resuspended yeast (ADY1: Run 1, \blacksquare and Run 2, \square) and washed resuspended yeast (ADY2: Run 1, \bullet and Run 2, \circ)

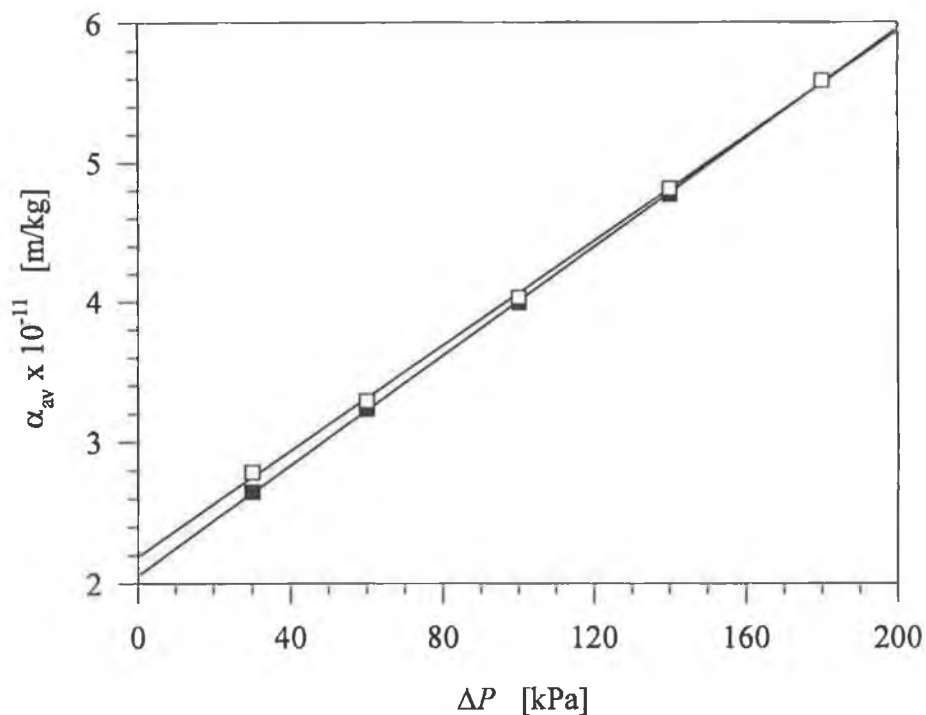


Figure 5.3 Specific cake resistance *versus* applied pressure, for cultured baker's yeast (Run 1, ■ and Run 2, □).

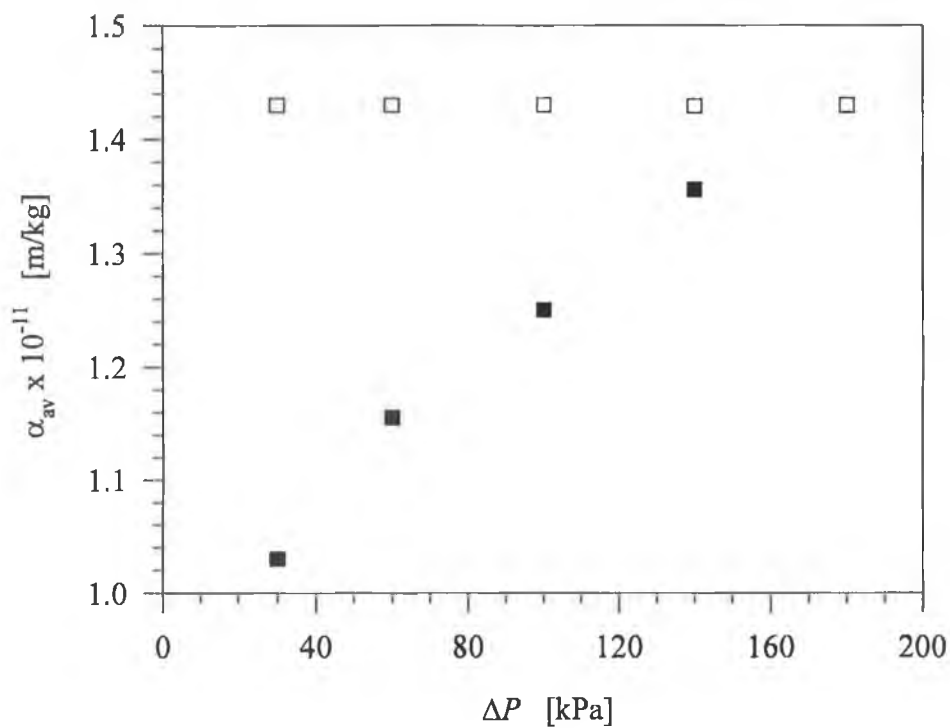


Figure 5.4 Specific resistance *versus* applied pressure for calcium carbonate (Run 1, ■ and Run 2, □).

In Figure 5.5 plots are given of α_o/S_v^2 versus L_{dm} for Run 1 and Run 2, for all the yeast suspensions studied. The dominant trend for both runs is for α_o/S_v^2 to decrease with increasing L_{dm} . This is consistent with the filtration behaviour of unstressed filter cakes of *K. marxianus*, as described in Chapter 4. The reduction in α_o/S_v^2 as L_{dm} increases is due to increasing cake voidage, as the mean cell morphology becomes more elongated, as was shown in Chapter 4.

The ADY1 point for Run 1 seems to be slightly inconsistent with the rest of the data in Figure 5.5. This may reflect the fact that the unwashed suspensions of Active Dry Yeast (ADY) contained cell aggregates, which were not considered in the image analysis measurements of S_v and L_{dm} , i.e. only single and double cells were considered for image analysis. Particle aggregation is known to increase cake voidage (Tiller *et al.*, 1987), therefore this may explain why α_o/S_v^2 for Run 1 of ADY1 is much lower than expected. It should be noted that the ADY2 suspension was observed to contain considerably fewer aggregates than ADY1. This was possibly due to aggregates being broken down by centrifugal forces during the washing stage. Therefore, the cake voidage would be expected to be lower, and α_o/S_v^2 higher, than that of a filter cake produced from ADY1 suspensions. It can be seen that α_o/S_v^2 for Run 2 of ADY1 is in much better agreement with the other data. Again this is probably due to aggregates being broken down by high compressive forces during filtration at high pressure. Finally it should be noted that cultured cell suspensions of *K. marxianus* and baker's yeast, consists of freely dispersed cells.

Figure 5.6 is a plot of k_c versus L_{dm} for all the microbial suspensions studied. As found in Chapter 4, the compressibility of cakes produced by cultured cell broths, increases as the cells become elongated. The ADY suspensions appear to have greater than expected compressibility coefficient, i.e., the trends observed in Chapter 4 showed that k_c increased with increasing L_{dm} for all the range of L_{dm} studied.

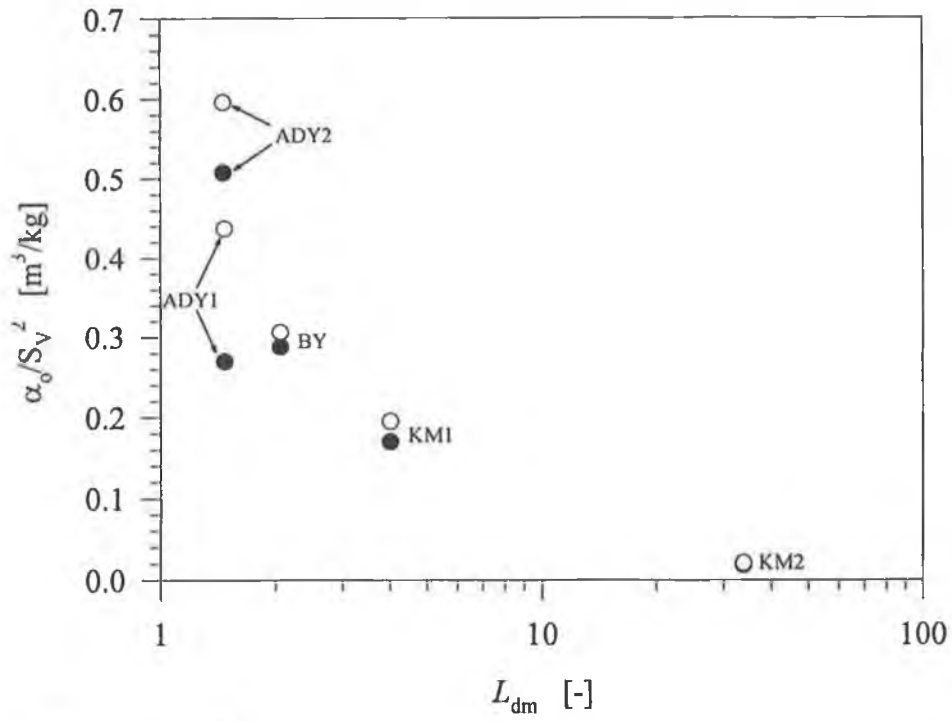


Figure 5.5 α_0/S_v^2 versus L_{dm} for all yeast suspensions. Symbols: ● Run 1 and ○ Run 2.

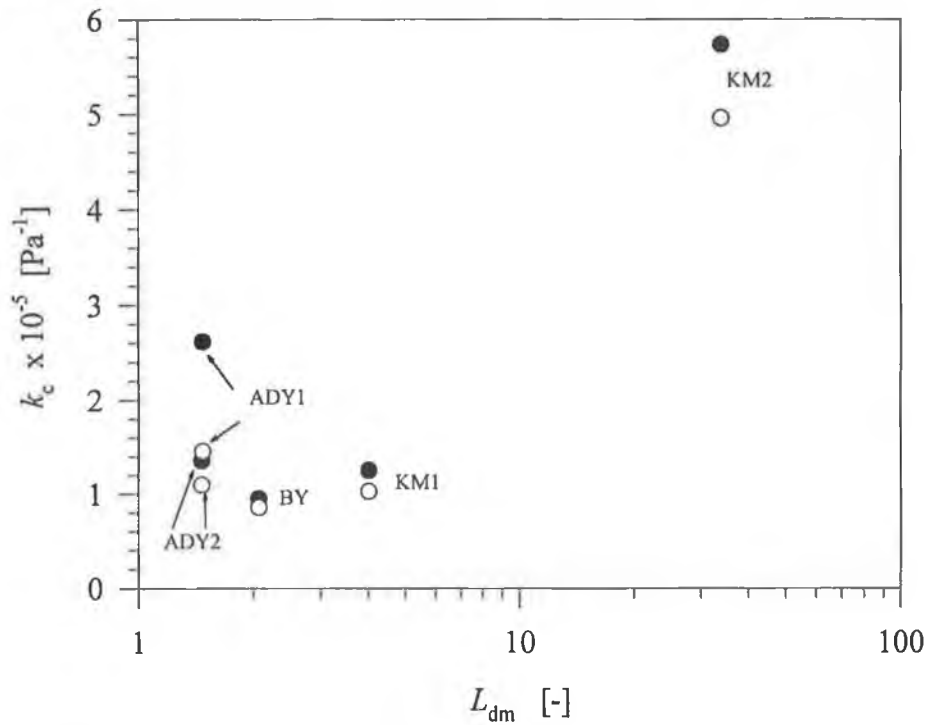


Figure 5.6 k_c versus L_{dm} for all yeast suspensions. Symbols: ● Run 1 and ○ Run 2.

In particular the measured compressibility coefficient for the ADY1 suspension, Run 1 was much higher than expected based on the findings in Chapter 4. This again may be due to the presence of aggregates. The action of the applied pressure would appear to be able to breakdown these aggregates (Tiller *et al.*, 1987), a phenomenon which is most likely irreversible. This is consistent with ADY suspensions giving the greatest degree of filter cake irreversibility for the yeast suspensions, as is clear from Figure 5.2. Another possible explanation for the high compressibility coefficients of ADY may be that cell walls of rehydrated yeast suspensions are usually damaged due to the drying process. It is possible that enhanced cake compressibility is due to greater cell deformability.

5.3 Conclusions

It can be seen that the yeast suspensions filtered in this study all show a linear relationship between α_{av} and ΔP , which is in agreement with the results of Chapter 4 and those of Tanaka *et al.*, (1997). This is in contrast with the relationship between α_{av} and ΔP for calcium carbonate where linearity was not observed. Furthermore, it was shown that cake compression for the cultured yeast suspensions was predominantly reversible. This is the opposite of what was observed for calcium carbonate where filter cake compression is irreversible. This suggests that the mechanism of filter cake compression is different for suspensions of microorganisms and inorganic suspensions.

The filtration behaviour of the resuspended active dry yeasts and cultured baker's yeast were in relatively good agreement with that observed for suspensions of *K. marxianus*. However, there was some evidence that aggregates present in unwashed ADY suspensions affect filter cake voidage and result in an increase in compressibility. Damage to the cell wall of ADY suspensions could also account for the higher than expected compressibility of these suspensions.

The results in this chapter indicate that cell compression may be significantly different for microbial suspensions and inorganic suspensions. This indicates that the mechanisms known to occur during compression of inorganic filter cakes may not be applicable to filter cakes of microorganisms. In Chapter 6, filter cake compression will be modelled in an attempt to qualitatively explain some of the phenomena relating to the compression of filter cakes comprised of microorganisms shown in Chapter 4 and this chapter.

CHAPTER 6

MODELLING FILTER-CAKE COMPRESSIBILITY

6.1 Introduction

The relationship between the mean specific resistance and applied pressure has commonly been assumed to be the same as that used for inorganic suspensions, i.e. a power-law relationship. However, in Chapter 4 and Chapter 5 it was shown that a linear relationship between α_{av} and ΔP existed for all morphologies of *K. marxianus* filtered. Also a linear relationship was found to hold for both resuspended and cultured baker's yeast in Chapter 5. These findings are in good agreement with recent work by Tanaka *et al.*, (1997), which showed a linear relationship between α_{av} and ΔP existed for a number of different yeast strains. Furthermore, it was shown in Chapter 5 that the compression of microbial filter cakes was predominately reversible in nature, while that of an inorganic filter cake was irreversible. All this suggests that the filter cake compressibility for microbial suspensions in general, and yeast suspensions in particular, is different from filter cake compressibility for inorganic suspensions.

There has been a considerable amount of theoretical research into filter cake compressibility of inorganic suspensions (e.g. Tiller, 1953; Tiller *et al.*, 1987) and in related fields where the pressure drop across packed beds of compressible material is important (e.g., Chase and Willis, 1992; Verhoff and Furnaic, 1983). Some of this theoretical work has been applied to qualitatively describe filtration of highly compressible biological material (Cleveland *et al.*, 1995; Soresen *et al.*, 1996). However, these models were based on the empirical equations of Tiller and Leu (1980) and consequently do not allow the affect of cake voidage to be accounted for explicitly.

In this chapter the filter cake compressibility of microbial suspensions will be analysed from a theoretical viewpoint. A model is developed in an attempt to theoretically describe the experimental findings given in Chapter 4 and Chapter 5. The model describes the relationship between the local specific resistance, local voidage and compressive pressure. However, the model does not attempt to describe the actual mechanism of filter cake compressibility.

The objective of the model is to describe the relationship between α_{av} and ΔP , i.e. to determine a theoretical basis for the linear relationship observed in plots of α_{av} versus ΔP . The accuracy of extrapolating plots of α_{av} versus ΔP to determine α_0 will be analysed. Also the relation between null stress voidage and filter cake compression will be investigated. Finally, the effect of applying the Kozeny-Carman equation directly to filtration data will also be studied.

6.2 Model development

The model outlined here, describes fluid flow through a pre-formed compressible filter cake, i.e. similar to experimental set-up used in Chapter 4 and Chapter 5. The mean specific resistance can be determined from the following expression (Tiller and Leu, 1980)

$$\alpha_{av} = \Delta P_c / \int_0^{\Delta P_c} [1/\alpha] dP_s \quad [6.1]$$

where α_{av} is the mean specific resistance, α is the local specific resistance, P_s is the local compressive pressure and ΔP_c is the pressure drop across the filter cake. In this study ΔP_c is assumed to be equal to the applied pressure, ΔP , i.e., negligible membrane resistance. This is in agreement with the dead-end filtration studies in this thesis, where the membrane resistance was found to be negligible in comparison to the cake resistance.

When filtering inorganic suspensions the mean specific resistance is determined by using an empirical expression relating the local resistance to the solid compressive pressure, P_s , such as (Tiller and Leu, 1980),

$$\alpha = \alpha_o \left[1 + \frac{P_s}{P_x} \right]^{n1} \quad [6.2]$$

where α_o is the unstressed cake resistance, P_x is a scaling factor and $n1$ is the index of compressibility. However, this approach does not explicitly take into account the role of voidage in cake compressibility. In the model presented here the local specific resistance is described by the Kozeny-Carman equation

$$\alpha = \frac{k_o [1 - \varepsilon] S_v^2}{\varepsilon^3 \rho_p} \quad [6.3]$$

where k_o is the Kozeny constant, S_v is the mean specific surface area and ρ_p is the particle density, taken to be equal 1000 kg/m³. Therefore, it is assumed that the Kozeny-Carman equation is locally valid within the filter cake, thus allowing for the voidage to be incorporated in the analysis. This approach has been used elsewhere (Tiller, 1953; Chase and Willis, 1992). Equation 6.3, together with an expression relating local voidage and compressive pressure, can be substituted into equation 6.1 and the resulting expression can be solved numerically at constant applied pressure. In this study two relationships between compressive pressure and local voidage were analysed. The first relationship between compressive pressure and local voidage used, is that given by Verhoff and Furjanic (1983) for the compression of bacterial material,

$$\varepsilon = \frac{\varepsilon_o}{1 + bP_s} \quad [6.4]$$

and the following expression used with the blood cell work of Zydney and Colton, (1989)

$$bP_s = \left(\frac{\varepsilon_0}{\varepsilon} \right) + \left(\frac{\varepsilon}{\varepsilon_0} \right) - 2 \quad [6.5]$$

Equation 6.5 can be rearranged to give a quadratic equation and solved to give

$$\varepsilon = \frac{[bP_s + 2] - \sqrt{[bP_s + 2]^2 - 4}}{2\varepsilon_0} \quad [6.6]$$

The constant, b (the compressibility factor), is a measure of filter cake or packed bed compressibility.

6.3 Solution method

The model was numerically integrated using Simpsons rule in the Matlab™ software package. S_v was set equal to 10^6 m^{-1} , i.e., the same magnitude as S_v determined for *K. marxianus* cells in Chapter 4. Initially k_0 was taken to be equal to 5 and in later simulations it was allowed to increase with increasing voidage as was shown to occur in Chapter 4 and with work done elsewhere (e.g. Mauret and Renaud, 1997). Kozeny's constant was replaced by the following linear function

$$k_0 = 5 \left[\frac{\varepsilon}{\varepsilon_0} \right] \quad [6.7]$$

For a set null stress voidage, ε_0 , in the range of 0.1-0.9, the mean specific resistance was determined every 2.5 kPa between 0.0-200 kPa. Subsequently linear regression analysis was carried out between the applied pressure and mean specific resistance. This allowed determination of the unstressed cake resistance, $\alpha_{0/\text{model}}$, and k_c in accordance with the linear model. The unstressed cake resistance for any null set voidage can also be determined using equation 6.3 alone, $\alpha_{0/\text{Eq6.3}}$, i.e., the *true* unstressed cake resistance. The difference between the two unstressed resistance terms was expressed as the *percentage error*,

$$\text{percentage error} = 100 \left[\frac{\alpha_{o/\text{Eq6.3}} - \alpha_{o/\text{model}}}{\alpha_{o/\text{Eq6.3}}} \right] \quad [6.8]$$

Using equation 6.8, a positive value for *percentage error* indicates the *true* unstressed specific resistance is being under predicted by the extrapolation and a negative value indicates the *true* unstressed specific cake resistance is being over predicted.

6.4 Model predictions of relationship between α_{AV} and ΔP

A sample of model predictions for the model based on the Verhoff and Furnaic relationship are shown in Figure 6.1, for constant k_o and in Figure 6.2 for variable k_o . Model predictions for the Zydney and Colton model are shown in Figure 6.3 and Figure 6.4. Further model predictions for different null stress voidages and values of the compressibility factor, b , are shown in Table 6.1.

It can be seen the model solution based on the Verhoff and Furnaic relationship, predicts an apparently linear relationship between α_{av} and ΔP , (Figure 6.1, Figure 6.2). In all simulations the regression coefficient, R^2 , was greater than 0.99. The model predicts almost completely linear behaviour over the range of experimental pressures used in Chapter 4 and Chapter 5. However, at low pressures (< 30 kPa), there is some curvature in the plots, when k_o is constant.

There is more curvature apparent in the plots of α_{av} versus ΔP , when the model is based on Zydney and Colton relationship, (Figure 6.3, Figure 6.4). The curvature in the plots of α_{av} versus ΔP is most pronounced at low pressures (below 30 kPa) in all simulations. Also at low values of b ($< 5 \times 10^{-6} \text{ kPa}^{-1}$), there is curvature in plots of α_{av} versus ΔP at pressures greater than 30 kPa. Consequently the regression coefficient was less than 0.98 in certain situations. However, over the range of experimental pressures used in Chapter 4 and Chapter 5 the plots appear linear in most cases.

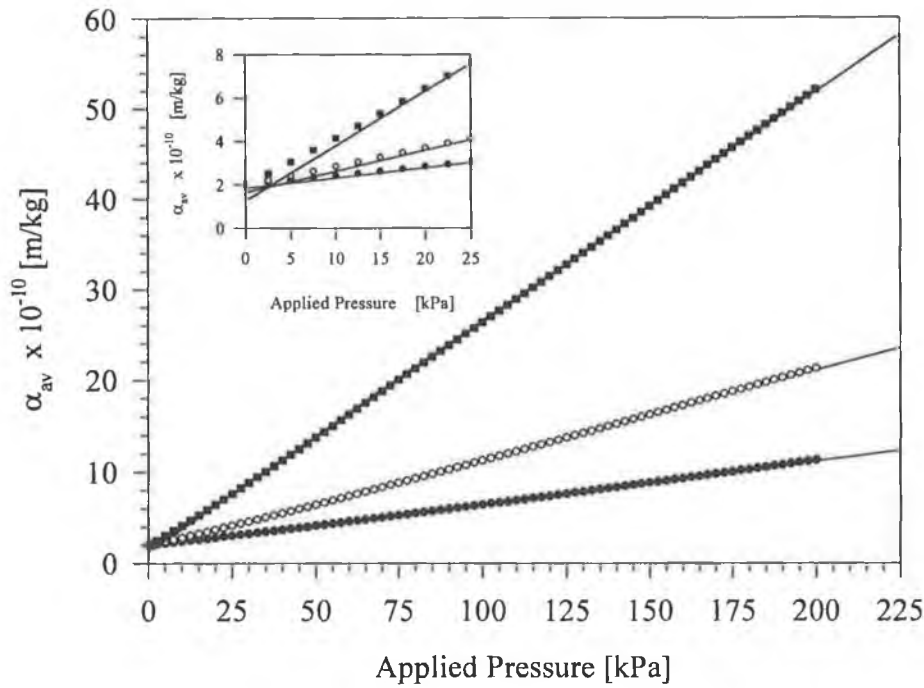


Figure 6.1 Relationship between α_{av} and ΔP , Verhoff and Furnaic model, constant k_0 , $\epsilon_0 = 0.5$. Symbols: \bullet $b=1 \times 10^{-5} \text{ kPa}^{-1}$; \circ $b=2 \times 10^{-5} \text{ kPa}^{-1}$ and \blacksquare $b=5 \times 10^{-5} \text{ kPa}^{-1}$. Lines: linear regression. The relationship at small applied pressures is shown in insert.

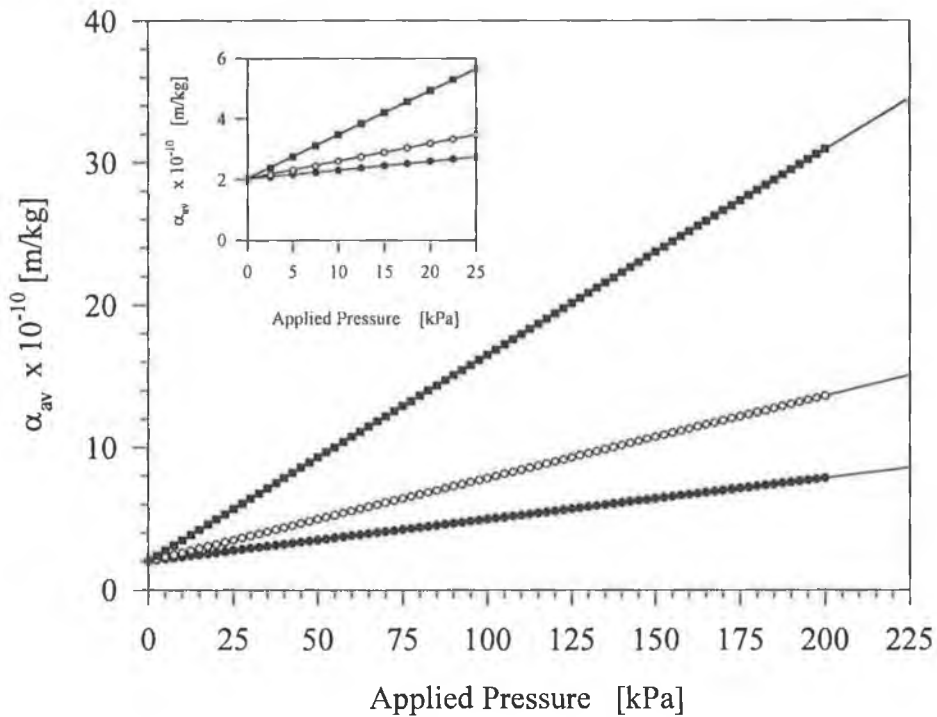


Figure 6.2 Relationship between α_{av} and ΔP , Verhoff and Furnaic model, variable k_0 , $\epsilon_0 = 0.5$. Symbols and lines as in Figure 6.1.

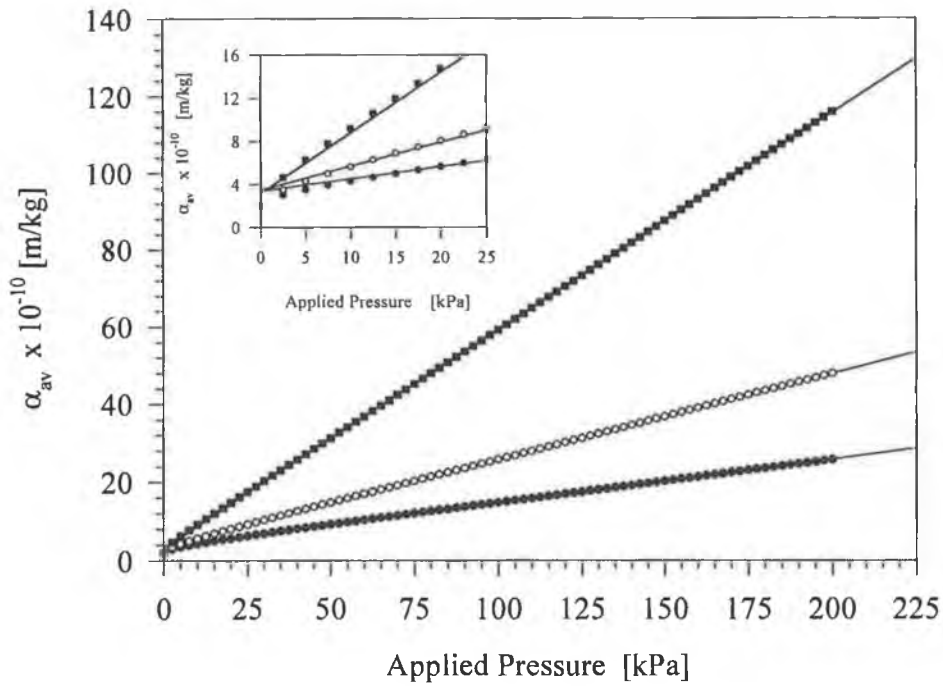


Figure 6.3 Relationship between α_{av} and ΔP , Zydney and Colton model, constant k_0 , $\epsilon_0 = 0.5$. Symbols and lines as in Figure 6.1.

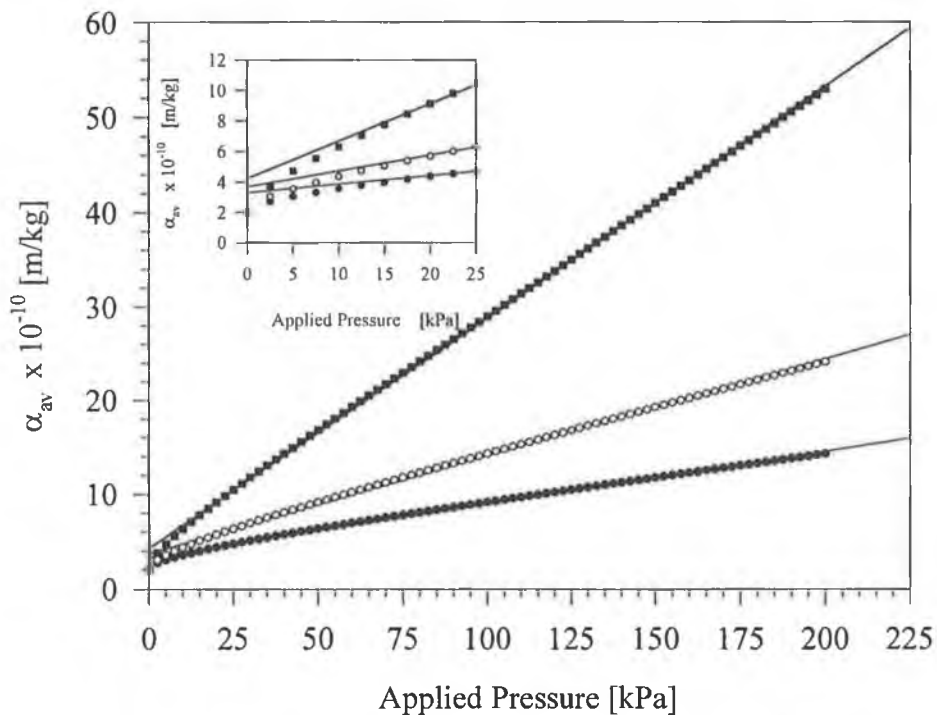


Figure 6.4 Relationship between α_{av} and ΔP , Zydney and Colton model, variable k_0 , $\epsilon_0 = 0.5$. Symbols and lines as in Figure 6.1.

Table 6.1 Model predictions for various null stress voidages and values of b .

ϵ_o	b $\times 10^5$ (kPa ⁻¹)	$\alpha_o/\text{Eq6.3}$ $\times 10^{-11}$ (m/kg)	Verhoff and Furnaic model			Zydney and Colton model		
			α_o/model $\times 10^{-11}$ (m/kg)	k_c $\times 10^5$ (kPa ⁻¹)	% error	α_o/model $\times 10^{-11}$ (m/kg)	k_c $\times 10^5$ (kPa ⁻¹)	% error
k_o constant								
0.2	0.1	50	49.92	0.17	0.17	62.15	0.51	-24.31
	1.0		46.32	2.07	7.37	78.53	2.77	-57.07
	10		24.95	42.76	50.10	62.48	35.21	-24.97
0.5	0.1	2	2.00	0.21	0.19	2.60	0.61	-29.83
	1.0		1.83	2.54	8.34	3.38	3.33	-69.16
	10		0.95	53.85	52.40	2.67	42.52	-33.41
0.8	0.1	0.2	0.20	0.35	-0.04	0.30	0.93	-51.81
	1.0		0.18	3.98	7.31	0.43	4.65	-118.9
	10		0.09	83.69	53.07	0.34	58.08	-75.58
k_o variable								
0.2	0.1	50	50.00	0.11	-0.00	58.60	0.32	-17.20
	1.0		50.04	1.12	-0.07	74.67	1.38	-49.34
	10		50.13	11.17	-0.27	99.47	8.81	-98.95
0.5	0.1	2	2.00	0.15	-0.04	2.46	0.41	-22.92
	1.0		2.02	1.44	-0.85	3.31	1.70	-65.46
	10		2.06	14.04	-2.79	4.61	10.45	-130.4
0.8	0.1	0.2	0.20	0.28	-0.50	0.28	0.68	-45.42
	1.0		0.21	2.40	-6.73	0.44	2.44	-127.7
	10		0.23	21.20	-17.41	0.69	13.66	-250.8

When the model is based on the Verhoff and Furnaic relationship and k_0 is taken to be constant, it can be seen, in Table 6.1, that the *percentage error* increases with increasing values of b . The positive value of the *percentage error* indicates that there is upward curvature in plots of α_{av} versus ΔP . When k_0 is allowed to vary in accordance with equation 6.7, the *percentage error* is low except in simulations with both high voidages and high values of b . When the model is based on the Zydney and Colton relationship it can be seen from Table 6.1, that the *percentage error* is always significant and increases with null stress voidage. In most cases, the *percentage error* is greater than when the model is based on the Verhoff and Furnaic relationship.

Allowing k_0 to vary according with the voidage, as with equation 6.7, does not significantly alter the general observations. In Table 6.1 it can be seen that allowing k_0 to vary, decreases the magnitude of the *percentage error* using the Verhoff and Furnaic model and increases the magnitude of the *percentage error* when using the Zydney and Colton model. This is because allowing k_0 to decrease with decreasing voidage, decreases the affect of voidage on the local specific resistance and will subsequently reduce the impact of pressure on the mean specific resistance, i.e. will reduce upward curvature in plots of α_{av} versus ΔP and enhance downward curvature in these plots.

Numerous theoretical relationships exist between Kozeny constant and local voidage, one such being (Happel and Brenner, 1965),

$$k_0 = \frac{2\varepsilon^3}{(1-\varepsilon) \left[\ln \left\{ \frac{1}{1-\varepsilon} \right\} - \frac{(1-[1-\varepsilon]^2)}{(1+[1-\varepsilon]^2)} \right]} \quad [6.9]$$

Sample calculations using equation 6.9, the Verhoff and Furnaic model and the Zydney and Colton model are given in Figures 6.5 and 6.6 respectively.

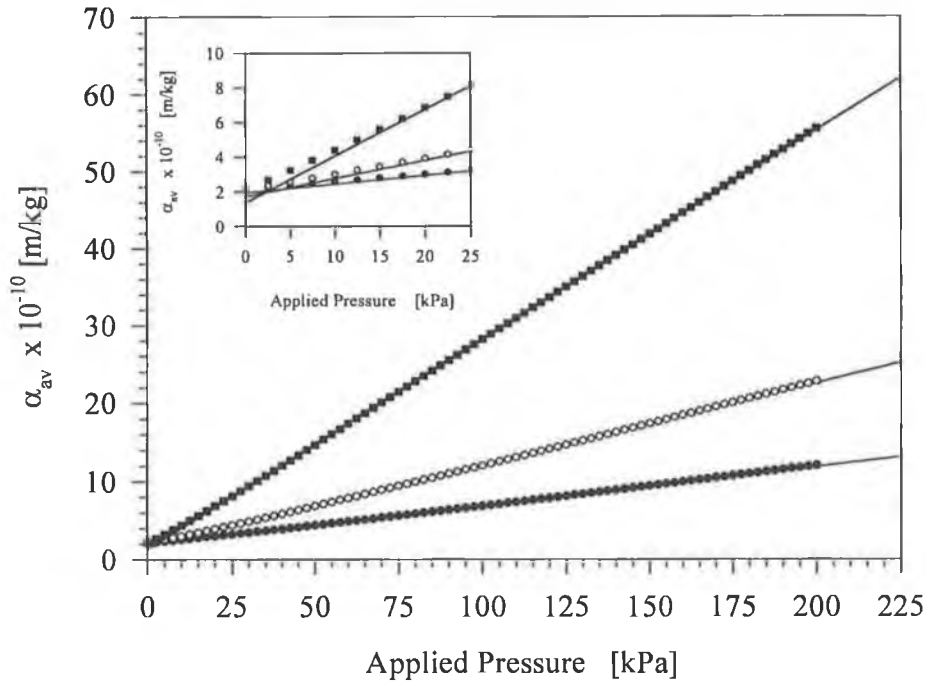


Figure 6.5 Relationship between α_{av} and ΔP , Verhoff and Furnaic model, $\epsilon_0 = 0.5$, k_0 varies according to equation 6.9. Symbols and lines as in Figure 6.1.

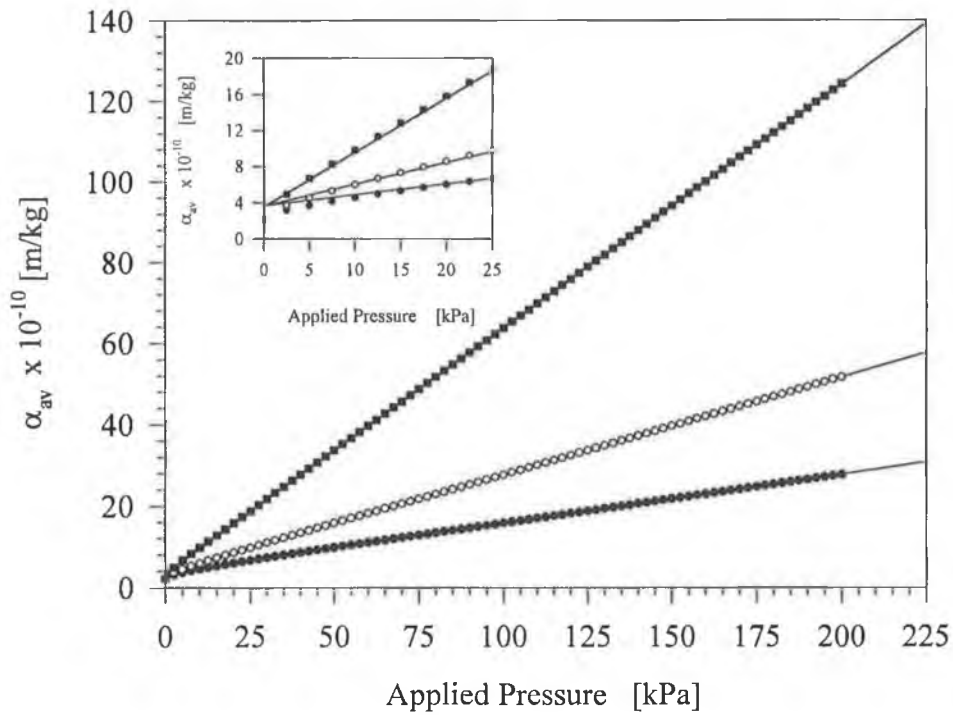


Figure 6.6 Relationship between α_{av} and ΔP , Zydney and Colton model, $\epsilon_0 = 0.5$, k_0 varies according to equation 6.9. Symbols and lines as in Figure 6.1.

It can be seen that using an alternative relationship between k_0 and voidage does not significantly alter the linearity of the plots in the experimental range used in Chapter 4 and Chapter 5.

The simulations shown here give a theoretical basis for the observed linearity in plots of α_{av} versus ΔP shown in Chapter 4 and Chapter 5, particularly, when the model is based on the Verhoff and Furnaic relationship between voidage and compressive pressure. However, it can be seen in the inserts of Figure 6.1-6.6 that there is, in some instances, considerable deviation between the unstressed cake resistance determined by equation 6.3 and the intercept obtained using linear regression analysis. This is clearly obvious from the *percentage error* values given in Table 6.1. Therefore, it is important to note that whilst the relationship between α_{av} and ΔP may appear linear, the extrapolated intercept may not represent the true null stress resistance.

However, even if the error in the unstressed cake resistance was in the region of 50-100% as indicated in Table 6.1, the general observations made in Chapter 4 and Chapter 5 are unlikely to be significantly affected, due to $\alpha_0 \rho / S_v^2$ decreasing two orders of magnitude over the range of morphologies filtered.

6.5 An alternative approach to the linearity between α_{av} and ΔP

In the previous section a model was presented which approximated the linear relationship between α_{av} and ΔP . However, the analysis in section 6.4 indicates that linearity may not hold in all cases, particularly at low pressures or at high compressibility. An alternative approach to filter cake compression is given here, whereby a solution is presented to describe linearity between α_{av} and ΔP for all pressures and degrees of compressibility.

For inorganic suspensions, equation 6.2 is normally used to relate the local specific resistance to the solid compressive pressure. Equation 6.1 can be integrated using equation 6.2 to give (Tiller *et al.*, 1981),

$$\alpha_{av} = \frac{\alpha_o [1 - n1] \frac{\Delta P_c}{P_x}}{\left[1 + \frac{\Delta P_c}{P_x} \right]^{[1-n1]} - 1} \quad [6.10]$$

When $\Delta P_c/P_x \gg 1$, equation 6.10 can be reduced to a power law relationship,

$$\alpha_{av} = \alpha_o [1 - n1] \left[\frac{\Delta P_c}{P_x} \right]^{n1} \quad [6.11]$$

Equation 6.11 is used as the basis for the power law relationship, that is often applied to plots α_{av} versus ΔP (see Section 2.2.5, equation 2.9), when filtering inorganic suspensions (Tiller *et al.*, 1987) or microbial suspensions (e.g., Nakanishi *et al.*, 1987).

However, when the value of $n1$ is taken equal to 2, equation 6.10 is reduced to the following linear relationship,

$$\alpha_{av} = \alpha_o \left[1 + \frac{\Delta P_c}{P_x} \right] \quad [6.12]$$

In equation 6.12, $1/P_x$ is equivalent to k_c .

The relationship between local voidage can then be described using equation 6.2 (assuming S_v is not affected by cake compression),

$$\frac{k'' [1 - \epsilon]}{\epsilon^3} = \frac{k_o [1 - \epsilon_o]}{\epsilon_o^3} \left[1 + \frac{P_s}{P_x} \right]^2 \quad [6.13]$$

where k'' is Kozeny's constant at a local voidage of ϵ .

Therefore it can be seen that existing filtration theory includes as a special case ($n=2$) a linear relationship between α_{av} and ΔP (assuming ΔP_c is equal to ΔP). Obviously using equation 6.10 and $n=2$ to describe filter cake compression, allows the entire range of pressures to be described by a linear function. However, it should be noted that the results in Figure 6.1 to Figure 6.6 indicate that while a linear relationship may be observed over the experimental range of pressures used, that it may be incorrect to assume the relationship can be extrapolated to zero applied pressure. Therefore experimental research is required to determine if the linear relationship is applicable at low pressures. This could probably be achieved by filtering using gravity as the driving force of filtration.

6.6 The affect of null stress voidage on filter cake compression

The affect of null stress voidage on the predicted value of k_c for both models and for a wide range of values of the compressibility factor, b , was tested. The results are shown in Figure 6.7, where k_c/b is plotted versus the null stress voidage, ϵ_0 . It can be seen in all cases that k_c/b increases and hence k_c increases with increasing values of ϵ_0 . This is in qualitative agreement with the experimental results shown in Chapter 4. Furthermore it is in agreement with the experimental results of Oolman and Liu (1991) and Lu and Yu (1993), where it can be seen that increasing filter cake voidage coincided with increasing filter cake compressibility. This could also explain the observed phenomena whereby as cell morphology deviates from spherical the compressibility index, n , increases (Nakanishi *et al.*, 1987; Tanaka *et al.*, 1994), if it is assumed that the null stress voidage increases as cell populations become more elongated (Ju and Ho, 1988; Chapter 4).

Furthermore, it has been shown that for a wide range of inorganic suspensions, the index of compressibility, n , increases with voidage (Tiller and Kwon, 1998). Therefore it may be expected that when filtering microbial suspensions that any benefit obtained from forming cakes with high voidage will be partially offset by higher compressibility.

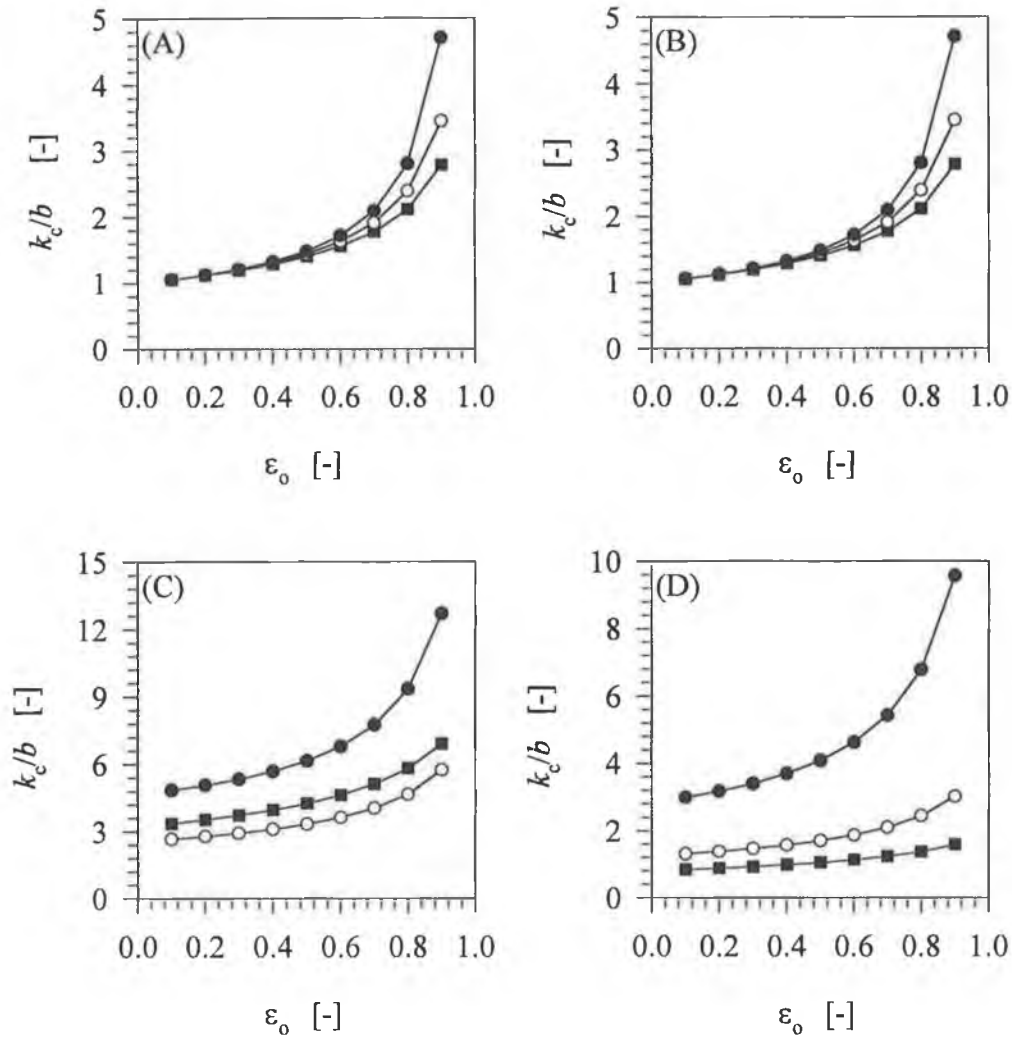


Figure 6.7 Plots of ϵ_0 versus k_c/b . (A) Verhoff and Furnaic model, constant k_0 , (B) Verhoff and Furnaic model, variable k_0 , (C) Zydney and Colton model, constant k_0 , (D) Zydney and Colton model, variable k_0 . Symbols: ● $b = 1 \times 10^{-4} \text{ kPa}^{-1}$; ○ $b = 1 \times 10^{-5} \text{ kPa}^{-1}$ and ■ $b = 1 \times 10^{-6} \text{ kPa}^{-1}$.

However, it should be noted that the magnitude of the increase in the compressibility coefficient, k_c , with increasing L_{dm} shown in Chapter 4 and Chapter 5, cannot be explained by the voidage dependency shown here. In order to achieve a similar magnitude increase in k_c over the range of L_{dm} values tested in Chapter 4 and Chapter 5, b has to increase with increasing L_{dm} . Furthermore it should be noted that the compressibility index, n , can vary substantially for different

microorganisms which have similar morphologies, (Nakanishi *et al.*, 1987; Tanaka *et al.*, 1994a). Therefore factors other than filter cake voidage must have an affect on filter cake compressibility. Therefore considerable research into the mechanism of filter cake compressibility of microorganisms is required before these factors can be elucidated fully.

6.7 Model predictions for the voidage gradient in filter cakes and calculation of the average cake voidage.

When filter cakes undergo compression a voidage gradient is formed within the filter cake (e.g., Sorensen *et al.*, 1996). In this section, the model presented in section 6.2, will be used to determine the voidage gradient within filter cakes and to subsequently determine the average cake voidage of a compressed filter cake.

The average cake voidage can be determined from (Zydney and Colton, 1989),

$$\varepsilon_{av} = \frac{1}{L_b} \int_0^{L_b} \varepsilon dz \quad [6.14]$$

where L_b is the filter cake depth and z is the distance away from the membrane cake interface. The position z within the filter cake can be determined from (Tiller, 1953)

$$z = L_b \frac{\int_{P_s}^{\Delta P} \frac{\varepsilon^3}{[1-\varepsilon]^2} dP_s}{\int_0^{\Delta P} \frac{\varepsilon^3}{[1-\varepsilon]^2} dP_s} \quad [6.15]$$

For a particular applied pressure, ΔP (assuming $\Delta P \approx \Delta P_c$), the position z was determined at a compressive pressure, P_s , by solving equation 6.15. The compressive pressure used was increased from zero to the applied pressure, in increments of $1/80^{\text{th}}$ of the applied pressure. Therefore, at each position z within

the filter cake, the local voidage can be determined using the compressive pressure and either equation 6.4 or 6.5. (In the following simulations the Verhoff and Furnaic model was used with k_0 taken to be constant and equal to 5.0). Subsequently the voidage data is integrated over the entire cake depth using equation 6.14 giving the average cake voidage, ϵ_{av} , for the particular applied pressure, ΔP .

The average cake voidage as a function of applied pressure is shown in Figure 6.8. At low to medium values of b the average voidage continually decreases over the range of ΔP used here. For highly compressible cakes, the average voidage becomes almost completely independent of applied pressure at high pressure. This is in qualitative agreement with the experimental findings of Ofsthun (1989) with yeast cells and the theoretical predictions of Cleveland *et al.* (1995) and Sorensen *et al.* (1996). However, for compressible cakes, α_{av} will continue to increase with applied pressure, despite ϵ_{av} reaching an asymptotic value. This apparent contradiction can be explained by the voidage profiles through the filter cake.

Shown on Figure 6.9 are the voidage profiles for the filter cake of high compressibility ($b = 10^{-4}$). In Table 6.2, the average cake voidage, ϵ_{av} and the mean specific resistance, α_{av} , for the three applied pressures used in Figure 6.9 are shown. The average voidages are nearly independent of the applied pressure because throughout most of the filter cake (away from the membrane), the voidage gradient is not steep and is very similar at all pressures. However, at a thin layer near the membrane the voidage gradient is at its steepest and voidage values here are more pressure dependent than in the rest of the filter cake (Insert, Figure 6.9). The layer is too thin to have a significant impact on the average voidage (as shown in Table 6.2), but it is this layer next to the membrane that accounts for most of the cake resistance due to the low voidage within this region. Theoretical simulations of Sorensen *et al.* (1996) have showed similar theoretical predictions of thin layer formation next to the membrane that subsequently dominates filtration behaviour.

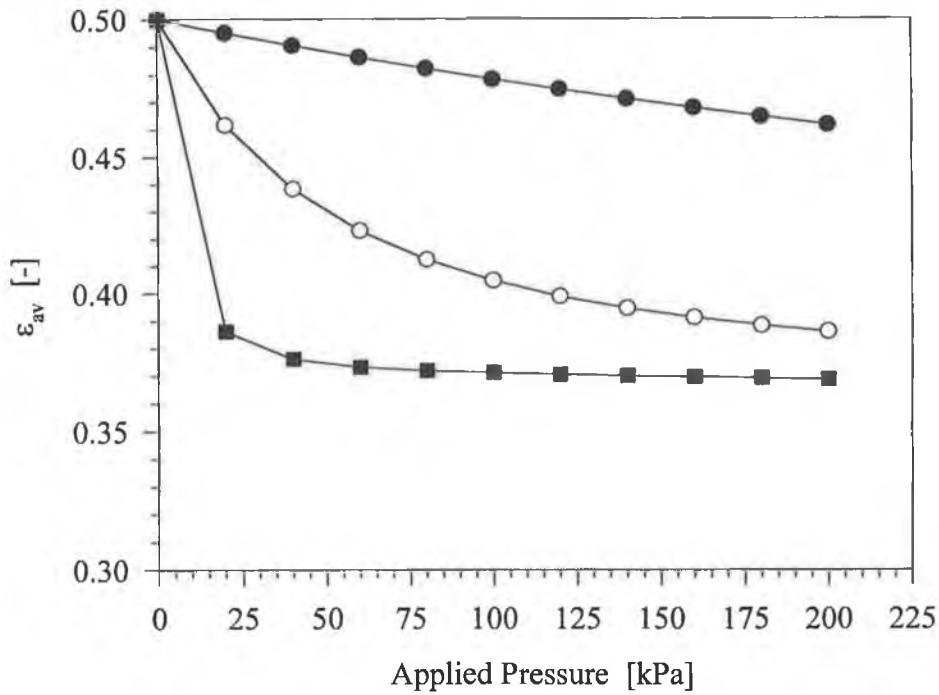


Figure 6.8 Relationship between ϵ_{av} and ΔP . Verhoff and Furnaic model, constant k_0 . Symbols: ● $b = 1 \times 10^{-6} \text{ kPa}^{-1}$; ○ $b = 1 \times 10^{-5} \text{ kPa}^{-1}$ and ■ $b = 1 \times 10^{-4} \text{ kPa}^{-1}$.

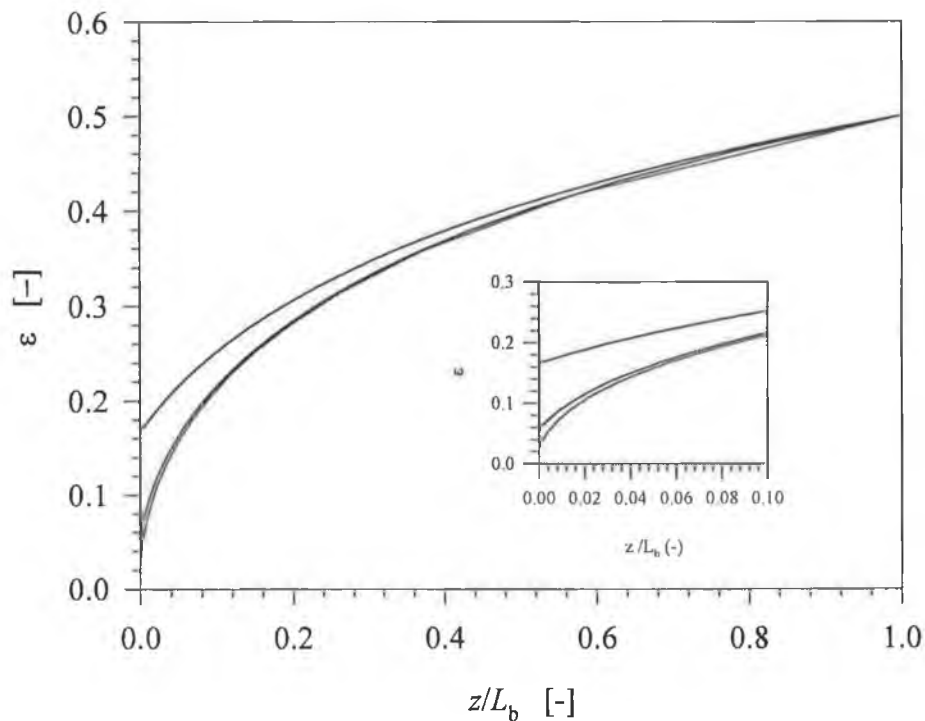


Figure 6.9 Relationship between ϵ and fractional position from cake membrane interface, z/L_b . Verhoff and Furnaic model, constant k_0 , $b = 10^{-4} \text{ kPa}^{-1}$. Lines applied pressure: — $0.2 \times 10^{-5} \text{ Pa}$; — $0.8 \times 10^{-5} \text{ Pa}$ and — $2.0 \times 10^{-5} \text{ Pa}$.

Table 6.2 The effect of applied pressure on average cake voidage for highly compressible filter cakes.

ΔP	ϵ_{av}	α_{av} (Model)
Pa		m/kg
2×10^4	0.386	1.13×10^{11}
8×10^4	0.371	4.18×10^{11}
2×10^5	0.368	1.04×10^{12}

$b = 10^{-4} \text{ kPa}^{-1}$, $\epsilon_0 = 0.5$, Verhoff and Furnaie model.

6.8 Implications of applying the Kozeny-Carman directly to filtration data

In the literature it common to find the Kozeny-Carman equation applied directly to filtration data to determine other cake parameters, without taking into account the effect of the voidage gradient within the filter cake (e.g. Nakanishi *et al.*, 1987). When this approach is taken, the Kozeny-Carman equation can be rewritten in the following form,

$$\alpha_{av} = \frac{k' [1 - \epsilon_{av1}] S_v^2}{\epsilon_{av1}^3 \rho_p} \quad [6.16]$$

where α_{av} is the mean specific resistance, ϵ_{av1} is the average cake voidage and k' is the Kozeny constant. Assuming a constant k' , equation 6.16 is used to compute the average filter cake voidage (e.g., Nakanishi *et al.*, 1987) once α_{av} is known or to compute Kozeny's constant when the ϵ_{av1} and α_{av} are known (e.g., Oolman and Lu, 1991).

However, this approach is likely to be in error when a voidage gradient exists within the filter cake due to filter cake compression. Furthermore, the average filter cake voidage may reach a constant value at high pressures (Ofsthun, 1989) and has been described theoretically in the previous section and by Cleveland *et al.* (1996) and Sorensen *et al.* (1996).

In this section, the model presented in section 6.2, is used to predict the voidage gradient through the filter cake and to then determine the *true* average cake voidage, ϵ_{av} , as outlined in section 6.7. The average cake voidage, ϵ_{av1} and the Kozeny constant k' , will also be determined using equation 6.16 so as to ascertain the effect of directly applying the Kozeny-Carman equation to filtration data.

In Figure 6.10, the *true* average cake voidage, ϵ_{av} (as determined in Section 6.7) as a function of applied pressure, is shown. Also shown are plots of the cake voidage, ϵ_{av1} , determined from the Kozeny-Carman equation, equation 6.16. In this case, ϵ_{av1} is determined by using the mean specific resistance as predicted by the model, i.e., α_{av} . Also k_o , S_v and ρ_p are set at the same values as used to determine ϵ_{av} . It can be seen from Figure 6.10, for slightly compressible filter cakes, that the predicted average voidage is in reasonable agreement with the *true* average voidage. However, for moderate to highly compressible filter cakes, the predicted average voidage is considerable lower than the *true* average voidage, particularly at the high end of the applied pressure range. The latter, is due to, the *true* average voidage reaching a near constant value, while the mean specific resistance continues to increase. Consequently, when equation 6.16 is used, the predicted ϵ_{av1} will continue to decrease in response the mean specific resistance increasing. Therefore, for compressible filter cakes, applying the Kozeny-Carman equation to filtration data to predict the average cake voidage, can result in considerable error.

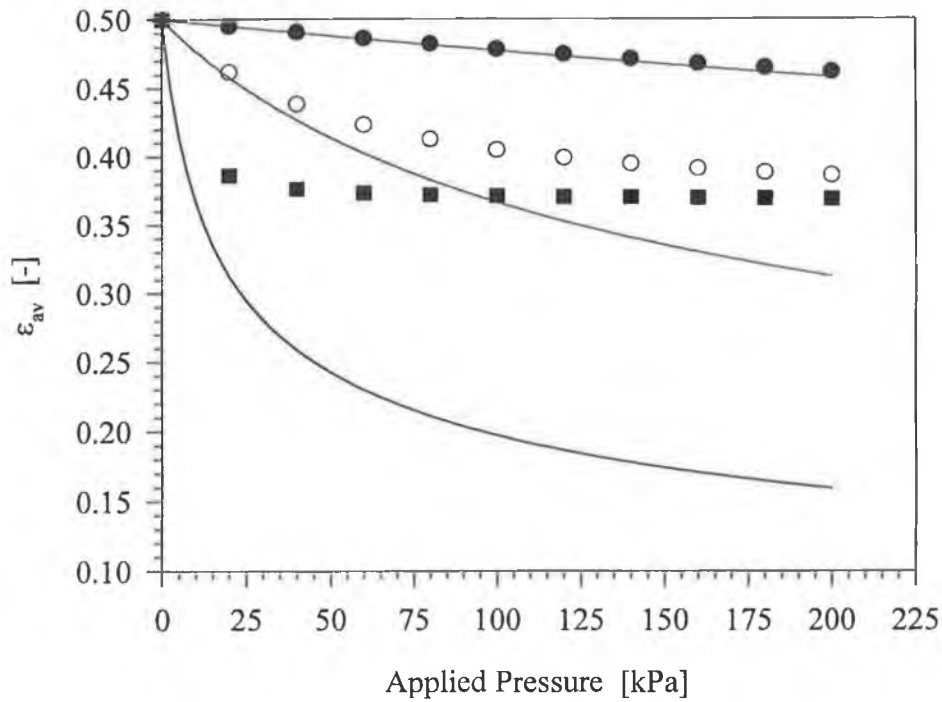


Figure 6.10 The effect of using the Kozeny-Carman equation to predict ϵ_{av1} . Verhoff and Furnaic model, constant k_o , $\epsilon_o = 0.5$. Symbols, ϵ_{av} : ● $b = 1 \times 10^{-6} \text{ kPa}^{-1}$; ○ $b = 1 \times 10^{-5} \text{ kPa}^{-1}$ and ■ $b = 1 \times 10^{-4} \text{ kPa}^{-1}$. Lines: ϵ_{av1} : — $b = 10^{-6} \text{ kPa}^{-1}$; — $b = 10^{-5} \text{ kPa}^{-1}$ and — $b = 10^{-4} \text{ kPa}^{-1}$

In Figure 6.11 the effect of using equation 6.16 to determine the Kozeny constant is shown. In this case the mean specific resistance and average cake voidage as determined by the model is applied to equation 6.16. The resulting equation is solved to predict the Kozeny constant, k' . It can be seen that when the filtration is carried out at low pressures or when the filter cakes has low compressibility that k'/k_o is close to unity, i.e. the predicted Kozeny constant is approximately correct. However, for highly compressible filter cakes it can be seen that Kozeny's constant can be considerably over predicted. Again this is due to the voidage gradients within the filter cake.

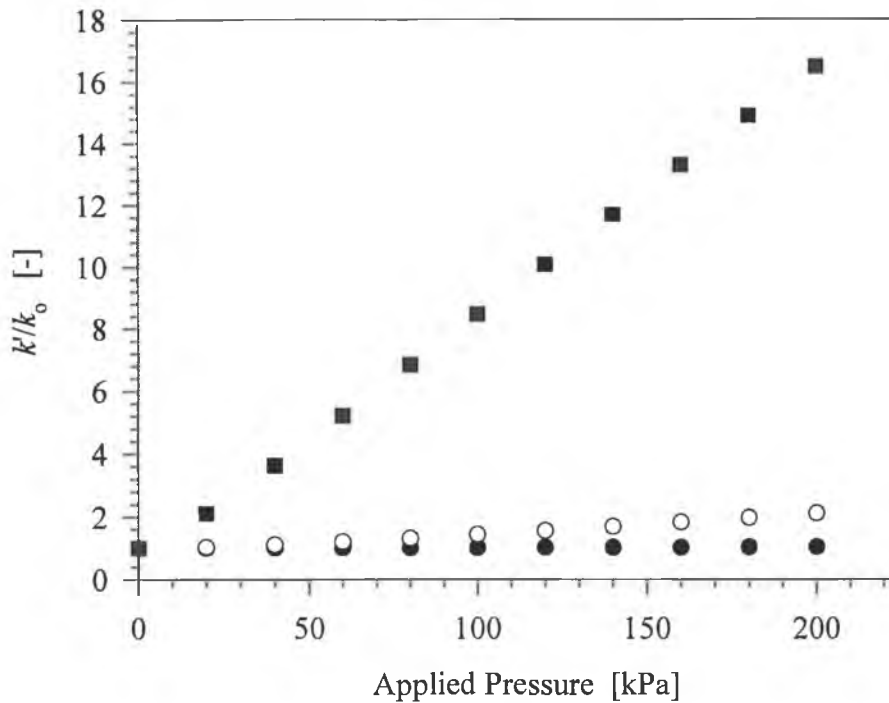


Figure 6.11 k'/k_0 Versus ΔP for various values of b . Symbols: ● $b = 1 \times 10^{-6} \text{ kPa}^{-1}$; ○ $b = 2 \times 10^{-5} \text{ kPa}^{-1}$ and ■ $b = 5 \times 10^{-4} \text{ kPa}^{-1}$.

6.9 Conclusions

In this chapter a model was presented to qualitatively describe filter cake compression. The model was found to predict a near linear relationship between α_{av} and ΔP as was found to occur experimentally in Chapter 4 and Chapter 5. However, the simulations showed that whilst it is possible to get a linear relationship between α_{av} and ΔP over an experimental range of pressures, the extrapolated null stress resistance may not be correct. It was also shown that the Tiller relationship, equation 6.10, between α_{av} and ΔP could be reduced to a linear expression if n_1 is set equal to 2.

Furthermore it was shown that the coefficient of compressibility increases with null stress voidage, thus partially explaining the increase in k_c with L_{dm} observed in Chapter 4.

The model was used to describe the voidage gradients within compressed filter cakes. Also it was shown, that when the filter cake had undergone significant compression, the average cake voidage becomes independent of the applied pressure, while α_{av} still increases with applied pressure. Finally it was shown that applying the Kozeny-Carman equation directly to filtration data without accounting for the voidage gradient could result in errors when determining either α_{av} or the Kozeny constant.

Experimental validation of the model is required. In order to do this, the voidage gradient within the filter cake will have to be determined experimentally. This may prove difficult with highly compressible cakes due to there being a steep voidage gradient close to the membrane which accounts for most of the cake resistance. Further experimental measurements of α_{av} at low pressures ($0-2 \times 10^4$ Pa) should be performed to determine if the linearity in the relationship between α_{av} and ΔP extends to zero pressure.

CHAPTER 7

CROSSFLOW MICROFILTRATION CHARACTERISTICS OF *K. marxianus*

7.1 Introduction

Crossflow microfiltration has attracted considerable research in the past two decades. This research can be divided into four main areas: (i) analysing the effects of process variables such as pressure, temperature, cell concentration and crossflow velocity; (ii) analysing cake formation and cake characteristics and subsequent determination of α_{av} in crossflow microfiltration; (iii) determination of fouling behaviour in crossflow microfiltration and (iv) modelling cake formation and flux behaviour in crossflow microfiltration.

When filtering cell suspensions, fouling of the membrane or cake layer by media components has been shown to have a significant impact on the filtration performance, as discussed in Chapter 2. However, it is difficult to ascertain the precise mechanism of fouling when combined with cake formation in crossflow microfiltration. The cake properties and consequently the cake resistance can be significantly different to that observed during dead-end filtration. This is due to (i) fouling of the cake layer by media components (Tanaka *et al.*, 1994c; Tanaka *et al.*, 1998); (ii) differences in cake voidages (Mackley and Sherman, 1992); (iii) shear induced arrangement of particles (Tanaka *et al.*, 1994b, 1996) and (iv) preferential deposition of small cells (Baker *et al.*, 1985; Foley *et al.*, 1993). Therefore the cake resistance may be different to those observed in dead-end filtration or vary when the operating parameters are changed. Consequently, interpretation of filtration behaviour is a complex process, where many different factors must be considered.

One approach used to separately analyse the effects of cake formation and fouling is that developed by Foley *et al.*, (1995b). In that study three different suspensions produced from resuspended baker's yeast, were filtered under the same operating conditions. These were, (i) resuspended cell suspensions, defined as unwashed cell suspensions, (ii) cell suspensions washed with saline using centrifugation, defined as washed cell suspensions and (iii) cell free supernatant produced by centrifugation. The washed cell suspensions gave better filtration fluxes than unwashed cell suspensions. This was probably due to fouling by macrosolutes occurring with the unwashed suspensions. Furthermore fouling was shown to occur when filtering the supernatant.

However, in that study the cake mass was not determined and subsequently cake resistances could not be determined. A similar approach is utilised in this study to determine the relative contribution of fouling to the observed filtration behaviour for *K. marxianus*. Furthermore by measuring the mass of cake formed for both washed and unwashed suspensions it is possible to determine the effect of fouling on cake formation in crossflow microfiltration.

It has been shown that particle polydispersity of the feed suspension can result in preferential deposition when filtering baker's yeast (Foley, 1993). *K. marxianus* is a dimorphic organism (O' Shea, 1998) and has a wide distribution of cell morphology as shown in Chapter 4. Consequently, preferential deposition could in theory contribute significantly to the filter cake resistance and hence filtrate flux. By measuring the rate of cake formation and using image analysis to determine the morphological parameters of the feed suspension and recovered filter cake it is possible to determine the relative contribution of preferential deposition to observed filtration behaviour.

In many studies with cell suspensions, the filter cake mass is not determined during crossflow microfiltration and consequently it is not possible to determine the cake resistance during crossflow microfiltration. Where the cake resistance has been determined during crossflow microfiltration, fouling effects are normally ignored.

Many of the observed phenomena in crossflow microfiltration, such as increasing specific cake resistance with increasing crossflow velocity (Riesmeier *et al.*, 1987; Riesmeier *et al.*, 1989) or the specific cake resistance exhibiting a minimum with respect to filtration pressure (Baker *et al.*, 1985; Riesmeier *et al.*, 1989; Schlupe and Widmer, 1996), could be due to fouling. It has been predicted in modelling work by Foley (1994) that the above phenomena *could* be caused by fouling.

In this study the impact of fouling on cake resistance is determined by measuring the reversible and irreversible components of fouling and assuming a simple fouling model where the increase in membrane resistance is proportional to the volume of filtrate passed through it. Furthermore the apparent specific resistance in crossflow microfiltration is compared with the dead-end specific resistance of the feed suspension and recovered crossflow filter cake. This allowed comparison of the composition of the crossflow filter cake and dead-end filter cakes.

In Chapter 4, different morphologies of *K. marxianus* were used to ascertain the role of cell morphology on dead-end filtration behaviour. For the crossflow microfiltration experiments reported here, three different morphologies of *K. marxianus* were used to ascertain the role of cell morphology in crossflow microfiltration. As with dead-end filtration, it is believed that by using a single microorganism which can exhibit a variety of morphological forms, the precise effects of cell size and shape on filtration behaviour can be elucidated more clearly than if a number of different microorganisms had been used.

Crossflow microfiltration is a relatively simple unit operation from an engineering perspective. However, as outlined in Chapter 2, many different factors can contribute to the crossflow microfiltration performance. The combined effects of process variables, cell morphology and fouling on filtration flux and cake resistance have not been previously researched in the same study. It is the objective of this chapter to elucidate the relative contribution to filtration behaviour, of some of the phenomena that are known to occur during crossflow microfiltration. This chapter focuses on the role of cell morphology and media constituents on the

filtrate flux, the rate of cake formation, preferential deposition, filter cake masses, the mean specific resistance, fouling and the reversible and irreversible components of the resistance to filtrate flow.

7.2 General observations in crossflow microfiltration

Crossflow microfiltration behaviour for a washed cell suspension, an unwashed cell suspension and spent medium, for a yeast like morphology ($L_{dm} = 3.24$) grown in whey medium is shown in Figure 7.1. Typical flux *versus* time behaviour can be observed for all three suspensions. The flux decreases rapidly during the first few minutes of filtration, then decreases slowly over the duration of the filtration run. In effect a pseudo steady state is reached. It can be observed that for the washed cell suspension, the flux values obtained during the pseudo steady state period are an order of magnitude greater than those obtained for the unwashed suspension. Furthermore it can be clearly seen that when filtering cell free spent medium the fluxes attained are less than those for washed cell suspensions. This suggests that fouling of the membrane or cake by macromolecules is occurring when crossflow filtering the unwashed cell suspension. This is in agreement with general observations of fouling during crossflow microfiltration with yeast suspensions (e.g., Foley *et al.*, 1995b; Patel *et al.*, 1989).

By comparison, there was little difference between the mean specific resistances measured at 100 kPa using dead-end filtration for the same unwashed and washed cell suspensions used in Figure 7.1. These resistances were determined as 7.39×10^{11} m/kg and 7.62×10^{11} m/kg respectively. This indicates a fundamental difference between crossflow microfiltration and dead-end filtration behaviour. These results suggest that fouling by macrosolutes may have a significant role in determining filtration performance in crossflow microfiltration, whereas in dead-end filtration the resistance to flow caused by membrane fouling was found to be negligible in comparison to the cake resistance.

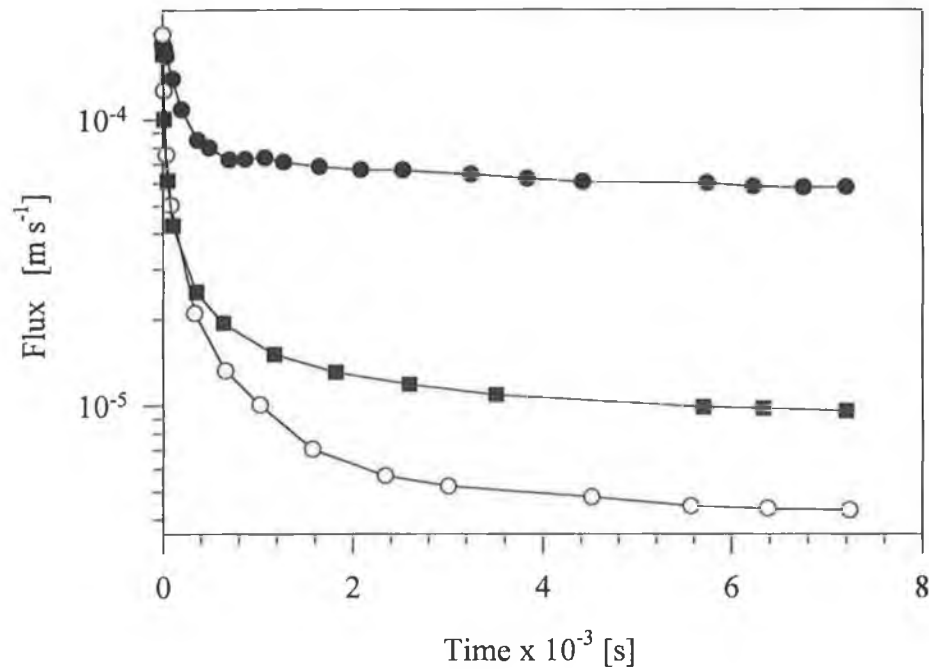


Figure 7.1 Filtration flux as a function of filtration time for a predominantly yeast-like morphology of *K. marxianus* grown in whey medium. $L_{dm} = 3.24$, $u = 0.5$ m/s, $\Delta P = 100$ kPa, $c \approx 17.5$ kg/m³. Symbols: ■ spent medium; ○ unwashed suspension and ● washed suspension.

As fouling appears significant during crossflow microfiltration, four different growth media are used to ascertain the effect of medium constituents on filtration behaviour. Washed cell suspensions are used to ascertain the affect of cell morphology on filtration behaviour, filter cake formation and specific cake resistance.

7.3 Flux patterns in crossflow microfiltration

In Figure 7.2, filtration fluxes during the two hour period of filtration are plotted for three different morphologies of *K. marxianus* grown in YEP_NL media. For each morphology filtered, the washed cell suspensions gave the greatest pseudo steady-state flux values. The qualitative filtration behaviour is similar to that observed in Figure 7.1.

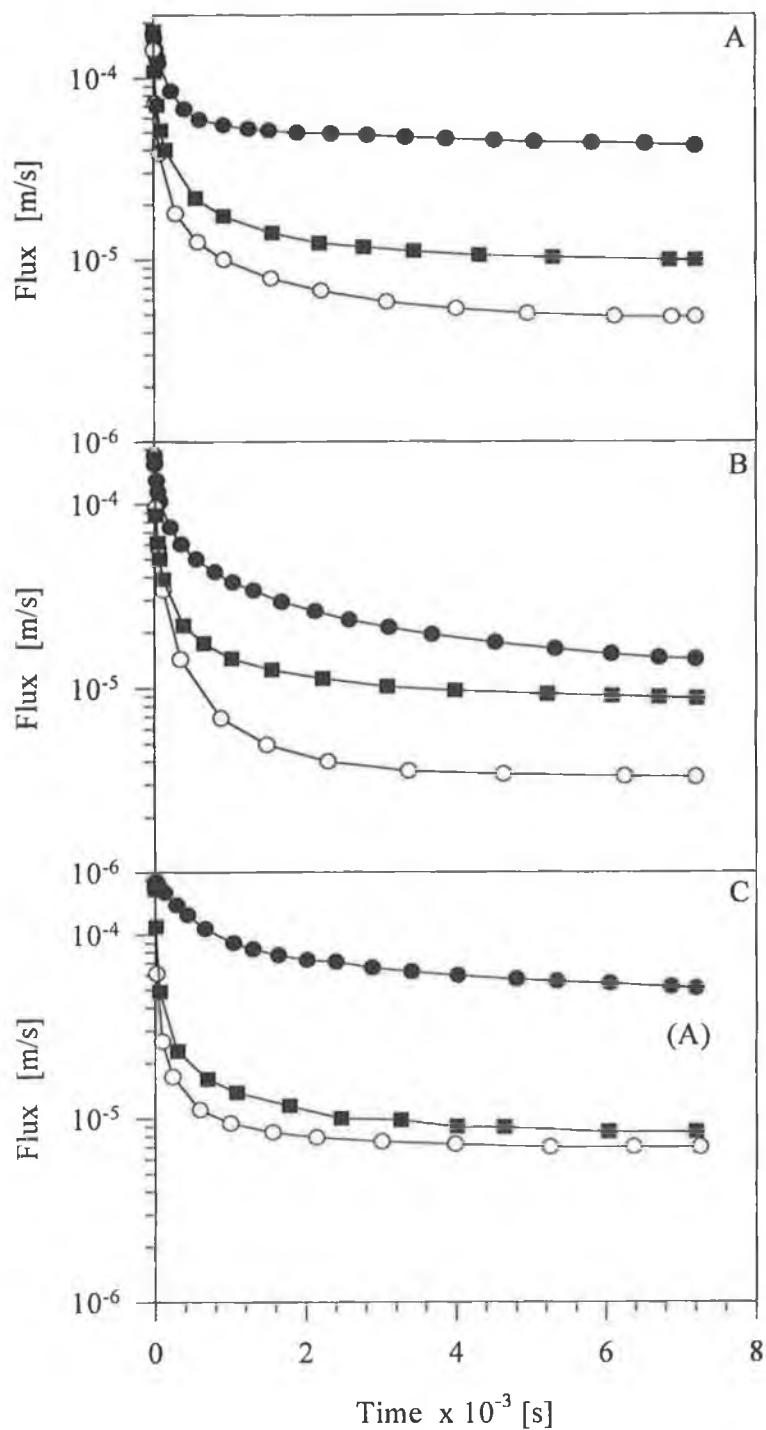


Figure 7.2 Filtration behaviour of *K. marxianus* grown in YEP_NL media. (A) Batch, 800 rpm; (B) Batch 500 rpm; (C) Continuous culture, dilution rate = 0.19 h⁻¹, $u = 0.5$ m/s, $\Delta P = 100$ kPa, $c \approx 17.5$ kg/m³. Symbols: ■ spent medium; ○ unwashed cell suspension and ● washed cell suspension.

The unwashed cell suspensions gave the lowest flux values, while the cell free spent medium gave flux values between the washed and unwashed suspensions. The different growth conditions resulted in three different mean cell morphologies for each growth medium. Cell suspensions grown in batch culture at 800 rpm agitation rate, produced the most yeast-like suspensions, L_{dm} values ranged between 2.92 to 3.45. Cell suspensions grown at an agitation rate of 500 rpm in batch culture, produced yeast suspensions more elongated than the 800 rpm batch cultures, L_{dm} values ranged between 4.42 to 5.31. Continuous cultures produced cell suspensions which were predominantly mycelial in nature, L_{dm} values ranged between 55 to 66.

For each of the three mean cell morphologies shown in Figure 7.2, the washed cell suspensions gave dramatically higher flux values throughout the filtration run than unwashed cell suspensions. This finding is consistent with previous research with washed and unwashed suspensions of resuspended baker's yeast (Foley *et al.*, 1995b) and baker's yeast resuspended in water and simulated media, (Patel *et al.*, 1987). The cell free spent medium gave higher fluxes than unwashed suspensions but lower than the washed suspensions. This suggests fouling by components of the spent medium contribute significantly to high resistances to filtrate flow observed when filtering unwashed cell suspensions. Numerous authors have demonstrated that fouling by macrosolutes contributes to the low fluxes observed during crossflow microfiltration of microbial suspensions (Boyaval *et al.*, 1996; Nagata *et al.*, 1989; Patel *et al.*, 1989; Tanaka *et al.*, 1998). The cell suspensions grown in the other media displayed similar flux patterns to that shown in Figure 7.2. This indicates that fouling by components in the spent medium contributes significantly to filtration behaviour of unwashed cell suspensions of *K. marxianus* regardless of the growth medium.

By comparison, Figure 7.3 summarises the dead-end filtration characteristics for washed and unwashed cell suspensions of *K. marxianus* grown in all four media. There was no detectable difference in filtration behaviour of washed and unwashed suspension.

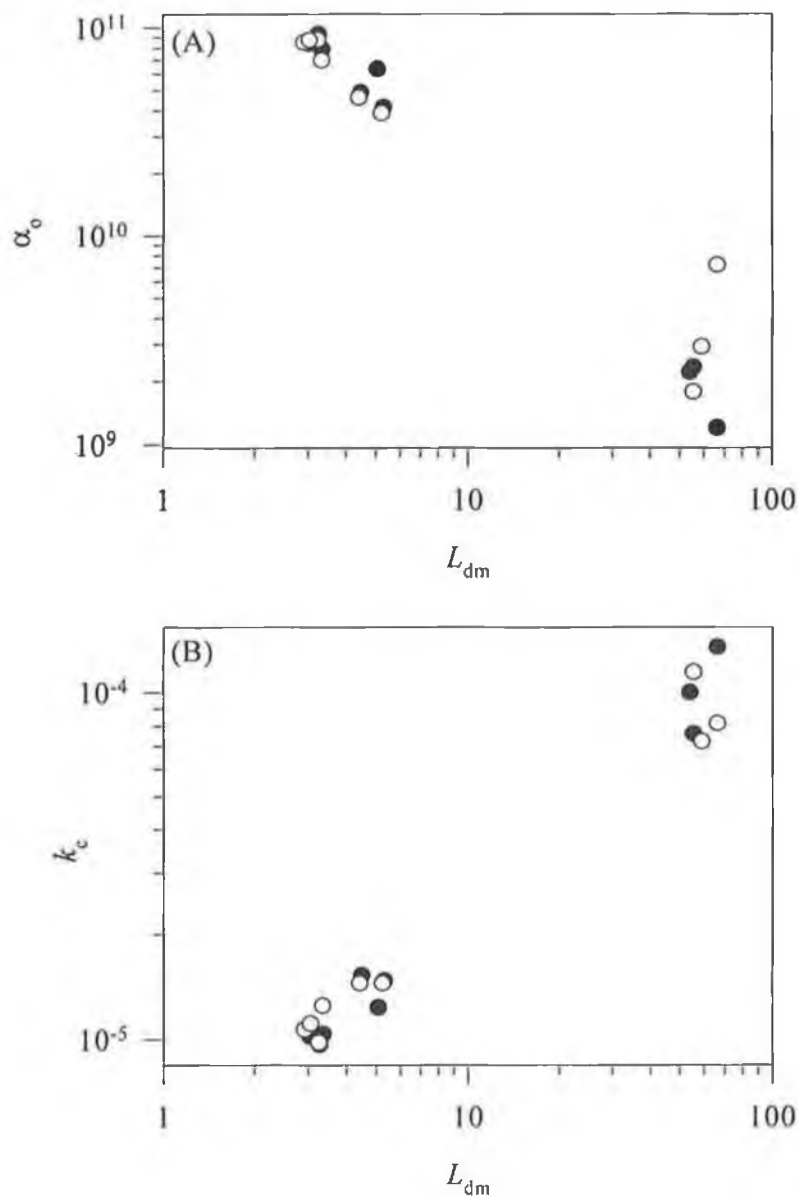


Figure 7.3 Dead-end filtration behaviour of *K. marxianus* grown in various media. (A) Unstressed cake resistance as function of L_{dm} (B) Compressibility as function of L_{dm} . Symbols: ○ washed suspension and ● unwashed cell suspension.

The measured null stress resistance, α_0 and compressibility coefficient, k_c is similar for cells of similar morphology, i.e., similar L_{dm} . Nor does the growth medium appear to have a detectable influence on the filtration behaviour in dead-end filtration. This indicates that neither fouling by media components nor growth

media is a significant factor in dead-end filtration. However, it appears that for all mean cell morphologies and growth media, fouling is a factor in crossflow microfiltration behaviour. It should be noted that the membrane used in dead-end and crossflow microfiltration were of different composition. The Carbosep membrane used for crossflow microfiltration is composed of a ZrO_2 filtering layer on a carbon support, whereas polysulphone membranes were used for dead-end filtration. This may have been a contributing factor in the observed differences between dead-end filtration and crossflow microfiltration behaviour.

It should be noted that cell suspensions grown under similar fermentation conditions but in different media, produce similar mean morphologies (L_{dm}) but with different S_v (0-10% difference in S_v). (Morphology data for washed cell suspensions and unwashed cell suspensions is given in Table 7.3 and Table 7.8 respectively). Therefore specific resistances measured at 100 kPa (transmembrane pressure drop used in crossflow microfiltration) differed, for cultures of similar morphology grown in different media, due to a size difference of the cells. Similarly it was noted that, washing cell suspensions caused a reduction in cell size, typically 5-10% increase in S_v .

Figure 7.4 shows plots of total resistance *versus* filtrate volume for each morphology using YEP_NL media. It can be seen the resistances are non-additive, i.e. in each case the sum of the washed suspension resistance and the spent medium resistance is not equal to the unwashed suspension resistance. Similar behaviour occurs with the cell suspensions grown in the other media and if the resistances are plotted as a function of time. In nearly all cases the sum of the resistances of washed suspensions and spent medium resistances are *less* than the unwashed resistances. This effect is greatest for the cells grown in batch culture, i.e. yeast-like morphologies. For mycelical suspensions (continuous cultures), the sum of the resistances from washed cell suspensions and spent medium were approximately equal to the unwashed suspension resistance. This may indicate that cell morphology impacts fouling. It should be noted that the filtrate fluxes for the cell free spent medium for all three morphologies are similar.

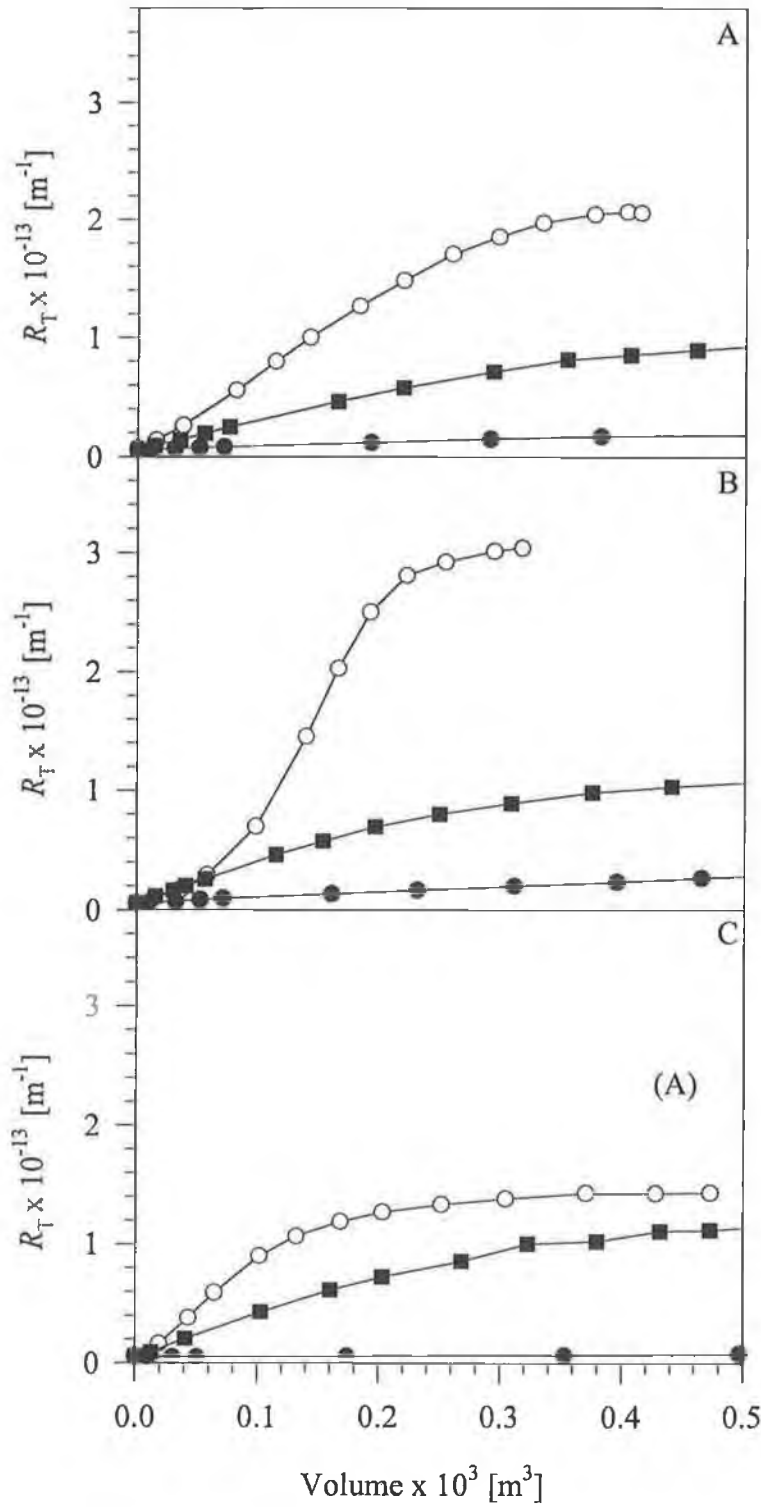


Figure 7.4 Total resistance as a function of filtrate volume for *K. marxianus* grown in YEP_{NL} media. (A) Batch, 800 rpm; (B) Batch 500 rpm; (C) Continuous

culture, dilution rate = 0.19h^{-1} . $u = 0.5$ m/s, $\Delta P = 100$ kPa. Symbols: ■ spent medium; ○ unwashed suspension and ● washed suspension.

The trends shown in Figure 7.4 are contrary to the observations of Foley *et al.*, (1995b). The authors on that occasion found the sum of the resistances for supernatant and washed cell suspensions to be *greater* than the resistances measured for unwashed cell suspensions. The authors attributed it to yeast cells protecting the membrane pores from fouling. The difference in the additive behaviour between the results here and those of Foley *et al.* (1995b), may be due to the nature of the suspensions, cultured suspensions as opposed to resuspended, i.e. the fouling agents would be different. Other factors may also be responsible such as different membrane types and/or operating conditions.

The reason why the unwashed cell suspensions have a higher total resistance than the sum of washed and spent medium resistances, is unclear at present. However, one possible explanation, is that the cells in the unwashed suspensions act as "secondary membranes" (Arora and Davis, 1994), and as filtration progresses both the membrane and cell cake become fouled or clogged. Cake fouling has been shown to occur with both yeast (Tanaka *et al.*, 1994c) and bacterial cell suspensions (Tanaka *et al.*, 1998). Furthermore it was shown in Chapter 4 that yeast morphologies form less porous filter cakes than mycelial morphologies. Thus mycelial cakes may allow media components to pass through more freely than filter cakes comprised of yeast morphologies, i.e., are less prone to fouling.

There are two factors worth mentioning before a more in-depth comparison of results: (i) fouling appears to occur when filtering washed cell suspensions, as steady state fluxes are never attained. Thus, washing may not take out all the components in the media (other than cells) that cause fouling; (ii) due to different growth conditions, cell biomass was different for each case. Hence, doing filtration at a constant concentration of 17.5 kg/m³ may have resulted in the retention of more medium components during the dead-end filtration stage of the suspension preparation for the more dilute cultures.

7.4 Spent medium and fresh medium studies

Figure 7.5 shows the relationship between filtrate flux and time for spent medium and fresh unfermented medium. In Table 7.1 filtration data for the filtration experiments shown in Figure 7.5 is given. The irreversible resistance, R_{irrev} , and reversible resistance, R_{rev} , is related to the total resistance, R_{T} , by the following expression,

$$R_{\text{T}} = R_{\text{mo}} + R_{\text{rev}} + R_{\text{irrev}} \quad [7.1]$$

Where R_{mo} is the clean membrane resistance. In Figure 7.5 and Table 7.1 it can be seen that the pseudo steady state flux of the spent medium appears to be independent of the growth conditions. Also the growth medium appears to have little impact on the filtrate fluxes of the spent medium, even though the fresh whey based media gave substantially better fluxes than the peptone media. It should be noted that spent whey based media give marginally better fluxes (approximately 5-20%) than either the peptone media, as indicated in Table 7.1.

Intuitively it may be expected that spent medium gives higher fluxes than the fresh medium (as occurs with YEP_{NL} media), due to utilisation of medium components during fermentation, some of which may cause fouling. However, this clearly does not occur with the whey media. It may be that some fermentation product, e.g. enzymes, proteins, lipid etc. also contribute to the fouling of the spent media. This could explain the lower fluxes obtained with the spent medium for the whey and whey2 media, compared to the fresh medium. It has previously been shown that *K. marxianus* produces a wealth of fermentation products (Ku and Hang, 1992). Some products of fermentation may have controlled the fouling behaviour of the spent medium. This may be the reason why the filtration of all the spent media gives similar results.

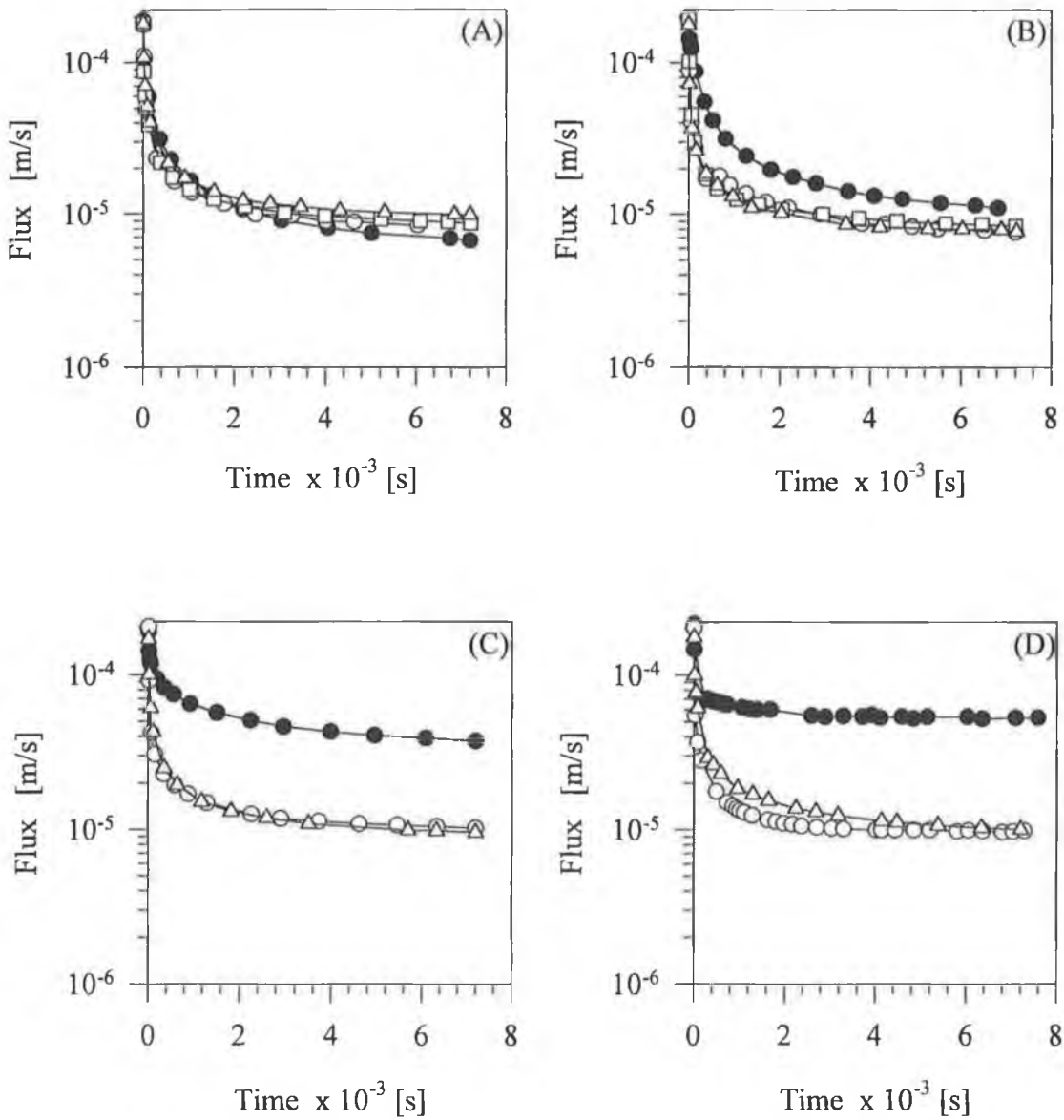


Figure 7.5 Filtration behaviour of spent and original media. (A) YEP_NL (B) YEPL, (C) Whey, (D) Whey2. $u = 0.5$ m/s, $\Delta P = 100$ kPa. Symbols: \triangle 800 rpm batch; \square 500 rpm batch; \circ continuous culture and \bullet fresh medium.

It can be seen from Table 7.1 that in all cases there is a considerable degree of reversible fouling (38-80% of total fouling) for the spent media. This suggests the formation of a cake layer by small aggregates present in the media. Similar results can be seen with the filtration data of the fresh media.

Table 7.1 Two hour fluxes and fouling behaviour for spent and fresh media.

Medium	Growth conditions	$J_{2\text{hrs}}$ m/s x 10^6	1R_T m ⁻¹ x 10^{-11}	R_{irev} m ⁻¹ x 10^{-11}	R_{rev} m ⁻¹ x 10^{-11}
YEPL					
Fresh	N/A	10.87	91.97	18.18	68.74
Spent	500 rpm/Batch	8.38	119.24	39.36	74.64
Spent	800 rpm/Batch	7.76	123.80	18.01	100.14
spent	Cont. Culture	7.40	135.02	30.02	100.12
YEP _N L					
Fresh	N/A	6.76	148.50	5.52	137.65
Spent	500 rpm/Batch	8.73	114.00	46.43	62.00
Spent	800 rpm/Batch	9.91	100.88	21.50	73.82
Spent	Cont. Culture	8.44	118.00	37.50	74.85
Whey					
Fresh	N/A	37.40	26.76	6.03	15.44
Spent	800 rpm/Batch	9.60	104.20	46.75	51.57
Spent	Cont. Culture	10.20	98.05	39.07	54.05
Whey2					
Fresh	N/A	53.20	18.78	11.20	2.90
Spent	800 rpm/Batch	10.00	99.50	56.10	37.70
Spent	Cont. Culture	9.88	101.21	47.66	48.60

¹ Total resistance after 2 hours filtration.

Ultrafiltering boiled whey medium was used to produce whey2 medium. This should remove any aggregates formed by protein denaturation during the boiling stage. Therefore less aggregates would be expected to be present after autoclaving

than with the whey medium. Consequently, less reversible fouling would be expected when filtering whey₂ medium than when filtering whey medium, as shown in Table 7.1. Similarly the neutralised peptone in YEP_{NL} medium should produce less aggregates than the peptone used for YEPL medium according to the manufacturers of the product. However, there is no evidence of this in Table 7.1 as reversible fouling is greater for fresh YEP_{NL} medium than fresh YEPL medium.

There appears to be a substantial difference between the degree of irreversible fouling of fresh and spent medium. For all media there appears to be considerably less irreversible fouling for the fresh medium than for the spent medium. For whey media the total fouling is much less for the fresh medium than the spent medium. Furthermore for the spent peptone-based media a greater fraction of the fouling is reversible, compared to the whey based media. This would indicate differences in the composition of the fermentation product.

The relationship between total filtration resistance and filtrate volume is shown in Figure 7.6 for fresh YEP_{NL} medium. It can be seen that the total resistance, R_T , is more than an order magnitude greater during crossflow microfiltration compared with dead-end filtration, Figure 7.6 (A). However, it can be seen that the rate of increase of R_T is nearly identical during the early stages of crossflow microfiltration and dead-end filtration (as shown in Figure 7.6 (B)) even though two different membrane types were used. (Dead-end filtration was conducted using polysulphone membranes whereas crossflow filtration experiments were conducted using carboxepharse membranes.) This may suggest that fouling is similar during dead-end filtration and the early stages of crossflow microfiltration. The difference in the magnitude of R_T may be due to the crossflow microfiltration membrane having a lower porosity than the dead-end filtration membrane.

For dead-end filtration of YEP_{NL} fresh media, R_{rev} was determined as $7.25 \times 10^{10} \text{ m}^{-1}$ and R_{irev} determined as $1.83 \times 10^{10} \text{ m}^{-1}$. Therefore, during dead-end filtration most of the increase in fouling is attributable to reversible fouling. This mirrors what occurs during crossflow microfiltration, as shown in Table 7.1.

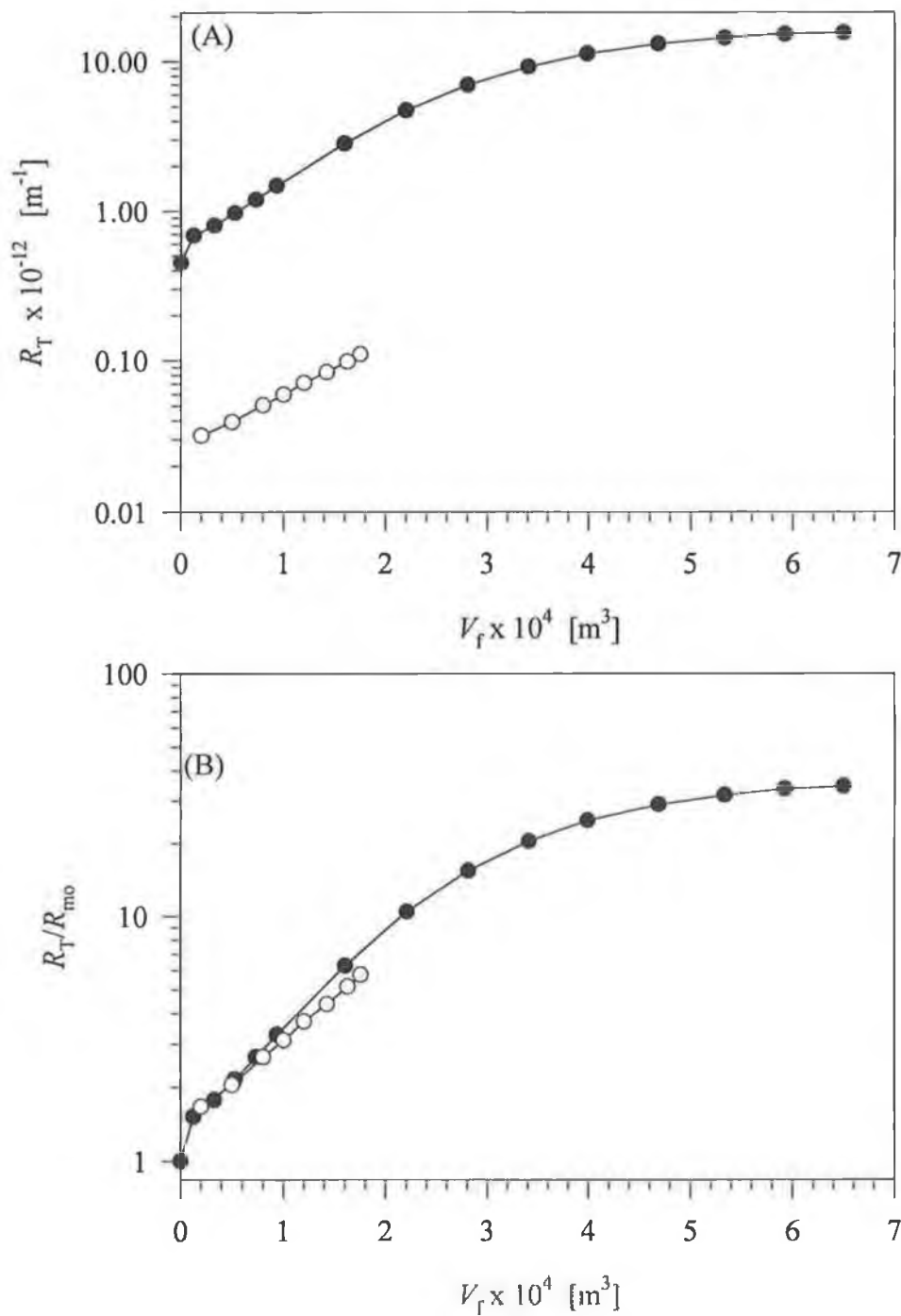


Figure 7.6 Comparison between dead-end filtration and crossflow microfiltration of fresh YEP_NL media. (A) R_T versus V_f , (B) R_T/R_{mo} versus V_f . Symbols: ● crossflow microfiltration, $u = 0.5$ m/s, $\Delta P = 100$ kPa and ○ dead-end filtration, $\Delta P = 100$ kPa.

The spent media and fresh media studies have demonstrated that a significant drop in the filtrate flux can be expected, due to fouling of the carboxepharose membrane by medium components. Varying the growth medium or growth conditions does not appear to significantly affect the filtrate fluxes observed. Furthermore a significant percentage of the total resistance after two hours of filtration is due to irreversible fouling.

7.5 Washed suspensions

An important feature of the crossflow microfiltration of washed cell suspensions is that steady state flux is not obtained. Figure 7.7 shows the filtrate flux for a washed yeast suspension (800 rpm batch culture, Whey medium). The suspension filtered in Figure 7.7 gave the closest approximation of steady state flux behaviour of all washed suspensions used in this study. Also shown in Figure 7.7 is the cake mass as a function of filtration time, (as determined by technique described in Chapter 3, Section 3.14.12). It can be seen after approximately 600 seconds that the cake mass reaches a steady state value. This is mirrored by the filtration flux data, whereby the filtration flux decays rapidly for the first 600 seconds and then approaches a near steady state, i.e., pseudo steady state. After 600 seconds of crossflow microfiltration, the filtrate flux is approx. 7.5×10^{-5} m/s and continues to decrease at a slower rate to 5.8×10^{-5} m/s after 2 hours of filtration. For other washed cell suspensions, the rate of decrease of flux with respect to time during the pseudo steady state period was typically found to be greater than shown in Figure 7.7.

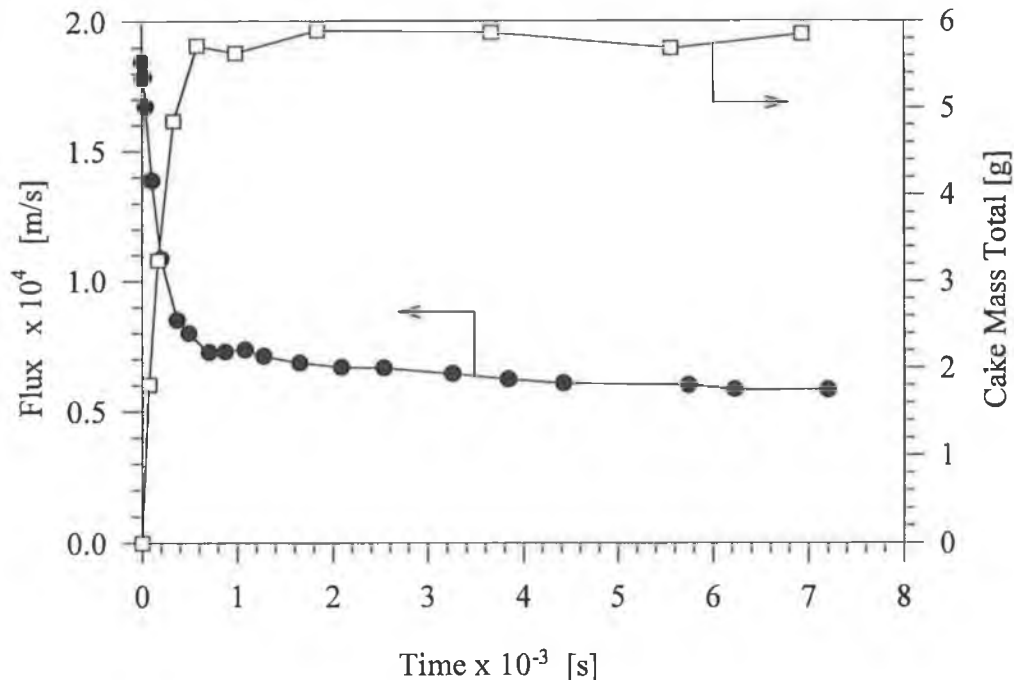


Figure 7.7 Filtrate flux and cake formation for a washed suspension of *K. marxianus*. Whey media, 800 rpm, Batch culture, $c \approx 17.5 \text{ kg/m}^3$, $u = 0.5 \text{ m/s}$, $\Delta P = 100 \text{ kPa}$.

7.5.1 Cake formation and flux behaviour of washed cell suspensions

Cake formation of cell suspensions of different mean morphology and grown in different media is shown in Figure 7.8. In nearly all cases cake formation is complete or nears completion after 10-15 minutes of cross-flow filtration. However, the filtrate flux continues to decline throughout the 2 hours of cross flow filtration for all experiments using washed cell suspensions. Therefore the secondary decrease in flux is not attributable to cake formation.

The method used to determine cake mass during filtration is based on monitoring the cell concentration in the feed reservoir as described in Chapter 3. It is a modified form of the technique previously described by Flynn *et al.*, (1990). Other techniques have been used to determine cake mass such as a cell lysis technique (Riesmeier *et al.*, 1987) and weighing the cake at the end of microfiltration (Tanaka *et al.*, 1993).

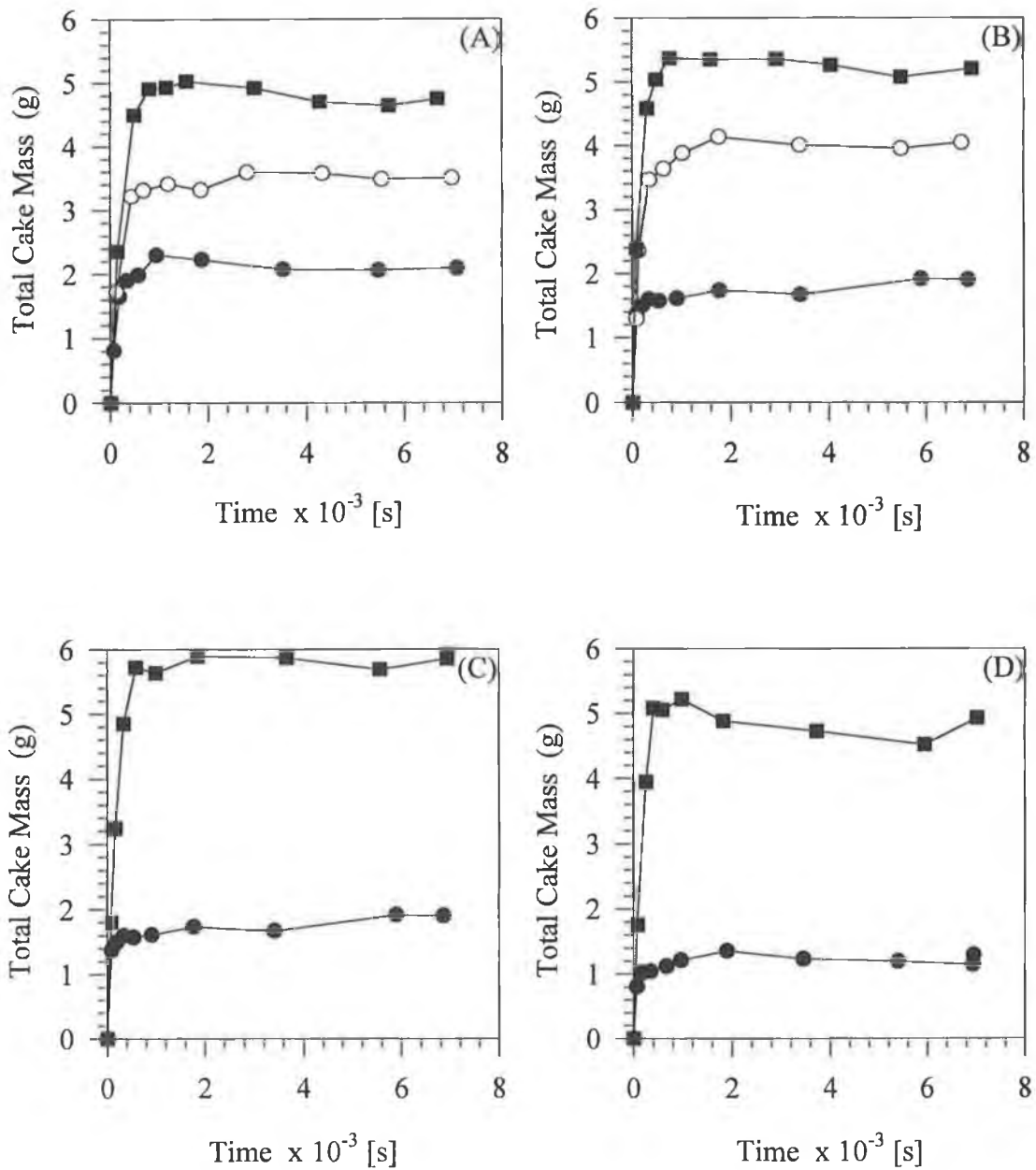


Figure 7.8 Cake formation during cross flow filtration of washed suspensions of *K. marxianus*. (A) YEP_{NL}, (B) YEPL, (C) Whey, (D) Whey2. $u = 0.5$ m/s, $\Delta P = 100$ kPa, $c \approx 17.5$ kg/m³. Symbols: ■ 800 rpm batch culture; ○ 500 rpm batch culture and ● continuous culture.

However, these techniques require the filtration to be stopped in order to determine the cake mass. The method used here can in theory be applied to any module configuration and requires only small sample volumes for analysis.

Using wet weight analysis to determine the cake mass was prohibitive as the sample volume required to accurately determine the cell concentration was too large. Determining the reservoir cell concentration using optical density measurements as applied by Flynn *et al.* (1990) could also be utilised. However, during trials, using optical density measurements resulted in considerable scatter in the determined cake masses. This is probably due to the higher cell concentrations used here compared with Flynn *et al.*, (1990), where most of the cells in the feed reservoir were deposited to form the filter cake. Furthermore at low cell concentrations the optical density is proportional to the cell concentration, however, at higher cell concentrations the optical density becomes almost independent of the cell concentration. Therefore the method utilised here would appear to be a simple and accurate method of determining cake masses.

In Figure 7.8 it appears that the steady state cake mass obtained is morphology dependent. Increasing L_{dm} results in a reduction in cake mass. Similar trends were found to occur with each growth medium. There are a number of possible reasons why cake mass decreases with L_{dm} . Firstly increasing L_{dm} has been shown, in Chapter 4, to cause an increase in cake voidage in dead-end filtration. Therefore, while there is a considerable difference in the cake mass for each morphology, there may not be much difference in cake height. Cake formation is expected to cease once a critical shear stress is surpassed. The shear stress will increase with increasing cake height and will be similar for all morphologies at the end of cake formation if the cake heights are similar.

Secondly it is well established that particle deposition is size dependent (Blake *et al.*, 1992; Foley *et al.*, 1995a). For a given trans-membrane pressure drop and crossflow velocity, only particles smaller than a critical size will deposit. For cell suspensions of high L_{dm} , the fraction of cells with a size less than the critical size is small, therefore less deposition should occur with these suspensions. In this study the particle size (mean cell volume) increases with increasing L_{dm} .

Fouling by other suspension components could affect cake formation. However, possible fouling affects do not appear to detract from the general observations made here as cake formation is completed within minutes of filtration commencing. During this time, limited filtration and hence fouling would have occurred.

The most likely cause of the decrease in flux after cake formation is completed is fouling by other components in the washed suspension. Other possible reasons for the flux to continue dropping after cake formation is complete, include time dependent compression or rearrangement of particles within the cake and these will be dealt with in more detail in the following sections.

In Figure 7.9 the impact of switching feed suspension from washed cell suspension to a saline suspension is shown. After two hours of filtration were completed the feed was switched from cell suspension to a saline suspension (1% concentration). The last hour of filtration with cell suspension and subsequent 30 minutes of filtration with the saline suspension is shown in Figure 7.9. The arrows indicates the switch in feed from cell suspension to saline suspension. For the suspensions grown on YEP_NL medium shown in Figure 7.9, the flux during the saline filtration stage remains the same as the 2 hour flux value or increases slightly (500 rpm culture). Cell suspensions grown in the other media displayed the same behaviour.

It was noted that the saline in the reservoir became slightly cloudy during the saline filtration stage and that cells were present in the reservoir. This suggests some form of shear induced particle removal from the filter cake. However, the concentration of cells in the reservoir during the saline filtration stage was extremely low. It was not possible to determine accurately what percentage of the cake is removed during the saline filtration stage. It was estimated using cell counts that only a fraction of the cake (<5%) was removed during this stage. This suggests the filter cake remains largely intact during the saline filtration stage.

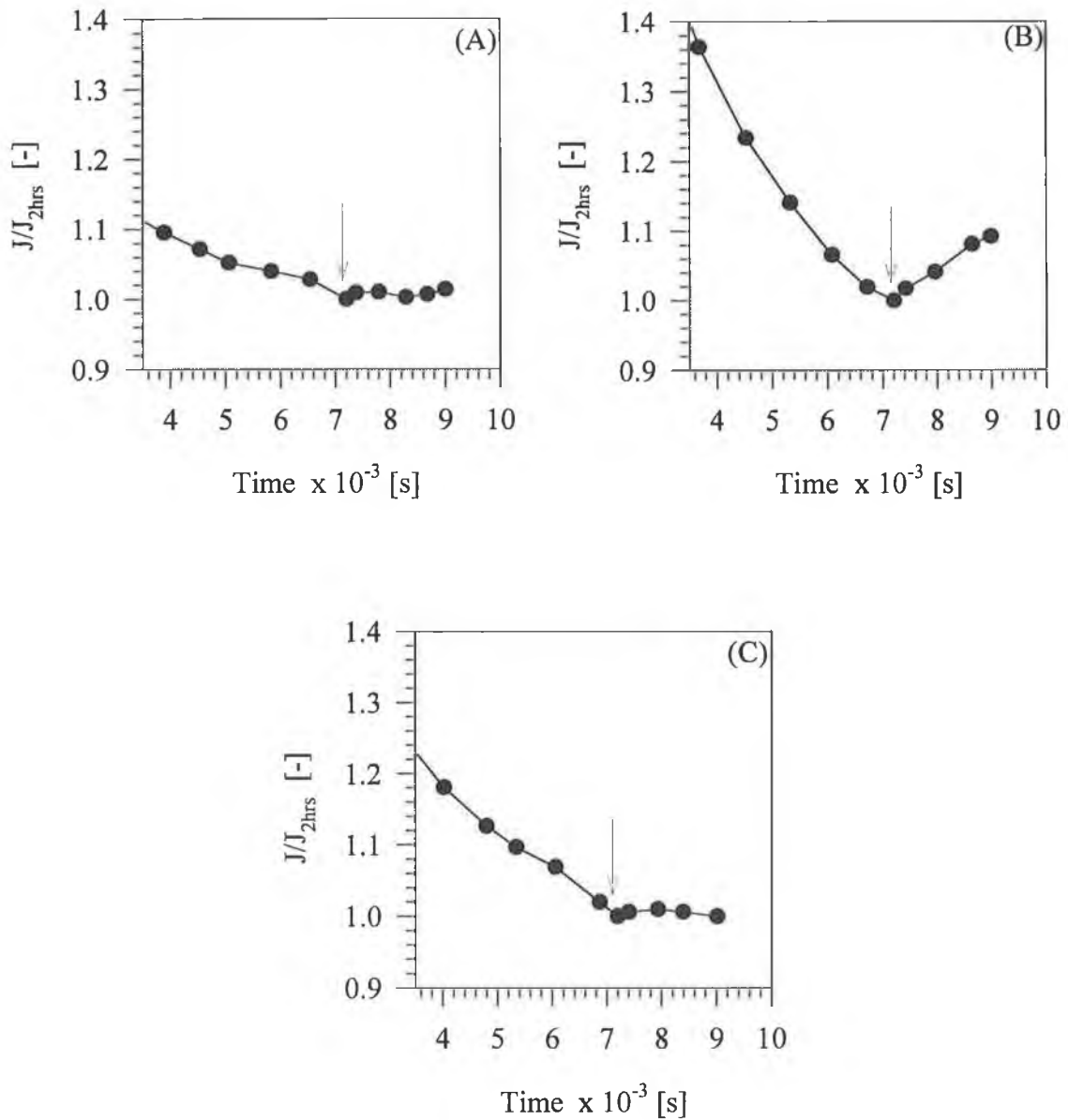


Figure 7.9 The effect of switching the feed suspension from cell suspensions to saline for YEP_{NL} media. (A) Batch, 800 rpm; (B) Batch 500 rpm; (C) Continuous culture, dilution rate = 0.19 h^{-1} . $c \approx 17.5 \text{ kg/m}^3$, $u = 0.5 \text{ m/s}$, $\Delta P = 100 \text{ kPa}$. Arrows indicate switch in feed.

If time dependant compression of the filter cake was occurring (Riesmeier *et al.*, 1987), then the filtrate flux should continue to decrease during the saline filtration stage. However, the filtrate flux remains constant or increases indicating that this does not occur. If the filter cake produced during filtration was partially a flowing

cake (Davis and Birdsell, 1987), then an increase in flux would be expected. In this case, a reduction in the filtrate flux would be expected as there would be less cells in the feed suspension (cell concentration would be dependant on amount of cells removed) to replace the removed cake. Therefore boundary layer formation does not appear to be occurring or at least not impacting filtration fluxes.

During the pseudo steady state the cake mass is constant (Figure 7.8) and time dependent compression does not appear to be occurring as discussed above. Therefore cake affects can be neglected as the cause of the continual decrease in flux during the pseudo steady state period of crossflow microfiltration. The washing stage in theory should remove all the fouling components. However, even after using multiple wash stages using either dead-end filtration or centrifugation does not result in *true* steady state fluxes. It may be that the washing stage used in the preparation of the washed suspensions does not remove all components in the media that cause fouling.

In particular there is evidence of particulate matter in the washed cell suspensions, as shown in Figure 7.10. These particles are much smaller than the cells and consequently sizing of the particles by image analysis was not possible to do accurately. These particles are also present in unwashed suspensions, therefore they do not appear to be a product of the cell washing stage.

When viewed under a microscope, the recovered crossflow filter cakes had a greater concentration of these particles (per unit cell volume) than was in the original suspension or reservoir at the end of filtration, i.e. recovered cake suspensions looked 'dirtier', as shown in Figure 7.10 (C). Furthermore cell pellets of the recovered filter cake, were formed by centrifugation. These had a layer of black material deposited at the bottom of the cell pellet. This layer was not noticeable in centrifugation pellets of the original washed suspension or retentate samples taken after two hours of filtration.

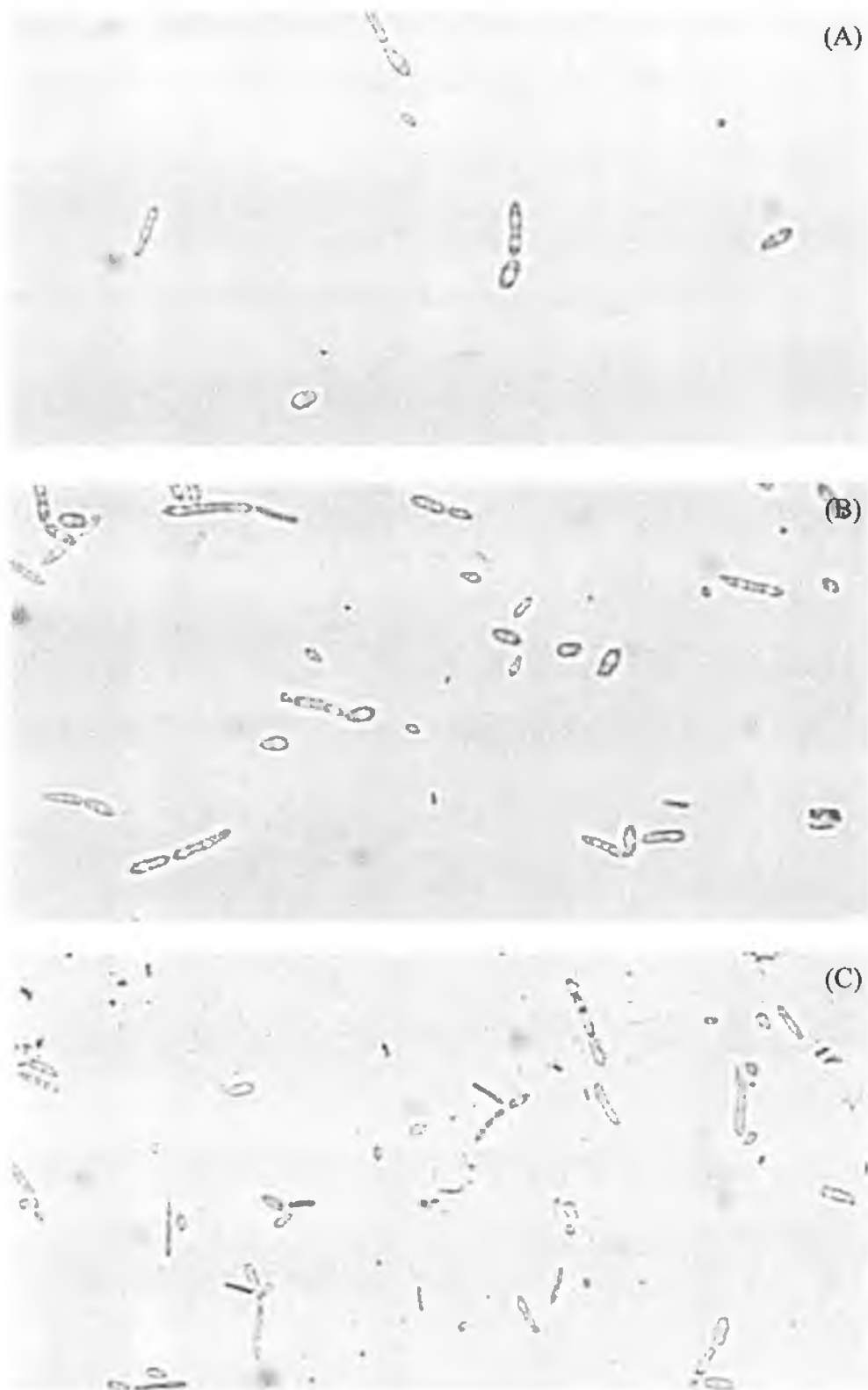


Figure 7.10 YEP_NL media 500 rpm batch culture. (A) washed suspension, (B) retentate after 2 hours and (C) recovered cell cake. Magnification factor 200X.

There are several possible sources for the particles. These may have been present in the original media (Tanaka *et al.*, 1993). Sterilisation of media has been shown to produce precipitates of similar size (Nagata *et al.*, 1989). Alternatively they may be the product of cell autolysis during fermentation or cell lysis caused by shear forces during crossflow microfiltration (Chan *et al.*, 1992).

In Figure 7.11, the flux data for washed suspensions is plotted, for each growth medium. A number of observations can be made from these plots. In the initial stages the filtrate flux decreases more rapidly for the yeast-like morphologies (batch cultures) than for mycelial suspensions (continuous cultures).

This is probably due to the yeast morphologies forming filter cakes with greater mass as shown in Figure 7.7. Furthermore in dead-end filtration, yeast morphologies have higher specific resistances than more elongated cell suspensions. Therefore the total resistance would be expected to be considerably higher for yeast suspensions than for mycelial suspensions.

Secondly the most yeast-like suspensions (batch, 800 rpm), give a closer approximation to a true steady state flux than either the 500 rpm batch cultures or continuous cultures. Possibly the greater cake mass here protects the membrane more from fouling (Foley *et al.*, 1995b), or there may be a lower concentration of aggregates (as observed in Figure 7.10) in the 800 rpm suspensions.

Finally, the filtration fluxes for the 500 rpm batch cultures (peptone-based mediums) behave similarly to 800 rpm batch cultures initially but give lower fluxes later in the filtration. This indicates a greater concentration of aggregates in these suspensions. This is possibly due to the low biomass of 500 rpm fermentations (~20g/l) compared to 800 rpm fermentations (34-40g/L). Therefore a greater fraction of the original suspension is required to obtain a cell concentration of 17.5 g/L. If the concentration of fines were the same in both media then more of the fine particles would be present in the 500 rpm washed cell suspensions, hence greater fouling would occur.

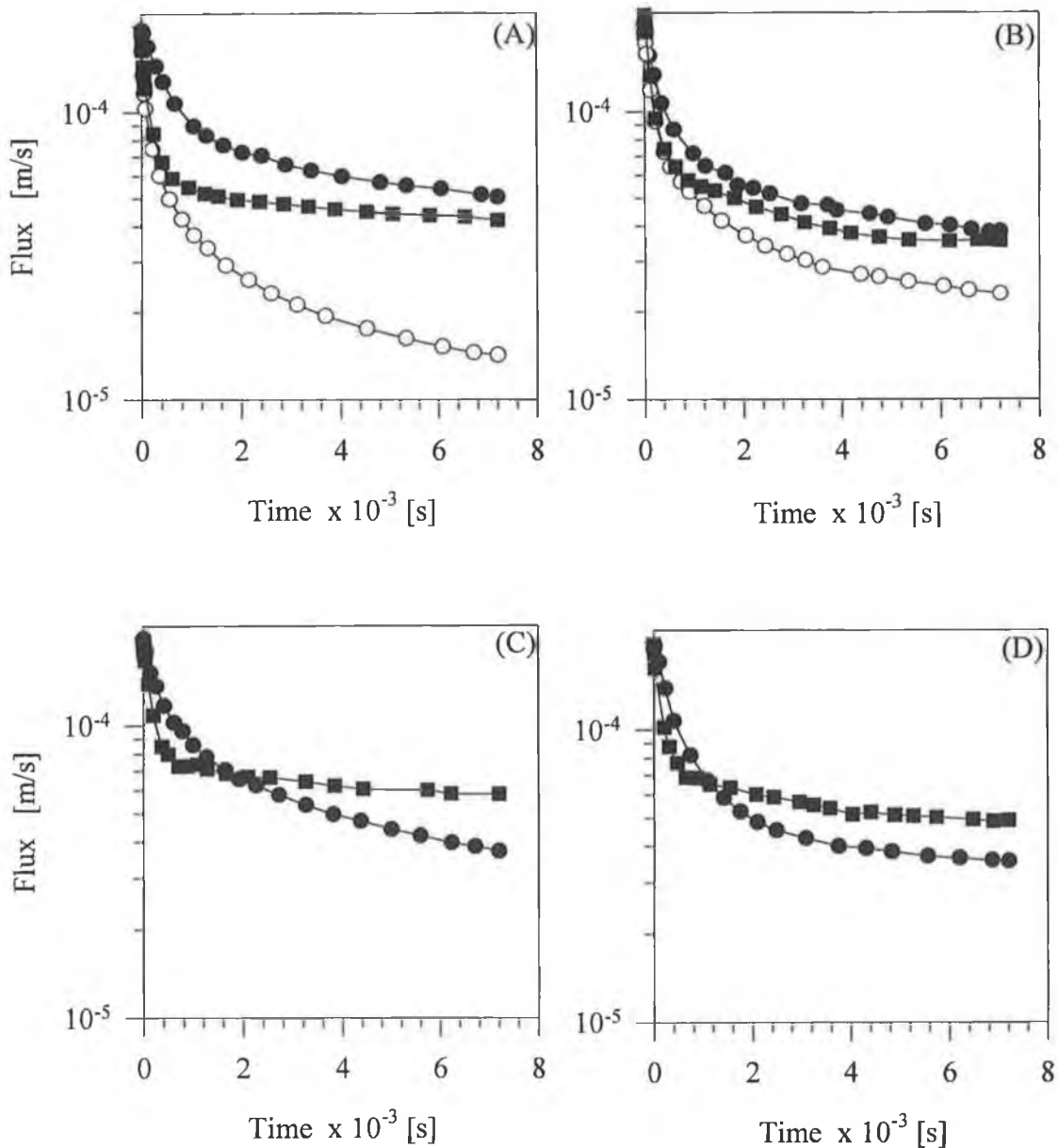


Figure 7.11 Effect of cell morphology on filtration behaviour of *K. marxianus*. (A) YEP_NL media (B) YEPL media (C) Whey media, (D) Whey2 media. $u = 0.5$ m/s, $\Delta P = 100$ kPa, $c \approx 17.5$ kg/m³. Symbols: ■ 800 rpm batch; ○ 500 rpm batch and ● continuous culture.

Obviously the size, amount and properties of the fine particles in the suspensions are going to influence the filtration behaviour of the washed suspensions. Also, other properties such as cake mass and particle size will also influence the

behaviour. Likewise phenomena such as shear induced arrangement and preferential deposition may also play a role in filtration behaviour here.

Figure 7.12 shows the data in Figure 7.11 re-plotted, so as to compare filtration fluxes of suspensions with similar morphologies.

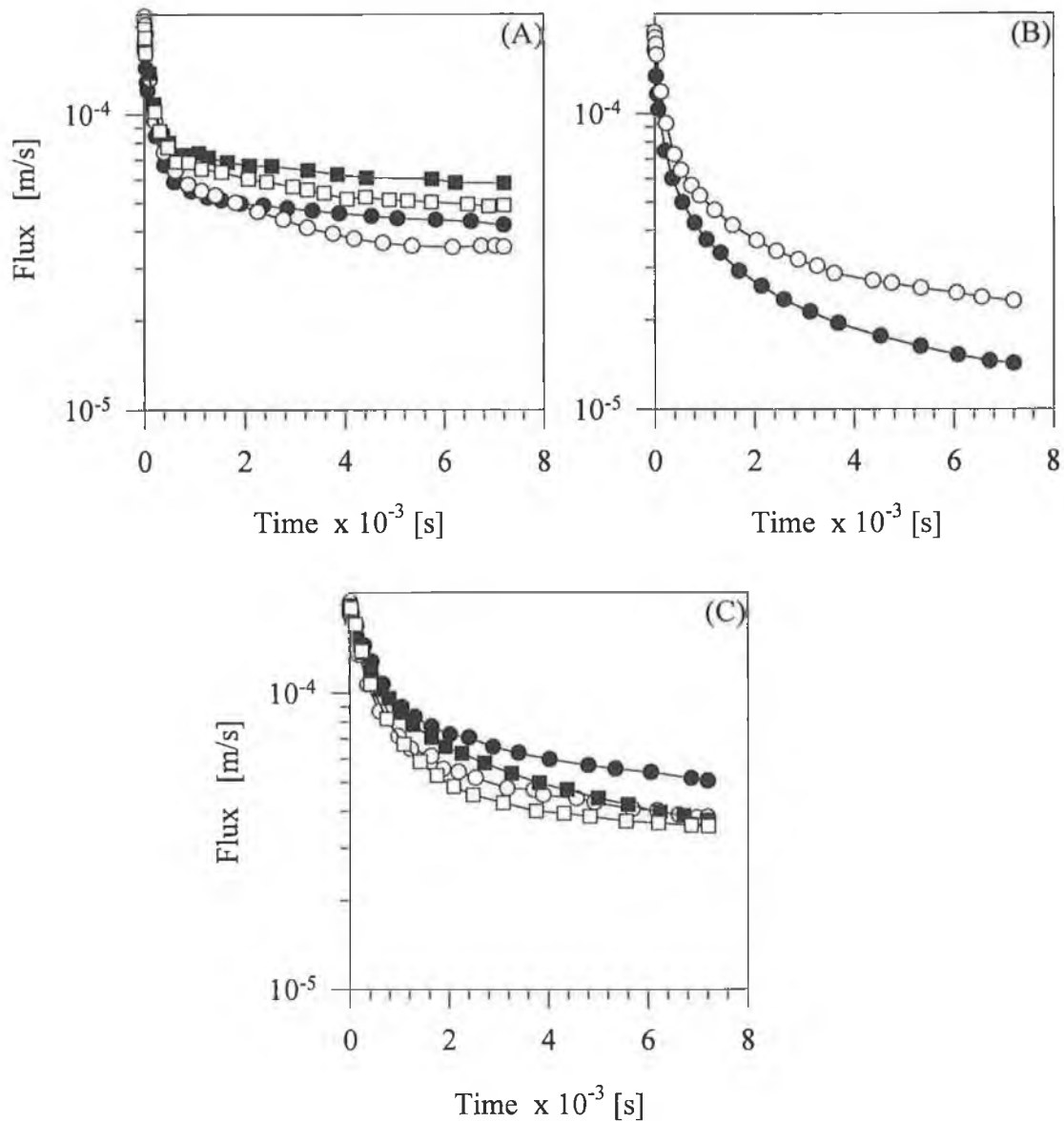


Figure 7.12 The effect of growth medium on the filtration flux of washed cell suspensions. (A) 800 rpm batch culture, (B) 500 rpm batch culture, (C) continuous culture. $u = 0.5$ m/s, $\Delta P = 100$ kPa, $c \approx 17.5$ kg/m³. Symbols: \square Whey; \blacksquare Whey2; \circ YEPL and \bullet YEP_NL.

In all cases the flux decline during the initial stages is similar for suspensions of the same morphology. Differences in the flux values later in the run may be due to differences in L_{dm} and S_v (as shown in Table 7.3). However, no clear relationship is obvious for the three morphologies.

7.5.2 Reversibility of fouling and cake recovery

Table 7.2 gives values of total resistance, reversible resistance, irreversible resistance and cake recovery for the washed cell suspensions. Cake recovery was high for the yeast suspensions, i.e., 85% or greater, whereas for mycelial suspensions it appeared low. Furthermore clumps of cells were noticed going into solution during the caustic wash stage after filtration of mycelial suspensions. This did not occur with yeast morphologies.

For all the batch culture suspensions, the recovered cake mass was determined using the technique described in Section 3.14.11, Chapter 3. The two suspensions marked with “*” was where the mass of the recovered cake was determined using the above technique, however for these mycelial suspensions the centrifugation pellet was small. Furthermore, the wet weight analysis stage was not possible to complete, as clumps sheared from the pellet when removing supernatant during the washing stage. The weight of the centrifugation pellet formed from the recovered crossflow filter cake suspension, was less than 0.5 g. This weight includes the weight of a water layer on top of the centrifugation pellet which was not removed as it contained the cells sheared from the pellet. Therefore the maximum possible cake mass recovered was less than 0.5g. Hence, less than 40% of the crossflow filter cake was recovered (probably much less if a mycelial morphology is assumed, and hence high pellet voidage, as shown in Chapter 4).

The suspensions marked by “**” indicates where the recovered cake mass was determined by a modified form of the technique described in Section 3.14.11. In these cases, the dry weight concentration of the recovered cake suspension was determined and then converted into a wet weight concentration, by multiplying by

wet to dry weight ratio. Thus, the wet weight of the recovered cake suspension was determined without need for centrifugation. The cake mass is a product of the wet weight cell concentration and the recovered cake suspension volume.

Table 7.2 Two hour fluxes, fouling behaviour and cake recovery for washed cell suspensions.

Medium / Growth conditions	$J_{2\text{hrs}}$ m/s x 10^6	R_T m ⁻¹ x 10^{-11}	R_{irev} m ⁻¹ x 10^{-11}	R_{rev} m ⁻¹ x 10^{-11}	% Cake Recovery
YEPL					
500 rpm / Batch	2.3	43.3	21.0	16.97	95
800 rpm / Batch	3.5	28.31	12.4	11.30	85
Cont. Culture	3.8	26.17	15.11	5.76	24**
YEP _N L					
500 rpm / Batch	1.42	70.21	17.89	46.25	92
800 rpm / Batch	4.31	23.85	5.83	12.32	94
Cont. Culture	5.05	19.76	13.1	1.46	<40*
Whey					
800 rpm / Batch	5.82	17.1	4.57	7.16	87
Cont. Culture	3.72	26.0	16.25	4.55	<40*
Whey2					
800 rpm / Batch	4.80	20.4	6.23	9.08	91
Cont. Culture	3.50	28.13	19.72	3.13	20**

* Undetermined poorly formed pellet, estimated cake recovery value. Less than 0.5g pellet weight formed from recovered cake.

** Determined from dry weight concentration.

A low cake recovery for mycelial suspensions is reflected by a high percentage of the total resistance being irreversible. Thus it may be, the mycelial cells have different surface properties to yeast cells, such that the mycelial cells adhere more to the membrane. Or the cake that forms may be highly entangled due to the cell morphology in these suspensions. It may be that a certain degree of cell adhesion to the membrane occurs in all cases, and that in the case of mycelial suspensions, the cells that adhere to the membrane can hold the entire cake on the membrane due to cell enmeshment.

For the yeast-like suspensions cake recovery was much higher than for the mycelial suspensions but in no case was it 100%. It may be that cake recovery was complete and cell losses during dead-end filtration and centrifugation stages used to determine the recovered cake mass, accounts for the difference. However, even for these suspensions a considerable fraction of the total resistance, R_T , was due to the irreversible fouling. This could be due pore plugging or fines penetrating the cell cake and interacting with the membrane surface and membrane pores. Moreover there is a greater degree of irreversible fouling for the 500 rpm cultures than the 800 rpm batch cultures despite similar cake recovery values. This could be due to greater amount of fines in these suspensions as discussed earlier or that a more porous cake (due to the higher L_{dm} values) allows more fines to penetrate the cake and interact with the membrane.

7.5.3 Cake formation and morphology effects

Cell morphology has been shown to influence filtration behaviour (Yamasaki *et al.*, 1993a, 1993b; Hooper *et al.*, 1998). More specifically preferential deposition of smaller cells (Foley *et al.*, 1992) and shear-induced arrangement of cells (Tanaka *et al.*, 1994b) are dependant on the morphology of the cells in the feed suspension. These factors can account for the specific resistance increasing during crossflow microfiltration, and account for higher specific resistances experienced in crossflow compared to dead-end end filtration.

Table 7.3 shows the L_{dm} , S_v and mean cell volume, V_{cells} , for the feed suspensions and recovered filter cakes. It can be seen that the morphological characteristics of the feed suspensions and recovered cakes are similar. Note there is no image analysis data for the recovered cakes of mycelial suspensions. This was due to the cells becoming entangled with each other when the filter cake formed. It was not possible to separate the large clumps of mycelium sufficiently to give accurate morphology data for recovered crossflow microfiltration cakes. However, microscopic inspection of the filter cake showed that it comprised of cells of all morphologies and appeared to be similar to the feed suspension.

Table 7.3 Image analysis data for washed cell suspensions and recovered crossflow filter cakes. $u = 0.5$ m/s, $\Delta P = 100$ kPa, $c \approx 17.5$ kg/m³.

Media	Growth Conditions	Feed Suspension			Recovered Cake		
		L_{dm} —	S_v μm^{-1}	V_{cells} μm^3	L_{dm} —	S_v μm^{-1}	V_{cells} μm^3
YEP _{NL}	800 rpm	2.92	1.60	41.93	3.63	1.69	38.23
	500 rpm	5.25	1.64	61.43	4.05	1.50	57.10
	Continuous	58.9	2.23	260.5	—	—	—
YEPL	800 rpm	2.92	1.55	40.28	3.26	1.57	43.04
	500 rpm	4.42	1.57	58.20	4.42	1.59	55.60
	Continuous	56.0	2.10	286.1	—	—	—
Whey	800 rpm	3.26	1.44	55.39	3.04	1.37	57.32
	Continuous	55.4	2.17	263.1	—	—	—
Whey2	800 rpm	3.45	1.49	54.76	2.86	1.59	47.26
	Continuous	66.18	2.05	340.3	—	—	—

There is no evidence in Table 7.3 of preferential deposition occurring with washed yeast-like morphologies. This indicates that cake formation is similar to that observed during dead-end filtration, i.e. the cake mass should be proportional to the filtrate volume *during* the cake formation period of crossflow microfiltration (the first 15 minutes of crossflow microfiltration approximately). To verify if this occurs, a theoretical rate of cake formation, based on the assumption that all the cells in the filtrate deposit to form a filter cake, can be determined and compared to the increase in cake mass determined experimentally, as shown in Figure 7.8. The theoretical rate of cake formation can be determined as outlined below.

The calculated filtrate volume, V_f , at any time, t , can be determined from the following expression,

$$V_f = A \int_0^t J \quad [7.2]$$

The measured flux values were numerically integrated using Simpsons rule to giving filtrate volumes at different times. Consequently, the cake mass can be plotted as a function of filtrate volume.

Determination of the theoretical cake mass accounts for changes in the feed suspension cell concentration due to the initial stage of filtration being conducted in batch mode (equation 7.3) and due to cake formation for the remainder of the filtration period (equation 7.7).

During the initial batch period the cake mass, M_t is a product of the filtrate volume, V_f , and the initial cell concentration, c_0 , i.e.,

$$M_t = c_0 V_f \quad [7.3]$$

Equation 7.3 reflects the initial stage of filtration, i.e., the initial filtrate sample collected in batch mode to determine the filtrate fluxes early in the filtration run

(reference section 3.14.9, Chapter 3). The volume collected in the initial stage was small in comparison to the total filtrate volume over two hours of filtration and was typically in the region of 80 mL. The cake mass at any time during the total recycle phase is equal to sum of the cake mass, M_1 , at the end of the initial batch period, t_1 , and the product of suspension volume by the change in reservoir cell concentration during the total recycle phase, i.e.,

$$M_t = M_1 + V_s[c_1 - c_t] \quad [7.4]$$

where c_1 is the theoretical cell concentration at time t_1 after the filtrate collected during the initial batch stage is re-introduced to the feed reservoir and is determined from the following expression,

$$c_1 = \frac{c_o V_s - M_1}{V_s} \quad [7.5]$$

At any time during the total recycle phase, the cell concentration in the reservoir, c_t , can be determined from the following expression (refer appendix A),

$$c_t = c_1 e^{-\frac{(V_t - V_1)}{V_s}} \quad [7.6]$$

where V_1 is the filtrate volume collect during the batch period, i.e., 80 mL in most cases.

Inserting equation 7.6 into equation 7.4 yields,

$$M_t = M_1 + V_s \left[c_1 - c_1 e^{-\frac{(V_t - V_1)}{V_s}} \right] \quad [7.7]$$

For each washed cell suspension filtered, the theoretical cake mass was determined every 10 mL using equations 7.3-7.7 and the initial cell concentration, c_0 and filtrate volume, V_1 , which were determined experimentally.

In Figure 7.13 the measured and theoretical cake masses as a function of filtrate volume are plotted. The experimental filtrate volumes were determined using equation 7.2. It can be seen with yeast-like suspensions the filter cake forms at the same rate as predicted theoretically. Similar results were shown by Tanaka *et al.*, (1993) with yeast suspensions. In that study, the change in flux during the unsteady state period corresponded with that predicted using the specific resistance determined during dead-end filtration. Therefore, it would be expected that the morphology of the recovered filter cake for these suspensions to be similar to that of the original suspension. There may be preferential deposition occurring as cake formation nears completion, however it is unlikely to contribute significantly as most of the cake that forms, would have similar morphology as the original feed suspension.

Preferential deposition could possibly be occurring with mycelial suspensions. It can be seen from Figure 7.13 that the rate of cake formation is less than that predicted, i.e. not all particles deposited to form the filter cake. This may indicate preferential deposition. Since the cake formed rapidly for these suspensions it was not possible to obtain sufficient data-points during the cake formation period. Furthermore due to cell entanglement it was not possible to accurately determine the morphology of the recovered cake using image analysis. However, these suspensions would have a greater potential for preferential deposition occurring than yeast suspensions. This is due to these morphologies having a much broader distribution of cell size and shape.

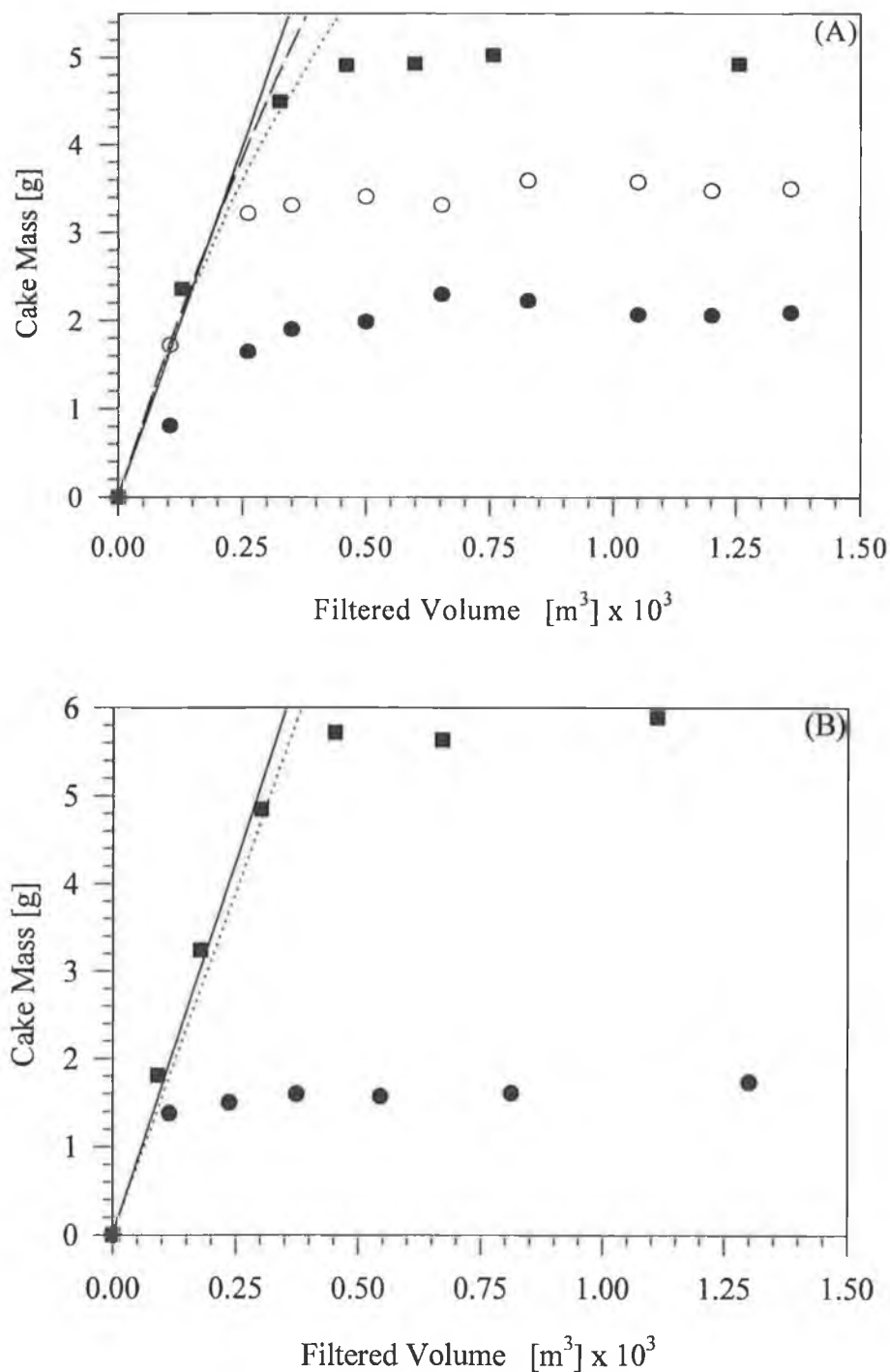


Figure 7.13 Cake mass as function of filtrate volume. (A) YEP_NL medium, (B) Whey medium, $u = 0.5$ m/s, $\Delta P = 100$ kPa, $c \approx 17.5$ kg/m³. Symbols: ■ 800 rpm batch culture; ○ 500 rpm batch culture; ● continuous culture. Lines: — theoretical prediction for 800 rpm batch culture; theoretical prediction for continuous culture; - - - - - theoretical prediction for 500 rpm batch culture.

In Figure 7.14, the two-hour flux value, $J_{2\text{hrs}}$, is plotted against the specific surface area, S_v , for the washed yeast suspensions. The specific surface area varied with the growth medium as can be seen in Table 7.3. Also plotted in Figure 7.14 is the flux value at the end of cake formation (10-14 minutes) for the 800 rpm suspensions *versus* S_v . It can be seen that the flux value decreases with increasing S_v . This is to be expected, as increasing S_v should causes increases in specific resistance and hence lower flux.

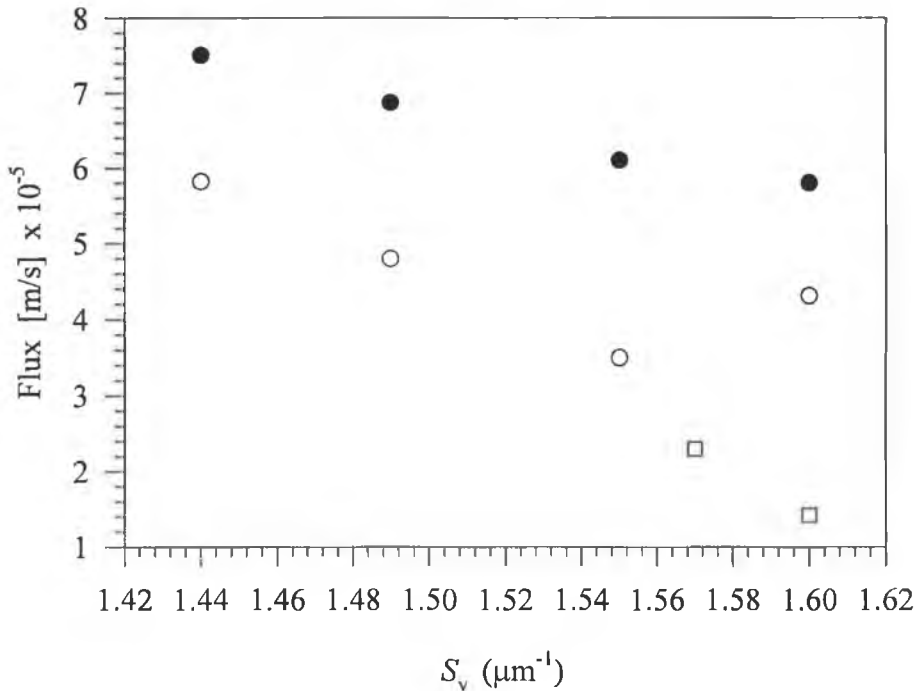


Figure 7.14 Relationship between filtrate flux and S_v . $u = 0.5$ m/s, $\Delta P = 100$ kPa, $c \approx 17.5$ kg/m³. Symbols: ● 800 rpm batch culture, J values at end of cake formation; ○ 800 rpm batch culture, $J_{2\text{hrs}}$ and □ 500 rpm batch culture, $J_{2\text{hrs}}$.

7.5.4 Evolution of specific resistance in crossflow microfiltration

Figure 7.15 shows the evolution of the apparent specific resistance during a crossflow microfiltration run of a yeast suspension. The apparent specific resistance is determined by assuming *no* membrane fouling and the apparent specific resistance at any time is determined from the following expression,

$$\alpha_{\text{app}} = \frac{R_T - R_{\text{mo}}}{M / A} \quad [7.8]$$

where R_T and M are the total resistance and mass deposited per unit area at time, t ,. R_{mo} is the clean membrane resistance, α_{app} is the apparent specific resistance and A is the crossflow microfiltration area.

In Figure 7.15 the apparent specific resistance is shown to increase throughout the filtration period. This is to be expected where membrane fouling occurs. The following expression relates the *true* cake resistance, α_{true} , with the apparent specific resistance when membrane fouling occurs (Foley, 1994),

$$\alpha_{\text{app}} = \alpha_{\text{true}} + \frac{R_m - R_{\text{mo}}}{M / A} \quad [7.9]$$

where R_m is the membrane resistance and R_{mo} is the clean membrane resistance. It can be clearly seen from Equation 7.9, that if the membrane resistance, R_m , increases throughout the filtration run then the apparent specific resistance will increase even if the true specific resistance remains constant.

It can be seen in Figure 7.15 that early in the filtration run that the apparent specific resistance is lower than the specific resistance measured for dead-end filtration, α_{av} . This may be due to the pressure drop across the cake being substantially lower than the transmembrane pressure drop in crossflow microfiltration.

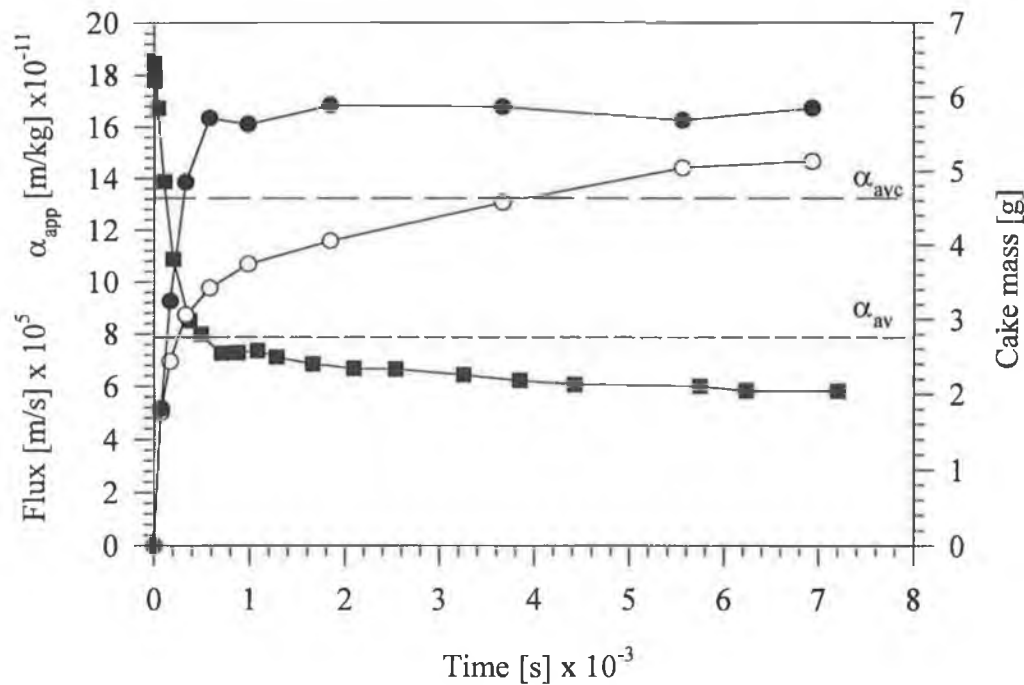


Figure 7.15 Evolution of the apparent specific resistance in crossflow microfiltration and comparison with dead-end filtration resistances. Whey medium, 800 rpm batch culture. $u = 0.5$ m/s, $\Delta P = 100$ kPa, $c \approx 17.5$ kg/m³. Symbols: ■ flux; ○ mean specific resistance in cross-flow filtration; ● cake mass.

Conversely, in dead-end filtration the pressure drop across the filter cake is approximately equal to the applied pressure, as the mean specific resistance is determined for a pre-formed filter cake. This occurs, due to the very high resistance of the crossflow microfiltration membrane in comparison to the dead-end membranes. Consequently, when dead-end filtration and crossflow microfiltration experiments are conducted at the same trans-membrane pressure drop, the crossflow filter cake will be less compressed and have a lower specific resistance than the dead-end filtration counterparts.

Before the cake mass reaches steady state the apparent specific resistance increases and becomes greater than that measured in dead-end filtration. Fouling may account for this but other factors should be considered. It may be that the structure of the crossflow filter cake is different from its dead-end filtration counterpart. It

has been shown that the specific resistance is greater in crossflow microfiltration, because the filter cake voidage is lower due to, shear dependant-particle packing (Mackley and Sherman, 1992; Sherman and Sherwood, 1993), or shear induce arrangement of cells (Tanaka *et al.*, 1994b). Alternatively, preferential deposition of smaller cells has been shown to occur in crossflow microfiltration (Baker *et al.*, 1985; Lu and Ju, 1989; Blake *et al.*, 1992; Foley *et al.*, 1995a). However, in the case of the latter there is little evidence of preferential deposition occurring here, as shown in Table 7.3.

Finally the mean specific resistance of the recovered cake measured by dead-end filtration, α_{avc} , is lower than the apparent specific resistance, α_{app} , of the crossflow filter cake later in the run. This is to be expected, as the recovered filter cake does not include the fouling material responsible for the irreversible fouling during crossflow microfiltration, whereas R_{rev} and R_{irev} have been used to determine α_{app} . The specific resistance of the recovered cake, α_{avc} , was greater than that measured for the original suspension, α_{av} . This occurs for all morphologies and growth media. This is possibly due to the fines that collected in the cake during crossflow microfiltration. As discussed earlier there was a greater concentration of these fines present when viewed under the microscope. Also, a black deposit was visible when centrifugation pellets of the recovered cake were formed.

Attempts to model the flux behaviour of the suspensions with the normally applied models such as the standard blocking model, cake filtration model or intermediate blocking model, proved inconclusive. This was probably due to cake formation and fouling occurring simultaneously. Figure 7.16 shows the relationship between total resistance and filtrate volume. It can be seen that different forms of the relationship between R_T and V_f are possible.

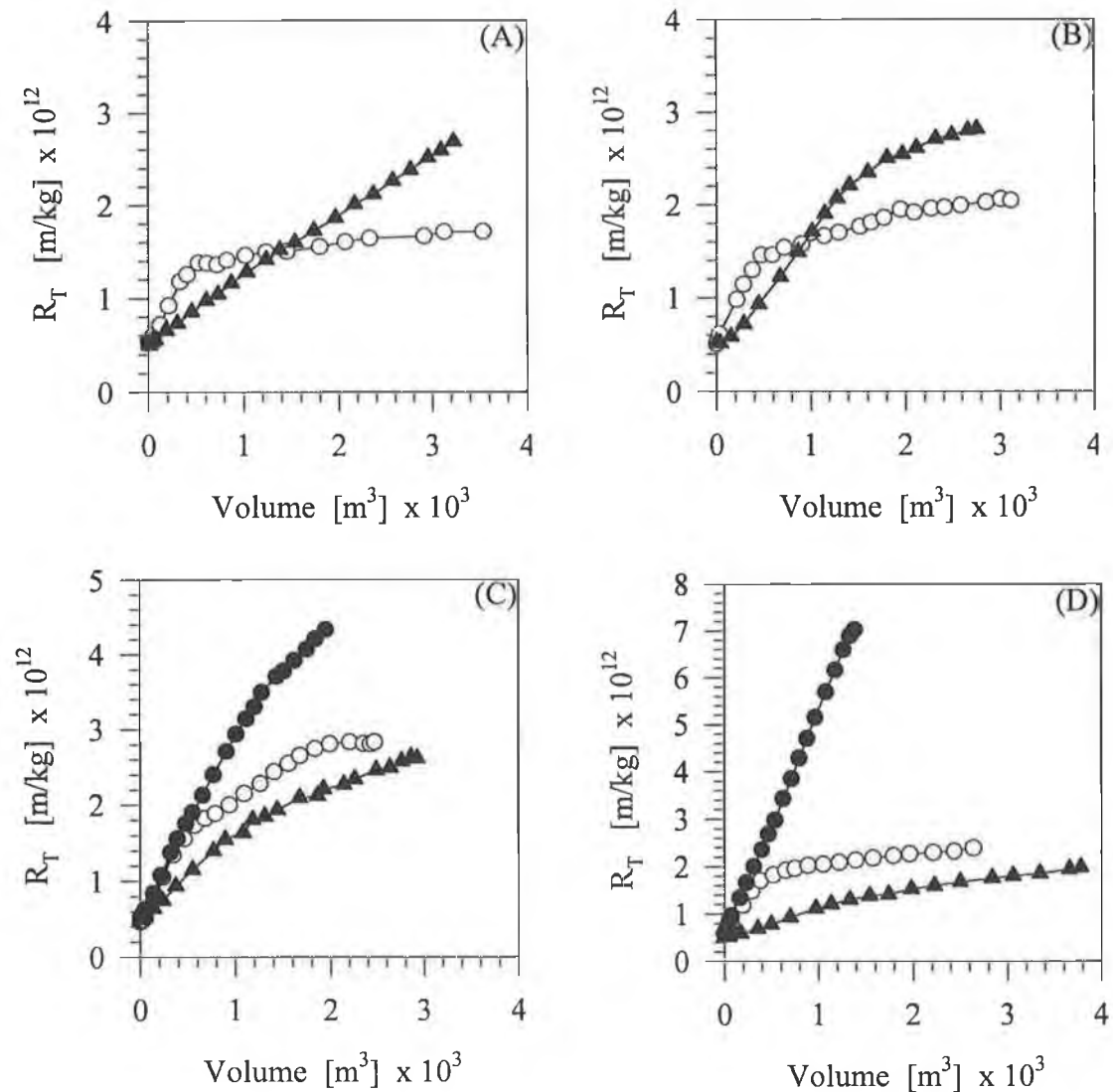


Figure 7.16 R_T as a function of filtrate volume. (A) Whey, (B) Whey2, (C) YEP_{NL}, and (D) YEPL medium, $u = 0.5$ m/s, $\Delta P = 100$ kPa, $c \approx 17.5$ kg/m³. Symbols: ○ 800 rpm batch culture; ● 500 rpm batch culture and ▲ continuous culture.

For the most yeast-like suspensions (800 rpm batch cultures), two distinct phases are apparent. The total resistance, R_T , increases sharply initially and then increases at a slower rate. The point of inflection corresponds to when cake formation ceases. For the other suspensions R_T increases linearly with filtrate volume or else the rate of change in R_T with filtrate volume slowly decays.

For the most yeast like suspension (800 rpm, batch cultures), the rate of fouling can be determined from the slope in plots of R_T versus V_f , after cake formation has been completed, i.e., the secondary increase in R_T as shown in Figure 7.16. The rate of change in R_T with respect to filtrate volume can be defined as the fouling coefficient K_{f1} , and determined from the following expression,

$$K_{f1} = S \quad [7.10]$$

where S is the slope of the second period filtration in plots of R_T versus V_f .

Furthermore the rate of fouling can be determined from the degree of irreversible fouling. If it is assumed that the increase in R_{rev} throughout the filtration run is proportional to the filtrate volume then a second fouling coefficient can be defined as K_{f2} . In this case K_{f2} can be determined from the following expression,

$$K_{f2} = \frac{R_{\text{rev}}}{V_{2\text{hrs}}} \quad [7.11]$$

where $V_{2\text{hrs}}$ is the volume of filtrate collected after two hours.

Table 7.4 shows the value of K_{f1} and K_{f2} determined for the cell suspensions grown at 800 rpm, batch culture.

Table 7.4 Fouling coefficient for the 800 rpm batch cultures.

Growth Media	$K_{f1} \times 10^{-14}$ m^{-4}	$K_{f2} \times 10^{-14}$ m^{-4}
YEPL	5.80	4.85
YEP _N L	2.05	2.21
Whey	1.25	1.29
Whey2	2.11	2.00

It can be seen there is excellent agreement between the fouling coefficient determined by both methods.

Subsequently if fouling is taken into account Equation 7.9 becomes,

$$\alpha_{\text{true}}^{\text{kf1}} = \frac{R_T - R_{\text{mo}} - K_{f1} V_f}{M / A} \quad [7.12]$$

$$\alpha_{\text{true}}^{\text{kf2}} = \frac{R_T - R_{\text{mo}} - K_{f2} V_f}{M / A} \quad [7.13]$$

The parameter, $\alpha_{\text{true}}^{\text{kf1}}$ is the *true* specific resistance when K_{f1} is used to determine fouling and $\alpha_{\text{true}}^{\text{kf2}}$ is the apparent specific resistance when K_{f2} is used to determine fouling.

In Figure 7.17 the apparent specific resistance determined by equation 7.8 and the *true* specific resistance determined by equation 7.12 and equation 7.13, for 800 rpm batch cultures are shown. Also shown are the mean specific resistances determined by dead-end filtration for the feed suspension α_{av} and the recovered cake, α_{avc} . It can be seen that when fouling is taken into account that the *true* specific resistance during crossflow microfiltration is in the region of $10\text{-}18 \times 10^{11}$ m/kg for all suspensions which is in relatively good agreement with the resistances measured for the recovered filter cakes.

However, they are 50-100% greater than the resistances measured for the feed suspensions. This is probably due to fouling of the cake layer by particulate matter. Tanaka *et al.* (1993) demonstrated that with baker's yeast grown on YEPD media, the specific resistance measured during crossflow microfiltration was the same as that determined during dead-end filtration.

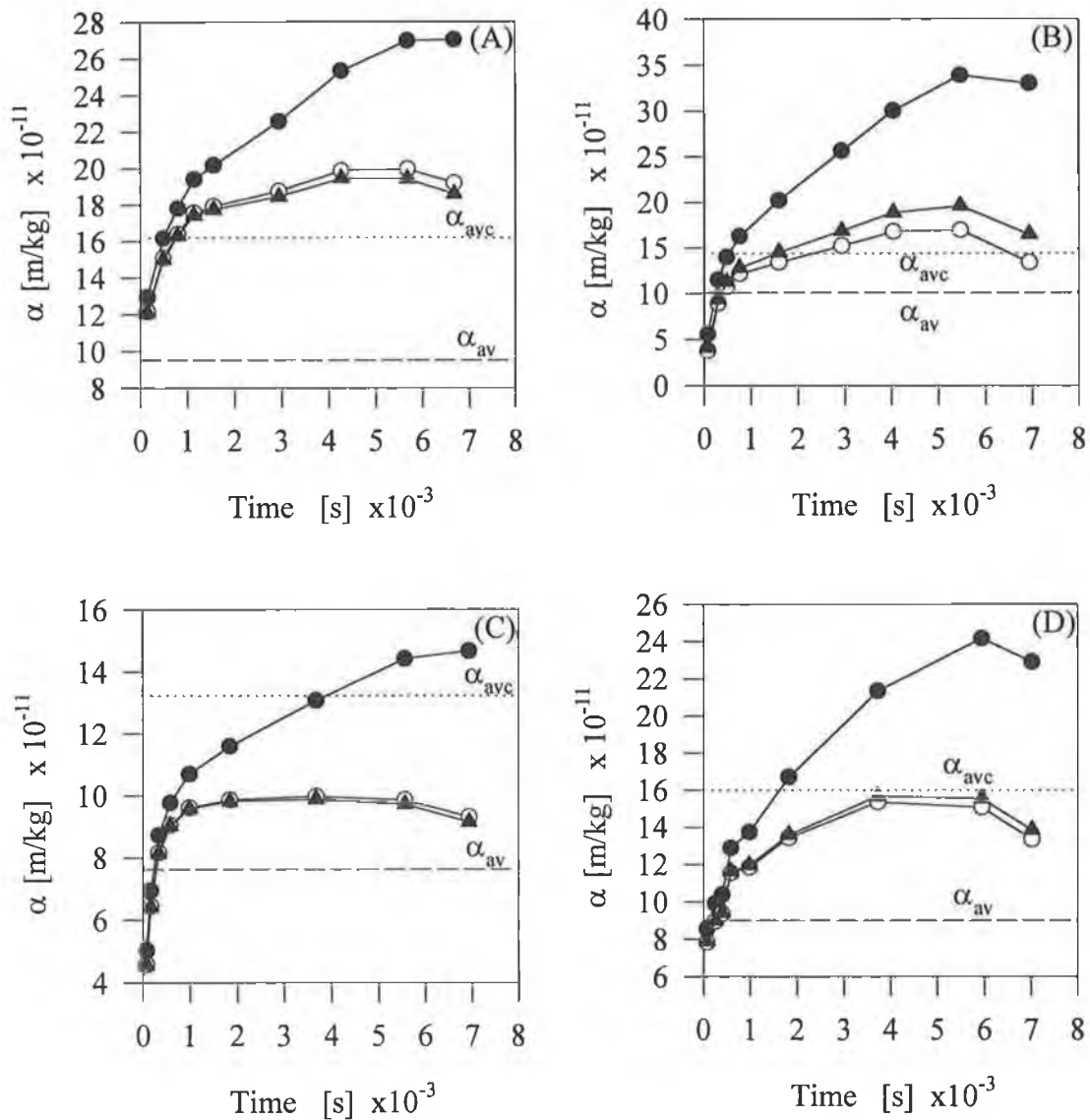


Figure 7.17 The specific resistance as a function of filtrate volume for batch (800 rpm) suspensions, $u = 0.5$ m/s, $\Delta P = 100$ kPa, $c \approx 17.5$ kg/m³. (A) YEP_{NL}, (B) YEPL, (C) Whey, and (D) Whey2 media. Symbols: ● α_{app} ; ○ α_{true}^{kf1} and ▲ α_{true}^{kf2} .

However, in a separate study it was shown that when filtering baker's yeast grown in molasses, the specific resistance measured during crossflow microfiltration was greater than that measured during dead-end filtration (Tanaka *et al.*, 1994c). It was suggested that the fines in the filter media caused fouling of the cake layer.

Therefore, if particulate matter is fouling the cake layer after the cells stop depositing to form a filter cake, then the *true* specific resistance will be greater in crossflow microfiltration than the mean specific resistance measured in dead-end filtration, α_{av} .

During dead-end filtration the fines will probably be distributed evenly throughout the filter cake, however, during crossflow microfiltration they can form a dense layer on the cake surface (Tanaka *et al.*, 1998). However, it may be possible that in certain cases the fines may migrate through the cake. This would be dependent on the size of the particles relative to the pore size in the filter cake and the electrostatic interactions between the particles and the cells.

By comparison, the *true* and apparent specific resistances for the 500 rpm batch cultures are shown in Figure 7.18. It can be seen the *true* and apparent specific resistances are significantly greater than those determined for the 800 rpm batch cultures. When fouling is taken into account for the 800 rpm cultures α_{true} appears to be relatively constant during the pseudo steady state period, however with the 500 rpm cultures it continues to rise throughout the filtration period. This suggests there is a much greater concentration of fines in the 500 rpm suspensions. This can be partly be attributed to the lower biomass yields of these cultures (approximately 50% of 800 rpm suspensions). Therefore, if the source of the fines are from the original media, then approximately twice the volume of the 500 rpm culture is required to give the 17.5 g/L concentration used for crossflow microfiltration and hence possibly twice the mass of fines.

Furthermore the specific resistance of the recovered cake for the 500 rpm batch cultures are similar to those determined for 800 rpm batch cultures. This is despite the specific resistances (true and apparent) during crossflow microfiltration being significantly greater for the 500 rpm batch suspensions. This suggests that the structure of the crossflow microfiltration filter cake is significantly different from the dead-end filtration filter cake.

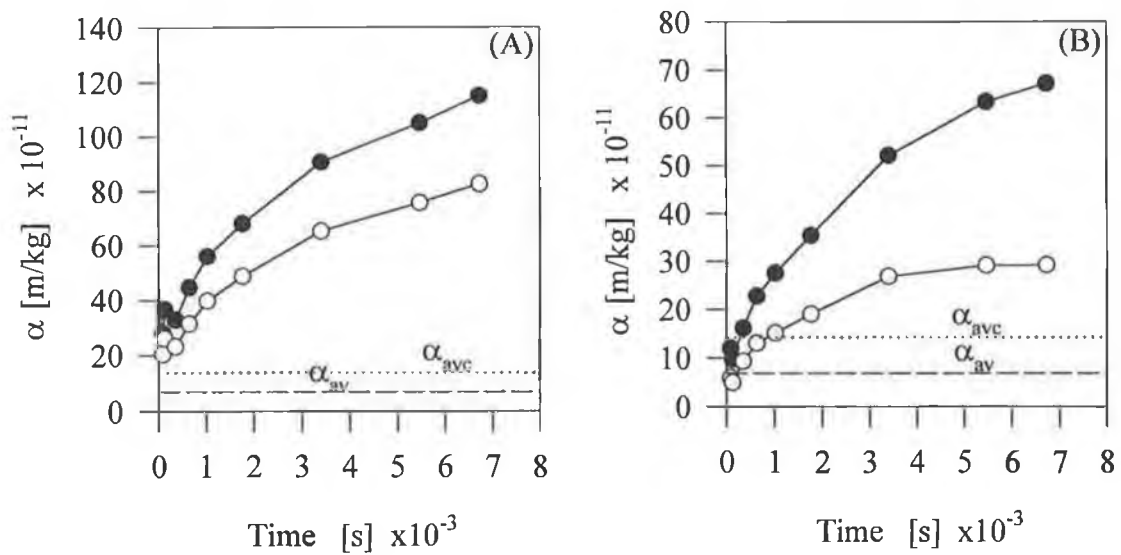


Figure 7.18 The specific resistance as a function of filtration time for 500 rpm batch cultures. (A) YEP_NL, (B) YEPL, (C) Whey, and (D) Whey2 media. $u = 0.5$ m/s, $\Delta P = 100$ kPa, $c \approx 17.5$ kg/m³. Symbols: ● α_{app} and ○ α_{true}^{kf2}

It may be that during crossflow microfiltration the fines deposit on top of the cake layer. This has been shown to occur when filtering *C. glutamicum*, where a thin layer of polymers formed on the cake surface, which had a very high resistance (Tanaka *et al.*, 1998). In this study, when the cake was recovered it was well mixed prior to carrying out dead-end filtration experiments. Subsequently the fines would be distributed evenly throughout the dead-end filter cake.

In Figure 7.19 the apparent specific resistance determined by equation 7.8 is shown for mycelial suspensions. The resistances determined are in most cases greater than those determined for the yeast suspensions. Furthermore they are in the region of an order of magnitude greater than those observed during dead-end filtration. There are several reasons why the determined resistances are so high in crossflow microfiltration. Preferential deposition of smaller cells (Foley *et al.*, 1993) may be occurring. There is some evidence of this as the cake mass of cake formed is less than that predicted by equations 7.3 to 7.7, as shown in Figure 7.13.

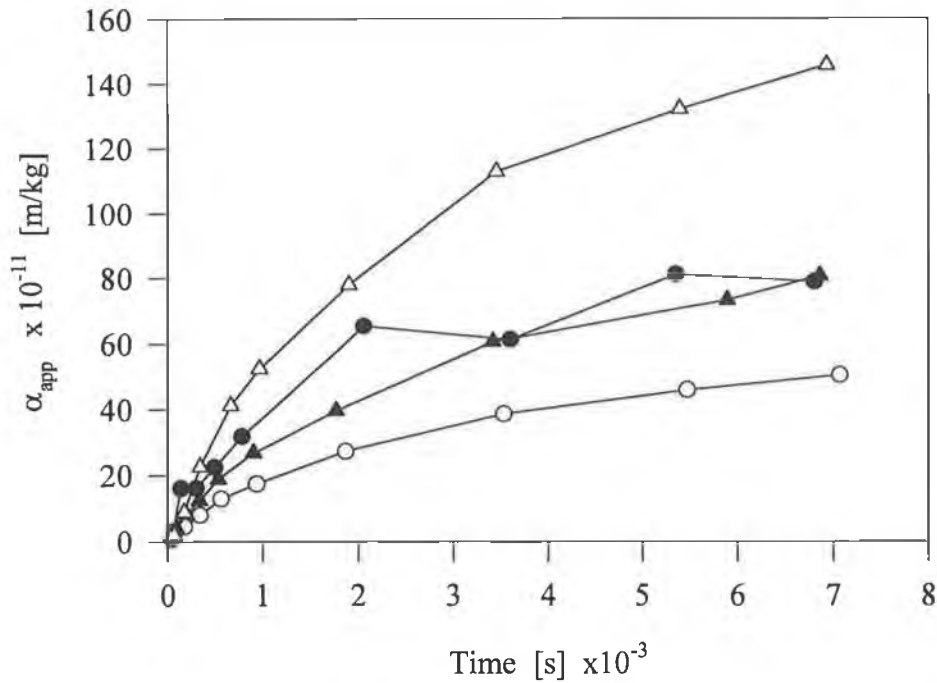


Figure 7.19 Apparent specific resistance as a function of filtration time for mycelial suspensions. $u = 0.5$ m/s, $\Delta P = 100$ kPa, $c \approx 17.5$ kg/m³. Symbols: ● YEPL; ○ YEP_NL; ▲ Whey and △ Whey2 medium.

Another factor could be the shear-induced arrangement of particles within the cake, producing a more tightly packed cake than formed in dead-end filtration (Tanaka *et al.*, 1994b, 1996). Fouling obviously will also be a factor for these suspensions. However, as it was not possible to recover the filter cake without using caustic it is difficult to ascertain the nature of fouling here. However, it is worth noting that the biomass yields for the mycelial suspensions are similar to those of the 800 rpm suspensions.

The results presented here indicate that there is significant difference in the filtration behaviour between the three morphologies and it would appear that fouling behaviour is more influenced by cell morphology than media composition.

7.5.5 Crossflow velocity

In Figure 7.20 the effect of crossflow velocity, u , on the two-hour flux value and steady state cake mass is shown. The flux value increases and the cake mass decreases with increasing u . This is in agreement with the general observations of other researchers, where as the cake mass decreases with crossflow velocity (Riesmeir *et al.*, 1987, Riesmeier *et al.*, 1989; Fordham and Ladva, 1989, Tanaka *et al.*, 1993), the filtrate flux normally increases (e.g., Sakai *et al.*, 1989; Li *et al.*, 1996). It can be seen that both the decrease in cake mass and increase in two hour flux are both linearly dependent on the crossflow velocity.

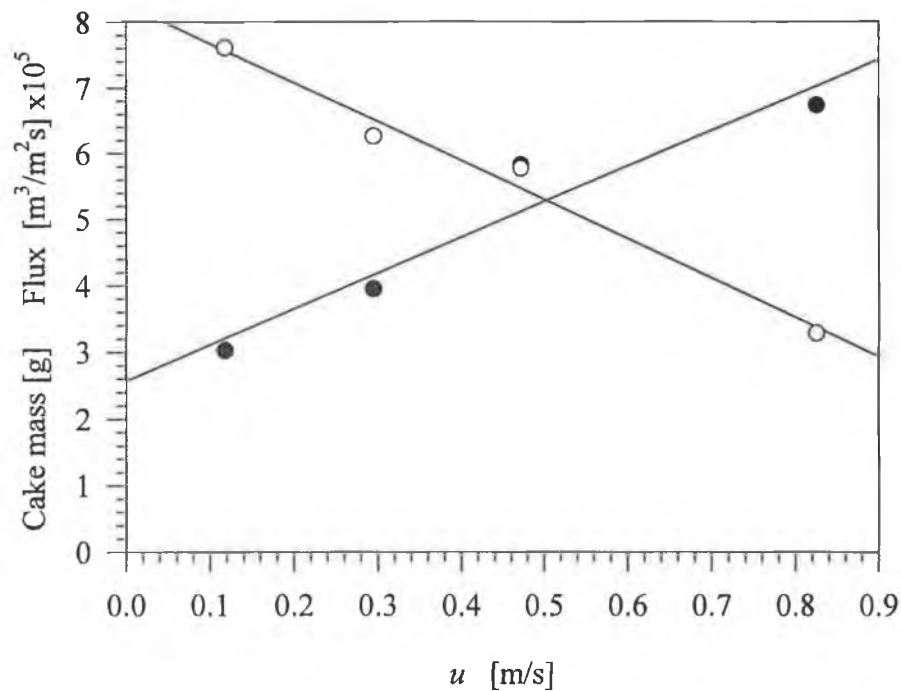


Figure 7.20 The effect of crossflow velocity on the pseudo steady state cake mass and filtration flux. Whey medium, $\Delta P = 100$ kPa, $c \approx 17.5$ kg/m³. Symbols: ● $J_{2\text{hrs}}$ and ○ Cake mass. Lines represent linear regression through data.

In Figure 7.21 the relationship between the *true* specific resistance determined from equation 7.13, and crossflow velocity is shown. It can be seen that the *true* specific resistance *decreases* with increasing crossflow velocity. This is in contrast

to research done elsewhere, where it has been shown that the specific resistance is *independent* of crossflow velocity (Baker *et al.*, 1985; Riesmeier *et al.*, 1989) or *increases* with crossflow velocity (Baker *et al.*, 1985; Riesmeier *et al.*, 1987; Riesmeier *et al.*, 1989; Tanaka *et al.*, 1998). It should be noted that there is no evidence of preferential deposition occurring in this study as in all cases cake formation occurred as predicted theoretically.

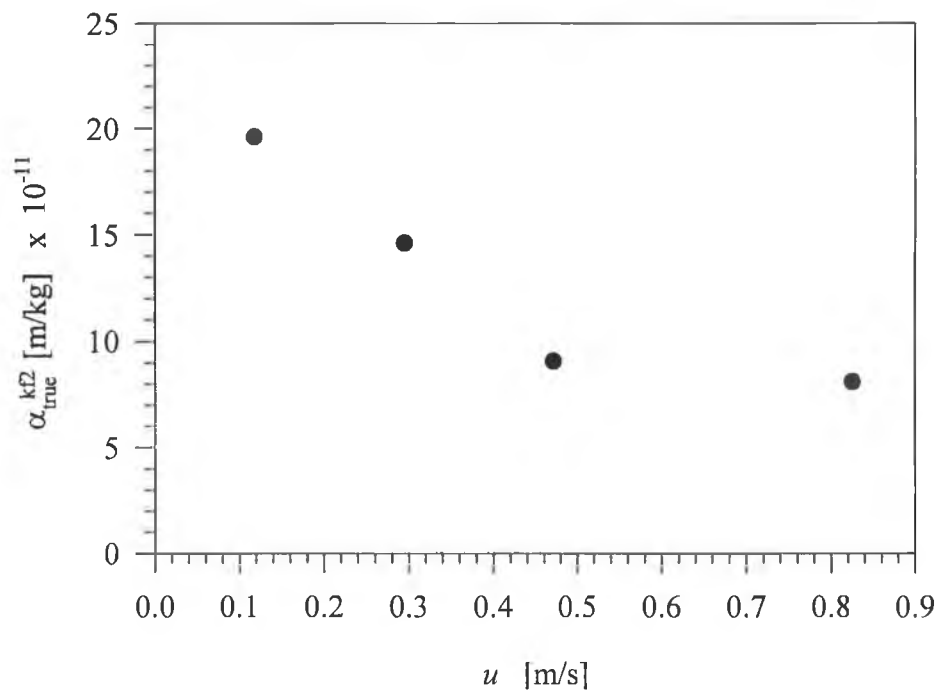


Figure 7.21 The effect of crossflow velocity on the *true* specific resistance determined after two hours of filtration. Whey medium, $\Delta P = 100$ kPa, $c \approx 17.5$ kg/m³.

One factor that may be causing the decrease in *true* specific resistance with increasing crossflow velocity is the pressure drop across the filter cake. It can be seen that in Table 7.5 that the pressure drop across the filter cake increases substantially as the crossflow velocity decreases. Thus the decrease in *true* specific resistance with crossflow velocity, may be due to cake compression decreasing as the pressure drop across the filter cake decreases (due to a decrease in cake mass).

This has been shown to occur in the theoretical study of Foley (1993). In Table 7.5, ΔP_c is calculated from the following expression,

$$\Delta P_c = \Delta P \frac{R_{rev}}{R_T} \quad [7.14]$$

Table 7.5 Effect of crossflow velocity on filtration flux and resistances for washed suspensions.

u	$J_{2hrs} \times 10^5$	$R_T \times 10^{-11}$	$R_{rev} \times 10^{-11}$	$R_{irev} \times 10^{-11}$	$\Delta P_c \times 10^5$
m/s	m^3/m^2s	m^{-1}	m^{-1}	m^{-1}	Pa
0.12	3.03	33.06	20.38	8.06	0.62
0.29	3.95	25.34	12.50	7.57	0.49
0.47	5.83	17.11	7.16	4.57	0.42
0.83	6.74	14.85	3.64	5.87	0.25

In Table 7.5 it can be seen that the degree of irreversible fouling tends to decrease with increasing crossflow velocity. This is in spite of the greater cake mass at lower crossflow velocities and less filtrate having passed through the membrane after two hours of filtration. This suggests that increasing crossflow velocity may tend to sweep away more of the fouling components in the retentate. Therefore it may be that less cake fouling is also occurring at higher crossflow velocities and that this also contributes to the decrease in *true* specific resistance with crossflow velocity as shown in Figure 7.21.

7.6 Unwashed suspensions

The effects of cell morphology and fermentation medium on the flux are shown in Figures 7.22 and 7.23. In all cases the flux drops rapidly in the first few minutes of filtration. The flux then slowly decays for the remainder of the filtration period. In Figure 7.23 it can be seen that in nearly all cases the flux values during the pseudo steady state period is largely independent of the growth medium. This would concur with the spent medium results, where fluxes were not significantly influenced by the growth media. During the pseudo steady state period, it appears that the mycelial suspensions have higher filtration fluxes than the yeast suspensions. Also the 800 rpm batch culture suspensions filtration fluxes are greater than those for the 500 rpm batch culture suspensions, as shown in Figure 7.22. This suggests that there is more fouling occurring with the 500 rpm suspensions. As discussed earlier the volume of cell suspension used for resuspension to give 17.5g/l may be a factor in the case of the 500 rpm cultures due to the lower biomass yields of these suspensions.

In Table 7.6 it can be seen reversible fouling is the dominant cause of the drop of flux for the yeast suspensions (batch cultures). For the mycelial suspensions the percentage of the total fouling that is irreversible is greater than for the yeast suspensions. This mirrors the filtration behaviour of the washed suspensions. Therefore, there may be a significant mass of cells adhering to the membrane when filter cakes formed by unwashed mycelial suspensions are being recovered, as was shown to occur for washed mycelial suspensions.

The degree of irreversible fouling for the suspensions is similar to that measured for the spent medium, as shown in Table 7.1. Therefore, there is no evidence that a cake layer protects the membrane from fouling. It is possible, however, that irreversible adhesion of cells onto the membrane may occur when filtering unwashed suspensions contributing to the measured irreversible fouling values. The high degree of reversible fouling suggests that a dense layer of cells, fines and rejected macromolecules forms on the membrane that is highly impermeable.

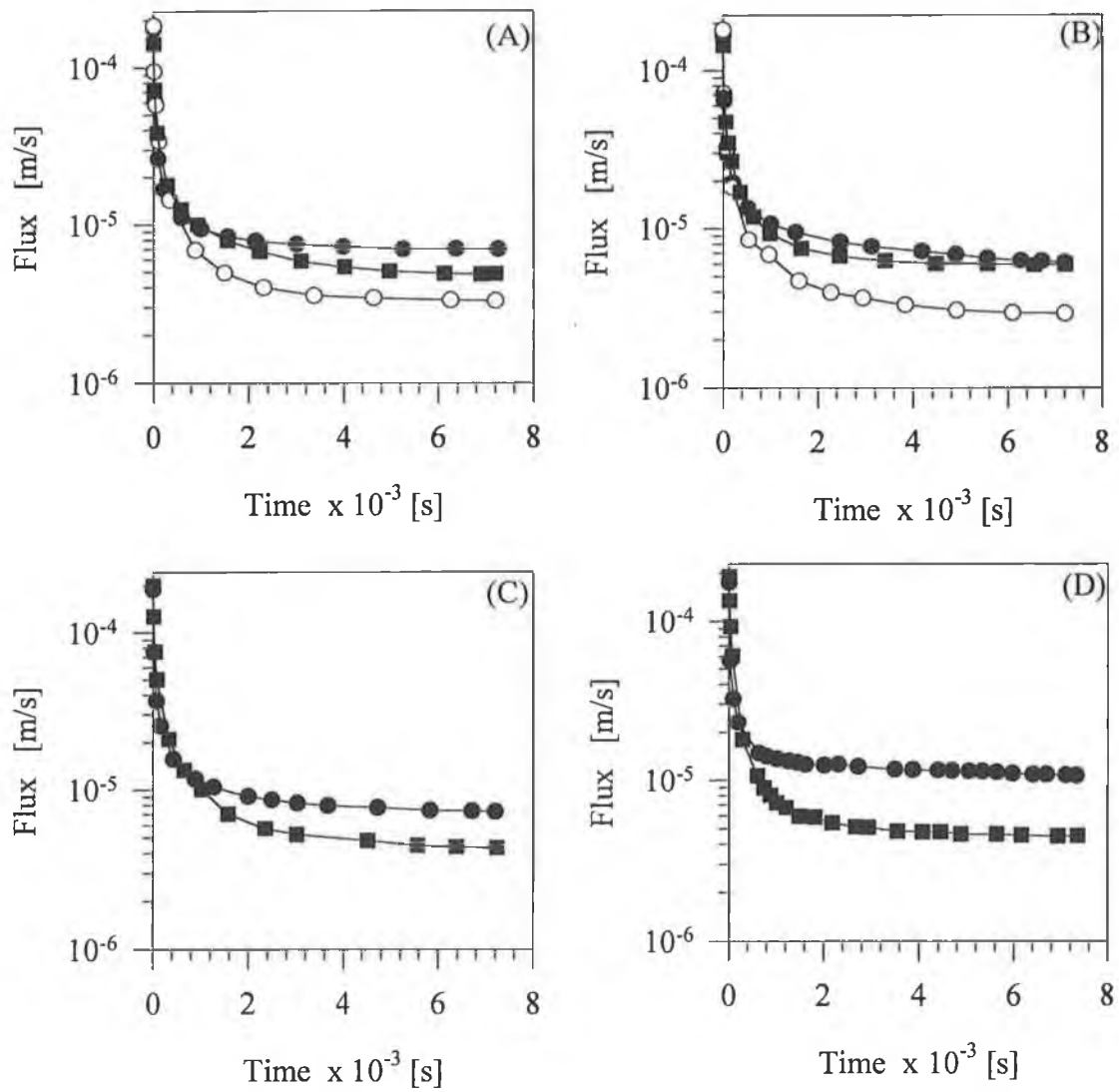


Figure 7.22 Effect of cell morphology on the filtration flux for unwashed suspensions. (A) YEP_NL (B) YEPL (C) Whey, (D) Whey2. $u = 0.5$ m/s, $\Delta P = 100$ kPa, $c \approx 17.5$ kg/m³. Symbols: ■ batch, 800 rpm; ○ batch, 500 rpm and ● continuous culture.

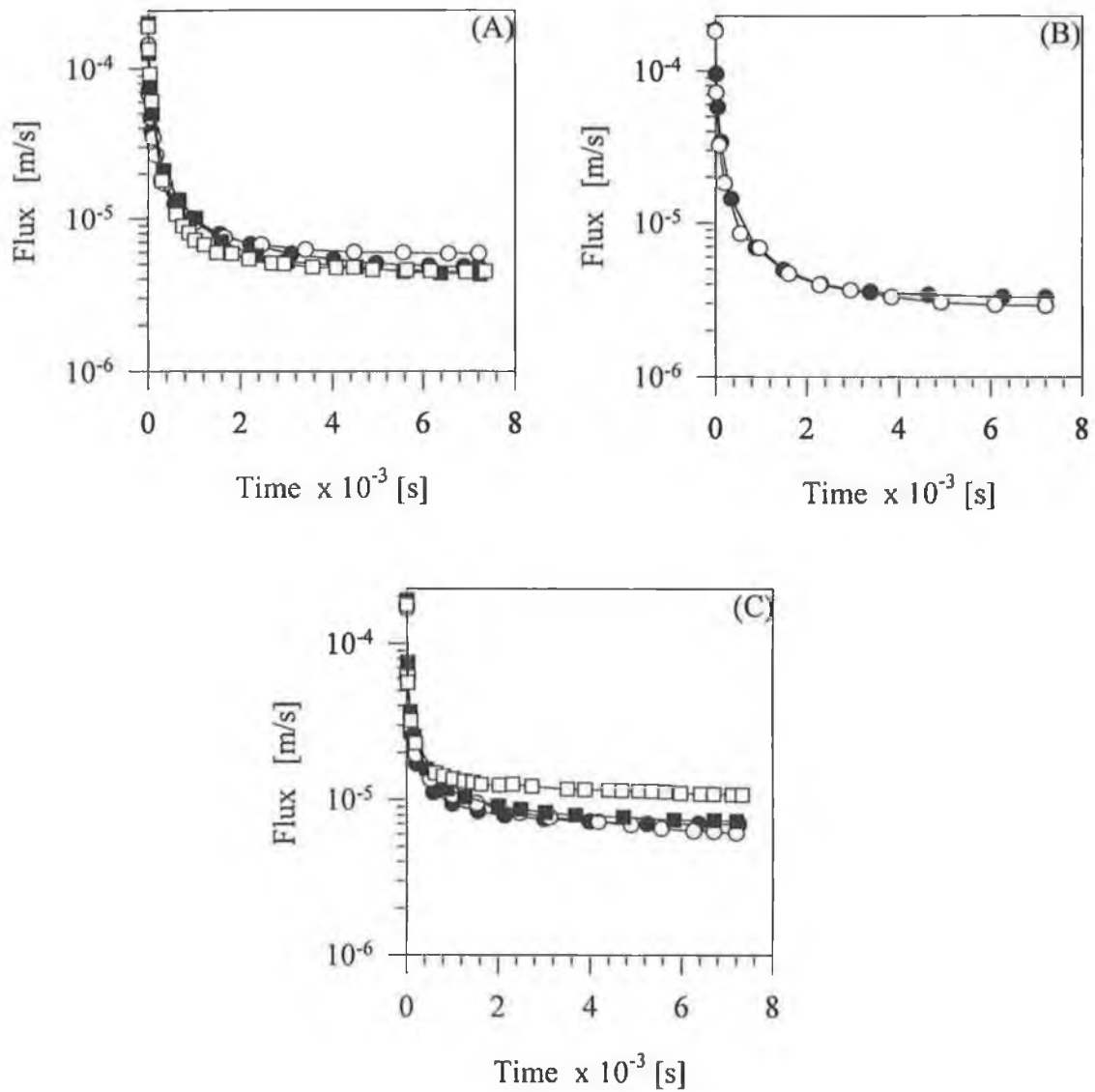


Figure 7.23 Effect of media on filtration flux of unwashed suspensions. (A) Batch, 800 rpm; (B) Batch 500 rpm; (C) Continuous culture, dilution rate = 0.19 h^{-1} . $u = 0.5 \text{ m/s}$, $\Delta P = 100 \text{ kPa}$, $c \approx 17.5 \text{ kg/m}^3$. ■ Whey, □ Whey2, ○ YEPL and ● YEP_{NL}. $u = 0.5 \text{ m/s}$, $\Delta P = 100 \text{ kPa}$.

Table 7.6 Two hour fluxes and fouling behaviour for unwashed suspensions.

Medium	/	$J_{2\text{hrs}}$	$^{\dagger}R_T$	R_{irev}	R_{rev}
Growth conditions		m/s x 10^6	$\text{m}^{-1} \times 10^{-11}$	$\text{m}^{-1} \times 10^{-11}$	$\text{m}^{-1} \times 10^{-11}$
YEPL					
500 rpm / Batch		2.91	343	36.4	301
800 rpm / Batch		5.94	168	14.5	147
Cont. Culture			115	33.9	75
YEP _N L					
500 rpm / Batch		3.29	304	27.4	271
800 rpm / Batch		4.86	206	24.4	174
Cont. Culture		6.97	143	70.4	66
Whey					
800 rpm / Batch		4.31	231	58.3	168
Cont. Culture		7.27	137	57.4	75
Whey2					
800 rpm / Batch		4.51	221	123	99
Cont. Culture		10.7	93.4	30.3	57

[†]Total resistance at 2 hours.

Cake masses for a number of unwashed suspensions are shown in Table 7.7. The cake masses appear to be much lower than for washed suspensions. This is to be expected if a force balance is considered. The rapid initial drop in flux would cause the cross flow velocity to flux ratio to increase rapidly. Subsequently the critical cross flow velocity to flux ratio which determines when cake formation ceases, would have been exceeded much more quickly for unwashed cell suspensions. This results in much thinner cell cakes than for the washed cell suspensions.

Table 7.7 Cake masses after 2 hours for unwashed cell suspensions.

Medium	Growth Conditions	Cake Mass [g]
YEP _N L	800 rpm	0.80
	500 rpm	0.30
YEPL	800 rpm	0.52
	500 rpm	0.42
Whey	Continuous	0.33

In Table 7.8 the L_{dm} , S_v and mean cell volume for feed suspensions and the recovered cakes of yeast-like suspensions. It can be seen the mean cell volume is significantly lower for the recovered cakes than the feed suspension. The parameter, L_{dm} is lower and S_v is higher, for the recovered cakes. This indicates that preferential deposition of smaller cells is occurring with unwashed cell suspensions.

This is in contrast with the behaviour observed with washed cell suspensions for yeast-like morphologies, as shown in Table 7.3. For washed cell suspensions the filter cake forms when the filtrate flux is large relative to that of the unwashed suspensions. For the latter, the filtrate flux decreases very rapidly to lower flux values than observed with washed suspensions. Therefore cake formation with unwashed cell suspensions will occur at lower flux values and hence lower flux/crossflow velocity ratios. The drag force from the filtrate may be sufficient to cause all cell morphologies to deposit with washed cell suspensions. With unwashed cell suspensions only the smaller cells are deposited due to the smaller filtrate drag forces. Finally, no definite conclusion can be made regarding preferential deposition of cells of different shape as the L_{dm} of the recovered cakes are not significantly different to those of the feed suspensions, though L_{dm} values tend to be lower.

Table 7.8 Morphology data for feed suspensions and recovered cakes for unwashed cell suspensions

Media	Growth Conditions	Feed Suspension			Recovered Cake		
		L_{dm} —	S_v μm^{-1}	V_{cells} μm^3	L_{dm} —	S_v μm^{-1}	V_{cells} μm^3
YEP _{NL}	800 rpm	3.34	1.52	50.26	2.47	1.75	24.96
	500 rpm	4.49	1.54	61.94	4.21	1.61	53.54
YEPL	800 rpm	3.26	1.48	52.05	3.13	1.66	35.31
	500 rpm	5.07	1.52	74.04	3.72	1.52	55.17
Whey	800 rpm	3.24	1.45	54.35	3.00	1.56	41.09
Whey2	800 rpm	3.05	1.49	47.45	3.06	1.53	43.14

In Figure 7.24, the specific resistance measured by dead-end filtration, of the feed suspension and recovered crossflow filter cake, is shown for cell suspensions grown in YEP_{NL} medium at 800 rpm in batch culture. It can be seen there is an order of magnitude of difference in the measured dead-end filtration specific resistances for the feed suspension and the recovered cake. In comparison, for the washed cell suspensions of the same culture, the difference between the dead-end filtration specific resistance of the feed suspension and the recovered filter cake is much less, approximately a factor of 2. This indicates that for the unwashed cell suspensions there is a greater mass of fouling material per unit cell volume in the cakes than for the washed suspensions. However, it should be noted that preferential deposition of smaller cells may account for some of the difference shown in Figure 7.24.

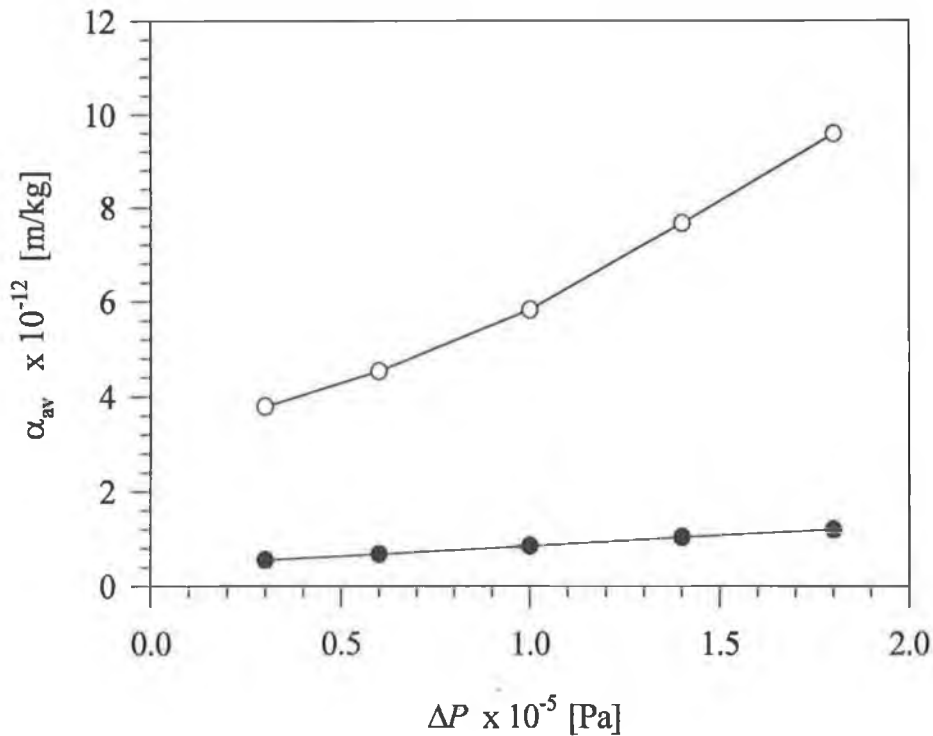


Figure 7.24 Specific resistance measured during dead-end filtration *versus* applied pressure for YEP_NL media 800 rpm, batch culture. Symbols: ○ recovered filter cake and ● feed suspension.

In Figure 7.25 the effect of switching the feed suspension from unwashed cell suspension to saline is shown. It can be seen, that in all cases there was a sharp increase in flux immediately after the feed suspension was changed and the flux then reached a relatively constant value. The increase in flux is partly due to a viscosity effect. The viscosity of spent medium is approximately 8-10% greater than that of water. Consequently, the flux during the saline filtration phase should increase by a similar magnitude if the filter cake was unaffected by the change in feed.

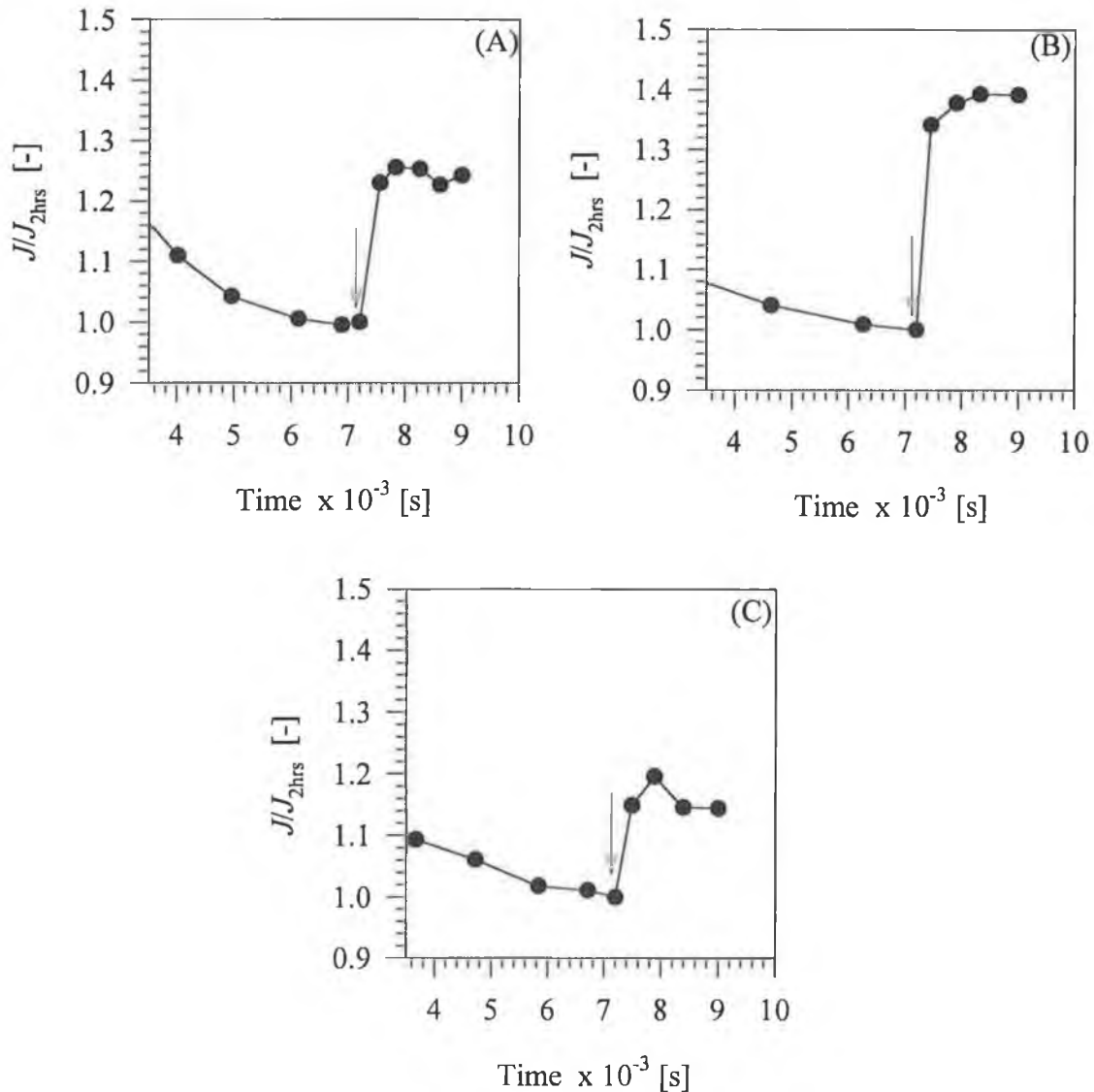


Figure 7.25 Saline filtration for unwashed suspensions grown in YEP_{NL} media. (A) Batch, 800 rpm; (B) batch, 500 rpm; (C) continuous culture, dilution rate = 0.19 h^{-1} . Arrows indicate switch in feed.

However, the increase in flux after switching the feed to saline, is in the region of 20 to 40 %, as shown in Figure 7.25. Therefore, some of the cake or fouling layer must be removed when the feed is switched to saline. It was noted that the contents in the reservoir became "turbid" almost instantly after changing the feed solution.

7.7 Conclusions

Fouling is an important factor in crossflow microfiltration of *K. marxianus*. This is particularly true in the case of unwashed suspensions, which result in significant differences in the filtration fluxes of washed and unwashed cell suspensions. However, dead-end filtration of washed and unwashed suspensions results in cakes with similar specific resistances, indicating fouling is not a factor here. Varying the growth conditions appears to influence the filtration behaviour in crossflow microfiltration more than using different growth media as can be observed in the filtration fluxes obtained for both washed and unwashed suspensions. However, the filtration flux of spent medium appears to be independent of the growth conditions and only slightly influenced by the culturing media. This indicates cell morphology may impact filtration behaviour.

When filtering washed cell suspensions, the mass of cake formed decreases with increasing L_{dm} and mean cell volume. Furthermore, preferential deposition does not appear to occur with washed yeast-like suspensions as indicated by the cake formation rate and image analysis data. However, it does occur with unwashed yeast-like suspensions and possibly occurs with both washed and unwashed mycelial suspensions.

The specific resistances of washed cell suspensions are higher than those observed during dead-end filtration even if membrane fouling is considered. This indicates a degree of cake fouling by fines, occurring during crossflow microfiltration. There is microscopic evidence of this occurring, as shown in Figure 7.10, and due to the observed black deposit when cell pellets are formed by centrifugation. Also the specific resistance measured by dead-end filtration, of the recovered crossflow filter cakes are significantly greater than those for the original feed suspension, such that the differences in cake resistances cannot be solely explained by slight changes in cell morphology that were observed. The apparent specific resistances of mycelial filter cakes are greater than those determined for yeast morphologies. This is in contrast to dead-end filtration where the specific resistance is less for mycelial suspensions than for yeast suspensions.

This is probably due to the thinner cakes formed by mycelial suspensions, which would lead to a greater concentration of fines per cell volume in the filter cake, than would be the case with the larger cakes formed from yeast-like cells. However, it is also possible the nature of cake fouling is significantly different with mycelial suspensions due to the difference in cake structure. Also cake recovery of washed yeast filter cakes was significantly higher than with washed mycelial filter cakes, indicating possible differences in cake structure and cell membrane interactions.

For unwashed suspensions there would appear to be considerable rejection of macrosolutes during crossflow microfiltration which results in the low fluxes observed. The yeast-like suspensions give lower filtration fluxes possibly as result of greater cake fouling. Again this indicates that the nature of the cells, fouling material and membrane interactions are different for mycelial and yeast suspensions during crossflow microfiltration.

Finally it was shown that the cake mass decreased and filtrate flux increased with increasing crossflow velocity. Furthermore, it was shown that the specific cake resistance decreases with crossflow velocity which is contrary to filtration behaviour observed in the literature. This was probably due to the pressure drop across the filter cake decreasing due to decreasing cake mass, hence less cake compression. However, there was also evidence of fouling decreasing with increasing crossflow velocity.

Many of the techniques utilised in this study can be used to elucidate filtration performance with different cell morphologies of *K. marxianus*, operating conditions, micro-organisms and crossflow microfiltration modules and membranes. The approach developed here allows considerable information to be determined from a single cross flow filtration experimental set-up. By increasing the number of parameters measured during a filtration experiment it allows a greater understanding of the filtration process to be obtained.

CHAPTER 8

SUMMARY AND FUTURE WORK

8.1 Summary

While filtration of microorganisms has attracted considerable research over the last few decades, there are areas in the field where the published research is minimal. In particular dead-end filtration has been particularly neglected due to the emphasis on research into crossflow filtration. In crossflow filtration, cake formation and cake properties have received minimum attention and fouling is often ignored in subsequent analysis and modelling of the crossflow filtration behaviour. In particular the role of cell morphology has not been extensively studied in either dead-end filtration or crossflow filtration. In this thesis the use of a dimorphic microorganism and computer-aided image analysis has proved to be a powerful tool combination in elucidating the fundamental relationships between mean cell morphology and filtration behaviour.

In Chapter 4 and Chapter 5, a linear relationship was found to exist between α_{av} and ΔP for all morphologies of *K. marxianus*, resuspended active dry yeast and cultured baker's yeast over the entire range of pressures employed. The relationship between α_{av} and ΔP allowed the null stress resistance to be determined, thus uncoupling cake packing and compressibility effects. The null stress resistance was found to decrease as the mean cell morphology became more mycelial in nature, suggesting random packing of cells in the filter cake. The Kozeny-Carman equation coupled with a relationship for null stress voidage, ϵ_0 , determined from centrifugation studies, and the mean aspect ratio, L_{dm} , gives a reasonably good description of the relation between morphology and specific cake resistance at zero compressive pressure.

Also in Chapter 4 and Chapter 5, it was shown that as L_{dm} increases that filter-cake compressibility, defined as k_c , increases. A possible mechanism for compression was described which could account for the dependence of compression on cell morphology. The mechanism is based on cells being most deformable at sub-unit joins and branch points. Furthermore in Chapter 5 it was shown that cake compression for the yeast filter cakes was predominantly reversible, whereas with calcium carbonate filter cakes it was completely irreversible. In Chapter 6 a model was presented to qualitatively describe filter cake compression. The model was found to predict a near linear relationship between α_{av} and ΔP as was found to occur experimentally in Chapter 4 and Chapter 5. It was also shown that the Tiller relationship relating α_{av} and ΔP could be reduced to a linear expression if n_1 is equal to 2. Furthermore it was shown that the coefficient of compressibility increases with null stress porosity. This partially explains the increase in k_c with L_{dm} observed in Chapter 4 and Chapter 5.

In Chapter 7, the crossflow filtration behaviour of *K. marxianus* was explored. Washed and unwashed suspensions of various mean cell morphologies of *K. marxianus* grown in different media were used to analyse cake formation and fouling. It was shown that crossflow filtration behaviour is significantly different to that observed during dead-end filtration. In particular it was shown that fouling is significant during crossflow filtration whilst it is negligible during dead-end filtration. Varying the cell morphology (growth conditions) appears to influence the filtration behaviour in crossflow filtration more than using different growth media for both washed and unwashed cell suspensions. However, the filtration flux of spent medium appears to be independent of the growth conditions and only slightly influenced by the culturing media. For unwashed suspensions there would appear to be considerable rejection of macrosolutes during crossflow filtration that results in the lower fluxes compared to washed suspensions. The results indicated that the nature of the cells, fouling material and membrane interactions are different for mycelial and yeast suspensions during crossflow filtration. Furthermore by switching the feed to saline solution during the pseudo steady state period it was shown that the cell cake remains largely intact and thus is not significantly influenced by shear.

It was also shown in Chapter 7, using a novel technique to determine cake mass, that the mass of cake formed, decreases with increasing L_{dm} and mean cell volume, for washed cell suspensions. Furthermore, preferential deposition does not appear to occur with washed yeast-like suspensions as indicated by the cake formation rate and image analysis data. However, it does occur with unwashed yeast suspensions and possibly occurs with both washed and unwashed mycelial suspensions.

The specific resistance of washed cell suspensions increases throughout filtration and is higher than observed during dead-end filtration even if membrane fouling is considered. This indicates a degree of cake fouling by fines occurring during crossflow filtration. Also the specific resistance, measured by dead-end filtration, of the recovered crossflow filter-cakes is significantly greater than those for the original feed suspension. The apparent specific resistance of mycelial filter cakes are greater than that determined for yeast morphologies. This is in contrast to dead-end filtration where the specific resistance is less for mycelial suspensions than for yeast suspensions. Cake recovery of washed yeast filter cakes was significantly higher than with washed mycelial filter cakes, indicating possible differences in cake structure and cell membrane interactions.

Also in Chapter 7 it was shown that the cake mass decreased and filtrate flux increased with increasing crossflow velocity. Furthermore, it was shown that the specific cake resistance decreases with crossflow velocity, which is contrary to filtration behaviour observed in the literature. This was probably due to the pressure drop across the filter cake decreasing due to decreasing cake mass, thus reducing less cake compression. However, there was also evidence of fouling decreasing with increasing crossflow velocity.

8.2 Recommendations for future work

While many areas of filtration have been elucidated in this thesis there is still a considerable amount of research needed in order to understand the fundamental basis of filtration behaviour on a universal scale. The approach and methods employed in this thesis could be used to gain a more in-depth understanding if used with other microorganisms or filtration configurations.

The relationship between α_{av} and ΔP needs to be fully re-investigated for other microorganisms and for bacterial cells in particular. It should be established if the null stress resistance of all microorganisms could be related to cell morphology as shown in Chapter 4. If a linear relationship between α_{av} and ΔP was found for a wide range of other microorganisms, it may indicate that a fundamental mechanism governs cake compression for microorganisms. Even if it was not found to hold for bacterial cells it may be that yeast and bacterial filter-cakes compress differently. New approaches could be developed to determine if cell deformation and/or particle rearrangement occurs during filter-cake compression. Attempts to correlate cell wall composition and cake compression may indicate the influence of the cell wall during compression. In particular *K. marxianus* would be a useful micro-organism to use, due to the fact that a single organism could be used and also due to its filtration characteristics being well established in this thesis.

The modelling of cake compression presented in Chapter 6 indicates that measuring α_{av} at low pressures (<20 kPa) is required to ascertain if α_{av} can be extrapolated to zero pressure to give the null stress specific resistance. Plotting either the compressibility coefficient or compressibility index against the null stress cake voidage for a wide range of microorganisms would elucidate the extent to which voidage affects compressibility. Also the impact of ionic strength, pH and modifying the surface properties of cells (Hodgson *et al.*, 1993) on compressibility with a variety of microorganisms, may indicate the importance of other factors.

Filtering washed, unwashed and cell free spent media in crossflow filtration helped simplify some of the complexities of crossflow filtration. This approach was successfully employed with resuspended bakers yeast (Foley *et al.*, 1995a). It is a simple approach that could be employed with any cell suspension and filtration configuration, to determine the extent of fouling by media components.

In Chapter 7 numerous parameters such as cake mass as a function of time, measurement of the degree of reversible and irreversible fouling, cake recovery, switching the feed to saline, image analysis of recovered cake and dead-end filtration of the original suspension and recovered cake were measured for each filtration run. Measuring a wide range of parameters for the same experimental set-up helped elucidate the mechanisms involved during crossflow filtration of *K. marxianus*. A similar approach could be adopted when filtering other suspensions to help minimise the ambiguity that remains when only flux measurements are taken. Biochemically assaying the media components would further add to understand the mechanisms involved when filtering *K. marxianus* suspensions. Alternatively, using minimal medium would make an interesting comparison to the complex media used here and may possibly eliminate fines. Using a similar approach used in this thesis while varying ΔP_{tm} would help elucidate the role of trans-membrane pressure drop in crossflow filtration. Depositing a cake of washed cells and switching the feed to cell free spent media could determine if the membrane is protected by deposited cells as suggested by Foley *et al.* (1995a).

The method utilised in this study for determining cake mass during filtration, is simple in nature and could be employed with a variety of microorganisms without the need to interrupt filtration as occurs with other methods (Riesmeier *et al.*, 1987). It would allow an easy and quick method to determine the evolution of α_{av} during filtration. Filtering more dilute suspensions than used in Chapter 7 and monitoring the feed suspension morphology as employed by Foley (1993) would help understand the preferential deposition that was shown to occur with unwashed cell suspensions of *K. marxianus*.

APPENDIX A

CAKE FORMATION IN CROSSFLOW FILTRATION EQUATIONS

At the start of crossflow filtration the reservoir cell concentration is c_0 . It is assumed that the cake forms as in dead-end filtration, i.e. all the cells in the filtrate prior to filtration deposit to form a cake. During the initial batch period the reservoir cell concentration will remain constant assuming dead-end filtration behaviour. Consequently, at the end of the batch period the deposited cake will be a product of the cell concentration and filtrate volume i.e.,

$$M_1 = c_0 V_1 \quad [\text{A1.1}]$$

At the end of the batch period the filtrate is re-introduced into the reservoir. This dilutes the concentration in the system, i.e.,

$$c_1 = \frac{c_0 V_s - M_1}{V_s} \quad [\text{A1.2}]$$

Consequently at the start of the total recycle mode phase, (time, t_1), the reservoir cell concentration is c_1 and the deposited cake mass is M_1 . During the total recycle phase the rate of change of cake mass, M_t , is equal to the rate of deposition of cells, i.e.,

$$\frac{dM_t}{dt} = A c_t J \quad [\text{A1.3}]$$

Also the rate of increase in the cake mass is related to the rate of decrease in cell concentration by the following expression,

$$\frac{dM_t}{dt} = -V_s \frac{dc}{dt} \quad [\text{A1.4}]$$

Equation A1.4 can be inserted into equation A1.3 to give,

$$V_s \frac{dc}{dt} = -AcJ \quad [\text{A1.5}]$$

Re-arranging equation A1.5 gives,

$$\frac{1}{c} dc = \frac{-AJ}{V_s} dt \quad [\text{A1.6}]$$

Equation A1.6 can be integrated between the limits (t_1, c_1) and (t, c) , i.e.,

$$\int_{c_1}^c \frac{1}{c} dc = \frac{-AJ}{V_s} \int_{t_1}^t dt \quad [\text{A1.7}]$$

However the solution of the integral on the right hand-side of equation A1.7 is,

$$A \int_{t_1}^t J dt = V_f - V_1 \quad [\text{A1.8}]$$

where V_1 is the filtrate volume at time t_1 .

Hence the solution of equation of A1.7 is,

$$\ln(c) - \ln(c_1) = \frac{-(V_f - V_1)}{V_s} \quad [\text{A1.9}]$$

Re-arranging equation A1.8 and getting the exponent of both sides gives,

$$\frac{c_t}{c_1} = e^{\frac{-(V_t - V_1)}{V_s}} \quad [\text{A1.10}]$$

Therefore at any time, t , the cell concentration, c_t , is given by

$$c_t = c_1 e^{\frac{-(V_t - V_1)}{V_s}} \quad [\text{A1.11}]$$

The cake mass at any time during the total recycle phase is equal to sum of the cake mass at the end of the initial batch period and the product of suspension volume by the change in concentration during the total recycle phase, i.e.,

$$M_t = M_1 + V_s [c_1 - c_t] \quad [\text{A1.12}]$$

Inserting equation A1.11 into A1.12 gives,

$$M_t = M_1 + V_s \left[c_1 - c_1 e^{\frac{-(V_t - V_1)}{V_s}} \right] \quad [\text{A1.13}]$$

REFERENCES

- Arora N. and R.H. Davis, (1994)
Yeast cake layers as secondary membranes in dead-end microfiltration of bovine serum albumin.
J. Membrane Sci., 92, 247-256
- Aubert M.C., Elluard M.P. and H. Barnier, (1993)
Shear stress induced erosion of filtration cakes studied by a flat rotating disk method.
J. Membrane Sci., 84, 229-240
- Baker R.J., Fane A.G., Fell C.J.D. and B.H. Yoo, (1985)
Factors affecting flux in crossflow filtration.
Desalination, 53,81-93
- Bashir I. and M. Reuss, 1992
Dynamic model for crossflow microfiltration of microbial suspensions in porous tubes.
Chem. Eng. Sci., 47, 189-203
- Belfort G., (1998)
Coiled Membrane Filtration System.
U.S. patent 5,626,758, May 6
- Bell D.J. and R.J. Davis (1987)
Cell harvesting of oleaginous yeast by crossflow filtration.
Biotechnol. Bioeng., 29, 1176-1178
- Blake N.J., Cumming I.W. and M. Streat, (1992)
Prediction of a steady state crossflow filtration using a force balance model.
J. Membrane Sci., 68, 205-216
- Blanpain P., Hermia J., and M. Lenoel, (1993)
Mechanisms governing permeate flux and protein rejection in the microfiltration of beer with a cyclopore membrane.
J. Membrane Sci., 84, 37-51
- Bowen W.R. and Q. Gan, (1991)
Properties of microfiltration membranes: Flux loss during constant pressure permeation of Bovine Serum Albumin.
Biotechnol. Bioeng., 38, 688-696.
- Bowen W.R., (1993)
Understanding flux patterns in membrane processing of protein solutions and suspensions.
Trends Biotechnol., 11, 451-460

- Bowen W.R. and X. Cao, (1998)
Electrokinetic effects in membrane pores and the determination of Zeta potential.
J. Membrane Sci., 140, 267-273
- Boyaval P., Lavenant C., Gesan G. and G. Daufin, (1996)
Transient and stationary operating conditions on performance of Lactic acid bacteria crossflow microfiltration.
Biotechnol. Bioeng., 49, 78-86
- Brady, D., Rose P.D. and J.R. Duncan, (1994)
*The use of hollow fiber crossflow microfiltration in bioaccumulation and continuous removal of heavy metals from solution by *Saccharomyces cerevisiae*.*
Biotechnol. Bioeng., 44, 1362-1366
- Cabral J.M.S., Casale B. and C.L. Cooney, (1985)
Effect of antifoam agents and efficiency of cleaning procedures on the crossflow filtration of microbial suspensions.
Biotechnol. Lett., 7, 749-752
- Capannelli G., Bottino A., Gekas V. and T. Tragardh, (1990)
Protein fouling behaviour of ultrafiltration membranes prepared with varying degrees of hydrophilicity.
Process Biochem. International, December, 221-224
- Carman P.C., (1937)
Fluid flow through a granular bed.
T. I. Chem. Eng., 15, 150-156
- Chan W.K., Belfort M. and G. Belfort, (1991)
*Protein overproduction in *Escherichia coli*: RNA stabilisation, cell disruption and recovery with a crossflow microfiltration membrane.*
J. Membrane Sci., 18, 225-242
- Chandavarkar C. and C.L. Cooney, (1990)
Mathematical modelling of flux decline caused by protein aggregation.
ACS National meeting, Washington D.C., August.
- Chase G.G. and M.S. Willis, (1992)
Compressive cake filtration.
Chem. Eng. Sci., 47, 1373-1381
- Chellam S. and M.R. Wisener (1998)
Evaluation of crossflow filtration models based on shear-induced diffusion and particle adhesion: Complications induced by feed suspension polydispersivity.
J. Membrane Sci., 83-97

- Cleveland T.G., Tiller F. M. and J.B. Lee, (1996)
Theory of filtration of highly compactable biosolids.
Water Sci. Technol., 34, 299-306
- Davis R.H. and S.T. Birdsell, (1987)
Hydrodynamic model and experiments for crossflow microfiltration.
Chem. Eng. Commun., 49, 217-234
- Davis R.H. and D.T. Leighton, (1987)
Shear-induced transport of a particle layer along a porous wall.
Chem. Eng. Sci., 49, 217-234
- Defrise D. and V. Gekas, (1988)
Microfiltration membranes and the problem of microbial adhesion - a literature survey.
Process Biochem., August, 105-116
- Dolejs V. and P. Mikulasek, (1997)
Creeping flow of generalised Newtonian fluid through a fixed and fluidized bed of spherical particles.
Chem. Eng. Process., 36, 111-117
- Elmaleh S. and L. Abdelmoumni, (1997)
Crossflow filtration of an anaerobic methanogenic suspension.
J. Membrane Sci., 131, 261-274
- Fane A.G., Fell C.J.D., Hodgson P.H., Leslie G. and K.C. Marshall, (1991)
Microfiltration of Biomass and Biofluids: effects of membrane morphology and operating conditions.
Filtr. Separat., Sept/Oct, 332-340
- Fane A.G., Fell C.J.D. and A.G. Waters, (1983)
Ultrafiltration of protein solutions through partially permeable membranes – the effect of adsorption and solution environment.
J. Membrane Sci., 16, 211-224
- Field R.W., Wu D., Howell J.A. and B.B. Gupta, (1995)
Critical flux concept for microfiltration fouling.
J. Membrane Sci., 100, 259-272
- Flemming H.C., Schaule G., Griebe T. and A. Tamachkiarowa, (1997)
Biofouling – the Achilles heel of membrane processes.
Desalination, 113, 215-225
- Flynn C., Geoffroy P. and G. Foley, (1990)
A novel technique for the study of cake formation during cross-flow microfiltration of microbial cells.
Biotechnol. Tech., 5, 325-328

- Foley G. (1993)
Experimental and theoretical studies of factors affecting cake formation and membrane fouling in crossflow microfiltration.
PhD Thesis, UCD
- Foley G., (1994)
Membrane fouling in crossflow filtration: Implications for measurement of the steady state specific resistance.
Biotechnol. Tech., 8, 743-746
- Foley G., MacLoughlin P.F. and D.M. Malone, (1995b)
Membrane fouling during constant flux crossflow microfiltration of dilute suspensions of active dry yeast.
Separ. Sci. Technol., 30, 383-398
- Foley G., Malone D.M. and F. MacLoughlin, (1995a)
Modelling the effects of particle polydispersity in crossflow filtration.
J. Membrane Sci., 99, 77-88
- Fordham E.J. and H.K.J. Ladva, (1989)
Crossflow filtration of benolite suspensions.
PhysicoChem. Hydrodyn., 11, 411-439
- Fowler J.D. and C.R. Robertson, (1991)
Hydraulic permeability of immobilised bacterial cell aggregates.
Appl. Environ. Microb., 57, 102-113
- Free M.L., Zhu J.S. and B.M. Moudgil, (1998)
Use of a new particle contact probability filtration rate model to determine effect of particle size distribution in filtration.
Separ. Sci. Technol., 33, 57-66.
- Gatenholm P., Fane A.G. and C.J.D. Fell, (1988)
Influence of the membrane structure on the composition of the deposit layer during processing of microbial suspensions.
Desalination, 70, 363-378
- Gehlert G., Luque S. and G. Belfort, (1998)
Comparison of Ultra- and Microfiltration in the presence and absence of secondary flow with polysaccharides proteins and yeast suspensions.
Biotechnol. Progr., 14, 931-942
- Gesan G., Daufin G. and U. Merin, (1995)
Performance of whey crossflow microfiltration during transient and stationary operating conditions.
J. Membrane Sci., 100, 271-281

- Grace H.P., (1953)
Resistance and compressibility of filter cakes.
Chem. Eng. Prog., 49, 303-318
- Hadzismajlovic D.E. and C.D. Bertram, (1998)
Flux enhancement in laminar crossflow microfiltration using a collapsible-tube pulsation generator.
J. Membrane Sci., 142, 173-189
- Happel J. and H. Brenner, (1965)
Low Reynolds number hydrodynamics, Chapter 8,
Prentice Hall, Englewoods Cliffs, NJ.
- Hermia J., (1982)
Constant pressure blocking filtration laws- application to power-law non-newtonian fluids.
T. I. Chem. Eng., 60,183-187
- Hodgson P.H., Leslie G.L., Schneider R.P., Fane A.G., Fell C.J. and K.C. Marshall, (1993)
Cake resistance and solute rejection in bacterial microfiltration: The role of the extracellular matrix.
J. Membrane Sci., 79, 35-53
- Hooper L.A., Hollein H.C. and C.S. Slater, (1998)
Microfiltration of Streptomyces rimosus: Cell harvesting process studies.
Separ. Sci. Technol., 33, 1747-1765
- Howell J.A., Field R.W. and D. Wu, (1993)
Yeast cell microfiltration: Flux enhancement in baffled and pulsatile flow systems.
J. Membrane Sci., 80, 59-71
- Hwang K.J., Liu H.S. and W.M. Lu, (1998)
Local properties of cake in cross-flow microfiltration of submicron particles.
J. Membrane Sci., 138, 181-192
- Hwang K. J., Wu Y. S. and W.M. Lu, (1996)
The surface structure of cake formed by uniform-sized rigid spheroids in cake filtration.
Powder Technol., 87, 161-168
- Jiratananon R., Uttapap D. and P. Sampranpiboon, (1998)
Crossflow microfiltration of a colloidal suspension with the presence of macromolecules.
J. Membrane Sci., 140, 57-66
- Ju L.-K. and C.S. Ho, (1988)
Correlation of cell volume fractions with cell concentration in fermentation media.
Biotechnol. Bioeng., 32, 95-99

Junker B.H., Timberlake S., Bailey F.J., Reddy J., Prud'homme and K. Gbewonyo, (1994)

Influence of strain and medium composition on filtration of Escherichia coli suspensions.

Biotechnol. Bioeng., 44, 539-548

Kavanagh P.R. and D.E. Brown, (1987)

Cross-flow separation of yeast cell suspensions using a sintered stainless steel filter tube.

J. Chem. Technol. Biotechnol., 38, 187-200

Kawakatsu T., Nakajima M., Nakao S. and S. Kimura (1995)

Three-dimensional simulation of random packing and pore blocking phenomena during microfiltration.

Desalination, 101, 203-209

Kawakatsu T., Nakao S. and S. Kimura, (1993)

Macromolecule rejection with compressible and incompressible cake layer formed in crossflow microfiltration.

J. Chem. Eng. Japan, 26, 656-661

Kelly S., Opong W.S. and A.L. Zydney, (1993)

The influence of protein aggregates on the fouling of microfiltration membranes during stirred cell filtration.

J. Membrane Sci., 80, 175-187

Kobayashi T., Ono M., Shibata M. and N. Fujii, (1998)

Cut-off performance of Escherichia coli by charged and noncharged polyacrylonitrile ultrafiltration membranes.

J. Membrane Sci., 140, 1-11

Kroner K.H., Schutte H., Hustedt H. and M. R. Kula, (1984)

Crossflow filtration in the downstream processing of enzymes.

Process Biochem., 19, 67-74

Ku M.A. and Y.D. Hang, (1992)

Production of yeast lactase from sauerkraut brine.

Biotechnol. Lett., 14, 925-928

Le S.L., (1987)

Recovery of beer from tank bottoms with membranes.

J. Chem. Technol. Biotechnol., 37, 59-66

Le M.S. and P.J. Biligheimer, (1985)

Membranes in downstream processing.

Chem. Eng. - London, 416, 48-53

- Le M.S., Spark L.B. and P.S. Ward, (1984a)
The separation of Aryl Acrylamidase by crossflow microfiltration and the significance of enzyme/cell debris interaction.
J. Membrane Sci., 21, 219-232
- Le M.S., Spark L.B., Ward P.S. and N. Ladwa, (1984b)
Microbial Asparaginase recovery by membrane processes
J. Membrane Sci., 21, 307-319
- Leighton D. and A. Acrivos, (1987)
The shear-induced migration of particles in concentrated suspensions.
J. Fluid Mech., 181, 415-439
- Leu W., (1986)
Principles of compressible cake filtration.
In: **Encyclopaedia of Fluid mechanics Vol. 5** (N. Chermisinoff Ed.),
Wiley New York, USA,
- Li S.L., Chou K.S., Lin J.Y., Yen H.W. and I.M. Chu, (1996)
Study of the microfiltration of Escherichia coli containing fermentation broth by a ceramic membrane filter.
J. Membrane Sci., 110, 203-210
- Liberge R., Colinart P., Fessier P., and H. Renon, (1994)
Data and model for progressive fouling in cross-flow microfiltration of yeast on three industrial mineral membranes.
Ind. Eng. Chem. Res., 33, 1310-1318
- Liu T. and D. Yu, (1993)
Morphological measurements on Penicillium chrysogenum broths by rheology and filtration methods.
Biotechnol. Bioeng., 42, 777-784
- Lu W. M. and K. J. Hwang (1993)
Methods of cake formation in constant pressure filtration.
Separ. Technol., 3, 122-132
- Lu W.M. and S.C. Ju, (1989)
Selective particle deposition in crossflow filtration.
Separ. Sci. Technol., 24, 517-540
- Maa Y. and C. Hsu, (1996)
Membrane fouling in sterile filtration of recombinant human growth hormone.
Biotechnol. Bioeng., 50, 319-328
- Mackley M.R. and N.E. Sherman, (1992)
Crossflow cake filtration mechanisms and kinetics.
Chem. Eng. Sci., 47, 3067-3085

- Maiorella B., Dorin G., Carion A. and H. Harano, (1991)
Crossflow microfiltration of animal cells.
Biotechnol. Bioeng., 37, 121-126
- Matsumoto Y. and Y. Totsuka, (1992)
Microfiltration of mixed microorganism and protein solutions.
Kagaku Kogaku Ronbun., 18, 677-683
- Mauret E. and M. Renaud (1997)
Transport Phenomena in multi-particle systems-I. Limits of the applicability of capillary model in high bed voidages – application to fixed beds of fibers and fluidized beds of spheres.
Chem. Eng. Sci., 52, 1807-1817
- McCarthy A.A., Walsh P.K. and G. Foley, (1996)
On the relation between filtrate flux and particle concentration in batch crossflow microfiltration.
Separ. Sci. Technol., 31, 1615-1627
- McDonagh R.M., Fell C.J.D. and A.G. Fane
Surface charge and permeability in the ultrafiltration of non-flocculating colloids.
J. Membrane Sci., 1984, 21, 285-294
- Milewski J.V., (1978)
The combined packing of rods and spheres in reinforcing plastics.
Ind. Eng. Chem. Prod. Res. Dev., 17, 363-367
- Mota M., Teixeira J. and A. Yelshin, (1998)
Tortuosity in Bioseparations and its application to food process.
2nd European Symposium on Biochemical Engineering Science, Porto, 93-98
- Moulin P., Serra C., Rouch J.C., Clifton M.J. and P. Aptel, (1996)
Dean vortices in coiled tubular membranes.
J. Membrane Sci., 114, 235-244
- Mourot P., Lafrance M. and M. Oliver, (1989)
Aseptic concentration of living cells by crossflow filtration.
Process Biochem., 24, 3-8
- Nagata N., Herouvis K.J., Dziejwski D.M. and G. Belfort, (1989)
Cross-flow membrane microfiltration of a bacterial fermentation broth.
Biotechnol. Bioeng., 34, 447-466
- Nakanishi K., Tadokoro T. and R. Matsuno, (1987)
On the specific resistance of cakes of microorganisms.
Chem. Eng. Commun., 62, 187-201

- Nakao S., Nomura S. and S. Kimura, (1990)
Transport phenomena of the crossflow microfiltration process,
Proc. 5th World Filtration Congress Vol. 1, Nice 5-8 June, p. 564
- Nolan G.T. and P.E. Kavanagh, (1992)
Computer simulation of random packing of hard spheres.
Powder Technol., 72, 149-155
- Nolan G.T. and P.E. Kavanagh, (1993)
Computer simulation of random packings of spheres with Log-normal distributions.
Powder Technol., 76, 309-316
- Ofsthun, N.J., (1989)
Crossflow membrane filtration of cell suspensions.
PhD Thesis, MIT
- Ogden G.E. and R.H. Davis, (1990)
Experimental determination of the permeability and relative viscosity for fine latexes and yeast suspensions.
Chem. Eng. Commun., 91, 11-28
- Oolman T. and T. Liu, (1991)
Filtration properties of microbial suspensions.
Biotechnol. Prog., 7, 534-539
- O'Shea D.G., (1998)
Morphological studies of Kluyveromyces marxianus var. marxianus NRRLy2415 in suspensions culture: A study incorporating computer aided image analysis.
PHD Thesis, DCU
- O'Shea D.G. and P.K. Walsh, (1996)
Morphological characterisation of the dimorphic yeast Kluyveromyces marxianus var. NRRLy2415 by semi-automated image analysis.
Biotechnol. Bioeng., 51, 679-690
- Patel P.N., Mehaia, M.A. and M. Cheryan, (1987)
Cross-flow membrane filtration of yeast suspensions.
J. Biotechnol., 5, 1-16
- Pritchard M. and J.A. Howell, (1990)
The concentration of yeast suspensions by crossflow filtration.
In: **Separations for Biotechnology 2** (D. L. Pyle, Ed.)
Elsevier Science, London, 65-73
- Puncochar M. and J. Drahos, (1993)
The Tortuosity concept in fixed and fluidized beds.
Chem. Eng. Sci., 48, 2173-2175

- Quirk A.V. and R.J. Woodrow, (1984)
Bacterial cell debris removal by tangential flow filtration.
Enzyme Microb. Technol., 6, 201-206
- Redkar S. and R.H. Davis, (1993)
Crossflow microfiltration of yeast suspensions in tubular filters.
Biotechnol. Prog., 9, 625
- Redkar S. and R.H. Davis, (1995)
Crossflow microfiltration with high frequency reverse filtration.
AIChE J., 41, 501-508
- Redkar S., Kuberkar V. and R.H. Davis, (1996)
Modelling of concentration polarization and depolarization with high frequency backpulsing.
J. Membrane Sci., 121, 229-242
- Riesmeier B., Kroner K.H. and M.R. Kula, (1987)
Studies on secondary layer formation and its characterisation during crossflow filtration of microbial cells.
J. Membrane Sci., 34, 245-266
- Riesmeier B., Kroner K.H. and M.R. Kula, (1989)
Tangential filtration of microbial suspensions: Filtration resistances and model development.
J. Biotechnol., 12, 153-172
- Romero C.A and R.H. Davis, (1991)
Experimental verification of the shear induced hydrodynamic diffusion model for crossflow microfiltration.
J. Membrane Sci., 62, 249-273
- Rushton A., Hosseini M. and I. Hassan, (1980)
The effect of velocity and resistance on filtercake resistance.
J. Sep. Proc. Technol., 1, 35
- Sakai K., Ozawa K., Ohashi K., Yoshida R. and H. Sakurai, (1989)
Low temperature plasma separation by crossflow filtration with microporous glass membranes.
Ind. Eng. Chem. Res., 28, 57-64
- Schluep T. and F. Widmer, (1996)
Initial transient effects during crossflow microfiltration of yeast suspensions.
J. Membrane Sci., 115, 133-145
- Sherman N.E. and J.D. Sherwood, (1993)
Crossflow filtration: Cakes with variable resistance and capyure efficiency.
Chem. Eng. Sci., 48, 2913-2918

- Shimizu Y., Matsushita K. and A. Watanabe, (1994)
Influence of shear breakage of microbial cells on cross-flow microfiltration flux.
J. Ferment. Bioeng., 78, 170-174
- Sims K.A. and M. Cheryan, (1986)
*Crossflow microfiltration of *Aspergillus niger* fermentation broth.*
Biotechnol. Bioeng. Symp., 17, 495-505
- Smith A.E., Moxham K.E. and P.J. Middelberg, (1998)
On uniquely determining cell-wall material properties with the compression experiment.
Chem. Eng. Sci., 53, 3913-3922
- Sohn H.Y. and C. Moreland, (1968)
The effect of particle size distributions on packing density.
Can. J. Chem. Eng., 46, 162-174
- Sorensen P.B., Agerbaek M.L., and B.L. Sorensen, (1996)
Predicting cake filtration using specific flowrate.
Water Environ. Res., 68, 1151-1155
- Taddei C., Aimar P., Howell J.A. and J.A. Scott, (1990)
Yeast cell harvesting from cider using microfiltration.
J. Chem. Technol. Biotechnol., 47, 365-376
- Takai R., Abe H., Watanbe H., Hasegawa H. and Y. Sakai, (1987)
Average specific cake resistance determined in the presence of sedimentation in filtration of starch slurry under constant pressure.
J. Food Process Eng., 9, 265-275
- Tanaka T., Abe K.I., Asakawa H., Yoshida H. and K. Nakanishi, (1994a)
Filtration characteristics and structure of cake in crossflow filtration of bacterial suspension.
J. Ferment. Bioeng., 78, 455-461
- Tanaka T., Abe K.I. and K. Nakanishi, (1994b)
*Shear-induced arrangement of cells in cake during crossflow filtration of *Escherichia coli* cells.*
Biotechnol. Technol., 8, 57-60,
- Tanaka T., Itoh H., Itoh K., Nakanishi K., Kume T. and R. Matsuno, (1995)
Crossflow filtration of bakers yeast with periodical stopping of permeation flow and bubbling.
Biotechnol. Bioeng., 47, 401-404
- Tanaka T., Kamimura R, Fujiwara R. and K. Nakanishi, (1994c)
Crossflow filtration of yeast broth cultivated in molasses.
Biotechnol. Bioeng., 43, 1094-1101

- Tanaka T., Kamimura R., Itoh K., Nakanishi K. and R. Matsuno, (1993)
Factors affecting the performance of crossflow filtration of yeast cell suspension.
Biotechnol. Bioeng., 41, 617-624
- Tanaka T., Tsuneyoshi S., Kitazawa W. and K. Nakanishi, (1997)
Characteristics in crossflow filtration using different yeast suspensions.
Separ. Sci. Technol., 32, 1885-1898
- Tanaka T., Usui K., Kouda K. and K. Nakanishi, (1996)
Filtration behaviours of rod-shaped bacterial broths in unsteady state phase of crossflow filtration.
J. Chem. Eng. Japan, 29, 973-981
- Tanaka T., Usui K. and K. Nakanishi, (1998)
*Formation of the gel layer polymers and its effect on the permeation flux in crossflow filtration of *Corynebacterium glutamicum* broth.*
Separ. Sci. Technol., 33, 707-722
- Tiller F.M., (1953)
The role of porosity in filtration.
Chem. Eng. Prog., 49, 467-479
- Tiller F.M. and J.H. Kwon, (1998)
Role of porosity in filtration: XIII. Behaviour of highly compactible cakes.
AIChE J., 44, 2159-2167
- Tiller F.M. and W.F. Leu, (1980)
Basic data fitting in filtration.
J. Chinese Inst. Chem. Engrs., 11, 61-70
- Tiller F.M., Weber W. and O. Davies, (1981)
Clogging phenomena in the filtration of liquefied coal.
Chem. Eng. Prog., 77, 61-68
- Tiller F.M., Yeh C.S. and W.F. Leu, (1987)
Compressibility of particulate structures in relation to thickening, filtration and expression.
Separ. Sci. Technol., 22, 1037-1063
- Tong Y., Makoto H., Takanashi H., Tano T., Kubota F., Goto M., Nakashio F. and M. Matsumoto, (1998)
Extraction of lactic acid from fermented broth with microporous hollow fibre membranes.
J. Membrane Sci., 143, 81-91
- Tracey E.M. and R.H. Davis, (1994)
Protein fouling of track-etched polycarbonate microfiltration membranes.
J. Colloid Interf. Sci., 167, 104-116
- Vassilieff C.S., (1992)

- Convective model of crossflow filtration.*
Adv. Colloid Interf. Sci., 40, 1-36
- Verhoff F.H. and J.J. Furnaic, (1983)
Compressible packed bed fluid dynamics with applications to a glucose isomerase reactor.
Ind. Eng. Chem. Proc. Des. Dev., 22, 192-198
- Visvanathan C. and R. Ben Aim, (1989)
Studies on colloidal membrane fouling mechanisms in crossflow microfiltration.
J. Membrane Sci., 45, 3-15
- Wakeman R.J., (1975)
Packing densities of particles with log normal size distributions.
Powder Technol., 11, 297-299
- Wakeman R.J., Sabri M.N. and E.S. Tarleton, (1991a)
Factors affecting the formation of wet compacts.
Powder Technol., 65, 283-292.
- Wakeman R.J. and E.S. Tarleton, (1991b)
Colloidal fouling of microfiltration membranes during the treatment of aqueous feed streams.
Desalination, 83, 35-52
- Warren R.K., MacDonald D.G. and G.A. Hill, (1991)
*Crossflow filtration of *Saccharomyces cerevisiae*.*
Process Biochem., 26, 337-342
- Willis M.S., Collins R.M. and W.G. Bridges, (1983)
Complete analysis of non-parabolic filtration behaviour.
Chem. Eng. Res. Des., 61, 96-109
- Winzeler H.B. and G. Belfort, (1993)
Enhanced performance for pressure-driven membrane processes: The argument for fluid instabilities.
J. Membrane Sci., 80, 35-47
- Xu-Jiang Y., Dodds J. and D. Leclerc, (1995)
Cake characteristics in crossflow and dead-end microfiltration.
Filtr. Separat., September, 795-798
- Yamasaki H., Lee M.S., Tanaka T. and K. Nakanishi, (1993a)
Improvement of performance for crossflow membrane filtration of pullulan broth.
Appl. Microbiol. Biotechnol., 39, 21-25
- Yamasaki H., Lee M.S., Tanaka T. and K. Nakanishi, (1993b)
Characteristics of crossflow filtration of pullan broth.
Appl. Microbiol. Biotechnol., 39, 26-30

Yu A.B., Bridgewater J. and A. Burbidge, (1997)
On the modelling of the packing of fine powders.
Powder Technol., 92, 185-194

Zou R.P. and A.B. Yu, (1996a)
Wall effect on the packing of cylindrical particles.
Chem. Eng. Sci., 51,1177-1180

Zou R.P. and A.B. Yu (1996b)
Evaluation of the packing characteristics of mono-sized non-spherical particles.
Powder Technol., 88, 71-79

Zydney A.L., (1985)
PhD Thesis, MIT

Zydney A.L., Saltzman W. M. and C.K. Colton, (1989)
Hydraulic resistance of red cell beds in an unstirred filtration cell.
Chem. Eng. Sci., 44, 147-159